Crystallization studies and application of innovative solid polymer electrolytes for lithium batteries

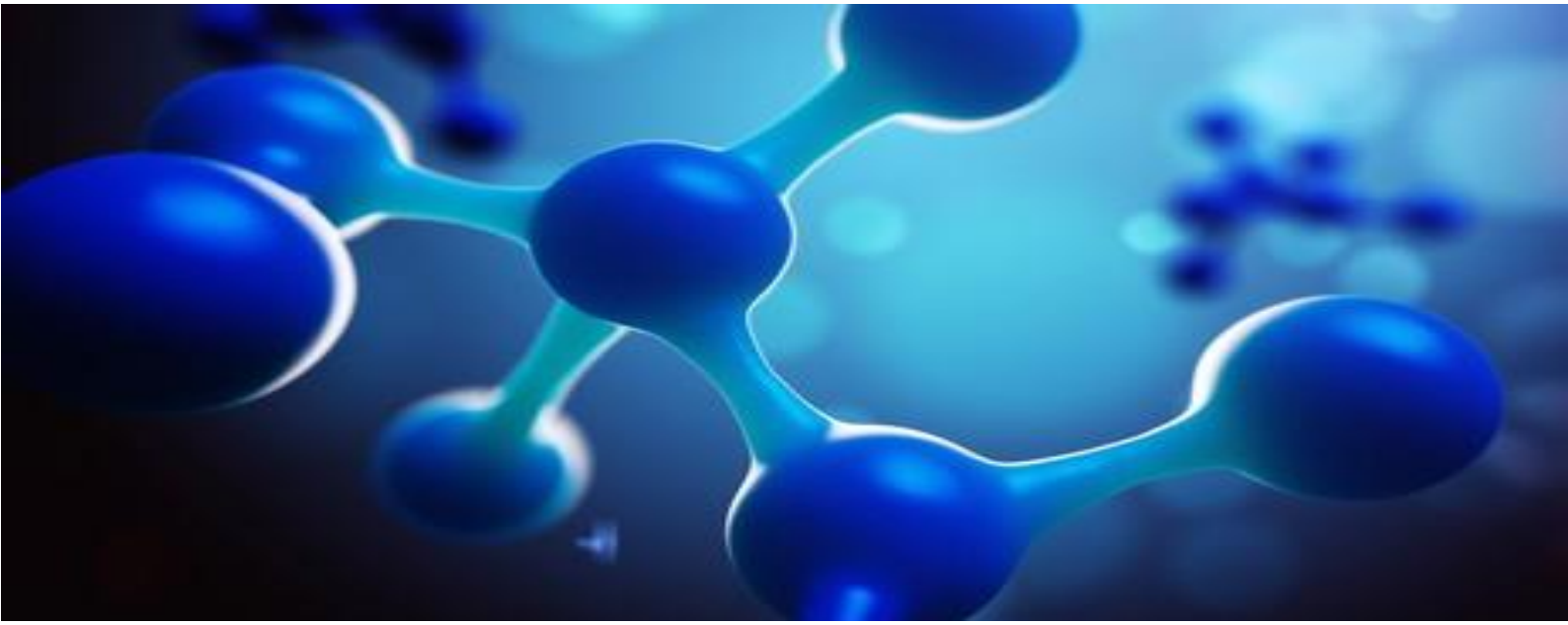

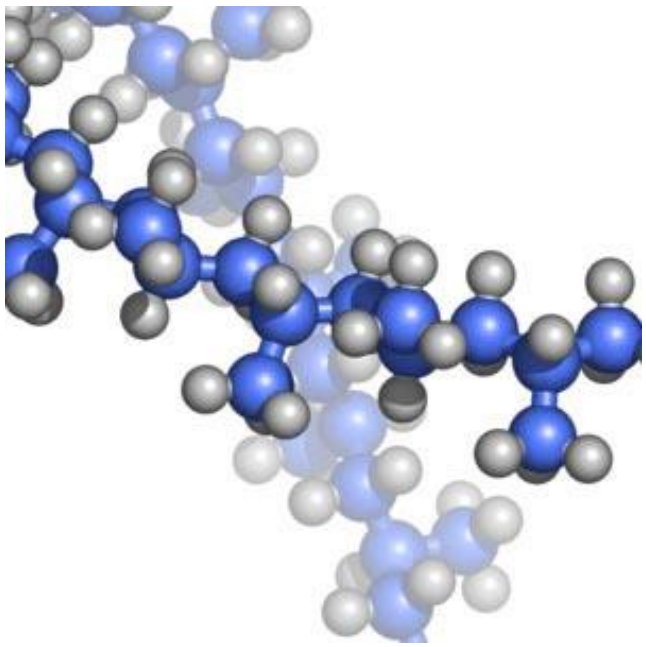

eman ta zabal zazu

Universidad del País Vasco

Euskal Herriko Unibertsitatea

Jorge Luis Olmedo Martínez

PhD Thesis, 2021

Donostia, San Sebastián

Crystallization studies and application of innovative solid polymer electrolytes for lithium batteries

Jorge Luis Olmedo Martínez

Thesis Advisors:

Prof. Alejandro J. Müller Prof. David Mecerreyes

Department of Polymers and Advanced Materials: Physics, Chemistry and Technology, Faculty of Chemistry, University of the Basque Country UPV/EHU

Universidad del País Vasco Euskal Herriko Unibertsitatea

POLYMAT

Basque Center for Macromolecular Design and Engineering

A mi mamá

Porque esto es en gran parte un logro tuyo, no tengo palabras para agradecerte por tanto.

Te amo con todo mi corazón, siempre.

Acknowledgments

Quiero agradecer al Consejo Nacional de Ciencia y Tecnología (CONACyT), México por la beca 471837.

A mis asesores, el Prof. Alejandro Müller por la oportunidad brindada y todo lo que me enseño, al Prof. David Mecerreyes, por todo el apoyo brindado durante este tiempo. A todos los profesores del POLYMAT, siempre demostraron gran profesionalismo y capacidad. A Inés Plaza, por su invaluable ayuda en todo momento.

A todos mis compañeros de trabajo de ambos grupos: Innovative Polymer Group y Advanced Multiphasic Polymer Group: Prof. Agurtzane Mugica, Prof. Manoli Zubitur, Prof. Maria Forsyth, Dr. Haritz Sardon, Dr. María Virginia Candal, Dr. Leire Meabe, Dr. Luca Porcarreli, Dr. Antonella Galastegui, Dr. Miryam Criado, Dr. Esther Udabe, Dr. Nerea Casado, Dr. Edgar Gutiérrez, Maria Rosaria Caputo, Eider Matxinandiarena, Nicolas María, Dr. Jon Maiz, Dr. Ricardo Pérez, Valentina Pirela, Elena Gabirondo, Michele Pastorio, Dr. Maryam Safari, Álvaro Gómez, Fermin Elizalde, Sara Marina, Marta Alvarez, Dr. Nicolas Goujon, Marine Lechartier, Mariana Allasia, Dr. Daniela Minudri, Ainhoa Fernández, Jorge Coba, Yilong Liao, Soline Vauthier, Diulia Quites, Maria Regato, Dr. Andere Basterretxea, Dr. Coralie Jahanno, Xabier Lopez.

A Rafael del Olmo y Ana Suárez, por su compañía, amistad, y tiempo compartido en Australia y San Sebastián.

A los mexicanos que me hicieron sentir no tan lejos de México, Dr. Claudia de León, Dr. Gregorio Guzmán, Dr. Irma Flores y Dr. Diego Magaldi.

A mis amigos en México, Lorena Zamarrón, Dr. Paola Cárdenas, Claudia Hernández y Flor Valdez las cuales siempre estuvieron presentes durante estos cuatro años.

A mis primos Bertha Pérez y Álvaro Martín, por su gran amistad y apoyo siempre. Fueron mi salvavidas más de una vez.

A Aurelie Destephen, por su amistad y los años compartidos viviendo en el mismo piso.

A mis padres, Jorge Olmedo y Pilar Martínez, así como a mis hermanos, César Olmedo y Jessica Olmedo, por su apoyo incondicional, por mostrarme que aún en las pruebas más difíciles de la vida, las podemos superar estando juntos. Quiero agradecer que durante este tiempo en el doctorado, nació mi primer sobrino, Esteban, el cual es una bendición en mi vida.

Table of Content

Abstract

In this work, different polymer electrolyte systems were studied with the objective of being used in lithium batteries. The polymeric systems developed were prepared with the purpose of solving some of the safety problems presented by this type of materials, such as polarization effects within the battery, the poor mechanical properties of the electrolyte and the flammability of the electrolyte. Polyethylene oxide (PEO) is the most widely used polymer in solid polymer electrolytes due to its ability to dissolve lithium salts and high ionic conductivities at temperatures above 70 ºC, but it has some disadvantages, such as poor mechanical properties and low ionic conductivity at room temperature.

In this thesis, PEO was used and the effect of the addition of lithium salt (LiTFSI) and different polymers on the crystallinity of PEO was studied. The electrolyte systems studied in this thesis are based on employing the strategies of blending and on using block copolymers. The electrolytes were characterized by different techniques such as: differential scanning calorimetry (DSC), polarized light optical microscopy (PLOM), electrochemical impedance spectroscopy (EIS), dielectric spectroscopy (DS), the flammability of the electrolytes was evaluated in a microcalorimeter, among other techniques. In addition, the electrolytes that presented the best values of ionic conductivity and mechanical properties were evaluated in symmetrical cells and lithium batteries.

The following is a summary of each of the results chapters:

Chapter III studied different aliphatic polyethers with the incorporation of LiTFSI and evaluated the effect of the number of methylene units in the repeating unit of the polymer on the crystallinity of the polymers, as well as the effect of LiTFSI concentration on the ionic conductivity. It was found that, LiTFSI acts as a diluting agent for aliphatic polyethers, which reduces the crystallization rate and crystallization temperature of these polymers. It was observed that, as the number of methylene units in the repeating unit increases the ionic conductivity decreases, PEO is the polyether with the highest conductivity values. The Flory-Huggins theory was applied to demonstrate that LiTFSI is a thermodynamic diluent for these polymers, with the results obtained by applying these equations

the thermodynamic equilibrium melting temperature and the equilibrium melting enthalpy for poly(oxydecamethylene) were calculated for the first time.

Given the results obtained in Chapter III, in **Chapter IV**, blends of PEO and poly(1,6-hexanediol) (PHD) were prepared, the first thing was to study the blends of the polymers without LiTFSI, in this part, it was concluded that the blends are partially miscible, and that the miscibility between these polymers is a function of the composition of the blend. By incorporating LiTFSI in the 80PEO/20PHD blend, it was shown that the lithium salt prefers to dissolve in PEO, while PHD remains crystalline at high concentrations of LiTFSI, the main conclusion of this Chapter is that the blending of two semi-crystalline polymers may be one of the keys to improve the mechanical properties of polymer electrolytes.

Chapter V presents a single-conduction polymer electrolyte system, meaning that only the lithium cation moves through the electrolyte, and the anion remains immobile. Blends of PEO and PLiMTFSI were prepared in a wide range of compositions (between 5 and 70 wt%). The polymer-polymer interaction parameter (χ_{12}) was calculated, and its value is negative, indicating that over the entire range of compositions the polymers are miscible. In addition, the effect of the molecular weight of both polymers was studied, varying these two parameters (composition and molecular weight) we were able to find an ideal relationship between the polymers as well as the molecular weights with which the electrolyte presents the highest conductivity (50 PEO/50 PLiMTFSI with PEO of 100,000 g mol^{-1} and PLiMTFSI of 50,000 g mol^{-1}).

By means of dielectric spectroscopy, the ionic conductivity equation was decomposed, being able to know the contribution of ion mobility and density, with this study it was demonstrated that the most important parameter is ion mobility.

In Chapter V, a single-conduction electrolyte was prepared, which in theory has many advantages in terms of battery safety, since there is no polarization inside the battery, but the PEO/PLiMTFSI electrolytes presented poor mechanical properties, for this reason, and as a continuation of Chapters III and IV, in **Chapter VI**, two electrolyte systems of ternary composition were developed, having as common components PEO and poly(lactic acid) (PLA)

systems. PLA was added with the purpose of increasing the mechanical properties of the systems, in addition, PLA has a high melting temperature (T_m), around 160 ºC, which allows the use of these electrolytes at high temperatures in a safe way. The systems developed were PEO/PLA/LiTFSI and PEO/PLA/PLiMTFSI. By means of DSC, it was demonstrated that PEO and PLA in the presence of LiTFSI or PLiMTFSI are partially miscible. Additionally, the lithium cation supplier materials prefer to dissolve in PEO, this effect was reflected in the mechanical properties, as the elastic modulus of both systems increased. In addition, the electrolytes showed stability at high potentials (>4 V), which is a safety requirement for these materials. The best electrolytes were evaluated in symmetrical cells at 100 °C, both systems showed good performance, offering the possibility of obtaining safe electrolytes for high temperature batteries.

In **Chapter VII**, different polyphosphoester copolymers were used to be evaluated as polymer electrolytes, the advantage of these copolymers is the flame resistance property, which is characteristic of the phosphoester groups, these copolymers have a central block of PEO, which can complex lithium salts. It is important to note that these copolymers were sent to POLYMAT from the CERN Institute, Belgium. When LiTFSI was added, these copolymers had very low mechanical properties, so taking advantage of the polymerizable double bonds in the copolymer, it was decided to crosslink the polymers to increase the mechanical properties. By means of FTIR it was concluded that the lithium cations are also complexed by the phosphoester groups, and this causes an increase in the lithium transport number. The flame retardant properties were evaluated in a microcalorimeter, showing that these properties are maintained in the electrolytes. Finally, the electrolyte with the highest ionic conductivity was evaluated in a lithium/electrolyte/LiFePO4 cell, which showed a coulombic efficiency >98% after 100 cycles.

Chapter I

1. Introduction

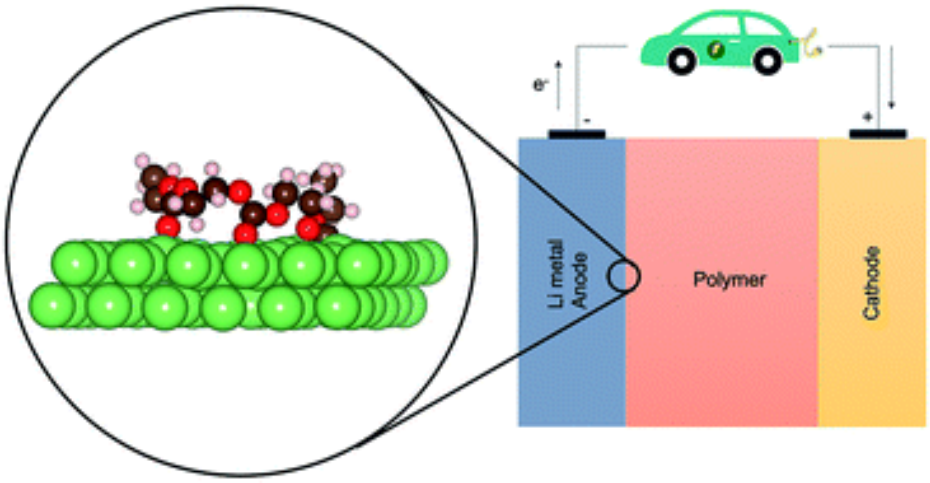

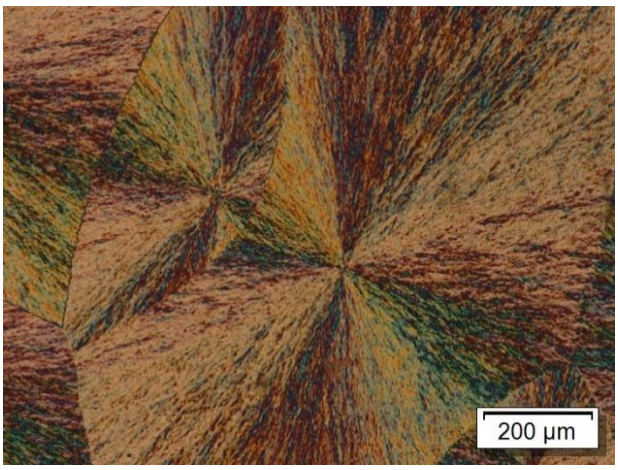

1.1 General Introduction

The use of lithium batteries has become increasingly important in recent decades, due to the rapid exhaustion of non-renewable fossil fuels and the associated environmental problems. Lithium batteries for energy storage devices, electric vehicles, and hybrid electric vehicles are the main goal in the development of these electronic devices [1].

In recent years, tons of lithium batteries have been recalled due to explosion and fire accidents [2,3]. Battery safety is directly determined by battery chemistry, its operating environment, and the tolerance of the battery. The internal failure of a battery is caused by electrochemical system stability [4].

In the design of this type of battery, the electrolyte plays an indispensable role in ion conduction, and this is reflected in power density [5]. An ideal electrolyte should have mechanical, electrochemical, thermal, and voltage stability with good interface properties.

Recently, polymer electrolyte systems have been very attractive due to some desirable characteristics: volume accommodation of electrode charges during charge/discharge processes, flexibility for battery design with different configurations, absence of leakage, easy processability and continuous production. The research and development of solid polymer electrolytes (SPEs) began when Wright, *et al.*, found ionic conductivity in PEO/Na^+ ion complex in 1975 [6]. During the elaboration of solid polymer electrolytes (SPEs), various inorganic salts are added to a polymer host, and ion mobility is possible by enhancing the segmental movements of the polymer chains.

Polyethers have been identified as the best candidates as host polymers because of their ability to dissolve various of inorganic salts at high concentrations by ion complexation due to the interaction between oxygen and metal ions. Many researchers make different polymer electrolytes, such as polypropylene oxide (PPO) [7], polymethyl methacrylate (PMMA) [8], etc., to check their electrochemical performances at ambient conditions. Among all, polyethylene oxide (PEO), has been recognized as an excellent candidate for technological applications and fundamental studies due to its outstanding

properties: high dielectric constant, flexible ethylene oxide segments, ether oxygen atoms and ability to solvate different inorganic salts.

A polymer electrolyte can be defined as a membrane that possesses transport properties comparable to common ionic liquid solutions. The development of polymer electrolytes has attracted the attention of many researchers over the last four decades, with the aim of finding applications not only in lithium batteries, but also in other electrochemical devices. These polymer electrolytes have certain advantages over liquid electrolytes, e.g., no internal short circuit, no electrolyte leakage, and no undesirable reaction products on the electrode surface existing in liquid electrolytes [9].

Since PEO is the polymer with the best ionic conductivity, different strategies have been developed to improve some of the other properties necessary for a good polymeric electrolyte [10]:

- Preparation and crosslinking of polymer networks, random copolymers, block copolymers or combinations, also, with short ethylene oxide chains to reduce crystallization.
- Use of organic plasticizers to increase the flexibility of the host polymer chains (polyglycols).
- Addition of inorganic and/or organic additives, with the aim of reducing crystallization without reducing the mechanical properties of the system. These products are generally called composite electrolytes.
- Developing polymer blends to easily and economically combine the properties of two or more polymers.

In the present thesis, different electrolyte systems have been designed, with the purpose of improving some of the properties of solid electrolytes. Polymer blends, as well as block copolymers and polymer crisslinking were used as strategies to formulate solid polymer electrolytes with improved properties.

1.2 Objectives

The main objective of this thesis is to study different polymeric systems as solid polymer electrolytes (SPEs), which may present some advantages vs the current reference polymer PEO in lithium solid state batteries. In this PhD thesis we have investigated new polyethers, blending of the PEO with single-ion conducting polymers or alternative polymer families such as poly(phosphoesters). Particular attention has been paid to investigate the crystallinity aspects of PEO and other polyethers in the different systems and the relationship between crystallinity and ionic conductivity.

1.2.1 Specific objectives

- To determine the effect of LiTFSI on the ionic conductivity and crystallinity of different aliphatic polyethers.
- To study the effect of LiTFSI on the crystallization of a polyether blend.
- To determine the miscibility of PEO and a single-ion conductor PLiMTFSI blends, as well as obtain the contributions of ion mobility and density to the ionic conductivity of these electrolytes.
- To increase the mechanical properties of single-conducting and dual-conducting electrolytes by blending it with PLA, and to study the effect on electrochemical and crystalline properties of PLA in the system.
- To determine ionic conductivity properties and the flame retardant effect using different polyphosphoesters as SPEs matrix, as well as the performance of these solid polymer electrolytes in a lithium battery.

1.3 Structure of the Thesis

This thesis is divided into eight chapters, where the basic concepts are presented, as well as the methods and experimental techniques used, and the different systems studied. Next, a brief description of the content of each chapter is presented:

- **Chapter 1**. This Chapter presents a general introduction to the use and characteristics of solid polymer electrolytes (SPEs), the advantages they present in comparison with liquid electrolytes, as well as the areas of opportunity for the development of solid state batteries. Also, the basic concepts, which are necessary to understand the content of this thesis, are presented in this Chapter. Concepts that are related to the theory of SPEs, such as ionic conductivity, ion transport models, charge transfer number, as well as the effect of temperature and polymer crystallinity on conductivity are described in detail. In addition, crystallization theories and their mathematical models are described.

- **Chapter 2.** All materials, methods, and experimental techniques used in the development of the thesis are described therein, as well as the synthesis and preparation of blends used in the different chapters of the thesis.

- **Chapter 3.** The relationship between crystallization and ionic conductivity in different aliphatic polyethers is presented in this Chapter. The effect of the number of methylene units in the repeating unit and the concentration of lithium salt (LiTFSI) on the ionic conductivity and the crystallinity of the polyethers is studied. Moreover, it was proved by the Flory-Huggins theory that LiTFSI acts as a diluting agent for this type of polymers.

- **Chapter 4.** In this chapter, blends of polyethylene oxide (PEO) and poly(1,6 hexanediol) (PHD) were prepared, and LiTFSI was added. In this part of the thesis, we studied how is the crystallization process in the case of a blend of polymers that both can crystallize, and the affinity that LiTFSI has with these polyethers given the difference in the length of $-CH_2-$ in the repeating unit of the materials.

- **Chapter 5.** In this Chapter, blends of poly(ethylene oxide) (PEO) and poly(lithium 1-[3-(methacryloyloxy) propylsulfonyl]-1-(trifluoromethanesulfonyl) imide) (PLiMTFSI) were prepared in order to obtain lithium single ion polymer electrolytes. The miscibility of these polymers was studied (by means of the Flory-Huggins interaction parameter χ_{12}) as a function of the molecular weight of both, in addition, by

means of dielectric spectroscopy, the contribution of mobility and ion density in the ionic conductivity of the blends was obtained.

- **Chapter 6.** In this Chapter, ternary blends were investigated by adding PLA to the previously optimized PEO blends. A comparison between dual-ion conductivity and single-ion conductivity was carried out by investigating PEO/PLA/LiTFSI and PEO/PLA/PLiMTFSI blends. The objective, unlike in Chapters 3 and 5 is the incorporation of poly(lactic acid) (PLA) which helps to maintain the mechanical properties of the electrolytes at high temperatures, between the melting temperature (T_m) of PEO (>65 ºC) and that of PLA (<150 ºC). The crystallinity and ionic conductivity of these polymer electrolytes were studied and also studied in lithium symmetrical cells.
- **Chapter 7.** This chapter presents the use of polyphosphoester copolymers as solid polymer electrolytes in lithium batteries. Since these materials are normally used as flame retardants, they offer safety advantages in their use in these devices.
- **Chapter 8.** Finally, this chapter presents the general conclusions of the thesis.

This thesis studies different polymer systems that can be used as solid electrolytes in lithium batteries, in this first chapter the basic concepts in polymer crystallization theory are presented, as well as concepts related to the electrochemical characterization for electrolytes in lithium batteries.

1.4 Battery performance

Batteries consist of three fundamental components: (a) the anode, where the oxidation (loss of electrons) of the lithium takes place; (b) the cathode, where electrons are accepted, here the reduction reaction takes place; and (c) the electrolyte, that acts as a separator between the electrodes, the electrolyte must be an electrical insulator [11], but it must allow the flow of ions (Figure 1.1). In the

case of lithium batteries, the reactions that occur at the electrodes are reversible [12].

The anode and cathode are joined in the battery by the electrolyte, and on the outside, they are connected by an external conductor through which electrons flow [13].

When the battery is charged, all the lithium is in the anode. During the discharge process, lithium ions flow through the electrolyte to the cathode, and electrons flow from the anode to the cathode through the external circuit, powering the device to which it is connected.

As the lithium ions are at a higher electrochemical potential than at the cathode, they fall from the anode potential to the cathode potential. This is why the battery supplies power to the device to which it is connected.

The voltage provided by the battery depends on the potential difference between the cathode and the anode. The greater the potential, the higher the voltage obtained.

When all the lithium ions reach the cathode, the battery is completely discharged [14].

Battery charging is done by connecting the battery to an external power source such as the mains. Electrons from the grid enter the anode through the external circuit: this causes the lithium ions to leave the cathode and return to the anode through the electrolyte.

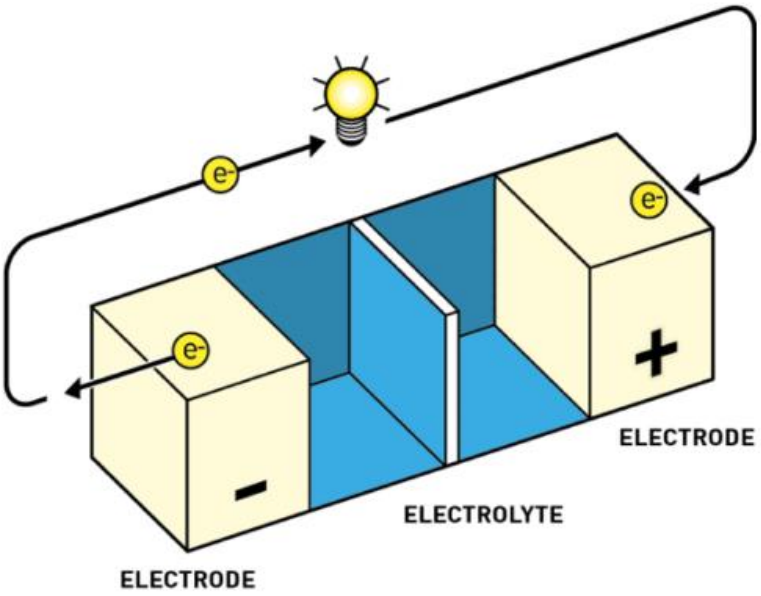

Figure 1.1. Different parts of a battery

1.5 Solid polymer electrolytes (SPEs)

Generally, SPEs are formed by inorganic salts dissolution in a polar polymer matrix that is able to conduct ions through the polymer chains. SPEs started to be studied in the mid 1970's, when Wright *et al*. discovered that PEO could be doped with different sodium and potassium salts [15]. Armand *et al*. later used these materials in lithium batteries and were the first to deduce that the ionic conductivity in PEO/salt systems takes place in the amorphous phase of the polymer [16].

1.5.1 Advantages and disadvantages of SPEs

The SPEs have the advantages of light volume, no liquid leakage, low cost, good flexibility, and do not cause battery volume expansion during charging and discharging, and can provide solutions for the safety problems in lithium batteries [17].

The principal disadvantages presented in SPEs are the low ionic conductivity shown compared with liquid electrolytes, in addition, to increase the ionic conductivity of these materials it is necessary to use amorphous polymers with a low T_g, which decreases the mechanical properties of the electrolyte. Table

1.1 shows the most important parameters and the values reuired to use these electrolytes in a practical way [18].

Table 1.1. The minimum requirements for all solid-state polymer electrolytes in lithium batteries.

Parameter	Requirement
Li^+ ion conductivity	$>10^{-5}$ S cm^{-1} at 25 ºC
Stable potential window	>4 V vs Li/Li^+
Mechanical property	>30 MPa
Thermal stability	>150 ºC
Limit oxygen index (LOI)	>27%

1.6 Ionic conductivity

Ionic conductivity is directly proportional to the concentration of charged species and their mobility, as expressed in the following equation:

$$\sigma = \sum n_i q_i \mu_i \tag{1.1}$$

where, q_i is the ionic charge, n_i is the number of free charge species and μ_i is the mobility of each charge carrier.

Ionic conductivity is usually determined by electrochemical impedance spectroscopy (EIS), by placing the electrolyte between two blocking electrodes (stainless steel). In this arrangement, the equivalent circuit is a resistor in series with interfacial capacitance (C_{dl}), where the bulk resistance (R_b) is related with the ionic conductivity (σ) of the electrolyte, by means of the following equation:

$$R_b = \frac{1}{\sigma}\frac{l}{A} \tag{1.2}$$

where, A is the interfacial surface area, l is the electrolyte thickness. R_b is determined by fitting the impedance response to the equivalent circuit presented in Figure 1.2.

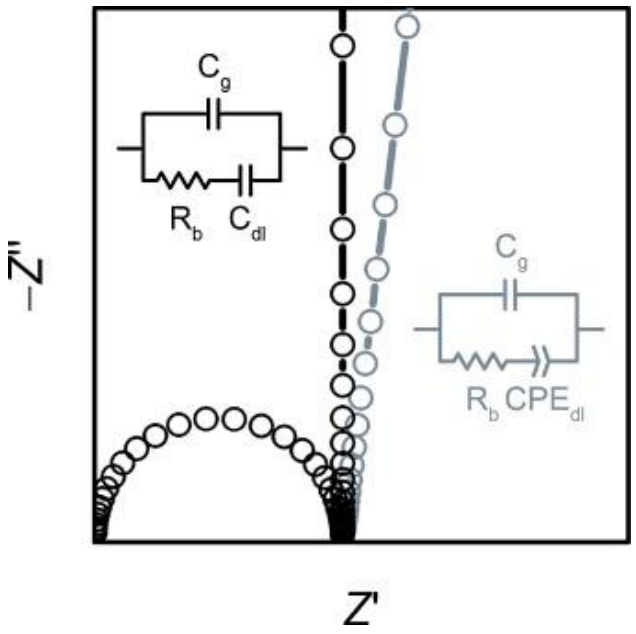

Figure 1.2. Equivalent circuits used in SPEs.

The glass transition temperature (T_g) is an important parameter in SPEs. The T_g corresponds to the beginning of the cooperative segmental movements of the polymer chain, normally in SPEs a low T_g is sought since it is related to the flexibility of the polymer. In models of Li transport in SPEs, which involve the coupling of lithium with the segmental movement of the polymer, a polymer with a low T_g is beneficial for ionic conductivity.

Figure 1.3 shows a plot of ionic conductivity as a function of the temperature for PEO/lithium salt system [19]. In the lower part is the conductivity of the PEO without salt, only with the impurities present in the synthesis. When lithium salt is added, the conductivity increases. At high temperatures, when the PEO is molten there is a high ionic conductivity due to the effect of temperature and to the fact that the polymer is completely amorphous. When the temperature decreases, the polymer crystallizes and the ionic conductivity is affected by this process. The presence of crystals restricts the ionic conductivity due to the dense molecular packing inside them, while the amorphous zones provide space for the lithium ions to move.

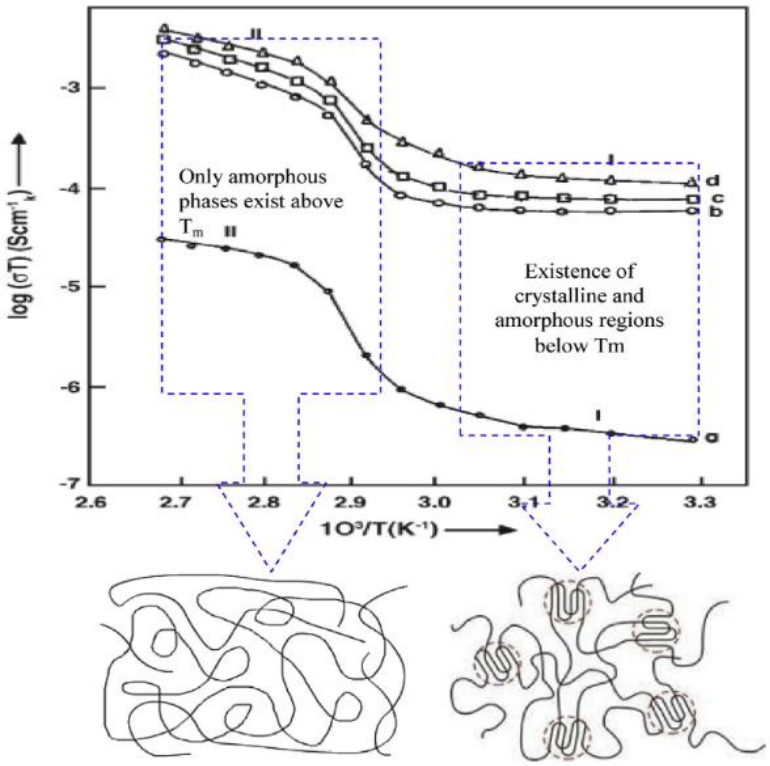

Figure 1.3. Effect of polymer crystallization on ionic conductivity

1.6.1 Ionic conduction mechanism in SPEs

Explaining the mechanism of ion transport in these systems is complex, due to the nature of SPEs, which have complex phase diagrams, where the crystalline phase is temperature dependent, and the complexation of ions with the polymer depends on the type of anion and cation [20]. Different theories have been developed to study the ionic conductivity mechanism, such as Arrhenius equation, Vogel-Tamman-Fulcher (VTF), William-Landel-Ferry equation, free volume model, and dynamic bond percolation model (DB1PM) model [21]. The ionic conductivity (σ) of SPEs is normally explained by Arrhenius and VTF equations.

The Arrhenius equation is used to explain the ionic conductivity mechanism of SPEs. A plot of ionic conductivity (σ) vs 100/T, is made according to equation 1.3:

$$\sigma = \sigma_0 \exp\left(\frac{-E_a}{k_B T}\right) \quad (1.3)$$

where, σ_0 is related to the number of charger carriers, T is the temperature in Kelvin, k_B is the Boltzmann constant, and E_a is the activation energy for the diffusion. The most important parameter in this equation is the activation energy. At lower E_a values, the ionic conductivity exhibits higher values. When the ionic conductivity behavior in a temperature range tends to be a straight line in an Arrhenius plot, the behavior is described by ion-hopping model [20].

Furthermore, the dynamics of the polymer is dependent on the polymer structure as well as the molecular weight. The behavior of ionic conductivity as a function of temperature that best describes the SPEs is the VTF model.

$$\sigma = \sigma_0 \exp\left(-\frac{B}{T - T_0}\right) \quad (1.4)$$

where, T_0 is the Vogel temperature (normally is T_g – 50 K), T_0 is interpreted as the temperature where the segmental mobility or the ionic conductivity drops to zero, B is associated with the activation energy of ionic movement

1.6.2 Lithium-ion transference number (t_{Li^+})

The transference number is defined as the ratio of the electric current derived from the cation (lithium) to the total current. If the transference number is close to 1, it means that the ionic conductivity in the polymer electrolyte is mainly accomplished by the cation. The advantage of a large transference number, is the reduction of the polarization concentration of electrolytes during charge-discharge cycles. In this way, higher power density can be produced. Although having a high transfer number is desirable, most polymer electrolytes use lithium salts, so the transfer number is less than 0.5 [22,23].

1.6.3 Bruce and Vincent Method to calculate lithium-ion transference number (t_{Li^+})

The most common method to calculate the lithium-ion transference number is that described by Evans, Vincent and Bruce (Bruce-Vincent method).

In this experiment, a Li/Li cell is polarized by a small potential difference (~10 mV) applied between the two electrodes until a steady-state (constant current) is reached. The Lithium-ion transference number is calculated by [24,25]:

$$t_{Li}^{+} = \frac{I_s(\Delta V - I_0 R_0)}{I_0(\Delta V - I_s R_s)} \quad (1.5)$$

where, ΔV is the potential applied (10 mV), I_0 is the initial current, I_s is the steady-state current, and R_0 and R_s are the interfacial resistance (obtained by electrochemical impedance spectroscopy (EIS)) before and after polarization, respectively.

1.6.4 Electrochemical stability window and mechanical stability

Lithium batteries operate up to 4 V vs Li/Li^+, therefore, an electrolyte with electrochemical stability in such voltage range is necessary. One advantage of SPEs is their electrochemical stability compared with liquid electrolytes, which tend to oxidize, at the cathode or reduce at the anode. Stable systems are able to form good solid electrolyte interface (SEI) layers in the interface electrode/electrolyte during the first cycles [26]. This layer is principally formed by the decomposition of the electrolyte, and helps to enhance the battery life.

Another important parameter is the mechanical properties of the electrolyte. Nevertheless, low Li-ion conductivity and poor mechanical properties are still the main challenges in the commercial development of SPEs [27]. Different methods are adopted for improving the polymer electrolyte system. Typically, they can be categorized into two approaches, polymer/polymer coordination and composite polymer electrolyte. Copolymerization, crosslinking, interpenetration, and blending are widely used as polymer/polymer coordination [28]. In recent years, many studies have been addressed to incorporate inert oxide ceramics particles into polymer electrolytes, in order to improve the mechanical properties, reduce polymer crystallinity, and thus solve the problem of low ionic conductivity of SPE. Different types of inert ceramics had been incorporated into the polymer, such as SiO_2 [29], Al_2O_3 [30], TiO_2 [31], zeolite, etc.

1.7 Principles of Thermal Characterization of Polymers

PEO is the most used host in the area of solid polymer electrolytes, and it is a semi-crystalline polymer. Even though the crystalline phase restricts the ionic conductivity, it is important to know the effect on the crystalline structure of PEO of the addition of lithium salts, as well as for other polymers.

1.7.1 Crystallization in Polymers

Crystallization is a phenomenon that depends on two processes: nucleation and growth. Crystallization of a polymer can only occur in a temperature range between the glass transition temperature (T_g) and the equilibrium melting temperature (T_m^0). The reason behind this behavior is that below T_g there is no movement of the polymeric chains, and at temperatures above T_m^0 the nucleation process is inhibited.

The nucleation rate ($\dot{N}$) and the growth rate (G) (Figure 1.4) depend in different ways on the supercooling. The maximum of $\dot{N}$ appears at higher supercooling. At lower temperatures, segmental mobility is reduced, and a greater number of small crystals are generated. On the contrary, at higher temperatures, crystalline growth is favored, forming a smaller number of larger crystals [32–34].

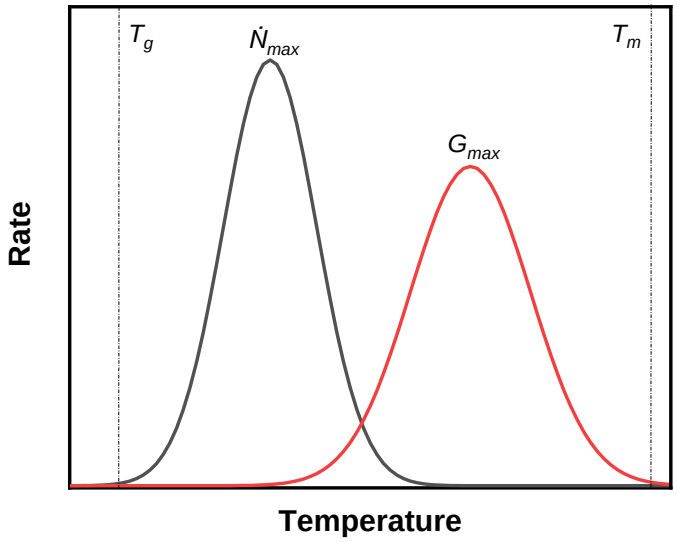

Figure 1.4. Schematic representation of nucleation rate ($\dot{N}$) and growth rate (G) as a function of temperature.

1.7.2 Crystal Growth and Morphology

Folded-chain lamellae are the fundamental unit of lamellar clusters, which grow to form supramolecular structures such as spherulites, axialites and hedrites [32,35]. The polymers of flexible character and with a large capacity to crystallize form spherical aggregates, called spherulites. These structures appear as birefringent structures observable under the polarized light optical microscope (PLOM) and generally show characteristic extinction patterns called maltese cross (Figure 1.5).

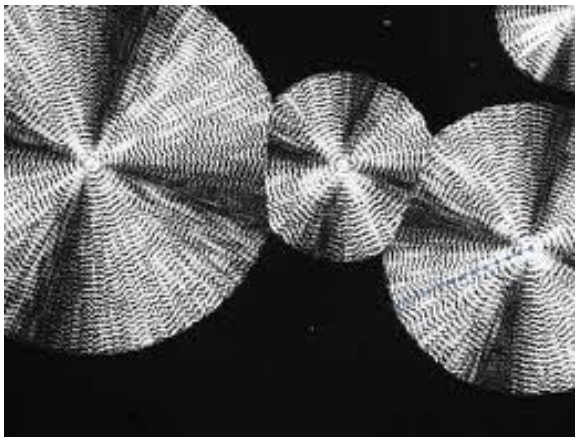

Figure 1.5. Maltese cross observed in a spherulite by means of PLOM [36].

It has been observed by transmission electron microscopy (TEM) that the internal zones of the spherulites consist of lamellae and are separated by amorphous interlamellar zones that grow radially. the chains are arranged perpendicular to the flat horizontal surface of the lamella, and are therefore tangential to the spherulite and to the direction of growth (Figure 1.6).

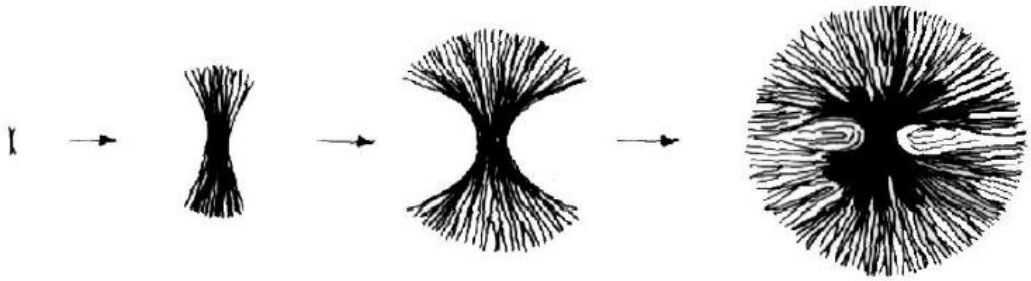

Figure 1.6. Diagram of the development of a spherulite from a homogeneous nucleus [34].

The primary lamellae extend from the center to the end of the spherulite, but along its growth axis, branches are formed by secondary lamellae.

At present, the model presented by Mandelkern [33] in 1964 is accepted, in which three fundamental regions are defined in the morphology of the spherulite: the first, the crystalline region formed by lamellae, the second, the amorphous region, of disordered conformation and the third, the interfacial region, of intermediate nature, formed by chain segments that form part of the lamellae, entering and leaving the interfacial region (Figure 1.7).

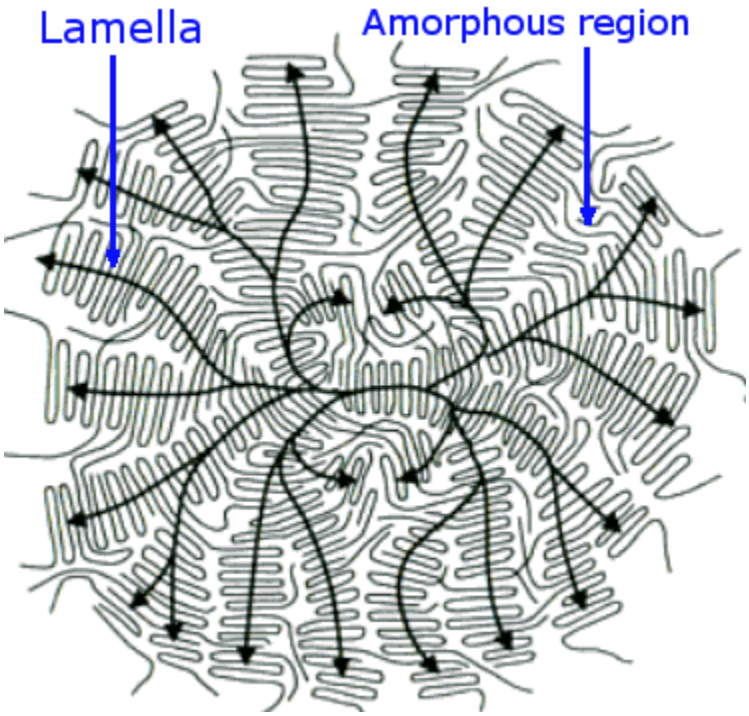

Figure 1.7. Amorphous and crystalline regions in spherulite.

The difference in size and morphology between spherulites of different polymers depends on the chemical nature, molecular weight and distribution, crystallization conditions and the density of nuclei present in the material.

1.7.3 Polymer Crystallization theories

1.7.3.1 Avrami Theory

The general Avrami equation applies to any type of crystallization. It describes the time evolution of the relative overall crystallization.

The Avrami equation was developed to quantify the transition between liquid-solid states. The equation can be expressed as follow [37,38]:

$$1 - V_c(t - t_0) = \exp\left(-K(t - t_0)^n\right) \tag{1.6}$$

where, t is the experimental time, t_0 is the induction time, V_c is the relative volumetric transformed fraction, n is the Avrami index, and K is the overall crystallization rate constant. (1 - V_c) is the amorphous fraction.

The Avrami index (*n*) is composed of two terms [39]:

$$n = n_d + n_n \tag{1.7}$$

where, n_s is the dimensionallity of the growing crystals, and this number can be 1, 2 or 3, for one, two or three-dimensional entities. n_n is the time dependence of the nucleation, this parameter can be 0 or 1, 0 corresponds to purely instantaneous (I) nucleation and 1 to purely sporadic nucleation (S). Table 1.2 shows the different combinations that can be obtained and the morphology that represents the Avrami index. The Avrami index (*n*) increases with increasing "dimensionality" of the growing crystal.

Table 1.2. Description of the different values of Avrami index (n).

Avrami Index	n_d	n_n	Description
1	1	0	Rod (I)
2	1	1	Rod (S)
2	2	0	Axialite (I)
3	2	1	Axialite (S)
3	3	0	Spherulite (I)
4	3	1	Spherulite (S)

The volume fraction (V_c) can be calculated as follows:

$$V_c = \frac{W_c}{W_c + \frac{\rho_c}{\rho_a}(1 - W_c)} \tag{1.8}$$

where, W_c is the crystalline mass fraction in the sample, ρ_c and ρ_a are the polymer densities of the crystalline and amorphous phases respectively. W_c is calculated from the following equation:

$$W_c = \frac{\Delta H(t)}{\Delta H_{total}} \quad (1.9)$$

where, $\Delta H(t)$ is the enthalpy as a function of time at a given crystallization temperature and ΔH_{total} is the maximum enthalpy value reached at the end of the isothermal crystallization process.

The crystallization half-time, $t_{50\%}$, is the time required to achieve 50% of the relative crystallinity of the polymer (1 - V_c = 0.5). It can be predicted by the Avrami theory, as follows:

$$t_{50\%} = \left(\frac{-ln(1 - V_c)}{k}\right)^{1/n} = \left(\frac{-ln0.5}{k}\right)^{1/n} \quad (1.10)$$

To obtain the Avrami parameters, the linearization of the Avrami equation is represented as follows:

$$log\left[-ln\left(1 - V_c(t - t_0)\right)\right] = log(K) + n\, log(t - t_0) \quad (1.11)$$

With this linearization it is possible to plot $ln[-ln(1-V_c)]$ vs $ln\ (t - t_0)$. If the crystallization kinetics follows the Avrami equation, then a straight line is obtained.

Figure 1.8 shows the plots that can be obtained from the Avrami equation and its linearization. These plots were obtained from de Origin® plug-in developed by Lorenzo, *et al.* [37].

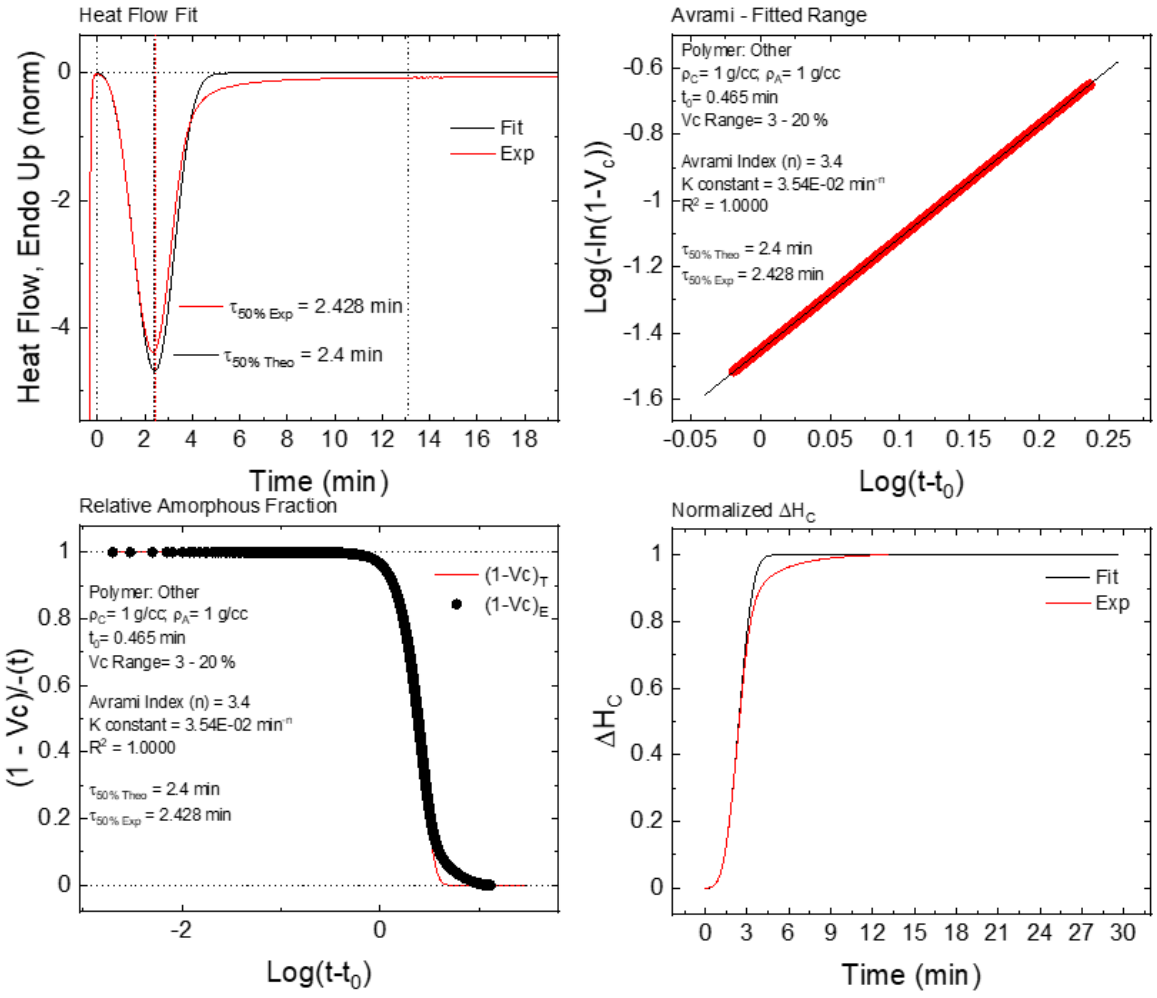

Figure 1.8. Avrami plots obtained through the Origin ® plug

1.7.3.2 Lauritzen and Hoffman Theory

This theory (LH) has been the dominant growth theory for polymer crystallization. One of the advantages of the LH is that it provides a simple form to connect microscopic parameters with macroscopic quantities.

The LF theory provides expressions for linear growth rate (G), i.e. spherulitic growth rate as a fuction of supercooling ($\Delta T = T_m^0 - T_c$), where T_m^0 is the equilibrium melting temperature, and T_c is the crystallization temperature. The linear growth rate is determined by polarized light optical microscopy (PLOM). The LH theory can be expressed as:

$$G(T) = G_0 \exp\left(\frac{-U^*}{R(T_c - T_\alpha)}\right) \exp\left(\frac{-K_g^G}{T_c \Delta T_f}\right) \quad (1.12)$$

where, G_0 is a pre-exponential growth rate constant. The fist term is related with molecular diffusion, U* is the activation energy for the transport of the polymer chains to the growth front (a value of 1500 cal/mol is usually employed), R is the gas constant, T_c is the crystallization temperature, T_α is the temperature at wich chain mobility ceases (normally is T_g – 30 K). The second term is the secondary nucleation term, ΔT is the supercooling (T_m^0 - T_c), and T_m^0 is calculated according to the Hoffman-Weeks extrapolation. The factor f is a temperature correction equal to $2T_c/(T_c+T_m^0)$, and K_g^G is a secondary nucleation constant that is proportional to the energy barrier for spherulitic growth.

The value K_g^G can be represented as:

$$K_g^G = \frac{j b_0 \sigma \sigma_e T_m^0}{k \Delta h_f} \quad (1.13)$$

where, j is determined by the crystallization regime and is equal to 4 for regime I and III, and is taken as 2 for regime II; b_0 is the width of the polymer chain, σ is the lateral surface free energy, σ_e is the fold surface free energy, k is the Boltzman constant, and Δh_f is the heat of fusion of a perfect crystal.

The LH theory analyzes the growth data acording to the competition between the rate of deposition of secondary nuclei (i) and the rate of lateral surface spreadig (g), resulting in three different regimes:

- Regime I: when $i << g$ and may be found at very low ΔT.
- Regime II: i is the order of g and occurs at moderate ΔT.
- Regime III: $i > g$ and is found at very high ΔT.

The overall crystallization kinetics is determined by the contributions of both nucleation and growth. The LH theory can be applied to the isothermal crystallization kinetics data collected by DSC. Following the equation:

$$\frac{1}{\tau_{50\%}}(T) = G_0^{\tau} \exp\left(\frac{-U^*}{R(T_C - T_\alpha)}\right) \exp\left(\frac{-K_g^{\tau}}{T\Delta T_f}\right) \quad (1.14)$$

The subscript τ is used to indicate that the parameters depend on the experimental data obtained by DSC, the subscript *G* indicates that the parameters were obtained by PLOM experimental data.

To apply the Lauritzen-Hoffman theory to the experimental data, the Origin ® plug in developed by Lorenzo, *et al* [37] was used. Figure 1.9 shows the plots obtained with this software.

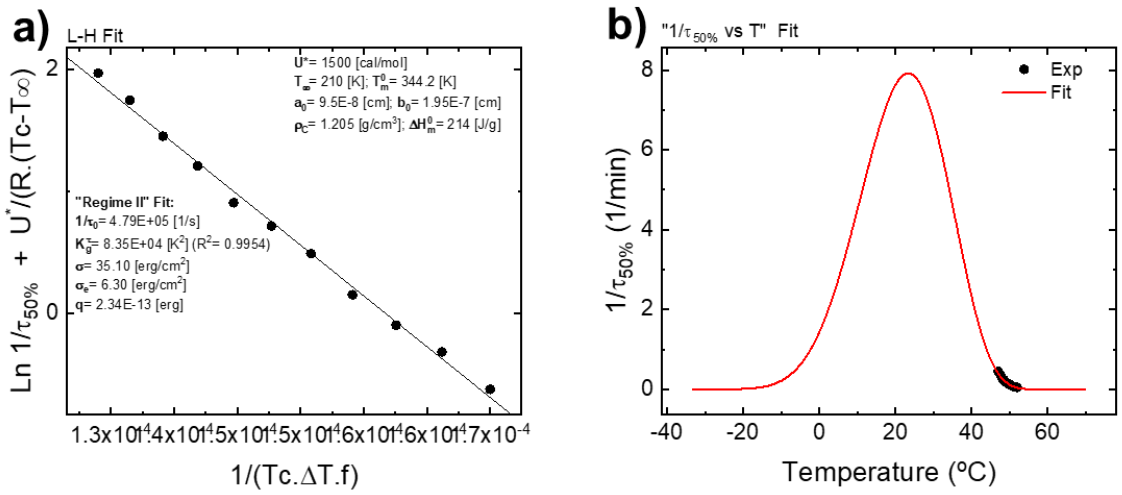

Figure 9. Lauritzen-Hoffman plots obtained through the Origin ® plug

1.8 Polymerization techniques

1.8.1 RAFT synthesis

The reversible addition fragmentation chain transfer (RAFT) process has grown into one of the most versatile and powerful polymerization techniques for the synthesis of complex polymeric architectures. RAFT is a reversible deactivation radical polymerization, also known as a controlled radical polymerization method [40]. One of the main advantages offered by this technique is a control in the molecular weight of the synthesized polymer, as well as a small value of dispersity.

The RAFT mechanism is depicted in Figure 1.10. Following activation (step I), the radical species add to the RAFT agent (chain transfer agent, CTA) to enter equilibrium between active and dormant species (steps III and V). The chain transfer steps that form the basis of the RAFT mechanism are degenerated as they involve a reversible transfer of the functional chain end-group (typically a thiocarbonylthio group, Z−C(= S)S−R) between the dormant chains (macroRAFT agent or macroCTA) and the propagating radicals. In an effective process, the rate of addition/fragmentation equilibrium is higher than that of the propagation, so there should be less than one monomer unit added per activation cycle; therefore, all chains will have a similar degree of polymerization (DP) at a given time. The overall process is comprised of the insertion of monomers between the R- and Z−C(=S)S-groups of a RAFT agent, which forms the α and ω end-group of the majority of the resulting polymeric chains [41].

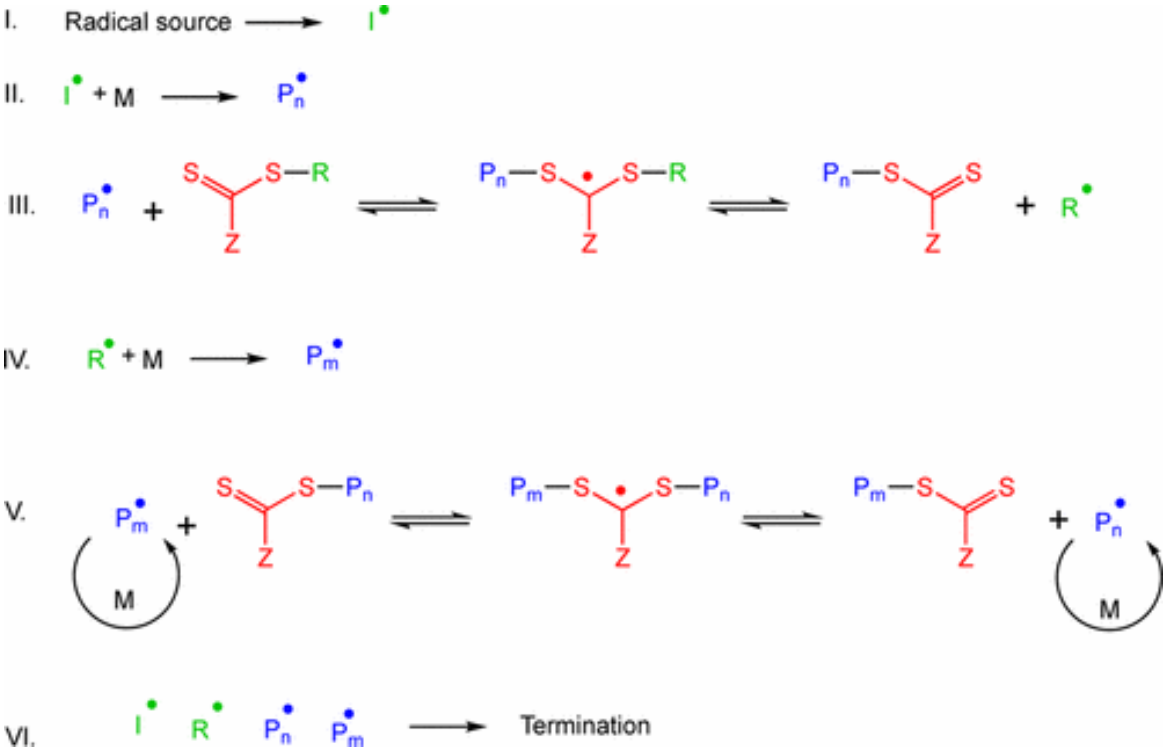

Figure 1.10. Proposed Mechanism of Reversible Addition−Fragmentation Chain Transfer Polymerization.

1.8.2 Inverse emulsion polymerization

In conventional emulsion polymerization, a hydrophobic monomer is emulsified in water using an oil in water emulsifier and polymerized using a water soluble initiator. The primary free radicals are generated in the aqueous phase and migrate to the monomer-water interface. Since the total surface area of the micelles is large relative to that of the monomer droplets, the probability is great that the diffusing radical will enter a micelle rather than a droplet. The initiation of polymerization in a monomer-containing micelle transforms it into a monomer-swollen polymer particle before the initial polymer radical is terminated. The rapid chain propagation is sustained by monomer diffusing from reservoir droplets and neighboring micelles, which have not captured a radical. In stage 2, the growth stage, no new particles are formed; those formed in stage 1 continue to grow until the supply of monomer or free radicals is exhausted [42].

In an inverse emulsion polymerization, an aqueous solution of hydrophilic monomer is emulsified in a continuous hydrophobic oil phase using a water in oil

emulsifier. The polymerization is initiated with either oil-soluble or water-soluble initiators [43]. Figure 1.11 shows a schematic representation of this system. The initiation of polymerization proceeds by a mechanism analogous to that of the conventional system, and submicroscopic particles of water-swollen hydrophilic polymer are generated in the continuous oil phase. This type of polymerization is used to obtain very high molecular weights.

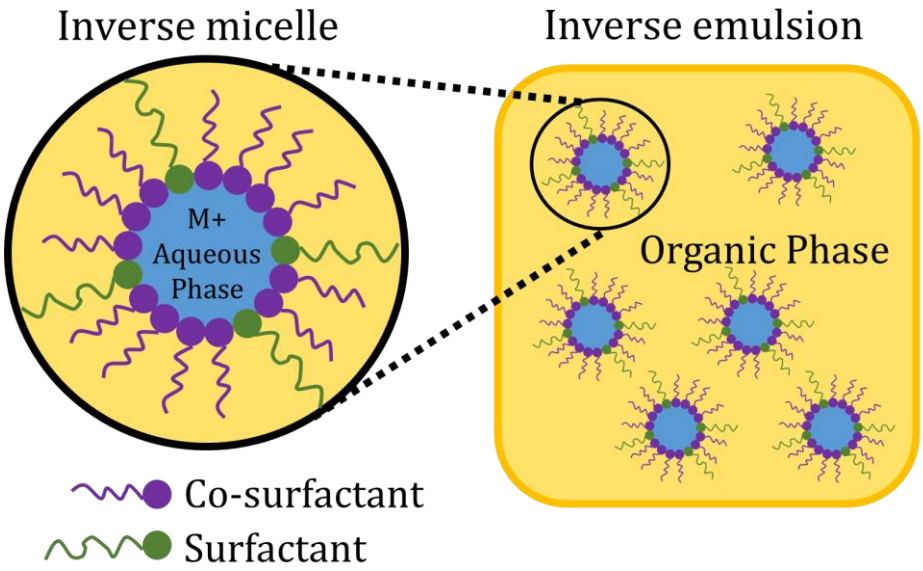

Figure 1.11. Schematic representation of an inverse emulsion polymerization.

1.9 References

[1] L. Yue, J. Ma, J. Zhang, J. Zhao, S. Dong, Z. Liu, G. Cui, L. Chen, All solid-state polymer electrolytes for high-performance lithium ion batteries, 5 (2016) 139–164. https://doi.org/10.1016/j.ensm.2016.07.003.

[2] D. Ren, X. Liu, X. Feng, L. Lu, M. Ouyang, J. Li, X. He, Model-based thermal runaway prediction of lithium-ion batteries from kinetics analysis of cell components, Applied Energy. 228 (2018) 633–644.

[3] Z. Chen, R. Xiong, J. Lu, X. Li, Temperature rise prediction of lithium-ion battery suffering external short circuit for all-climate electric vehicles application, Applied Energy. 213 (2018) 375–383.

[4] Y. Chen, Y. Kang, Y. Zhao, L. Wang, J. Liu, Y. Li, Z. Liang, X. He, X. Li, N. Tavajohi, A review of lithium-ion battery safety concerns: The issues, strategies, and testing standards, Journal of Energy Chemistry. (2020).

[5] Q. Li, J. Chen, L. Fan, X. Kong, Y. Lu, Progress in electrolytes for

rechargeable Li-based batteries and beyond, Green Energy & Environment. 1 (2016) 18–42. https://doi.org/10.1016/j.gee.2016.04.006.

[6] K. Murata, S. Izuchi, Y. Yoshihisa, An overview of the research and development of solid polymer electrolyte batteries, Electrochimica Acta. 45 (2000) 1501–1508.

[7] T.A. LaFollette, L.M. Walker, Structural and mechanical hysteresis at the order-order transition of block copolymer micellar crystals, Polymers. 3 (2011) 281–298. https://doi.org/10.3390/polym3010281.

[8] A. Manuel Stephan, K.S. Nahm, Review on composite polymer electrolytes for lithium batteries, Polymer. 47 (2006) 5952–5964. https://doi.org/10.1016/j.polymer.2006.05.069.

[9] A.M. Stephan, Review on gel polymer electrolytes for lithium batteries, European Polymer Journal. 42 (2006) 21–42. https://doi.org/10.1016/j.eurpolymj.2005.09.017.

[10] E. Quartarone, P. Mustarelli, A. Magistris, PEO-based composite polymer electrolytes, 110 (1998) 1–14.

[11] M. Marcinek, J. Syzdek, M. Marczewski, M. Piszcz, L. Niedzicki, M. Kalita, A. Bitner, P. Wieczorek, T. Trzeciak, M. Kasprzyk, P. Łęż, Z. Zukowska, A. Zalewska, W. Wieczorek, Electrolytes for Li-ion transport – Review, 276 (2015) 107–126.

[12] D.R. Wright, N. Garcia-Araez, J.R. Owen, Review on high temperature secondary Li-ion batteries, Energy Procedia. 151 (2018) 174–181.

[13] P. Tan, H.R. Jiang, X.B. Zhu, L. An, C.Y. Jung, M.C. Wu, L. Shi, W. Shyy, T.S. Zhao, Advances and challenges in lithium-air batteries, Applied Energy. 204 (2017) 780–806. https://doi.org/10.1016/j.apenergy.2017.07.054.

[14] C. Sun, J. Liu, Y. Gong, D.P. Wilkinson, J. Zhang, Recent advances in all-solid-state rechargeable lithium batteries, Nano Energy. 33 (2017) 363–386. https://doi.org/10.1016/j.nanoen.2017.01.028.

[15] D.E. Fenton, Complexes of alkali metal ions with poly (ethylene oxide), Polymer. 14 (1973) 589.

[16] C. Berthier, W. Gorecki, M. Minier, M.B. Armand, J.M. Chabagno, P. Rigaud, Microscopic investigation of ionic conductivity in alkali metal salts-poly (ethylene oxide) adducts, Solid State Ionics. 11 (1983) 91–95.

[17] F. Ran, S. Chen, Advanced Nanomaterials for Electrochemical-Based Energy Conversion and Storage, Elsevier, 2019.

[18] L. Yue, J. Ma, J. Zhang, J. Zhao, S. Dong, Z. Liu, G. Cui, L. Chen, All solid-state polymer electrolytes for high-performance lithium ion batteries, Energy Storage Materials. (2016). https://doi.org/10.1016/j.ensm.2016.07.003.

[19] S.B. Aziz, T.J. Woo, M.F.Z. Kadir, H.M. Ahmed, A conceptual review on polymer electrolytes and ion transport models, Journal of Science:

Advanced Materials and Devices. 3 (2018) 1–17. https://doi.org/10.1016/j.jsamd.2018.01.002.

[20] M.A. Ratner, Aspects of the theoretical treatment of polymer solid electrolytes: transport theory and models, Polymer Electrolyte Reviews. 1 (1987) 173–236.

[21] K.J. Laidler, The development of the Arrhenius equation, Journal of Chemical Education. 61 (1984) 494.

[22] R. Meziane, J.P. Bonnet, M. Courty, K. Djellab, M. Armand, Single-ion polymer electrolytes based on a delocalized polyanion for lithium batteries, in: Electrochimica Acta, 2011. https://doi.org/10.1016/j.electacta.2011.03.074.

[23] D.-W. Kim, J.-K. Park, H.-W. Rhee, Conductivity and thermal studies of solid polymer electrolytes prepared by blending poly(ethylene oxide), poly(oligo[oxyethylene]oxysebacoyl) and lithium perchlorate, Solid State Ionics. 83 (1996) 49–56. https://doi.org/10.1016/0167-2738(95)00238-3.

[24] J. Evans, C.A. Vincent, P.G. Bruce, Electrochemical measurement of transference numbers in polymer electrolytes, Polymer. 28 (1987) 2324–2328. https://doi.org/10.1016/0032-3861(87)90394-6.

[25] K. Pożyczka, M. Marzantowicz, J.R. Dygas, F. Krok, Ionic Conductivity and Lithium transference number of Poly(ethylene oxide):LiTFSI system, Electrochimica Acta. 227 (2017) 127–135. https://doi.org/https://doi.org/10.1016/j.electacta.2016.12.172.

[26] M.B. Pinson, M.Z. Bazant, Theory of SEI formation in rechargeable batteries: capacity fade, accelerated aging and lifetime prediction, Journal of the Electrochemical Society. 160 (2012) A243.

[27] J.W. Fergus, Ceramic and polymeric solid electrolytes for lithium-ion batteries, Journal of Power Sources. 195 (2010) 4554–4569.

[28] P. Yao, H. Yu, Z. Ding, Y. Liu, J. Lu, M. Lavorgna, J. Wu, X. Liu, Review on Polymer-Based Composite Electrolytes for Lithium Batteries, Frontiers in Chemistry. 7 (2019) 1–17. https://doi.org/10.3389/fchem.2019.00522.

[29] C.-W. Nan, L. Fan, Y. Lin, Q. Cai, Enhanced Ionic Conductivity of Polymer Electrolytes Containing Nanocomposite S i O 2 Particles, Physical Review Letters. 91 (2003) 266104.

[30] J.E. Weston, B.C.H. Steele, Effects of inert fillers on the mechanical and electrochemical properties of lithium salt-poly (ethylene oxide) polymer electrolytes, Solid State Ionics. 7 (1982) 75–79.

[31] P. Pal, A. Ghosh, Influence of TiO2 nano-particles on charge carrier transport and cell performance of PMMA-LiClO4 based nano-composite electrolytes, Electrochimica Acta. 260 (2018) 157–167.

[32] U.W. Gedde, M.S. Hedenqvist, Fundamental polymer science, Springer, 2019.

[33] L. Mandelkern, Crystallization of Polymers, 2nd ed. Vo, Cambridge

University Press, Cambridge, United Kingdom, 2002.

[34] G. Reiter, G.R. Strobl, Progress in understanding of polymer crystallization, Springer, 2007.

[35] J.M. Schultz, Polymer crystallization: the development of crystalline order in thermoplastic polymers, Amer Chemical Society, 2001.

[36] P. Enrique-Jiménez, J.F. Vega, J. Martínez-Salazar, F. Ania, A. Flores, Estudio del bandeado en esferulitas poliméricas mediante nanoindentación, (2017).

[37] A.T. Lorenzo, M.L. Arnal, J. Albuerne, A.J. Müller, DSC isothermal polymer crystallization kinetics measurements and the use of the Avrami equation to fit the data: Guidelines to avoid common problems, Polymer Testing. 26 (2007) 222–231. https://doi.org/10.1016/j.polymertesting.2006.10.005.

[38] U.L.F. Gedde, Polymer physics, Springer Science & Business Media, 1995.

[39] A.J. Müller, V. Balsamo, M.L. Arnal, Nucleation and crystallization in diblock and triblock copolymers, Block Copolymers II. (2005) 1–63.

[40] A.D. Jenkins, R.G. Jones, G. Moad, Terminology for reversible-deactivation radical polymerization previously called" controlled" radical or" living" radical polymerization (IUPAC Recommendations 2010), Pure and Applied Chemistry. 82 (2009) 483–491.

[41] S. Perrier, 50th Anniversary Perspective: RAFT Polymerization: A User Guide, Macromolecules. 50 (2017) 7433–7447.

[42] J.M. Asua, Emulsion polymerization: from fundamental mechanisms to process developments, Journal of Polymer Science Part A: Polymer Chemistry. 42 (2004) 1025–1041.

[43] J.W. Vanderhoff, E.B. Bradford, H.L. Tarkowski, J.B. Shaffer, R.M. Wiley, Inverse emulsion polymerization, in: ACS Publications, 1962.

Chapter II

2. Experimental Part

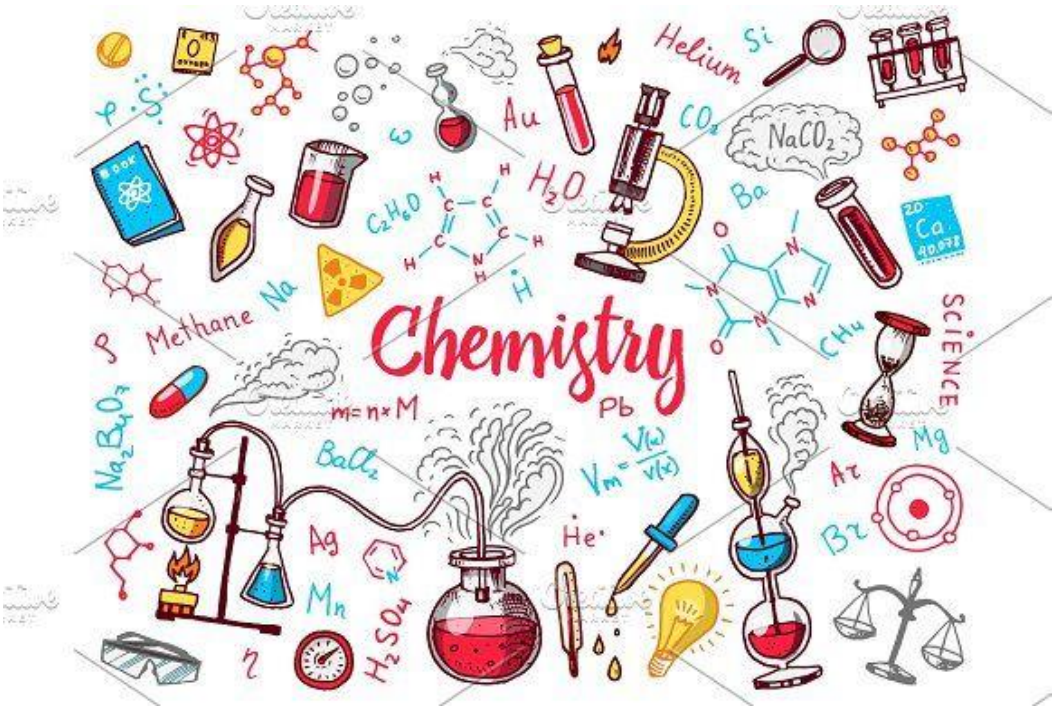

This chapter describes the characterization methods, materials as well as the synthesis and preparation of polymeric blends for each system presented in the thesis.

2.1 Characterization Methods

2.1.1 Differential Scanning Calorimetry (DSC)

This technique is very effective in determining the enthalpy changes of a substance. A DSC unit consists of two cells: in one cell an empty pan is placed as a reference, and in the other cell, a pan with the sample to be studied is placed. A power compensating DSC consists of two electronic heating circuits, the first is responsible for changing the temperature in the two furnaces at the speed indicated in the program, the second circuit keeps the temperature difference between the two furnaces equal to zero, since, when an exothermic or endothermic process occurs in the sample, this circuit compensates the temperature imbalance (by applying or substracting power to the sample cell) so that the temperatures in the furnaces remain constant.

This technique, applied to polymer science, allows determining changes in the polymer physical state or chemical composition when varying the temperature, such as: melting temperature (T_m), glass transition temperature (T_g), crystallization temperature (T_c) or cold crystallization temperature (T_{cc}), as well as the enthalpies corresponding to the mentioned transitions. In addition, from the melting or crystallization enthalpies it is possible to calculate the crystallinity degree of a polymer, by means of the following equation:

$$X_c = \frac{\Delta H_m}{f\ \Delta H_m^0} * 100 \qquad (2.1)$$

where ΔH_m is the measured melting enthalpy, ΔH_m^0 is the equilibrium melting enthalpy, and f is the weight fraction of the polymer of interest in the sample. A value of $\Delta H_m^0 = 214$ J g^{-1} was employed for PEO [1].

All DSC experiments were carried out in a Perkin Elmer III DSC, equipped with an Intracooler II cooling system, and nitrogen was used as the atmosphere for the experiments. The sample placed for the experiments was always around 5 mg. The different experiments performed in the DSC are explained below.

2.1.1.1 Non-isothermal DSC experiments

These tests were performed according to the following steps:

1. Heating from T_0 (25 ºC) to a T_f (between 20 - 30 ºC above the polymer melting peak), at a heating rate of 20 ºC min^{-1}.
2. Wait 3 min at T_f to erase the thermal history of the material.
3. Cooling from T_f down to -70 ºC at 20 ºC min^{-1}.
4. Isothermal step for 3 min at -70 ºC.
5. Heating from -70 ºC to T_f at 20 ºC min^{-1}.

2.1.1.2 Isothermal DSC experiments

In order to perform the isothermal experiments in the DSC, the following methodology was used, taking into account the recommendations suggested by Lorenzo, *et al*. [2]:

1. Wait 3 min at T_f to erase the thermal history of the material.
2. Cooling from T_f to T_c at 60 ºC min^{-1}.
3. Isothermal step at T_c for sufficient time to complete the crystallization process.
4. Heating from T_c to T_f at 20 ºC min^{-1}.

This procedure is repeated for 10 different T_c, starting from $T_{c,min}$, which is the minimum temperature at which no crystallization of the polymer occurs during cooling.

2.1.2 Polarized light optical microscopy (PLOM)

This technique uses an optical microscope equipped with two polarizing filters, placed below and above the sample to be analyzed. When the polarizers are crossed, light is allowed to pass only in the orthogonal direction. This means that the light is not transmitted through the polarizers when there is no sample or when the sample has an isotropic disordered structure, as in the case of amorphous polymers or semi-crystalline polymers in the melt. In the case where the polarizers are crossed and a semicrystalline polymer, a birefrigent sample, is to be observed, an interference phenomenon occurs (i.e., the crystals have the ability to reorient the polarization of the light), causing the light beam to pass through the polarizer. In this way, there are areas of the sample, the ordered anisotropic regions, which appear bright on a smooth or dark background, which corresponds to the fraction of amorphous or molten material. Polarized optical microscopy is, therefore, a suitable technique in the study of ordered regions of semicrystalline polymers.

In this thesis an OLYMPUS BX51 microscope was employed, this microscope has a programmable heating chamber Metter Toledo FP82 HT.

In this equipment two types of experiments were performed, the first one to obtain the spherulitic growth rate and the second one to obtain the density of nuclei as a function of time. To perform these tests, a thin film of the mixture to be studied was placed on a glass slide.

2.1.2.1 Spherulitic growth rate (*G*)

To calculate the spherulite growth rate (G) as a function of the isothermal crystallization temperature (T_c), the radius of a spherulite as it grew was measured by the following steps:

1. The thermal history of the material is erased by holding at T_f for 3 min.
2. Cooling from T_f to a selected crystallization temperature at 50 ºC min^{-1}.
3. An isolated small spherulite is located. The growth of the spherulite is recorded as a function of time, taking pictures at different times by means of a digital camera.

4. Afterwards, the radius is plotted as a function of time, a straight line is obtained, from the slope of which the growth rate of the spherulite is calculated.

5. These steps are repeated for 10 different T_c.

The nucleation density was calculated employing the images collected for spherulitic growth rate measurements and assuming that each spherulite grows from a single nucleus [3]. The number of spherulites when the image was saturated was divided by the volume of the sample within the observed field.

2.1.2.2 Nuclei density

The density of nuclei as a function of temperature was determined by counting the number of nuclei at T_c when the image is completely saturated with spherulites.

Furthermore, by taking into account the thickness of the polymer film as well as the area observed in the digital camera it is possible to obtain the volume. therefore, the nuclei density was calculated by means of the equation:

$$\rho_{nuclei} = N^{\circ}\, Nuclei/V \tag{2.2}$$

2.1.3 Thermogravimetric analysis (TGA)

Thermogravymetry is a technique in wich the mass sample is measured as a function of temperature or time. TGA is the most commonly used method to investigate the thermal decomposition processes of polymers. In TGA experiments, at heating rates around 10 ºC min^{-1}, a sample of around 5-15 mg is enough to ensure that it is in thermal equilibrium with the equipment used [4]. In the development of this thesis, this technique was used to determine the temperature at which the materials studied begin to decompose, the conditions for this study were the same in all cases, at 10ºC min^{-1} from 30ºC to 800ºC.

2.1.4 Dynamic mechanic thermal analysis (DMTA)

The study of elastic and viscoelastic materials under conditions of cyclic stress, strain, time or temperature is called dynamic mechanical thermal analysis (DMTA). This technique has far greater sensitivity to both macroscopic and molecular relaxation. DMTA probes the mechanical properties of a material as a function of temperature; for this, a small sinusoidal force is applied to the sample [5].

DMTA experiments were used to obtain the elastic modulus as a function of temperature, since this is one of the most important points for the application of SPEs.

These experiments were performed using rectangular samples of crosslinked polyphosphoesters electrolytes (10 × 10 × 5 mm), using a Triton 2000 DMA from Triton Technology in compression mode. The tests were performed at 1 Hz and the heating rate of 4 °C min^{-1} from −100 to 100 °C.

2.1.5 X-Ray (WAXS)

X-ray diffraction is a physical phenomenon that occurs when an x-ray beam of a certain wavelength interacts with a crystalline material. When the beam is incident on a solid material, part of the beam is scattered in all directions because of the electrons associated with the atoms or ions in the path, but the rest of the beam gives rise to the phenomenon of x-ray diffraction, provided that there is an orderly arrangement of atoms, and Bragg's Law is satisfied. This law relates the wavelength and the interatomic distance to the angle of incidence of the diffracted beam.

X-ray powder diffraction patterns were collected by using a Philips X'pert PRO automatic diffractometer operating at 40 kV and 40 mA, in theta-theta configuration, secondary monochromator with Cu-Kα radiation (λ = 1.5418 Å) and a PIXcel solid state detector (active length in 2θ 3.347º). Data were collected from 5 to 70° 2θ (step size = 0.026 and time per step = 60s.) at RT. 1º fixed soller slit and divergence slit giving a constant volume of sample illumination were used.

2.1.6 Gel Permeation Chromatography (GPC)

Gel permeation chromatography, also known as size exclusion chromatography (GPC-SEC), is a liquid chromatographic technique that evaluates the molecular weight distribution of a polymer. The peculiarity of this liquid chromatography lies in the fact that the stationary phase of its columns is capable of separating the components according to the size that the polymer chains occupy in the solution (hydrodynamic volume). The larger molecules migrate faster along the column than the smaller ones, because they are too large to enter the pores of the polymer gel particles that form the column. On the other hand, smaller molecules enter the pores and move more slowly along the column. This size is related, albeit indirectly, to the molecular weight of the separated chains. Thus, the technique is one of the most useful tools to characterize the molecular weight distribution of a polymer and its different averages.

The GPC instrument consisted of a pump (Shimadzu LC-20a), three columns in series (Styragel HR2, HR4, and HR6 with pore sizes ranging from 10^2 to 10^6 Å), and a differential refractometer (Waters 2410), and a dual λ absorbance detector (Waters 2487). 0.1 M LiCl in water was used as a mobile phase at flow rate of 1 mL min^{-1}, all the experiments were performed at 25 ºC.

2.1.7 Nuclear Magnetic Resonance (NMR)

Nuclear magnetic resonance is the technique that provides structural information. It is able to observe the nuclei of the atoms and to deduce the influence in each molecular environment on each of the atoms. In this way it is possible to know the general structure of the molecule to be studied.

The most abundant atoms in polymeric compounds, hydrogen (H) and carbon (C) can be easily observed with relatively small amounts of sample. Therefore, with this technique, it is possible to deduce the chemical structure of the polymeric compounds.

For the characterization of the single-ion conduction polymer, proton nuclear magnetic resonance (H^1-NMR) experiments were performed at room temperature in chloroform (CDCl3) and dimethyl sulfoxide (DMSO-d6) using a

Bruker AMX spectrometer (400 MHz). In all cases, 5 mg of sample was dosed in 700 µL of solvent.

2.1.8 Fourier Transform Infrared Spectroscopy (FTIR)

Infrared spectroscopy has long been recognized as a powerful tool for the characterization of polymers. This technique is based on the absorption of radiation in the infrared frequency range due to the molecular vibrations of the functional groups contained in the polymer chain [6].

The benefits that an FTIR offers compared to a dispersive infrared are in terms of spectral quality, speed of data collection, data reproducibility, and ease of maintenance and use.

An infrared spectrometer (Bruker Alpha-P) equipped with an attenuated total reflection (ATR) accessory was used in the development of this thesis. Spectra were obtained in the 4000-400 cm^{-1} range with a resolution of 4 cm^{-1}.

2.1.9 Electrochemical Impedance Spectroscopy (EIS)

The general principle of the EIS method is to apply a sinusoidal signal and to measure the characteristic response from the cell, which depends on the cell impedance. The input signal can either be current (galvanostatic) or voltage (potentiostatic).

The voltage V(t) and the phase shift φ are recorded as responses of the measurements. By using the following equation [7]:

$$\bar{Z} = \frac{V(t)}{I(t)} = \frac{\bar{V}\sin(\omega t)}{\bar{I}\cos(\omega t - \varphi)} = \overline{|Z|}\frac{\sin(\omega t)}{\cos(\omega t - \varphi)} \qquad (2.3)$$

where, $\bar{V}$ is the amplitude of the voltage signal, $\bar{I}$ is the amplitude of the current signal, ω is the angular frequency, φ is the phase shift, and is the absolute value of the impedance, *t* is time and $\overline{|Z|}$ is the absolute value of the impedance. Finally,

it is possible to separate the impedance in a real part (Z´) and an imaginary part (Z´´) by using φ again:

$$Z' = \overline{|Z|}\sin(\varphi) \tag{2.4}$$

$$Z'' = \overline{|Z|}\cos(\varphi) \tag{2.5}$$

$$\overline{|Z|} = \sqrt{Z'^2 + Z''^2} \tag{2.6}$$

Z´ and Z´´ can be displayed in a Nyquist plot in order to visualize the influence of the parameters.

The Nyquist diagrams obtained by measuring the impedance at different temperatures are usually fitted to an equivalent circuit. Figure 2.1 shows the equivalent circuit that was used to fit the experimental results obtained in this thesis.

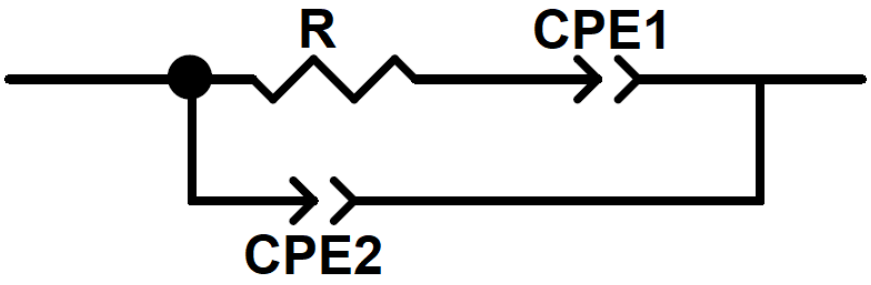

Figure 2.1. Equivalent circuit to fit the Nyquist diagrams for SPEs.

This technique is widely used in the electrochemical characterization of SPEs, for example, in the determination of ionic conductivity and the calculation of the lithium transport number.

Electrochemical impedance spectroscopy (EIS) was employed to determine ionic conductivity in an Autolab 302N potentiostat galvanostat at different temperatures (100 to 25 ºC). The electrolyte was placed in between two stainless

steel electrodes (of surface area = 0.5 cm^2). Measurements were obtained in the 100 kHz to 1 Hz range, with 10 mV amplitude. All samples had an average thickness of 0.1 mm.

2.1.10 Dielectric spectroscopy (DS)

Dielectric spectroscopy (DS) is frequently used to study the response of a sample subjected to an applied electric field of fixed or changing frequency. DS descrives the dielectric properties of a materias as a funcion of frequency. The ratio and microwave frecuency regions of the electromagnetic spectrum have been successfully made to interact with materials, so as to study the behavior of molecules. The interaction of applied alternating electric fields with dipoles possessing reorientation mobility in materias is also dealt by DS. DS is a poweful tool to study soft matter, whose principle is mainly to determine the frequency-dependent complex permittivity (ε) and DC electrical conductivity (σ). DS deals with current and voltage (amplitude and phase of an AC system) is used to evaluate the dielectric properties such as dielectric constant (ε´), dielectric loss (ε´´), etc, of polymers, polymer nanocomposites, and nanomaterials [8].

Dielectric measurements were conducted using a high-resolution Novocontrol Alpha analyzer. The isothermal experiments were performed in a frequency range between 10^{-1} and 10^6 Hz at different temperatures ranging from -100 to 100 ºC every 5 ºC with an applied AC voltage of 1 V root mean square amplitude. The samples were placed between two golden electrodes forming a parallel plate capacitor of about 0.2 mm thickness.

2.1.11 Microcalorimeter Test

Pyrolysis-combustion flow calorimetry (PCFC) measures the rate at which the heat of combustion of fuel gases is released by a solid during controlled pyrolysis in an inert gas stream. The fuel gases are mixed with excess oxygen and combusted at high temperatures, and the instantaneous heat of combustion of the flowing gas stream is measured by oxygen consumption calorimetry. Figure 2.2 is a schematic diagram showing how the component processes of flaming combustion are reproduced in pyrolysis-combustion flow calorimetry. The

apparatus is based on Susott's original concept [9–11] of linear programmed heating of milligram samples in an inert (nonoxidizing) atmosphere to separate the processes of char formation and gas phase combustion, which normally occur in a fire. In the present device, the sample is heated using a linear temperature program, and the volatile thermal degradation products are swept from the pyrolysis chamber by an inert gas and combined with excess oxygen in a tubular furnace at flame temperatures to force complete non flaming combustion (oxidation) of the fuel.

The maximum (peak) value of the PCFC heat release rate normalized for the initial sample mass and heating rate is a material flammability parameter with units of heat [release] capacity (J g^{-1} K^{-1}) which depends only on chemical composition of the sample and is proportional to the burning rate of the material in a fire. Time-integration of the PCFC heat release rate gives the heat of complete combustion of the pyrolysis gases, and the char yield is measured by weighing the sample before and after the test. If the pyrolysis is conducted in air so that there is no possibility of char remaining after the test, time-integration of the oxygen consumption signal gives the net heat of complete combustion of the solid, as would be determined in a high-pressure oxygen bomb calorimeter [12].

Micro calorimetry measurements were performed using a pyrolysis combustion flow calorimeter (PCFC) Fire Testing Technology FAA microcalorimeter. The mass of the sample was ≈5 mg, the experimental conditions were: a heating rate of 1 K s^{-1}, the specimen temperature was raised up to 700 °C, a combined gas flow rate of 100 cm^3 min^{-1}, an oxygen concentration of 20% O2 v/v in the combustor, and a combustor temperature of 900 °C. The results were obtained after averaging three samples. Heat release capacity (HRC) and heat released rate (HRR) were calculated based on the oxygen consumption, heating rate, flow rate and sample weight.

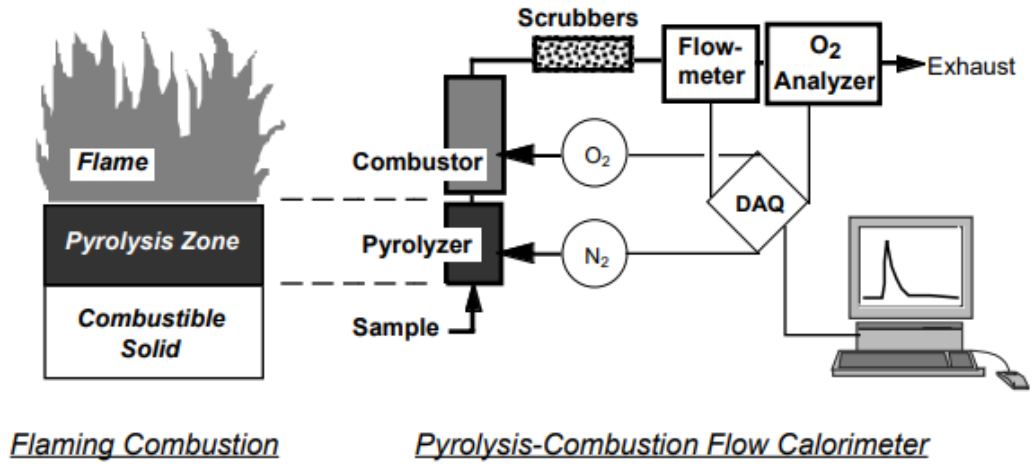

Figure 2.2. Schematic of flaming combustion and pyrolysis-combustion flow calorimetry.

2.1.12 Battery test

For the characterization of the batteries using the electrolytes developed in this thesis, two different methods were used:

2.1.12.1 Symmetrical Li/Li cells

Symmetric Li cells have the same material as the positive and negative electrodes (when cells are assembled one would already contain lithium and the other wouldn't). Although the cells have an average voltage of zero volts and are useless from a practical point of view, they can give vast information about reactions between electrode materials and polymer electrolytes [13].

Symmetrical cells were measured at 100 ºC after stabilization at that temperature for 24 h. The polymer electrolyte was sandwiched between two lithium disks. The effect of different current densities on the overpotential is analyzed using a Biologic VMP-3 battery inside an oven (Thermoscientific).

2.1.12.2 Full battery

A typical experiment for testing a battery's long term stability is cycling. For this, batteries are charged and discharged several hundreds of times and the capacity is measured.

Lithium iron phosphate (LFP) cathode composed by 60 wt% of active material, 10 wt% of conductive carbon (C65) and 30 wt% electrolyte was prepared in a water based slurry. The slurry was cast on aluminum foil and heated at 100 °C to remove the solvent. The loading mass of the active material in the electrodes was ~3 mg cm^{-2}. The Li^0/polymer electrolyte/LFP cells were assembled in the argon filled glove box. The galvanostatic charge–discharge studies were performed using a Biologic VMP-3 battery testing system at 70 °C inside an oven (Thermoscientific). These cells were subjected to three cycles for Solid Electrolyte Interface (SEI) at a rate of C/10 and then charged and discharged with a constant C-rate of C/10 for constant cycling, and the corresponding charge/discharge voltage range was between 2.5 and 4 V. The electrochemical characterization was performed in recently assembled cells and subjected at 2 h of stabilization.

2.2 Materials, synthesis and electrolyte preparation

2.2.1 Chapter III

2.2.1.1 Materials

Poly(ethylene oxide) (PEO) (M_W 2,000 g mol^{-1}) and polytetrahydrofuran P(THF) (M_w 2,000 g mol^{-1}) were purchased from Sigma Aldrich. Chloroform (99 %) was supplied by Scharlau and acetone (99.5 %) by Acros Organics. Finally, the lithium bis(trifluoromethane) sulfonimide (LiTFSI) (99.9 %) salt was purchased from Solvionic.

2.2.1.2 Synthesis of the linear polyethers

The aliphatic polyethers were synthesized following the methodology described by Basterretxea, *et. al*. [14]. Direct polycondensation of diols containing 6, 8, 10 and 12 methylene units was performed in solvent free conditions. The reaction was catalyzed by protic ionic liquids previously prepared by mixing methanesulfonic acid (MSA) and 1,5,7-triazabicyclo[4.4.0]dec-5-ene (TBD) in a 3:1molar ratio. The polymers are named using the following nomenclature: PEO = P1, Poly(THF) = P2 and the synthesized polymers with different number of methylene groups in their repeat units are poly(oxyhexamethylene) (P3) >

poly(oxyoctomethylene) (P4)> poly(oxydecamethylene) (P5)> poly(oxydodecamethylene) (P6) (Figure 2.3).

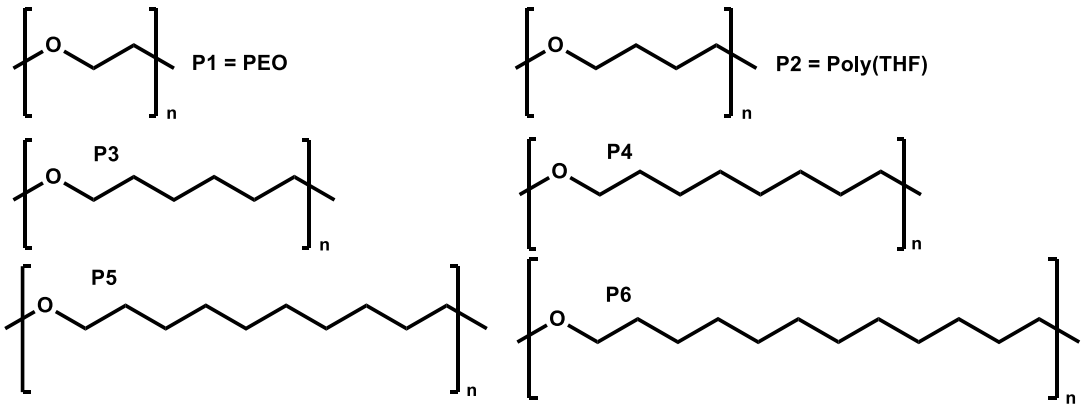

Figure 2.3. Chemical Structure of the different polyethers employed in Chapter III.

2.2.1.3 Elaboration of SPE solid polymer electrolytes

SPEs were prepared by solvent casting method. Polyethers and lithium salt were dissolved in a chloroform/acetone (90/10 v/v%) mixture. The solutions were directly cast onto a silicon mold. First, the membranes were dried at ambient conditions, and later, the total evaporation of the solvents was completed applying high vacuum at 90 ºC for 24 h. The SPEs were transferred into nitrogen filled glovebox to assemble the cell. In the first part, SPEs containing 30 wt% of LiTFSI were prepared (0.15 g of polymer and 0.064 g of salt in 3 mL of chloroform). Later, polymers P3 and P5, were selected to prepare SPEs with different concentrations of LiTFSI: 10, 30, 50, 80 and 90 wt% LiTFSI.

2.2.2 Chapter IV

2.2.2.1 Materials

1,6-hexanediol (99%) was purchased from Sigma-Aldrich and was dried in toluene before using it. Methanesulfonic acid (MSA, 99%), 1,5,7-triazabicyclo[4.4.0]dec-5-ene (TBD, 98%), chloroform ($CDCl_3$) and the rest of the solvents used in this work were supplied by Sigma-Aldrich and used as received. Poly(ethylene oxide) (PEO, M_v 100 kg mol^{-1}, powder) was purchased from Sigma-Aldrich. Finally, the lithium bis(trifluoromethanesulfonyl)imide (LiTFSI) (99.9%) salt was supplied by Solvionic.

2.2.2.2 Synthesis of PHD: Bulk Self-Condensation of 1,6-Hexanediol

In a 250 mL round bottom flask, 0.61 g of MSA and 0.25 g of TBD were weighed and heated at 90 ºC for 30 minutes under vigorous stirring. Once the protic ionic salt was prepared, 20 g of 1,6-hexanediol were added to the flask and it was heated up to 130 ºC for 24 h under vacuum. The temperature was increased to 150 °C for the next 24 h and then to 180 °C for the last 24 h. After 72 h the reaction was stopped by cooling it down at room temperature. For the purification, the material was dissolved in chloroform and precipitated in cold methanol. The resulted polymer was filtered and dried in the oven under vacuum at 40 °C, overnight. The NMR of the obtained polymer is presented in Figure 2.4.

2.2.2.3 Nuclear Magnetic Resonance (NMR) Spectroscopy.

^{1}H nuclear magnetic resonance (^{1}H-NMR) spectra were recorded in a Bruker Avance DPX 300 at 300.16 MHz of resonance frequency using deuterated chloroform ($CDCl_3$) as solvent at room temperature. Experimental conditions were as follows: 10 mg of sample; 3 s acquisition time; 1 s delay time; 8.5 μs pulse; spectral width 5000 Hz and 32 scans. Figure 2.4 present the NMR spectra for the synthesized poly(1,6-hexanediol) (PHD).

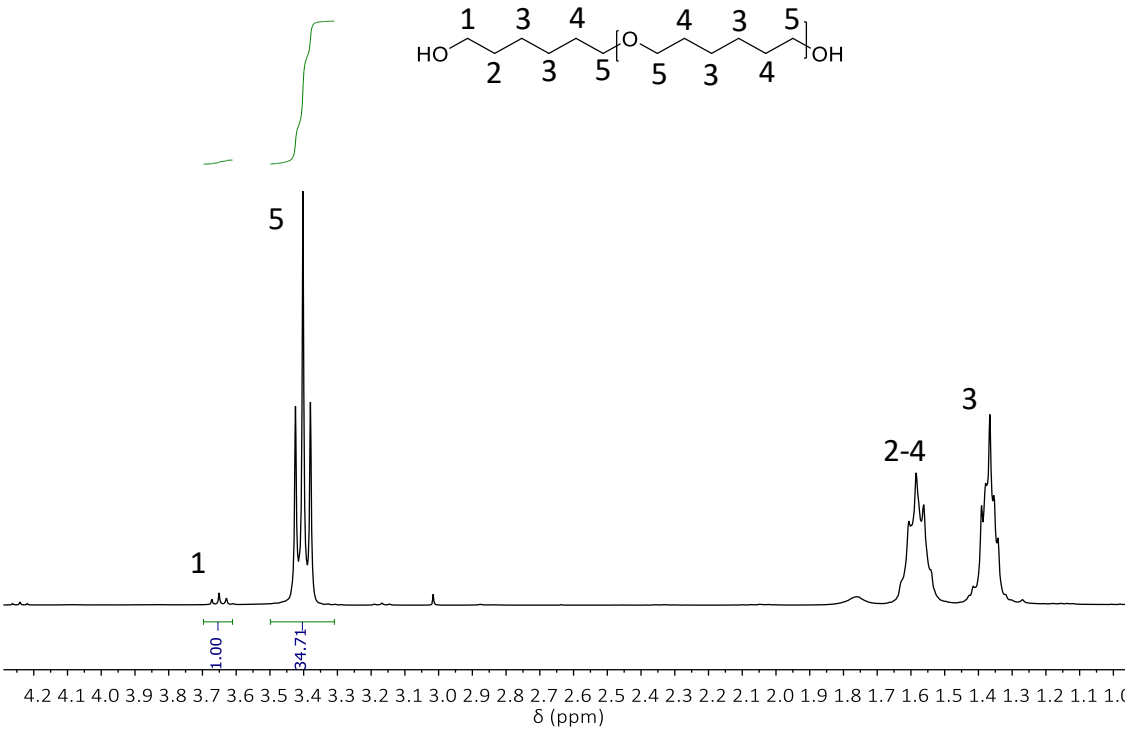

Figure 2.4. ^{1}H-NMR of PHD.

2.2.2.4 Calculation of molecular weight by ^{1}H-NMR

The signal of the ester (signal 5) was related with the proton that is next to the alcohol group, in order to know the value of the repeating units (*n*):

$$n = \frac{Contribution\ of\ signal\ 5}{Contribution\ of\ signal\ 1} = \frac{34.71}{1} = 34.71 \tag{2.7}$$

Afterward, the repeating unit value is multiplied by the molecular weight of the repeating unit and added the ending group molecular weight (18 g mol^{-1}):

$$Mn = (n * 100.17) + 18$$

$$Mn = (34.71 * 100.17) + 18 = \ 3494.90\ g\ mol^{-1} \tag{2.8}$$

The molecular weight of the polymer by ^{1}H-NMR is 3500 g mol^{-1}.

2.2.2.5 Blends preparation

Blends between PEO and PHD were prepared by a simple solvent evaporation method (Figure 2.5). Even when both polymers are soluble in chloroform, PEO (that tends to aggregate) is slightly less soluble than PHD, so it is added little by little under stirring. A series of 0.5 g samples was prepared with different weight percent of PEO/PHD: 80/20 (0.4 g/0.1 g, 16 mL of $CHCl_3$), 60/40 (0.3 g/0.2 g, 14 mL of $CHCl_3$), 50/50 (0.25 g/0.25 g, 12 mL of $CHCl_3$), 40/60 (0.2 g/0.3 g, 12 mL of $CHCl_3$) and 20/80 (0.1 g/0.4 g, 10 mL of $CHCl_3$).

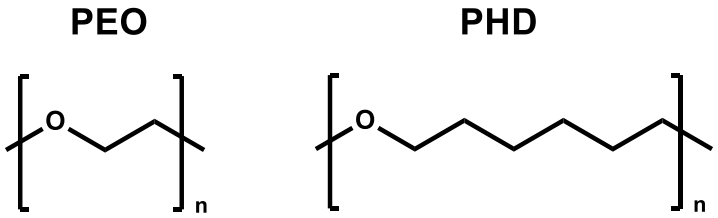

Figure 2.5. Chemical structure of the aliphatic polyethers used in Chapter IV.

The preparation of PEO/PHD blends with LiTFSI salt required some extra work. LiTFSI is indeed soluble in acetone or acetonitrile, but not in chloroform. On the other hand, the opposite is true for PHD, while PEO is soluble both in chloroform and acetonitrile (more easily in the latter). So, the blends with salt were dissolved in an acetonitrile/chloroform mixture, with a vol/vol% roughly equal to the one of the PEO/PHD in the blend. The PHD-rich blends with salt could be successfully dissolved also in a chloroform/acetone (90/10 vol%) mixture. It is worth specifying that the wt.% of LiTFSI is referred to the final total weight of the sample (Li salt included).

2.2.3 Chapter V

2.2.3.1 Synthesis of Poly (lithium 1-[3-(methacryloyloxy) propylsulfonyl]-1-(trifluoromethanesulfonyl) imide) (PLiMTFSI)

The lithium 1-[3-(methacryloyloxy) propylsulfonyl]-1-(trifluoromethanesulfonyl) imide monomer (LiMTFSI) was synthesized by three-step reactions according to literature procedures [15,16].

Step 1: 3-sulfopropyl methacrylate potassium salt reacts with thionyl chloride with a small amount of DMF to provide the sulfonyl chloride (Figure 2.6). A yield of 73.15% was obtained

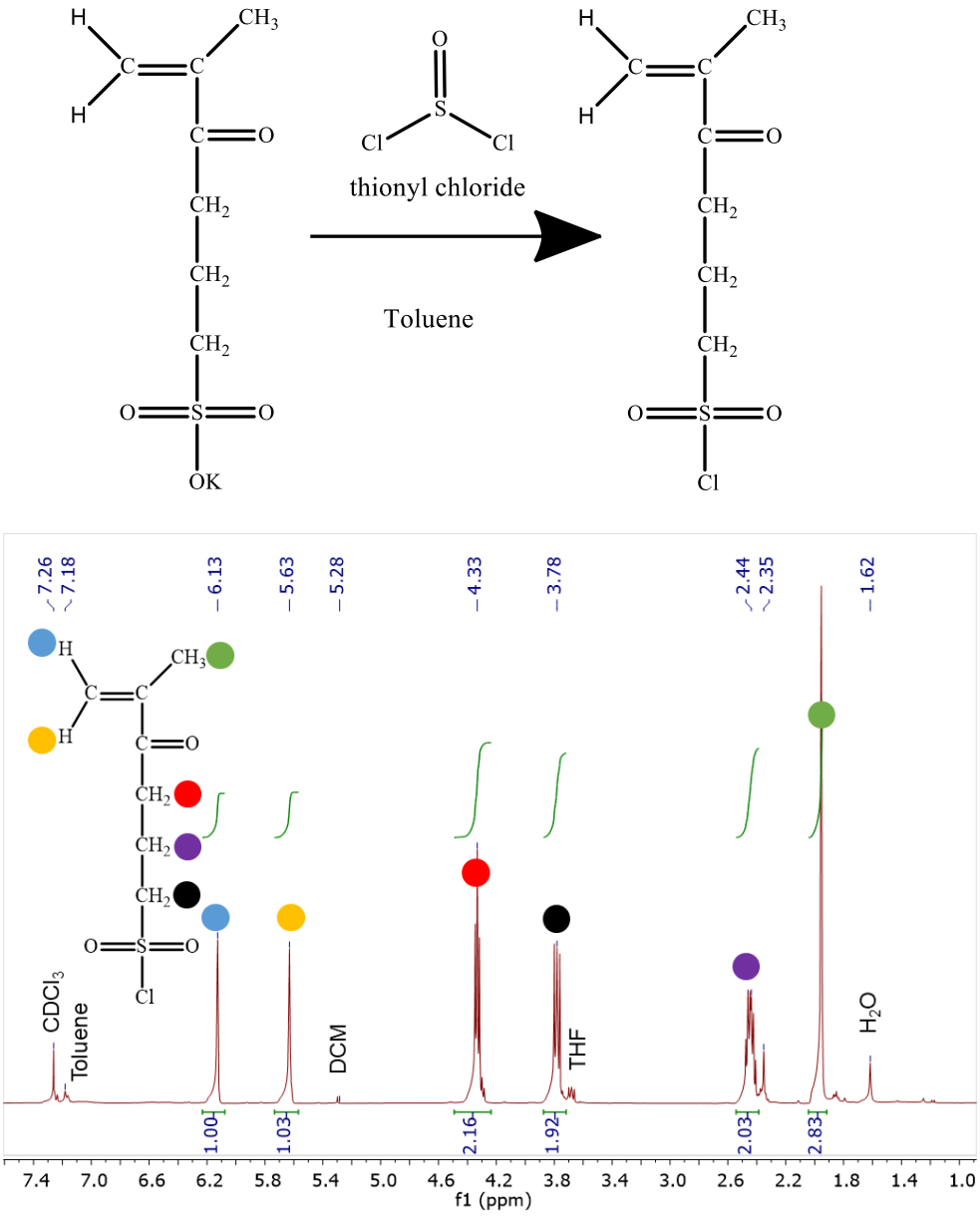

Figure 2.6. H^1-NMR of the product of the first reaction to obtain the monomer LiMTFSI.

Step 2: In the second step, it reacts with trifluoromethanesulfonamide in the presence of triethylamine, resulting in the formation of ammonium salt (Figure 2.7). A yield of 81% was obtained.

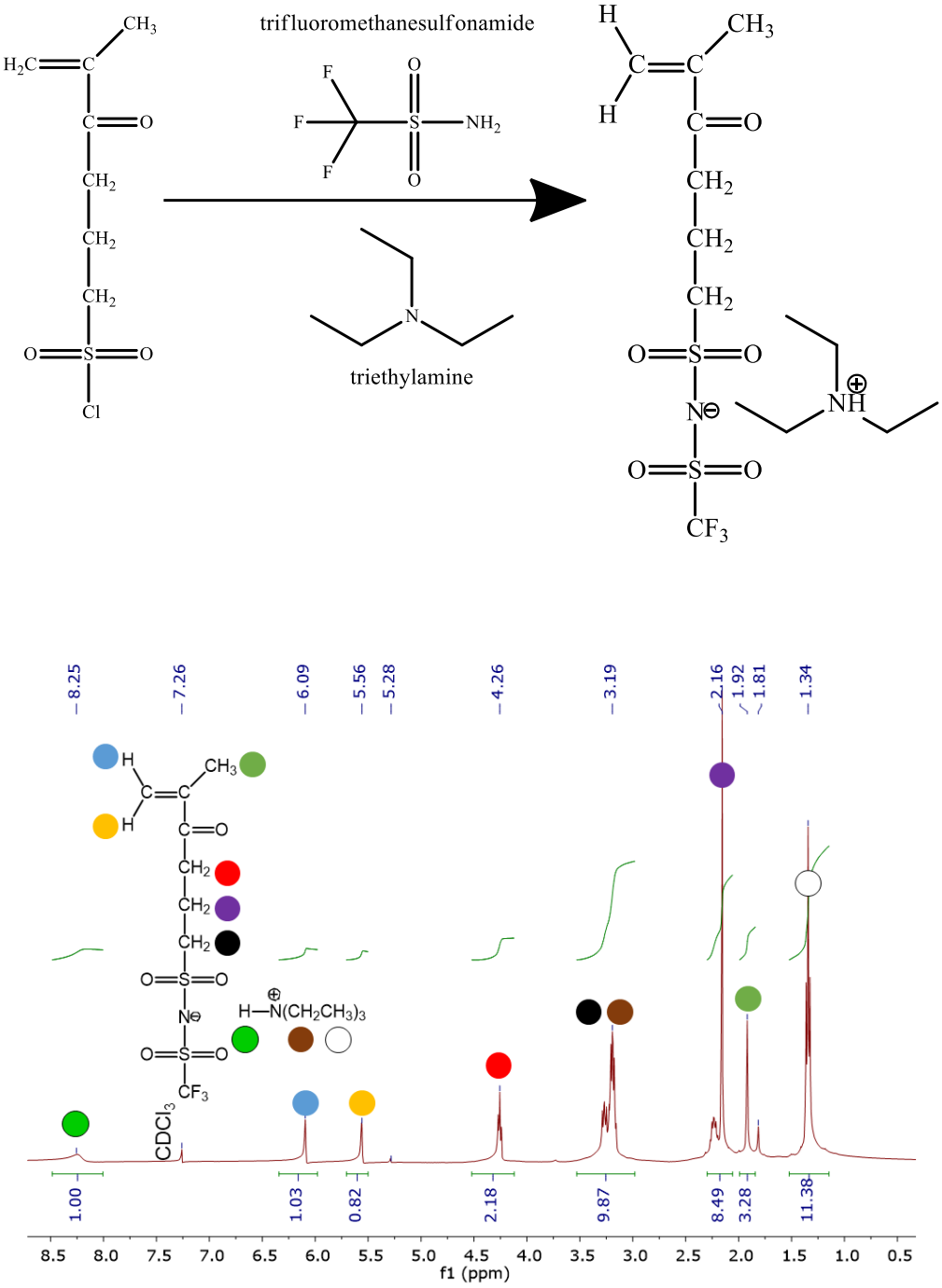

Figure 2.7. H[1]-NMR of the product of the second reaction to obtain the monomer LiMTFSI.

Step 3: Finally, this salt reacts with lithium hydrate to obtain the final monomer (Figure 2.8). A yield of 60% was obtained.

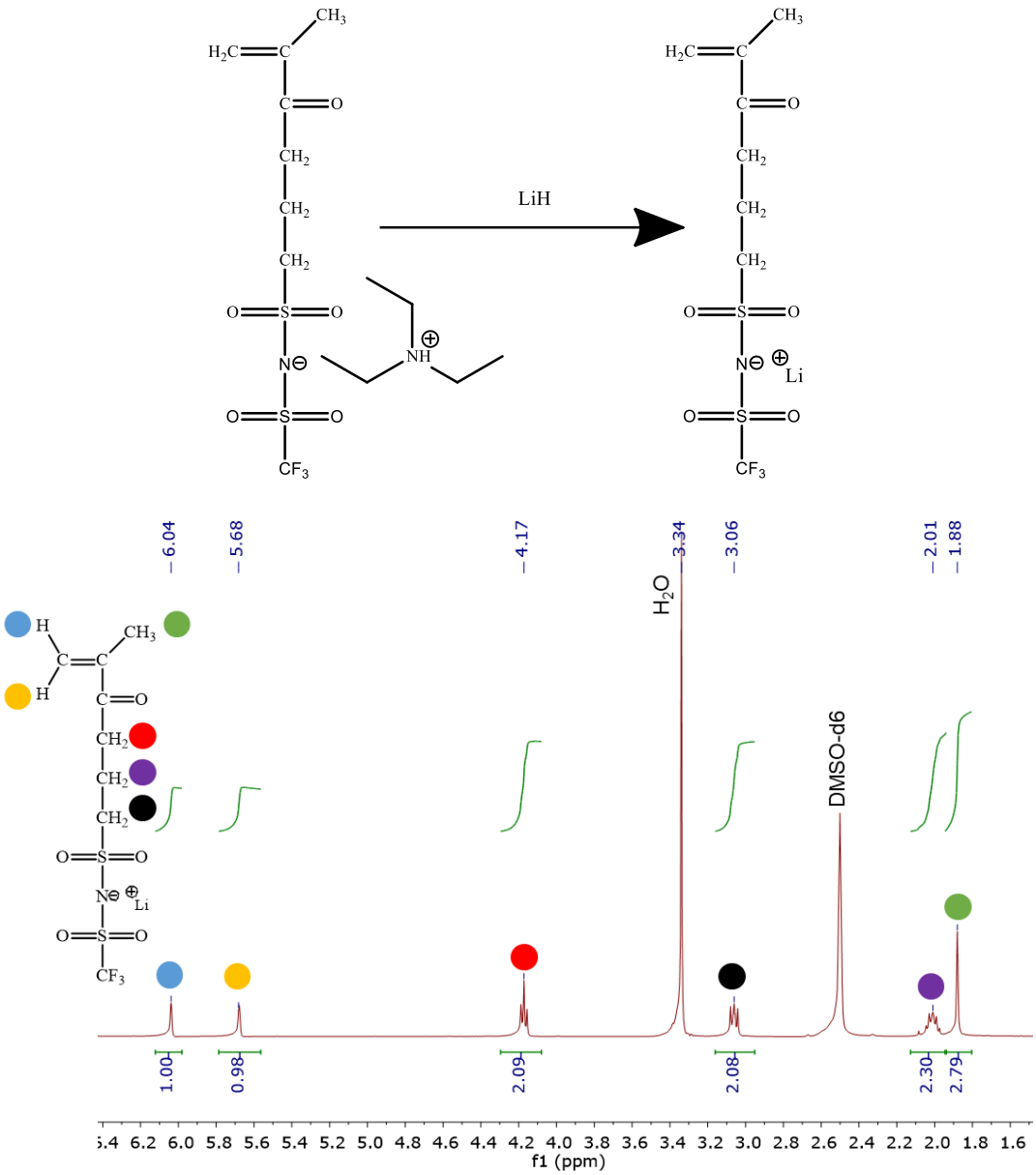

Figure 2.8. H[1]-NMR of the product of the third reaction to obtain the monomer LiMTFSI.

Poly (lithium 1-[3-(methacryloyloxy) propylsulfonyl]-1-(trifluoromethanesulfonyl) imide) (PLiMTFSI) was prepared by Reversible addition−fragmentation chain-transfer polymerization (RAFT) and inverse emulsion polymerization in order to obtain different molecular weights: 5 kg mol^{-1}, 50 kg mol^{-1} and a high molecular weight one. A degassed solution of LiMTFSI (1.5 g, 4.31 mmol), 4-cyano4-(phenyl-carbonthionylthio) (84 mg, 0.3 mmol for the 5 kg mol^{-1} polymer and 8.4, 0.03 mmol for the 50 kg mol^{-1} polymer) and AIBN (10 mg, 0.61 mmol for the 5 kg/mol polymer and 1 mg, 0.061 mmol for the 50 kg mol^{-1} polymer) in 5 g of DMF and a magnetic stir bar, was placed in a Schlenk tube.

RAFT polymerization was carried out at 90 ºC, under argon atmosphere for 24 h and then the polymer was precipitated in cold diethyl ether. Finally, the polymer was thoroughly dried at 60 ºC under high vacuum for 24 h.

Inverse emulsion polymerization was used to obtain a very high molecular weight PLiMTFSI. LiMTFSI (1.5 g, 4.31 mmol) was dissolved in 0.6 g of Milli-Q water, Isopal L (1.1 g) was used as an organic solvent, Span 83 (0.1 g) and Solftanol 90 (0.15 g) were selected as emulsifiers, and SMB (0.1 g), as initiator. The reaction was carried out at 70 ºC for 2 h under argon atmosphere and then the polymer was precipitated with cold diethyl ether. The polymer was purified by precipitation with diethyl ether and then centrifuged. Finally, the polymer was thoroughly dried at 60 ºC under high vacuum for 24 h.

Figure 2.9 shows the ^{1}H-NMR of the polymer after polymerization, where the characteristic peaks of the monomer (4.19 ppm) and the polymer (4.03 ppm) are presented, and the total conversion from monomer to polymer is calculated with the ratio of these two peaks.

Figure 2.10 shows the ^{1}H-NMR of the polymer after purification of the polymer by precipitation in diethyl ether and subsequent precipitation in the centrifuge. The spectrum no longer shows peaks corresponding to the lithium monomer, indicating that the polymer is clean.

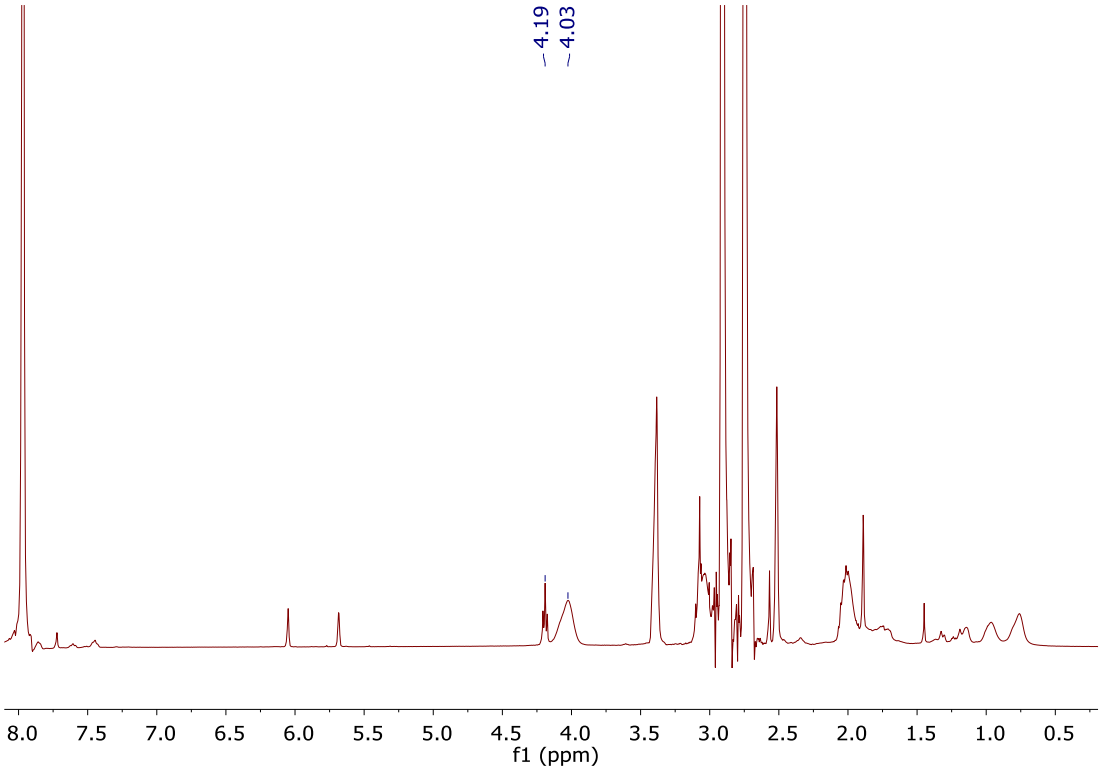

Figure 2.9. ^{1}H-NMR obtained after polymerization.

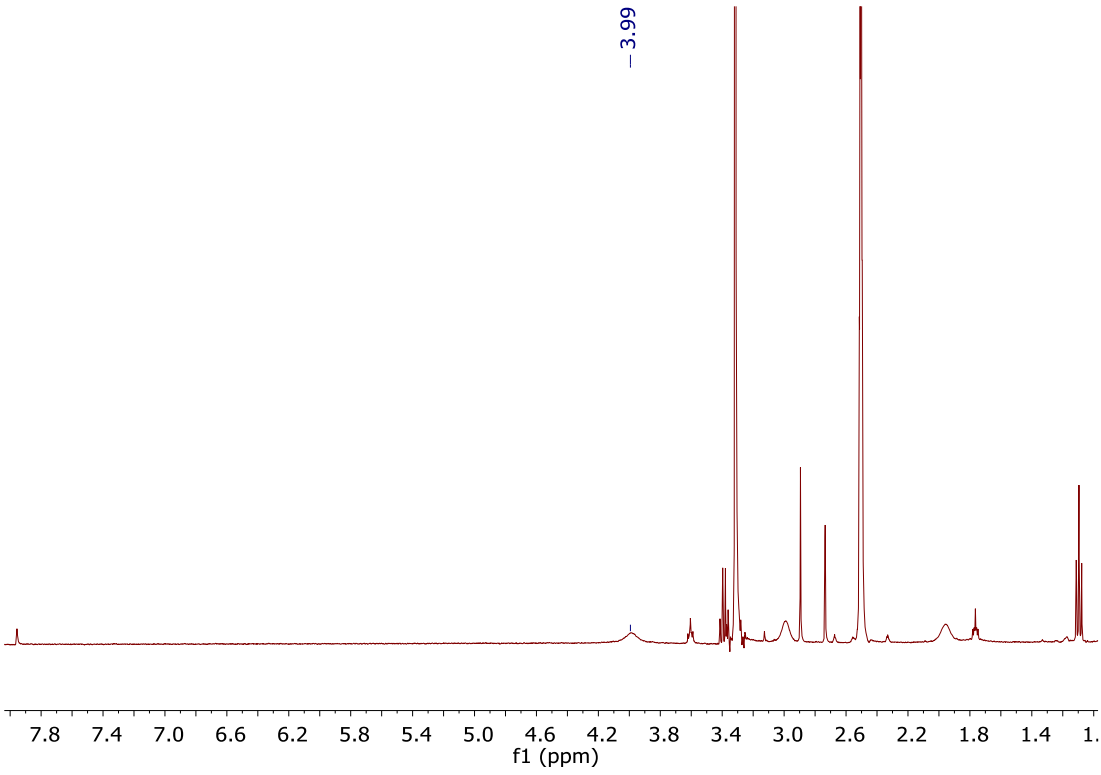

Figure 2.10. ^{1}H-NMR of PLiMTFSI after purification.

The M_W values of the prepared polymers are reported in Table 2.1. In the case of the high molecular weight polymer sample, the SEC measurements indicated that the *Mw* value is higher than 2,000 kg mol^{-1}, as it was out of the range of the SEC columns available. Our columns can only detect molecular weights lower or equal to 2,000 kg mol^{-1}.

Table 2.3. SEC of the synthesized polymers at 25 ºC, 0.1 M LiCl in water.

Expected molecular weight	M_n **(kg mol^{-1})**	M_w **(kg mol^{-1})**	$Đ$
PLiMTFSI 5 kg mol^{-1}	5.5	7.4	1.33
PLiMTFSI 50 kg mol^{-1}	44.9	59.2	1.32
PLiMTFSI >2,000 kg mol^{-1}	-	-	-

2.2.3.2 Preparation of Single Ion Solid Polymer Electrolytes by Blending PEO and PLiMTFSI (SIPE)

SIPE blend films were prepared by solvent casting method dissolving PEO and PLiMTFSI in water at 10 wt%. A family of blends mixing PEO of two different molecular weights (100 and 1,000 kg mol^{-1}) and PLiMTFSI of three different molecular weights (5, 50 and >2,000 kg mol^{-1}) at different compositions were prepared. The solutions with the mixture of the polymers were poured in silicone molds, and the solvent was let to evaporate slowly at room temperature (RT), then the obtained films were dried at 70 ºC under high vacuum to constant weight (Figure 2.11). A series of PEO/ PLiMTFSI blends were prepared with different weight compositions: 95/5, 90/10, 85/15, 80/20, 75/25, 70/30, 50/50 and 30/70 with PEO and PLiMTFI of different molecular weights.

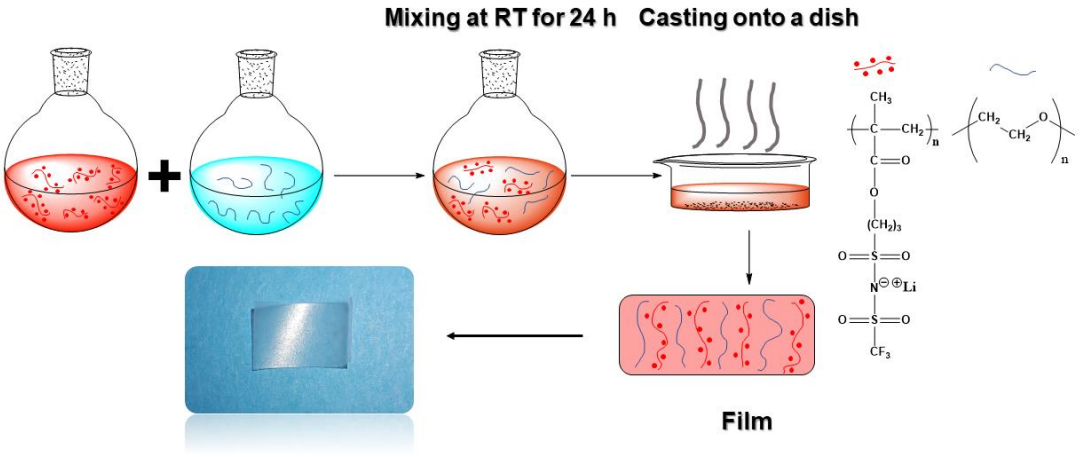

Figure 2.11. Preparation process of PEO/PLiMTFSI blends.

2.2.4 Chapter VI

2.2.4.1 Materials

Poly(ethylene oxide) (PEO) (with M_v value of 100 kg mol^{-1}, Sigma Aldrich), 3-sulfopropyl methacrylate potassium salt (98%, Sigma Aldrich), 4-cyano-4-(phenylcarbonothioylthio) pentanoic acid (CPADB >97%, Sigma Aldrich), hexane (Across), tetrahydrofuran (THF, Acros), dichloromethane (DCM, Across), 2,2′-Azobis(2-methylpropionitrile) (AIBN>98%, initiator, Sigma Aldrich), lithium hydride (LiH, Sigma Aldrich), N,N dimethylformamide (DMF, Across), poly(lactid acid) (PLA) (Ingeo 4032D, NatureWorks, M_n value of 107.3 kg mol^{-1} [17]), lithium bis(trifluoromethanesulfonyl)imide (LiTFSI), acetonitrile (ACN), and chloroform (99%) was supplied by Scharlau.

2.2.4.2 Preparation of solid polymer electrolytes

The blends were prepared by solvent casting using the amounts presented in Table 2.2. All blends were dissolved in chloroform/acetonitrile solution (70/30 v/v%) at 50 ºC for 12 h. In this chapter, PLiMTFSI of 50,000 g mol-1 was used, which was synthesized as explained in section 2.2.3.1.

The solutions were placed in a silicon mold to evaporate the solvents at room temperature. Then, the electrolytes were dried at 80 ºC for 12 h under vacuum.

Table 4.2. Composition of the different electrolytes prepared.

	PEO (g)	PLA (g)	LiTFSI (g)	PLiMTFSI (g)
60 PEO 40 PLA 0 wt% LiTFSI	1.5	1	0	-
60 PEO 40 PLA 5 wt% LiTFSI	1.425	0.95	0.125	-
60 PEO 40 PLA 10 wt% LiTFSI	1.35	0.9	0.25	-
60 PEO 40 PLA 15 wt% LiTFSI	1.275	0.85	0.375	-
60 PEO 40 PLA 30 wt% LiTFSI	1.05	0.7	0.75	-
50 PEO 50 PLiMTFSI 0 wt% PLA	1.25	0	-	1.25
50 PEO 50 PLiMTFSI 5 wt% PLA	1.1875	0.125	-	1.1875
50 PEO 50 PLiMTFSI 10 wt% PLA	1.125	0.25	-	1.125
50 PEO 50 PLiMTFSI 15 wt% PLA	1.0625	0.375	-	1.0625
50 PEO 50 PLiMTFSI 20 wt% PLA	1	0.5	-	1
50 PEO 50 PLiMTFSI 30 wt% PLA	0.875	0.75	-	0.875

2.2.5 Chapter VII

2.2.5.1 Synthesis of polyphosphoester copolymers

2.2.5.1.1 Poly(BEP-co-BenEP)-b-PEG-b-(BEP-co-BenP) block copolymer (P1 and P2).

Polyethylene glycol (M_w = 4000 g mol^{-1}) (4 g, 1 mmol for P1 and 2 g, 0.5 mmol for P2) was transferred in a round bottom flask and dried by three azeotropic distillations with anhydrous toluene. BenEP (2.5 g, 13.9 mmol) and BEP (2.5 g, 13.9 mmol) monomers were added in the flask. The mixture is then put under vacuum for 10 min 10 mL of anhydrous dichloromethane were then added under N_2 atmosphere. After complete solubilization, the mixture was cooled down to 0 °C, and 0.75 mL (5 mmol) of DBU was finally introduced under a N_2 atmosphere with a syringe equipped with a stainless-steel capillary. The polymerization medium was then stirred for 30 min. After concentration of the solution under vacuum, the copolymer was precipitated in cold diethyl ether. After decantation, the recovered copolymer was dissolved in methanol and dialyzed against methanol (MWCO = 3.5 kDa) overnight to remove impurities. After evaporation of methanol under vacuum, the copolymer was collected and characterized by NMR and SEC analyses.

2.2.5.1.2 P1 copolymer characterization

^{1}H NMR ($CDCl_3$) δ = 5.78 ppm (m, 10 H, –CH_2–CH=CH_2), 5.11 ppm (m, 20 H, CH_2=CH–CH_2), 4.25 ppm (m, 120 H, O–CH_2– CH_2–O and O–CH_2–CH_2–CH_2–CH_3 of BenEP + O–CH_2–CH_2–O, O–CH_2–CH_2–CH=CH_2 of BEP), 3.6 ppm (m, 360 H, O–CH2–CH2–O PEG), 2.41 ppm (m, 20 H, O–CH_2–CH_2–CH=CH_2) 1.62 ppm (m, 20 H, CH_2–CH_2–CH_2–CH_3), 1.46 ppm (m, 20 H, CH_2–CH_2–CH_2–CH_3) and 0.92 ppm (t, 30 H, CH_2–CH_2–CH_2–CH_3). ^{31}P NMR ($CDCl_3$) δ = −1.18 ppm and −1.32 ppm. M_n (^{1}H NMR) = 7600 g mol^{-1}, $Đ$ = 1.1 (SEC).

2.2.5.1.3 P2 copolymer characterization

^{1}H NMR ($CDCl_3$) δ = 5.78 ppm (m, 22 H, –CH_2–CH=CH_2), 5.11 ppm (m, 44 H, CH_2=CH–CH_2), 4.25 ppm (m, 264 H, O–CH_2–CH_2–O and O–CH_2–CH_2–CH_2–CH_3 of BenEP + O–CH_2–CH_2–O, O–CH_2–CH_2–CH=CH_2 of BEP), 3.6 ppm (m, 360 H, O–CH_2–CH_2–O PEG), 2.41 ppm (m, 44 H, O–CH_2–CH_2–CH=CH_2) 1.62 ppm (m, 44 H, CH_2–CH_2–CH_2–CH_3), 1.46 ppm (m, 44 H, CH_2–CH_2–CH_2–CH_3) and 0.92 ppm (t, 66 H, CH_2–CH_2–CH_2–CH_3). ^{31}P NMR ($CDCl_3$) δ = −1.18 ppm and −1.32 ppm. M_n (^{1}H NMR) = 11 000 g mol−1, $Đ$ = 1.1 (SEC).

2.2.5.1.4 Poly(BenEP-co-BEP) (50 mol% in BEP) random copolymer (P3)

TU (926 mg, 2.5 mmol) was transferred in a round bottom flask and dried by three azeotropic distillations with anhydrous toluene. BenEP (3.5 g, 19.6 mmol) and BEP (3.5 g, 19.6 mmol) monomers were added to the flask. The mix is then put under vacuum for 10 min 10 mL of anhydrous dichloromethane were then added under N_2 atmosphere. 2 mL of benzylic alcohol stock solution (5 mmol of benzylic alcohol in 100 mL of anhydrous CH_2Cl_2) (0.1 mmol) was added under a N_2 atmosphere. The mixture was cooled down to 0 °C, and DBU (0.4 mL, 2.8 mmol) was finally introduced under a N_2 atmosphere with a syringe equipped with a stainless-steel capillary. The reaction medium was stirred at 0 °C for 30 min. After concentration of the solution under vacuum, the copolymer was precipitated in cold diethyl ether. After decantation, the recovered copolymer was dissolved in methanol and dialyzed against methanol (MWCO = 1 kDa) overnight in order

to remove impurities. After evaporation of methanol under vacuum, the copolymer was collected and characterized by NMR and SEC analyses.

2.2.5.1.5 P3 copolymer characterization

^{1}H NMR ($CDCl_3$) δ = 7.5 (m, 5H, aromatic protons), 5.78 ppm (m, 20 H, –CH_2–CH=CH_2), 5.11 ppm (m, 40 H, CH_2=CH–CH_2), 4.25 ppm (m, 240 H, O–CH_2–CH_2–O and O–CH_2–CH_2–CH_2–CH_3 of BenEP + O–CH_2–CH_2–O, O–CH_2–CH_2–CH=CH_2 of BEP), 2.41 ppm (m, 40 H, O–CH_2–CH_2–CH=CH_2) 1.62 ppm (m, 40 H, CH_2–CH_2–CH_2–CH_3), 1.46 ppm (m, 40 H, CH_2–CH_2–CH_2–CH_3) and 0.92 ppm (t, 60 H, CH_2–CH_2–CH_2–CH_3). ^{31}P NMR ($CDCl_3$) δ = −1.18 ppm and −1.32 ppm. M_n (^{1}H NMR) = 7000 g mol^{-1}, $Đ$ = 1.1 (SEC).

2.2.5.2 Elaboration of solid polymer electrolytes

SPEs were prepared by a solvent casting method dissolving the polyphosphoester copolymers (0.15 g) and the lithium bis(trifluoromethanesulfonyl) imide (LiTFSI) (15 and 30 wt% respect to the copolymer amount) in ACN (3 mL). The solutions were dried on a silicon mold a room temperature for 24 hours, and after the SPEs were dried under high vacuum at 50 °C during 12 h.

The polyphosphoester named P1 and P3 were crosslinked to produce free-standing films by UV-Light using the next methodology. The crosslinked polymer electrolytes were preprepared by dissolving in acetonitrile the copolymer (0.15 g), lithium bis(trifluoromethanesulfonyl)imide (LiTFSI) (15 and 30 wt% respect the copolymer amount), the UV photoinitiator (2-hydroxy-2methyl-propiophenone (1 wt% respect the copolymer amount)) in 3 mL of acetonitrile. The solutions were stirred during 1 h, and they were cast onto a silicon mold. The solvent was evaporated at room temperature and later by applying high vacuum. Finally, the films were passed 3 times from a xenon arc lamp (Helios Italquartz, 45 mW cm^{-2}). Before each experiment, the crosslinked copolymers were dried under vacuum at 50 °C during 24 h. Figure 2 shows the structure of the crosslinked electrolytes.

2.3 References

[1] R.H. Beaumont, B. Clegg, G. Gee, J.B.M. Herbert, D.J. Marks, R.C. Roberts, D. Sims, Heat capacities of propylene oxide and of some polymers of ethylene and propylene oxides, Polymer. 7 (1966) 401–417. https://doi.org/https://doi.org/10.1016/0032-3861(66)90055-3.

[2] A.T. Lorenzo, M.L. Arnal, J. Albuerne, A.J. Müller, DSC isothermal polymer crystallization kinetics measurements and the use of the Avrami equation to fit the data: Guidelines to avoid common problems, Polymer Testing. 26 (2007) 222–231. https://doi.org/10.1016/j.polymertesting.2006.10.005.

[3] E. Quero, A.J. Müller, F. Signori, M.B. Coltelli, S. Bronco, Isothermal cold-crystallization of PLA/PBAT blends with and without the addition of acetyl tributyl citrate, Macromolecular Chemistry and Physics. 213 (2012) 36–48. https://doi.org/10.1002/macp.201100437.

[4] A. Witkowski, A.A. Stec, T.R. Hull, Thermal decomposition of polymeric materials, in: SFPE Handbook of Fire Protection Engineering, Springer, 2016: pp. 167–254.

[5] R.E. Wetton, R.D.L. Marsh, J.G. Van-de-Velde, Theory and application of dynamic mechanical thermal analysis, Thermochimica Acta. 175 (1991) 1–11.

[6] J.L. Koenig, Fourier transform infrared spectroscopy of polymers, Spectroscopy: NMR, Fluorescence, FT-IR. (1984) 87–154.

[7] D. Andre, M. Meiler, K. Steiner, C. Wimmer, T. Soczka-Guth, D.U. Sauer, Characterization of high-power lithium-ion batteries by electrochemical impedance spectroscopy. I. Experimental investigation, Journal of Power Sources. 196 (2011) 5334–5341.

[8] K. Deshmukh, S. Sankaran, B. Ahamed, K.K. Sadasivuni, K.S.K. Pasha, D. Ponnamma, P.S. Rama Sreekanth, K. Chidambaram, Chapter 10 - Dielectric Spectroscopy, in: S. Thomas, R. Thomas, A.K. Zachariah, R.K.B.T.-S.M. for N.C. Mishra (Eds.), Micro and Nano Technologies,

Elsevier, 2017: pp. 237–299. https://doi.org/https://doi.org/10.1016/B978-0-323-46140-5.00010-8.

[9] R.A. Susott, F. Shafizadeh, T.W. Aanerud, Quantitative thermal analysis technique for combustible gas detection, J. Fire Flammability;(United States). 10 (1979).

[10] R.A. Susott, Thermal behavior of conifer needle extractives, Forest Science. 26 (1980) 347–360.

[11] R.A. Susott, Characterization of the thermal properties of forest fuels by combustible gas analysis, Forest Science. 28 (1982) 404–420.

[12] R.E. Lyon, R.N. Walters, Pyrolysis combustion flow calorimetry, Journal of Analytical and Applied Pyrolysis. 71 (2004) 27–46. https://doi.org/10.1016/S0165-2370(03)00096-2.

[13] L.A. Middlemiss, A.J.R. Rennie, R. Sayers, A.R. West, Characterisation of batteries by electrochemical impedance spectroscopy, Energy Reports. 6 (2020) 232–241.

[14] A. Basterretxea, E. Gabirondo, C. Jehanno, H. Zhu, I. Flores, A.J. Müller, A. Etxeberria, D. Mecerreyes, O. Coulembier, H. Sardon, Polyether Synthesis by Bulk Self-Condensation of Diols Catalyzed by Non-Eutectic Acid–Base Organocatalysts, ACS Sustainable Chemistry & Engineering. 7 (2019) 4103–4111. https://doi.org/10.1021/acssuschemeng.8b05609.

[15] L. Porcarelli, M.A. Aboudzadeh, L. Rubatat, J.R. Nair, A.S. Shaplov, C. Gerbaldi, D. Mecerreyes, Single-ion triblock copolymer electrolytes based on poly(ethylene oxide) and methacrylic sulfonamide blocks for lithium metal batteries, Journal of Power Sources. 364 (2017) 191–199. https://doi.org/10.1016/j.jpowsour.2017.08.023.

[16] A.S. Shaplov, P.S. Vlasov, M. Armand, E.I. Lozinskaya, D.O. Ponkratov, I.A. Malyshkina, F. Vidal, O. V. Okatova, G.M. Pavlov, C. Wandrey, I.A. Godovikov, Y.S. Vygodskii, Design and synthesis of new anionic “polymeric ionic liquids” with high charge delocalization, Polymer Chemistry. 2 (2011) 2609. https://doi.org/10.1039/c1py00282a.

[17] Á. Kmetty, K. Litauszki, Development of poly (lactide acid) foams with thermally expandable microspheres, Polymers. 12 (2020) 463. https://doi.org/10.3390/polym12020463.

Chapter III

3. Effect of chemical structure and salt concentration on the crystallization and ionic conductivity of aliphatic polyethers

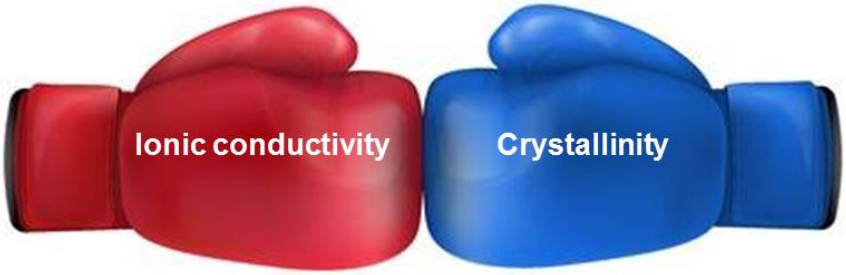

3.1. Abstract

Poly(ethylene oxide) PEO is the most widely used polymer in the field of solid polymer electrolytes for batteries. It is well known that the crystallinity of polymer electrolytes strongly affects ionic conductivity and electrochemical performance. Nowadays, alternatives to PEO are actively searched in the battery community showing higher ionic conductivity, electrochemical window or working temperature range. In this chapter, we investigated polymer electrolytes based on aliphatic polyethers with a number of methylene units ranging from 2 to 12. Thus, the effect of the lithium bis(trifluoromethanesulfone) imide (LiTFSI) concentration on the crystallization behavior of the new aliphatic polyethers and their ionic conductivity was investigated. In all the cases, the degree of crystallinity and the overall crystallization rate of the polymers decreases drastically with 30 wt% LiTFSI addition. The salt acted as a low molecular diluent to the polyethers according to the expectation of the Flory-Huggins theory for polymer-diluent mixtures. By fitting our results to this theory, the value of the interaction energy density (B) between the polyether and the LiTFSI was calculated, and we show that the value of B must be small to obtain high ionic conductivity electrolytes.

J.L. Olmedo-Martínez, L. Meabe, A. Basterretxea, D. Mecerreyes, A.J. Müller, Effect of chemical structure and salt concentration on the crystallization and ionic conductivity of aliphatic polyethers, Polymers. 11 (2019) 452. https://doi.org/10.3390/polym11030452.

3.2 Introduction

Dry solid polymer electrolytes (SPEs) have attracted great attention as safe alternatives to liquid electrolytes in different energy storage technologies such as lithium batteries for electric vehicles [1–3]. SPEs are formed by complexing an ionic salt within a polymer matrix. It is generally accepted that the ionic conductivity occurs in the amorphous part of the polymers, and the ion dynamics is governed by the segmental motion of the amorphous phases in polymers [4]. Several polymers and salts have been evaluated as SPEs such as poly(ethylene oxide) (PEO), poly(vinyl alcohol) (PVA), poly(methyl methacrylate) (PMMA), poly(ε-caprolactone) (PCL), polycarbonates (PC), chitosan (CS), poly(vinylpyrrolidone) (PVP), poly(vinyl chloride) (PVC), poly(vinylidene fluoride) (PVDF) and poly(ionic liquid)s [5,6], among other polymers. Different lithium salts have been employed, such as $LiClO_4$, $LiBF_4$, $LiPF_6$, LiFSI [7], and lithium bis(trifluoromethanesulfone) imide (LiTFSI). In particular, LiTFSI has been widely employed, as its low lattice energy favors salt dissolution and dissociation, leading to enhanced ionic conductivity [8].

Among all the polymers matrices, PEO is the most studied polymer electrolyte in lithium batteries. Due to its polarity, lithium salts can be easily dissolved in PEO, a fact that promotes the ion mobility [9–11]. The PEO/LiTFSI system has been widely studied because of the high dissociation and plasticizing abilities of LiTFSI that leads to better ionic conductivities, as compared to other salts. However, the low ionic conductivity obtained at low temperatures, the low lithium transference number, and the resulting high interfacial resistance are common problems for this electrolyte to be applied in lithium batteries. In these polymer electrolytes, the salt plays two roles, the introduction of ionic charge carriers and the suppression of crystallization of the PEO. Thus, Marzantowicz *et al*. studied the crystallization of PEO/LiTFSI by polarized optical microscopy and ionic conductivity simultaneously, and they found that the decrease of conductivity during crystallization is related to the reduction of amorphous conductivity pathways by growing spherulites [12]. An in-depth study of the crystallization behavior of PEO helped to understand the electrochemical properties of SPEs [13]. Generally, crystallization limits ionic conductivity. Consequently, different strategies have been developed to limit the crystallization

of PEO and improve the ionic conductivity in SPEs. Some of the strategies employed in this direction are synthesizing block and random copolymers [14,15], cross-linked polymer electrolytes [16] or adding nano-particles [17].

Furthermore, the crystallization kinetics of polymer electrolytes has a direct effect on the structure and properties of the SPEs. Sim *et al.* studied the effect of molecular mass of PEO and $LiClO_4$ content on the isothermal crystallization of PEO [18]. Their study reports a very large decrease in the isothermal crystallization rate with salt addition. In addition, they observed that the effect is more pronounced as the molecular weight of PEO increased. Additionally, Zhang *et al.,* investigated the crystallization behavior of PCL/$LiClO_4$, and the results indicated that Li salts affected the crystallization behavior of PCL without changing its crystalline structure [19].

Very recently, we have reported a new versatile synthetic pathway to a variety of aliphatic polyethers by organocatalyzed bulk self-condensation of aliphatic diols [20]. This prompted us to investigate the effect of chemical structure of the aliphatic polyethers and the salt concentration in the crystallinity of the polymer electrolytes. In this chapter, we prepared solid polymer electrolytes (SPEs) composed of aliphatic polyethers, with different methylene numbers in their repeating units (between 2 and 12) and several LiTFSI concentrations (10, 30 50 and 80 wt%). The objective in this chapter of the thesis is to study the effect of the chemical structure of the different polyethers and LiTFSI salt concentrations on the crystallization kinetics and ionic conductivity of polyethers/LiTFSI SPEs.

3.3 Results

The polymers are named using the following nomenclature: PEO = P1, Poly(THF) = P2 and the synthesized polymers with different number of methylene groups in their repeat units are poly(oxyhexamethylene) (P3) > poly(oxyoctomethylene) (P4)> poly(oxydecamethylene) (P5)> poly(oxydodecamethylene) (P6) (Figure 3.1).

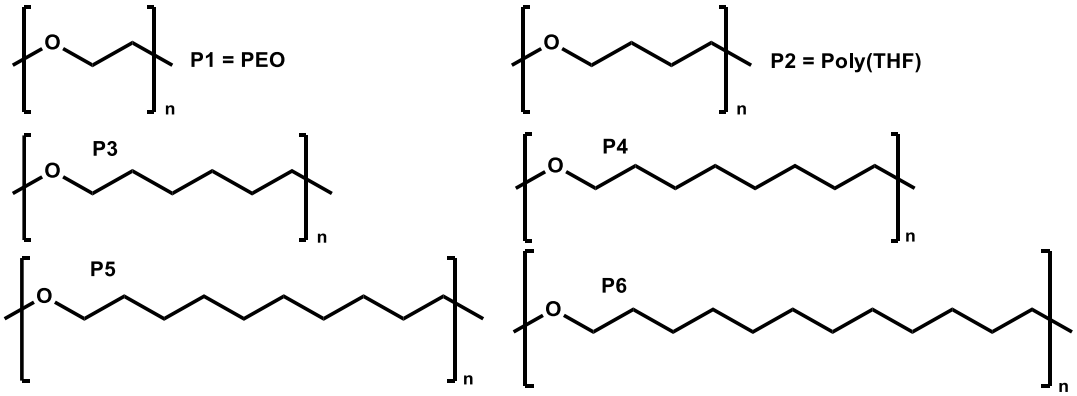

Figure 3.1. Chemical Structure of the different polyethers employed in this work.

3.3.1 Non-isothermal crystallization of aliphatic polyethers in the presence of LiTFSI

As mentioned before, poly(ethylene oxide) (PEO) is widely explored in the area of SPEs for lithium batteries [7]. Adequate coordination between different salts and PEO has been investigated for many years [21,22]. The crystallinity of PEO plays an important role, as it has been demonstrated that it can hinder ionic conductivity. Nevertheless, there are no reports on the ionic conductivity and the effect of crystallinity on other aliphatic polyethers with a higher amount of methylene units. For this reason, we first examined the thermal properties of pure polyethers and their mixtures with 30 wt% LiTFSI by DSC. In total, six different polyethers have been compared, (i) commercially available PEO (P1) with two methylene units, poly(tetrahydrofurane) PTHF (P2) with four methylene units, and the synthesized aliphatic polyethers with 6, 8, 10 and 12 methylene units respectively (P3, P4, P5, P5). All the studied polymers have a similar number average molar mass of around 2,000 g mol^{-1}.

As a reference, Figure 3.2a shows the cooling scans for the neat aliphatic polyethers. The crystallization temperature generally increases between 10 and 65 ºC as the number of methylene groups in the polyethers repeating units increases. The only exception being the P1 PEO sample, this sample also shows a bimodal distribution of crystallization temperatures whose origin is unknown as it would merit further studies outside the scope of the present work. As the number of methylene units increases, the polyethers start to behave in a similar

way to polyethylene showing a higher T_m, as the effect of the polar oxygen atom is progressively diluted by the aliphatic chain.

Additionally, Figure 3.2b shows the crystallization temperature of the polyether SPEs with 30 wt% LiTFSI. In all cases, homogenous SPEs were obtained, except for the SPE based on P6, as LiTFSI has poor solubility in P6. Figure 3.2b shows that P1 and P2 with 30% LiTFSI are completely amorphous materials. However, in the case of P3, P4, P5 and P6, the crystallization temperature decreases as compared with the neat polyethers, indicating that LiTFSI slows down the non-isothermal crystallization kinetics from the melt at 20 $^{o}C\ min^{-1}$.

Figure 3.2c represents the change in the melting temperature of the neat polyethers and the polyethers with 30 wt% of LiTFSI. As expected, the melting temperature increases with the number of methylene units and for any given polyether, it decreases with salt addition. The depression of the melting temperature with the addition of LiTFSI could be due to a dilution effect of the salt. This possibility is examined in detail below by varying the salt concentration in selected samples and applying the Flory-Huggins theory. Figure 3.2c also shows how the values of the equilibrium melting point change as a function of the number of methylene groups in the repeating units for synthesized polyethers. These values were obtained using the Hoffman-Weeks extrapolation for isothermally crystallized samples (Figure 3.7). The T_m^0 values also follow the same trend with the number of methylene units, as the apparent or experimentally determined melting points, as expected. In Figure 2c, the data for P1 and P2 are not reported, as the Hoffman-Weeks extrapolation yielded unsatisfactory data, a fact that maybe due to the lower molecular weight values for these samples.

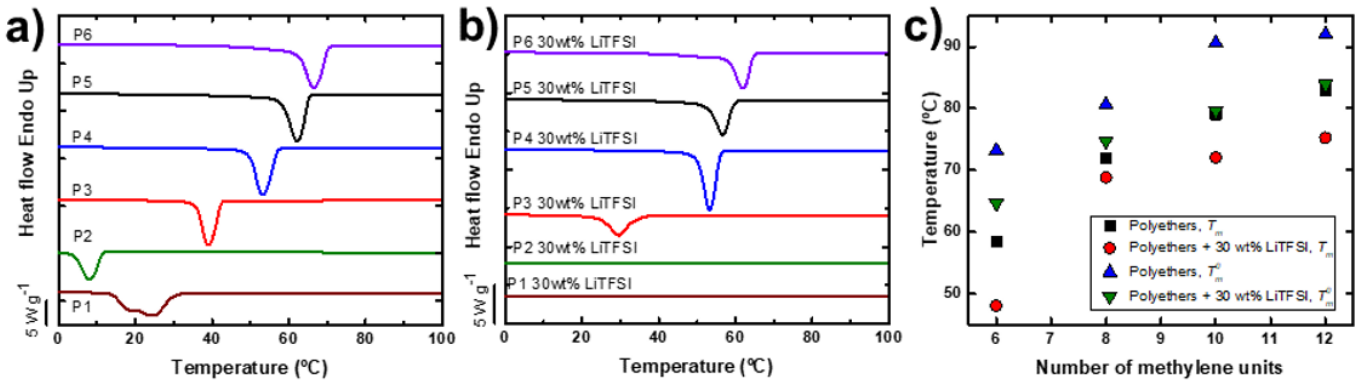

Figure 3.2. (a) DSC cooling scans of neat aliphatic polyethers, (b) DSC cooling scans of polymer electrolytes composed of aliphatic polyethers including 30 wt% LiTFSI, (c) Experimental melting peak values (T_m) (determined during the second DSC heating runs) and equilibrium melting point values (T_m^0) determined by the Hoffman-Weeks extrapolation procedure after isothermal crystallization.

Given the results obtained above, samples P3 and P5 were chosen in order to study in detail the effect of salt concentration on ionic conductivity and crystallization. P3 has the lowest T_m and T_c values, while P5 has one of the highest T_m and T_c values, from the series of long-chain polyethers synthesized in this work. We need to remark that the mixture of P6 and LiTFSI was not homogeneous, thus P6 was not chosen for further analysis.

P3 and P5 were evaluated with different salt concentrations: 10, 30, 50 and 80 wt% LiTFSI. The general trend of crystallization temperature of either polyether is to decrease gradually with the addition of salt (Figure 3.3). This trend can be attributed to a dilution effect of the salt. In other words, the salt acts as a solvent that depresses both the crystallization and melting temperature of the polyether. In addition, P3 is completely amorphous with 50 wt% or more LiTFSI, whereas in the case of P5, the SPE-P% is rendered amorphous only when 80 wt% LiTFSI is added.

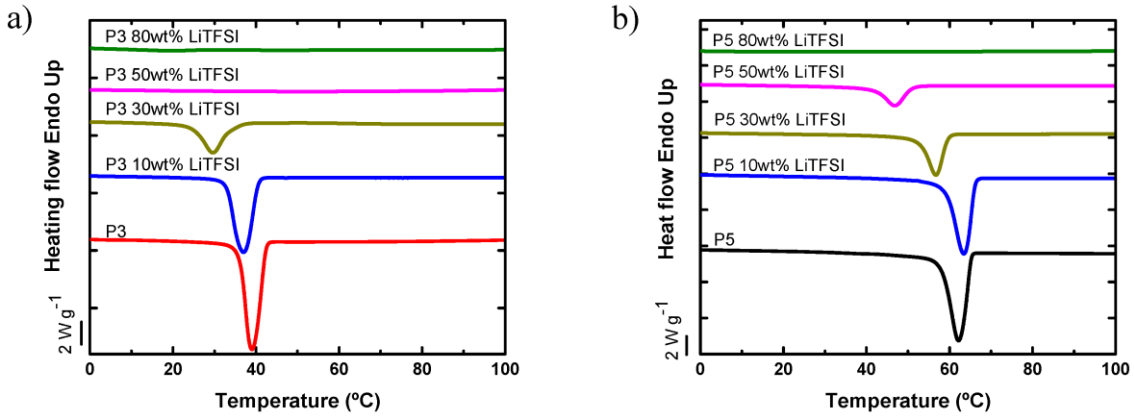

Figure 3.3. DSC cooling scans of neat P3 and P5 polyethers and their mixtures with different LiTFSI salt concentrations (SPEs): (a) P3, (b) P5.

3.3.2 Ionic conductivity of aliphatic polyethers in the presence of LiTFSI

The ionic conductivity of these solid polymer electrolytes (SPEs) was studied by impedance spectroscopy. Figure 3.4 presents the change in impedance for the different polyethers with 30 wt% LiTFSI, showing how the impedance decreases with increasing temperature.

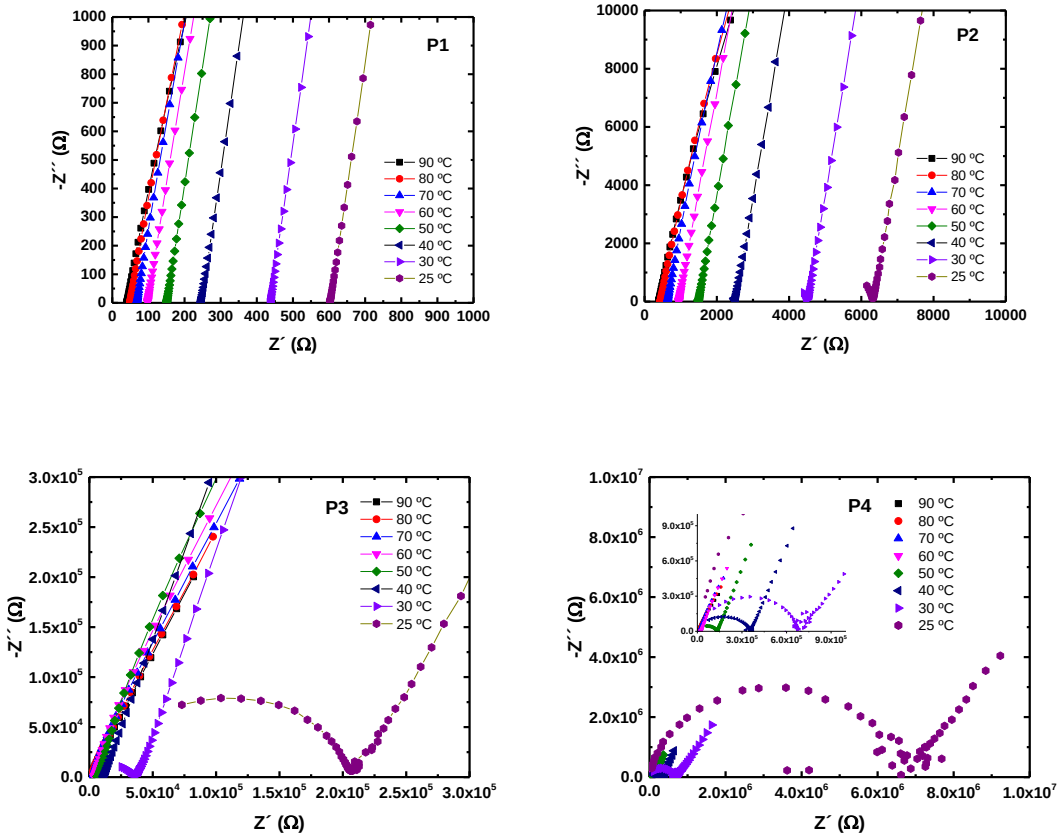

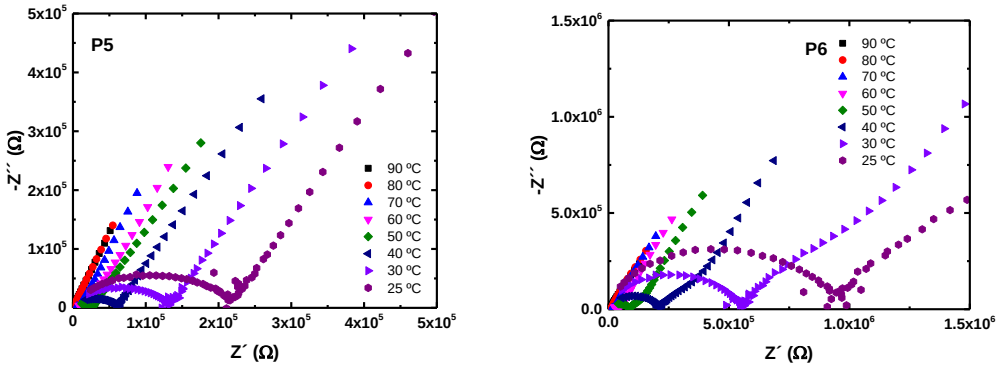

Figure 3.4. Nyquist plots of polyethers with 30 wt% LiTFSI.

The ionic conductivity of polymer electrolytes with different salt contents was evaluated. First, the ionic conductivity of all polyethers with 30% LiTFSI was analyzed, and the results are presented in Figure 3.5.

Figure 3.5a shows a decrease in ionic conductivity with the increase of the number of methylene groups along the repeating units of the polyethers employed. P1 and P2 provide the highest ionic mobility as they are amorphous. The amorphous nature of these materials can be deduced from their monotonic behavior in the Arrhenius representation plotted in Figure 3.5, and corroborated by DSC analysis, see Figure 3.2b.

Figure 3.5a also shows how the ionic conductivity of P3, P4, P5 and P6 dramatically decreases as soon as these polyethers crystallize below 70 ºC (see also Figure 3.2b) [23]. These data, where SPE-P1 provides the highest ionic conductivity, reveals that PEO is the best candidate, from the series of polyethers examined here, for hosting LiTFSI (ionic conductivity of $5 \cdot 10^{-4}$ S cm^{-1} at 70 °C and 4.8 10^{-5} S cm^{-1} at room temperature). This high ionic conductivity can be explained by the favorable helical wrapping of Li ions on the polyether chain, when the ether oxygens are separated by exactly two carbon atoms [6]. This favorable coordination shows the highest ionic conductivity of the entire polyether family.

It should be noted that the behavior of SPE-P6 in Figure 3.5a is out of the general trend (i.e., the trend of decreasing conductivity as the number of methylene groups in the polyether repeating unit increases), due to its

compromised solubility in the mixture of solvents and LiTFSI. Such poor solubility affects the homogeneity of the resulting SPE-P6.

Figure 3.5b reports the ionic conductivity and the activation energies (E_a) of the polyethers (except P6) at 90 ºC (a temperature at which all samples are in the melt) in the linear region (only molten state data were employed), these values were calculated using the Arrhenius equation [24]:

$$\sigma = \sigma_0 \exp(\frac{-E_a}{kT}) \tag{3.1}$$

where σ is the ionic conductivity, σ_0 is the pre- exponential factor, E_a is the activation energy, K the Boltzman contant and T the absolute temperature.

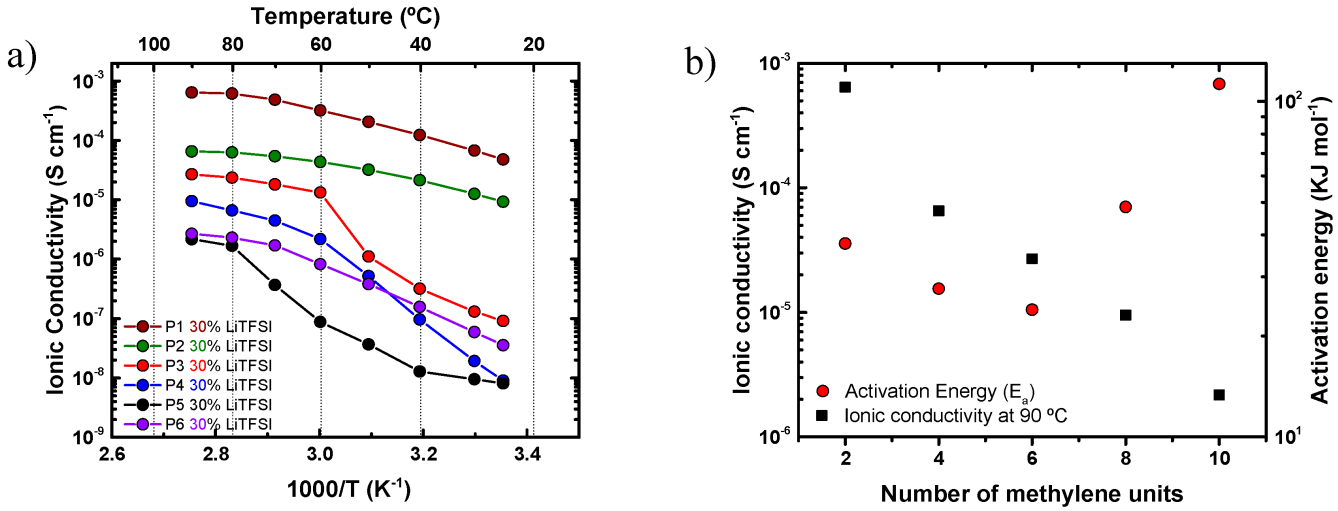

Figure 3.5. (a) Ionic conductivity of the polyethers with 30 wt% LiTFSI (b) Ionic conductivity of the polyethers with 30 wt% LiTFSI at 90 ºC and activation energy (E_a) calculated in the molten state for the SPEs.

For P1, P2 and P3, the activation energies obtained (E_a) are of the same order of magnitude, but for P4 and P6, the activation energy significantly increases. In addition, a large decrease in conductivity with respect to the number of methylene groups in the repeating units of the polyethers is observed as expected. As a result, the ionic conductivity decreases with increasing E_a. The activation energy values found in this work are similar to those reported in the literature [5].

Among the all SPEs, SPE-P3 and SPE-P5 were selected to study the effect of salt concentration (10, 30, 50, 80 wt% of LiTFSI) on the ionic conductivity, and the results are shown in Figure 3.6. The ionic conductivity of SPE-P3 increases with the increase of salt concentration from 10 wt% to 50 wt%, whereas the crystallinity decreases (Figure 3.3a). The optimum ionic conductivity value at room temperature is $2.05 \cdot 10^{-5}$ S cm^{-1}, with 50 wt% LiTFSI. At higher salt concentrations, the ionic conductivity of SPE-P3 decreases. In P5 is more evident the increase of ionic conductivity with the amount of salt, this value increases from $1.61 \cdot 10^{-9}$ S cm^{-1} with 10 wt% LiTFSI to $8.8 \cdot 10^{-6}$ S cm^{-1} with 80 wt% LiTFSI (at room temperature), and then with 90 wt% the conductivity drops two orders of magnitude. In both cases, the conductivity is lower than with PEO with 30 wt% LiTFSI.

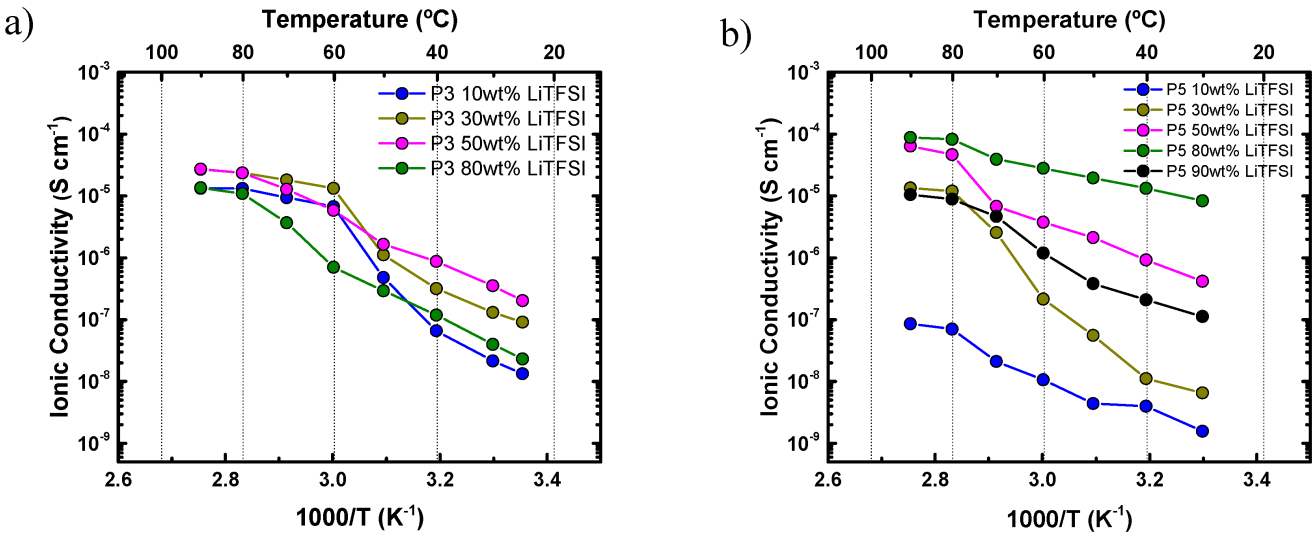

Figure 3.6. Ionic conductivity of SPE-P3 (a) and SPE-P5 (b) with different amounts of LiTFSI.

The degree of crystallinity (X_C) of the polyether components was calculated for the two families of SPEs, using the following equation:

$$X_C = \frac{\Delta H_m}{f\ \Delta H_m^0} * 100 \qquad (3.2)$$

where $\Delta H_m{}^0$ is the equilibrium melting enthalpy for the 100% crystalline polyether, ΔH_m is the experimental melting enthalpy of the sample, and f is the weight fraction of the polymer in the sample.

The values of ΔH_m^0 = 244.7 J g^{-1} for P3 and ΔH_m^0 = 258.3 J g^{-1} for P5 were employed. These values were obtained by the Flory Huggins theory, where ΔH_m^0 is denoted as ΔH_u (as explained below, in section 3.3.4). In both cases. Table 3.1 reports the crystallinity values obtained, and it is observed that the degree of crystallinity decreases as LiTFSI content increases, as expected if the salt is considered a diluent for the polyethers. This crystallinity reduction is one of the reasons why SPEs exhibit a larger ionic conductivity as the content of LiTFSI increases.

Table 3.1. ΔH_m and degree of crystallinity of SPE-P3 and SPE-P5 with different amount of LiTFSI.

Sample	ΔH_m (J g^{-1})	Crystallinity (%)
P1	149	69
P2	85	36
P3	127	51
P3 10 wt% LiTFSI	99	45
P3 30 wt% LiTFSI	49	29
P3 50 wt% LiTFSI	0	0
P4	145	56
P5	135	52
P5 10 wt% LiTFSI	119	51
P5 30 wt% LiTFSI	80	44
P5 50 wt% LiTFSI	47	36
P5 80 wt% LiTFSI	0	0
P6	142	53

3.3.3 Isothermal crystallization of aliphatic polyethers in the precence of LiTFSI

Isothermal crystallization experiments performed by DSC are useful to determine the overall crystallization kinetics of the polymeric samples employed here. These experiments are performed to study how the lithium salt concentration affects the overall crystallization kinetics of the different polyethers.

One of the important data needed to perform the Lauritzen-Hoffman adjustment is the value of T_m^0, which is calculated by means of the Hoffman-Weeks extrapolation. To perform the Hoffman-Weeks extrapolation, the samples

were heated after isothermal crystallization from their T_c values until melting, and the peak melting temperature (T_m) were recorded. As an example, the Hoffman-Weeks plots for P3, P4, P5 and P6 are shown in Figure 3.7. The straight line of the observed melting temperature against T_c intersects with the equilibrium line (red line $T_m = T_c$) [25–27]. From the extrapolations, we estimated the T_m^0 values for all the samples.

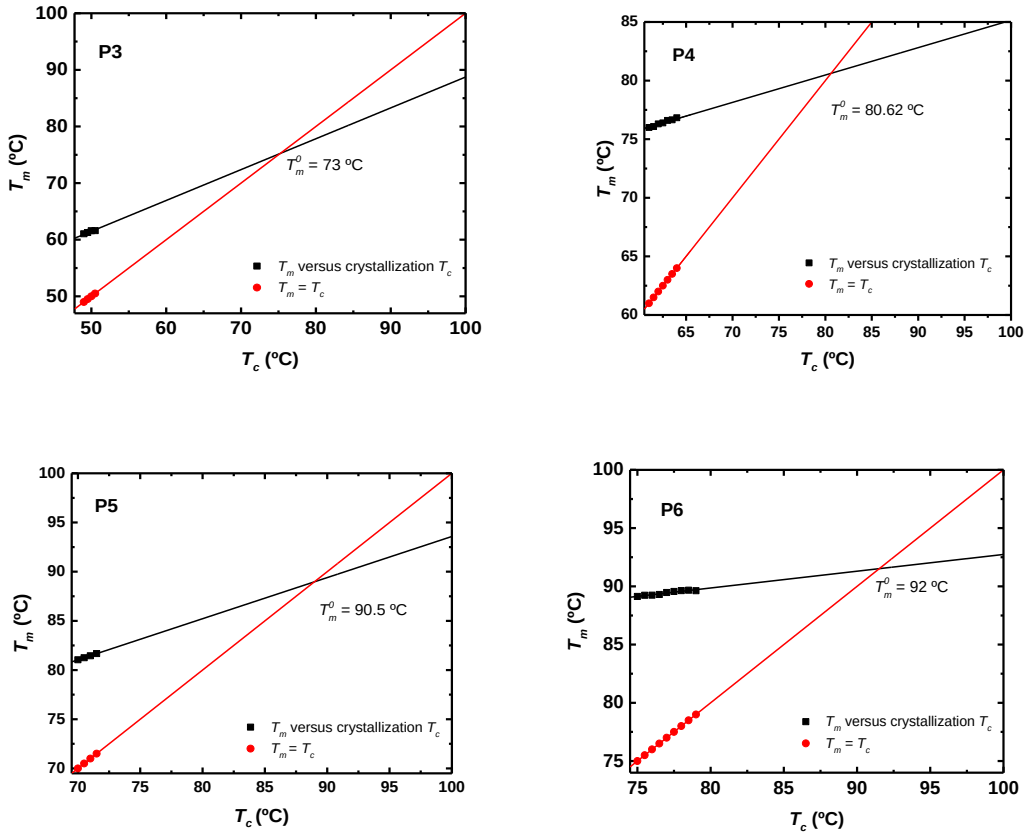

Figure 3.7. Hoffman- Weeks plots of neat polyethers

Figure 3.8a shows plots of the inverse of the half-crystallization time ($1/\tau_{50\%}$) as a function of the crystallization temperature (T_c) of the neat polyethers. The inverse of the half-crystallization time ($1/\tau_{50\%}$) is an experimentally determined value that is directly proportional to the overall crystallization rate [25,26]. The crystallization temperature values where the kinetics was able to be measured decrease as the number of methylene units decreases in the polyether repeating unit. If the supercooling is calculated as $\Delta T=T_m^0-T_m$, employing the equilibrium melting temperature values determined by the Hoffman-Weeks extrapolation (Figure 3.7), the overall crystallization kinetics can be represented as a function of supercooling. Figure 3.8b shows how the overall crystallization kinetics plots for the different polyethers are now much closer together (using the same relative temperature range), since the supercooling normalizes the plot with respect to thermodynamic effects. The supercooling required for crystallization decreases as the number of methylene units in the polyether increases (Figure 3.8b). This result is consistent with the non-isothermal crystallization data reported in Figure 3.3.

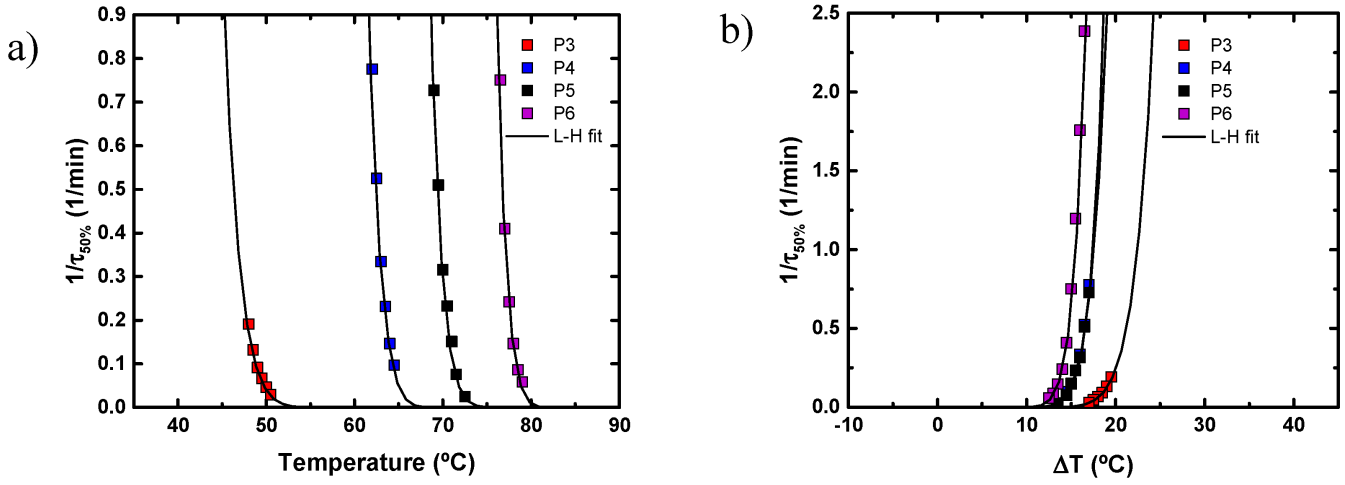

Figure 3.8. (a) Overall crystallization rate (expressed as the inverse of the half-crystallization time) versus isothermal crystallization temperature. (b) Overall crystallization rate (expressed as the inverse of the half-crystallization time) versus supercooling ($\Delta T=T_m^0-T_c$). Symbols: experimental data. Solid lines are fittings to the Lauritzen and Hoffman theory.

The overall crystallization rate of P3 and P5 with different amounts of LiTFSI (5-30 wt%) was studied and the results are presented in Figure 3.9. In the

case of the SPE-P3 samples, the crystallization rate decreases with salt content, a result that is explained by the dilution effect caused by LiTFSI. Similar results are obtained for SPE-P5 samples, except for the sample with 10 wt% LiTFSI, which exhibits a larger value than expected. Apart from this particular sample, all the rest behaved as expected and the results indicate that the overall crystallization kinetics of these polyethers is substantially depressed by the incorporation of LiTFSI. The best way to visualize this change in crystallization rate is to plot the overall crystallization rate at a constant temperature (45 ºC in case of P3 and 71 ºC for P5) as a function of LiTFSI content, as shown in Figure 3.9c. The results clearly show that the overall crystallization rate of polyethers P3 and P5 generally decrease with increasing LiTFSI content.

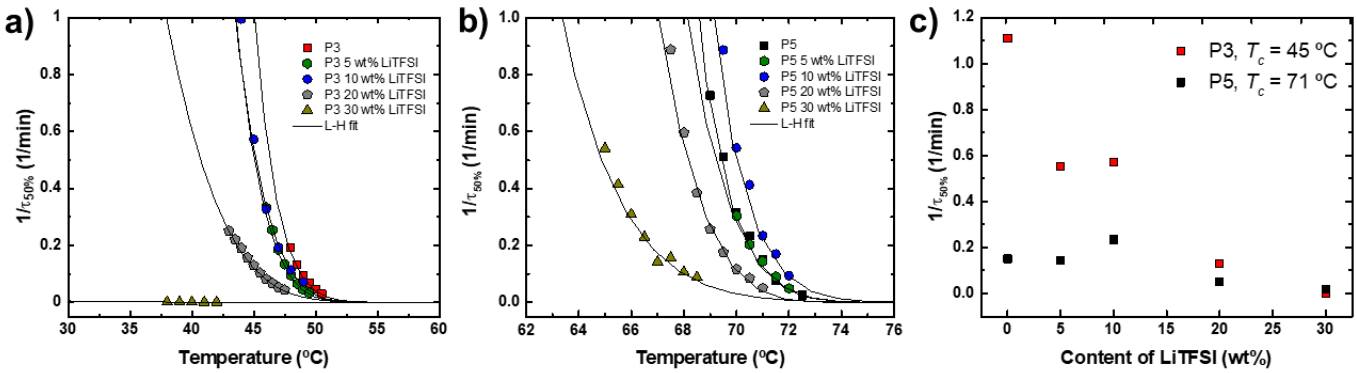

Figure 3.9. (a) Overall crystallization rate (expressed as the inverse of the half-crystallization time) versus isothermal crystallization temperature for P3 and SPEs-P3. (b) Overall crystallization rate (expressed as the inverse of the half-crystallization time) versus isothermal crystallization temperature for P5 and SPEs-P5. Symbols: experimental data. Solid lines are fittings to the Lauritzen and Hoffman theory. (c) Overall crystallization rate (expressed as the inverse of the half-crystallization time) versus the content of LiTFSI at a constant crystallization temperatures (notice that T_c values are different for each series), whose values are indicated in the legend.

3.3.4 Diluent effect of LiTFSI

LiTFSI may act as a solvent that depresses the melting temperature of polyethers [28]. In order to demonstrate if LiTFSI behaves like a low molecular weight diluent, we have employed the Flory-Huggins theory for polymer-diluent mixtures [27,29]. The fundamental equation can be written as:

$$\frac{\frac{1}{T_m}-\frac{1}{T_m^0}}{\upsilon_1}=\frac{R}{\Delta H_u}\frac{V_u}{V_1}\left(1-\frac{BV_1}{R}\frac{\upsilon_1}{T_m}\right) \quad (3.3)$$

where ΔH_u is the melting enthalpy per mole of repeating unit, V_u and V_1 are the molar volumes of the polymer repeating unit and the diluent respectively, υ_1 is the volume fraction of the diluent, B is the interaction energy density character of the polymer-diluent pair, T_m is the apparent melting temperature (taken from the DSC second heating run), and T_m^0 is the equilibrium melting temperature (determined by the Hoffman Weeks extrapolation method). All temperatures are expressed in Kelvin degrees and, R is the gas constant.

Figure 3.10 shows that the plot of $[(1/T_m - 1/T_m^0)/\upsilon_1] \times 10^3$ as a function of $(\upsilon_1/T_m) \times 10^3$ is a straight line. This linear relationship indicates that the Flory-Huggins theory is obeyed for LiTFSI and polyethers (P3-P5) mixtures, or in other words that LiTFSI acts as a diluent for the employed polyethers.

Table 3.2 shows the parameters used and the calculated values for SPE-P3 and SPE-5, after applying the Flory-Huggins theory.

Table 3.2. Calculated data for $(\upsilon_1/T_m) \times 10^3$ versus $[(1/Tm - 1/T_m^0)/\upsilon_1] \times 10^3$

Sample	υ_1	T_m (K)	T_m^0 (K)	$(\upsilon 1/T_m) \times 10^3$	$[(1/Tm - 1/T_m^0)/\upsilon 1] \times 10^3$
P3 5 wt% LiTFSI	0.038	329.78	330.36	0.1154	0.1398
P3 10 wt% LiTFSI	0.077	329.61	330.64	0.2339	0.1225
P3 20 wt% LiTFSI	0.158	327.59	329.02	0.4830	0.0838
P3 30 wt% LiTFSI	0.248	321.22	322.31	0.7587	0.0432
P5 5 wt% LiTFSI	0.038	353.9	354.6	0.1075	0.1423
P5 10 wt% LiTFSI	0.077	353.16	354.2	0.2183	0.1336
P5 20 wt% LiTFSI	0.158	348.28	350.6	0.4843	0.1200
P5 30 wt% LiTFSI	0.248	345.73	348.73	0.7049	0.1021

where T_m is the apparent melting point, T_m^0 is the equilibrium melting temperature, u_1 is the volume fraction of LiTFSI, ΔH_u is the melting enthalpy per mole of repeating unit [27].

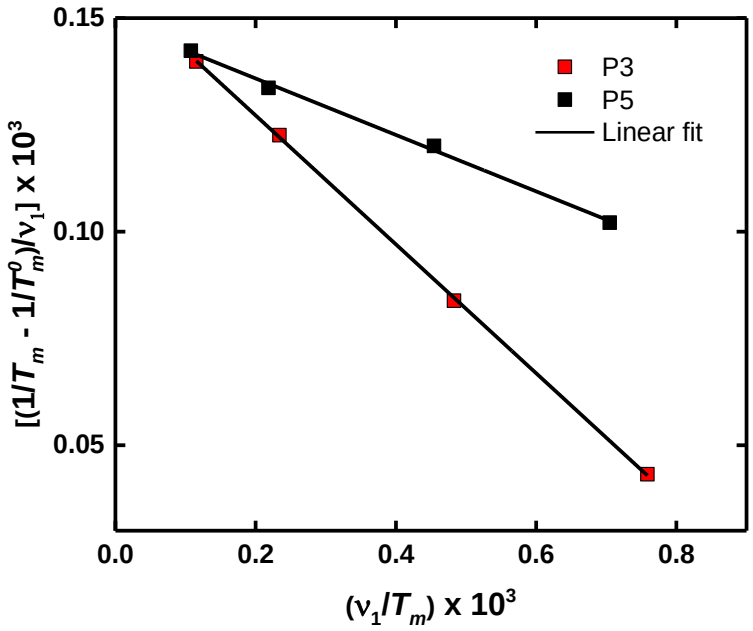

Figure 3.10. Graph of $[(1/T_m - 1/T_m^0)/u_1] \times 10^3$ as a function of $(u_1/T_m) \times 10^3$

From the intercept of the straight line it is possible to obtain the value of ΔH_u, whereas, from the slope, the value of B is determined. It has been demonstrated that the value of ΔH_u is a property of the crystallizing chain repeating unit and does not depend on the nature of the diluent. Therefore, it is a fundamental thermodynamic property of the polyether crystal that is directly related to its chain structure. ΔH_u is, therefore, the enthalpy of melting of a 100% crystalline material expressed as the heat of fusion per repeating unit [27]. The values obtained from Figure 10 for P3 are ΔH_u = 24,741 J mol^{-1} and B = 3.7 J cm^{-3}, and for P5, ΔH_u = 40,300 J mol^{-1} and B = 48 J cm^{-3}. The value of ΔH_u for P3 is similar to that reported in the literature [27], i.e., 23,640 J mol^{-1}.

In the case of P5, the value of the equilibrium melting temperature and equilibrium melting enthalpy are reported in this work for the first time, as far as the authors are aware. Figure 3.11 shows the data of some polyethers reported

in the literature [27] and the experimental values obtained here by the application of the Flory-Huggins theory to our data. It can be seen that the values of ΔH_u increase with the number of -CH_2- and in the case of P3 (6 methylene units) our value is very similar to that reported in the literature, as already mentioned. In addition, the value for P5 (10 methylene units) follows the expected trend.

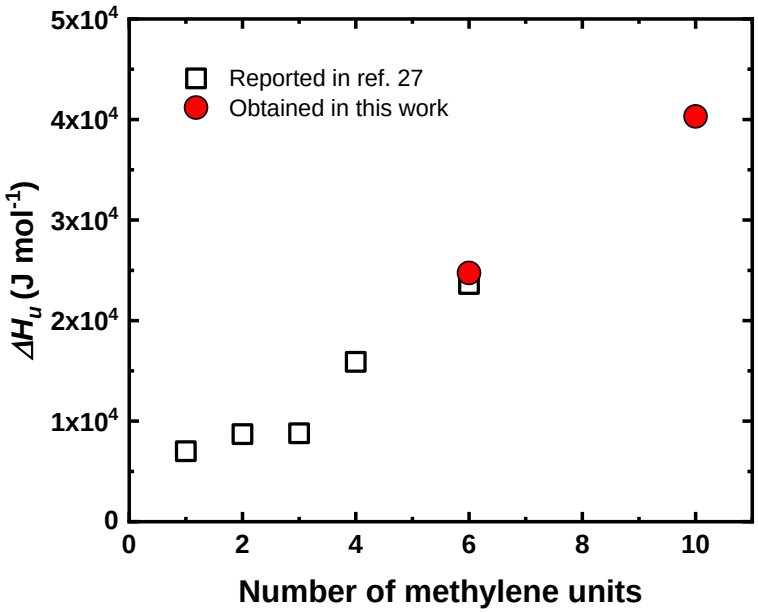

Figure 3.11. ΔH_u values of polyethers as a function of the number of methylene units in the repeating unit. The black points are values reported in the literature [27] and the red points are the values obtained in this work.

The value of *B* is related to the polymer-diluent interaction, and therefore it depends on the chemical structure of the diluent component. The different slopes that are observed in Figure 3.10 reflect differences in the Flory-Huggins interaction parameters for the mixtures. The Flory-Huggins polymer-diluent interaction parameter (χ_1) can be expressed as [29]:

$$\chi 1 = \kappa 1 - \psi 1 + 1/2 \tag{3.4}$$

where κ_1 and ψ_1 are enthalpic and entropic parameters related to the partial molar enthalpy $\Delta H_1 = RT\ \kappa_1 \upsilon_2^2$ and the partial molar entropy $\Delta S_1 = RT\ \psi_1\ \upsilon_2^2$. The enthalpic term can also be represented as:

$$\kappa 1 = BV1 / RT \quad (3.5)$$

As can be seen from the above equations, B is directly proportional to the enthalpic contribution (κ_1) to the Flory-Huggins parameter χ_1. The lower the value of χ_1, the higher is the thermodynamic interaction between the polymer and the diluent. The B values obtained from Figure 8 are B = 3.7 J cm^{-3} for P3, and B = 48 J cm^{-3} for P5. Therefore, LiTFSI is a better solvent for P3 than for P5, an expected result based on the chemical structure of P3 and P5, as the polarity degree within the polyether molecules decreases as the number of methylene units increases along the repeating unit. From the application of the Flory-Huggins theory, we can extrapolate the results to conclude that small values of B are necessary to increase the ionic conductivity.

3.4 Conclusions

In this chapter the impact of the chemical structure of aliphatic polyethers and salt concentration on crystallization rate, crystallization temperature, and ionic conductivity has been investigated. As a general observation, the LiTFSI salt acts as a diluent for all the aliphatic polyethers, reducing the crystallization rate and crystallization temperature. The ionic conductivities of the SPEs were obtained in the order of 10^{-8}-10^{-4} S cm^{-1} at 70 ºC. A higher number of methylene units in the polyether repeating unit causes a decrease in the ionic conductivity of the SPEs in the following order PEO (P1)> P(THF) (P2)> poly(oxyhexamethylene) (P3) > poly(oxyoctomethylene) (P4)> poly(oxydecamethylene) (P5)> poly(oxydodecamethylene) (P6) with 30 wt% of LiTFSI. The reason of this behavior is probably due to the decreasing solvation of lithium atoms in the same order. Additionally, as salt concentration increases, both crystallization temperature and melting enthalpies of the SPE-P3 and SPE-P5 were found to decrease. By applying the Flory-Huggins theory, we demonstrate that LiTFSI acts as a thermodynamic diluent for the polyethers examined. The interaction energy parameter (*B*) was calculated for SPEs prepared with P3 and P5. We show that the value of *B* must be small to obtain high ionic conductivity electrolytes. In the case of the poly(oxydecamethylene),

the value of the equilibrium melting temperature and equilibrium melting enthalpy are reported in this work for the first time.

3.5 References

[1] L. Porcarelli, C. Gerbaldi, F. Bella, J.R. Nair, Super Soft All-Ethylene Oxide Polymer Electrolyte for Safe All-Solid Lithium Batteries, Scientific Reports. 6 (2016) 19892. https://doi.org/10.1038/srep19892.

[2] E. Paillard, F. Alloin, L. Cointeaux, C. Iojoiu, J.Y. Sanchez, Poly(oxyethylene) electrolytes based on lithium nitrophenyl sulfonamide and hexanitrodiphenylamide, Electrochimica Acta. 57 (2011) 20–26. https://doi.org/10.1016/j.electacta.2011.05.006.

[3] A. Thiam, C. Antonelli, C. Iojoiu, F. Alloin, J.Y. Sanchez, Optimizing ionic conduction of poly(oxyethylene) electrolytes through controlling the cross-link density, Electrochimica Acta. 240 (2017) 307–315. https://doi.org/10.1016/j.electacta.2017.04.046.

[4] S.B. Aziz, T.J. Woo, M.F.Z. Kadir, H.M. Ahmed, A conceptual review on polymer electrolytes and ion transport models, Journal of Science: Advanced Materials and Devices. 3 (2018) 1–17. https://doi.org/10.1016/j.jsamd.2018.01.002.

[5] L. Meabe, T.V. Huynh, N. Lago, H. Sardon, C. Li, L.A. O'Dell, M. Armand, M. Forsyth, D. Mecerreyes, Poly(ethylene oxide carbonates) solid polymer electrolytes for lithium batteries, Electrochimica Acta. 264 (2018) 367–375. https://doi.org/10.1016/j.electacta.2018.01.101.

[6] J. Mindemark, M.J. Lacey, T. Bowden, D. Brandell, Progress in Polymer Science Beyond PEO — Alternative host materials for Li + -conducting solid polymer electrolytes, Progress in Polymer Science. 81 (2018) 114–143. https://doi.org/10.1016/j.progpolymsci.2017.12.004.

[7] Z. Xue, D. He, X. Xie, Poly(ethylene oxide)-based electrolytes for lithium-ion batteries, Journal of Materials Chemistry A. 3 (2015) 19218–19253.

https://doi.org/10.1039/c5ta03471j.

[8] O.E. Geiculescu, J. Yang, S. Zhou, G. Shafer, Y. Xie, J. Albright, S.E. Creager, W.T. Pennington, D.D. DesMarteau, Solid Polymer Electrolytes from Polyanionic Lithium Salts Based on the LiTFSI Anion Structure, Journal of The Electrochemical Society. 151 (2004) A1363. https://doi.org/10.1149/1.1773581.

[9] Y. Zhao, R. Tao, T. Fujinami, Enhancement of ionic conductivity of PEO-LiTFSI electrolyte upon incorporation of plasticizing lithium borate, 51 (2006) 6451–6455. https://doi.org/10.1016/j.electacta.2006.04.030.

[10] B.K. Choi, Y.W. Kim, Thermal history effects on the ionic conductivity of PEO-salt electrolytes, Materials Science and Engineering: B. 107 (2004) 244–250. https://doi.org/10.1016/j.mseb.2003.09.047.

[11] E. Quartarone, P. Mustarelli, A. Magistris, PEO-based composite polymer electrolytes, 110 (1998) 1–14.

[12] M. Marzantowicz, J.R. Dygas, F. Krok, A. Łasińska, Z. Florjańczyk, E. Zygadło-Monikowska, A. Affek, Crystallization and melting of PEO:LiTFSI polymer electrolytes investigated simultaneously by impedance spectroscopy and polarizing microscopy, Electrochimica Acta. 50 (2005) 3969–3977. https://doi.org/10.1016/j.electacta.2005.02.053.

[13] S.J. Park, A.R. Han, J.S. Shin, S. Kim, Influence of crystallinity on ion conductivity of PEO-based solid electrolytes for lithium batteries, Macromolecular Research. 18 (2010) 336–340. https://doi.org/10.1007/s13233-010-0407-2.

[14] D.R. Sadoway, Block and graft copolymer electrolytes for high-performance, solid-state, lithium batteries, Journal of Power Sources. 129 (2004) 1–3. https://doi.org/10.1016/j.jpowsour.2003.11.016.

[15] T. Niitani, M. Shimada, K. Kawamura, K. Kanamura, Characteristics of new-type solid polymer electrolyte controlling nano-structure, Journal of Power Sources. 146 (2005) 386–390. https://doi.org/10.1016/j.jpowsour.2005.03.102.

[16] J.F. Snyder, R.H. Carter, E.D. Wetzel, Electrochemical and mechanical behavior in mechanically robust solid polymer electrolytes for use in multifunctional structural batteries, Chemistry of Materials. 19 (2007) 3793–3801. https://doi.org/10.1021/cm070213o.

[17] M.M. Borgohain, T. Joykumar, S. V. Bhat, Studies on a nanocomposite solid polymer electrolyte with hydrotalcite as a filler, Solid State Ionics. 181 (2010) 964–970. https://doi.org/10.1016/j.ssi.2010.05.040.

[18] L.H. Sim, C.H. Chan, N.H.A. Nasir, The effect of molecular mass of PEO and the salt content on its isothermal crystallization behaviour for PEO:LiClO4electrolyte, AIP Conference Proceedings. 1250 (2010) 201–204. https://doi.org/10.1063/1.3469636.

[19] Y. Zhang, H. Huo, J. Li, Y. Shang, Y. Chen, S.S. Funari, S. Jiang, Crystallization behavior of poly(ε-caprolactone) and poly (ε-caprolactone)/LiClO4complexes from the melt, CrystEngComm. 14 (2012) 7972–7980. https://doi.org/10.1039/c2ce25126d.

[20] A. Basterretxea, E. Gabirondo, C. Jehanno, H. Zhu, I. Flores, A.J. Müller, A. Etxeberria, D. Mecerreyes, O. Coulembier, H. Sardon, Polyether Synthesis by Bulk Self-Condensation of Diols Catalyzed by Non-Eutectic Acid–Base Organocatalysts, ACS Sustainable Chemistry & Engineering. 7 (2019) 4103–4111. https://doi.org/10.1021/acssuschemeng.8b05609.

[21] A. Das, A.K. Thakur, K. Kumar, Exploring low temperature Li+ion conducting plastic battery electrolyte, Ionics. 19 (2013) 1811–1823. https://doi.org/10.1007/s11581-013-0898-x.

[22] Z.S. Wang, H. Kawauchi, T. Kashima, H. Arakawa, Significant influence of TiO2 photoelectrode morphology on the energy conversion efficiency of N719 dye-sensitized solar cell, Coordination Chemistry Reviews. 248 (2004) 1381–1389. https://doi.org/10.1016/j.ccr.2004.03.006.

[23] C. Tao, M.H. Gao, B.H. Yin, B. Li, Y.P. Huang, G. Xu, J.J. Bao, A promising TPU/PEO blend polymer electrolyte for all-solid-state lithium ion batteries, Electrochimica Acta. 257 (2017) 31–39. https://doi.org/10.1016/j.electacta.2017.10.037.

[24] J. Luo, A.H. Jensen, N.R. Brooks, J. Sniekers, M. Knipper, D. Aili, Q. Li, B. Vanroy, M. Wübbenhorst, F. Yan, L. Van Meervelt, Z. Shao, J. Fang, Z.H. Luo, D.E. De Vos, K. Binnemans, J. Fransaer, 1,2,4-Triazolium perfluorobutanesulfonate as an archetypal pure protic organic ionic plastic crystal electrolyte for all-solid-state fuel cells, Energy and Environmental Science. 8 (2015) 1276–1291. https://doi.org/10.1039/c4ee02280g.

[25] A.T. Lorenzo, M.L. Arnal, J. Albuerne, A.J. Müller, DSC isothermal polymer crystallization kinetics measurements and the use of the Avrami equation to fit the data: Guidelines to avoid common problems, Polymer Testing. 26 (2007) 222–231. https://doi.org/10.1016/j.polymertesting.2006.10.005.

[26] A.T. Müller, Alejandro J., Michell, R. M., Lorenzo, Isothermal Crystallization Kinetics of Polymers, in: Q. Guo (Ed.), Polymer Morphology: Principles, Characterization, and Processing, John Wiley & Sons, 2016: pp. 181–203. https://doi.org/https://doi.org/10.1002/9781118892756.ch11.

[27] L. Mandelkern, Crystallization of Polymers, 2nd ed. Vo, Cambridge University Press, Cambridge, United Kingdom, 2002.

[28] T.P. Gumede, A.S. Luyt, R.A. Pérez-Camargo, A.J. Müller, The influence of paraffin wax addition on the isothermal crystallization of LLDPE, Journal of Applied Polymer Science. 134 (2017) 1–7. https://doi.org/10.1002/app.44398.

[29] P.J. Flory, Principles of polymer chemistry, Cornell University Press, 1953.

Chapter IV

4. Polyether single and double crystalline blends and the effect of lithium salt on their crystallinity and ionic conductivity

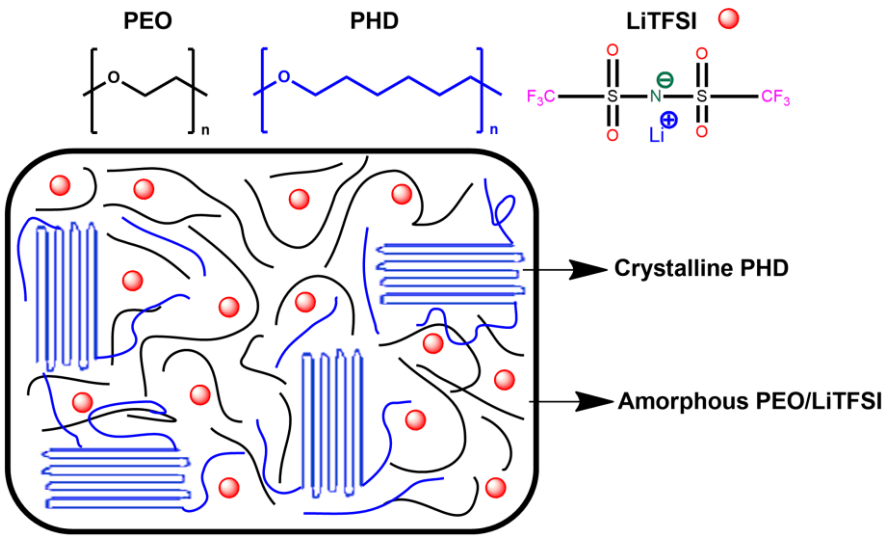

4.1 Abstract

In this chapter, blends of Poly(ethylene oxide), PEO, and poly(1,6-hexanediol), PHD, were prepared in a wide composition range. They were examined by Differential Scanning Calorimetry (DSC), Polarized Light Optical Microscopy (PLOM), and Wide Angle X-ray Scattering (WAXS). Based on the results obtained, the blends were partially miscible in the melt and their crystallization was a function of miscibility and composition. Crystallization triggered phase separation. In blends with higher PEO contents both phases were able to crystallize due to the limited miscibility in this composition range. On the other hand, the blends with higher PHD contents display higher miscibility and therefore, only the PHD phase could crystallize in them. A nucleation effect of the PHD phase on the PEO phase was detected, probably caused by a transference of impurities mechanism.

Since PEO is widely used as electrolyte in lithium batteries, the PEO/PHD blends were studied with lithium bis(trifluoromethanesulfonyl) imide (LiTFSI), and the effect of Li-salt concentration was studied. We found that the lithium salt preferentially dissolves in the PEO phase without significantly affecting the PHD component. While the Li-salt reduced the spherulite growth rate of the PEO phase within the blends, the overall crystallization rate was enhanced because of the strong nucleating effect of the PHD component.

The ionic conductivity was also determined for the blends with LiTFSI. At high temperatures (>70 °C), the conductivity is in the order of ~10^{-3} S cm^{-1}, and as the temperature decreases, the crystallization of PHD was detected. This improved the self-standing character of the blend films at high temperatures as compared to the one of neat PEO.

J.L. Olmedo-Martínez, M. Pastorio, E. Gabirondo, A. Lorenzetti, H. Sardon, D. Mecerreyes, A.J. Müller, Polyether Single and Double Crystalline Blends and the Effect of Lithium Salt on Their Crystallinity and Ionic Conductivity, Polymers. 13 (2021) 2097.

4.2 Introduction

Aliphatic polyethers are a broad class of polymers, nowadays used in a wide range of fields [1]. However, their industrial applications are limited to short-chain aliphatic polyethers. Commercially available short-chain aliphatic polyethers such as polyethylene oxide (PEO), polypropylene oxide (PPO) or polytetrahydrofuran (PTHF) are industrially obtained by ring-opening polymerization [2–4]. Recently, a sustainable route for the synthesis of medium- to long-chain aliphatic polyethers has been reported [5]. This synthetic method open the possibility of tuning the length of the aliphatic chain of polyethers, preparing different copolymers and fine tuning of their T_m and crystallinity [5–7].

One of the actual applications of PEO is as solid polymer electrolytes (SPEs) for lithium batteries of electric vehicles [8]. Polyethylene oxide (PEO) stands out as the main host polymer for polymer electrolytes, due to its excellent capability to dissolve lithium salts and because it exhibits high ionic conductivity values at relatively high temperatures (>70 °C) [9–11]. In particular, the polyethylene oxide (PEO)/lithium bis(trifluoromethanesulfonyl) imide (LiTFSI) system has been widely studied because of the high dissociation and plasticizing abilities of LiTFSI, that lead to better ionic conductivities compared to other salts [12,13]. However, the high crystallinity and the low mechanical strength of PEO are still issues to be improved [14]. Specifically, the crystallization limits the ionic conductivity due to the reduction of amorphous conductivity pathways caused by the spherulitic growth [15]. Many strategies have been attempted to improve the comprehensive performance of PEO-based electrolytes, such as: filler addition (e.g., nanoparticles [16,17]), synthesis of PEO copolymers (random, block [18] or graft [19]), crosslinking [20] or blending techniques [14,21,22]. In particular, blending can suppress crystallization, increasing the percentage of the amorphous phase, and as a result, the ionic conductivities of polymer electrolytes are improved. Compared to copolymerization of PEO, polymer blending technique is convenient, efficient, and low cost. Indeed, the main advantages of polymer electrolytes prepared via blending method are the simplicity of preparation and easy control of physical properties by compositional change, overcoming the serious drawback of preparing electrolytes by nontrivial synthesis methods, which are not very suitable for practical applications.

For this reason, different polymer blends have been studied to improve a specific property, for example, polycarbonates and polyesters [23–25], due their high anodic stability. Recently, Gao et al. reported a system polyether (PEO)/ poly(ether-acetal) (poly (1,3,6-trioxocane)) with LiTFSI; they showed that these polymers are miscible and, depending on the amount of LiTFSI in the blend, it is possible to obtain immiscible or miscible blends when a critical value is exceeded [26]. When obtaining completely miscible blends, the charge transport is favored.

Previously in our research group it was found that LiTFSI acts as a diluting agent for polyethers [27]. This is, of course, good for the improvement of the ionic conductivity, but it can compromise the mechanical properties of PEO due to the loss of crystallinity and self-standing character. In this article, a ternary PEO/PHD/LiTFSI system is studied, since both polymers present ionic conductivity when LiTFSI is added [27]. The goal of this article is to investigate the polyether blending and the ionic conductivity and its effect on the crystallinity of the individual homopolymers.

4.3 Results

4.3.1 Non-isothermal DSC of PEO/PHD blends

PEO/PHD blends were studied in the whole composition range to explore their miscibility and crystallization behaviour. One of the first clues that indicate miscibility between two polymers is the appearance of a single glass transition temperature (T_g). However, in this case, both polymers show low T_g (e. g. PEO ≈ -60 °C [28]) and are highly crystalline. For this reason, determining their T_g by DSC is difficult, as the change in specific heat is too small. Nevertheless, the DSC can provide valuable information via the crystallization and melting of the samples.

The non-isothermal DSC runs were carried out at 20 °C min^{-1}. In Figure 4.1, the experimental curves have been superimposed to scans that were denoted “theoretical”. They were calculated from the experimental DSC scans of the neat homopolymers, they were multiplied by their weight fraction in the blends and then added. In this way, these theoretical curves give an idea of how the

DSC traces should appear when there is no interaction whatsoever between the blend components.

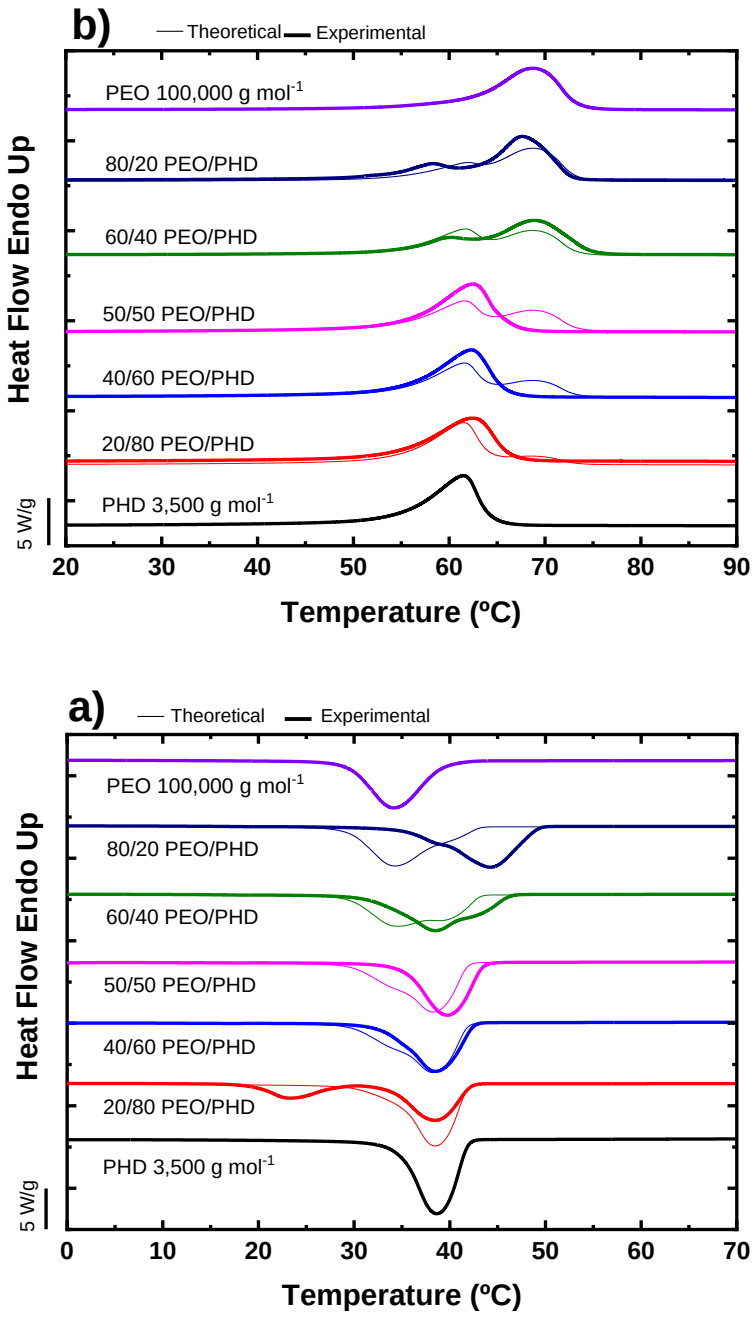

Figure 4.1. PEO/PHD blends: a) DSC cooling scans at 20 °C min^{-1} and subsequent DSC heating scans at 20 °C min^{-1}.

The presence of a double peak in Figure 4.1 indicates that phase separation takes place, while the presence of a single peak in the middle of the neat polymers could, in principle, indicate a single crystalline phase. Focusing on

the neat components, the T_m of PEO is higher than that of the PHD, while the opposite situation is observed in their crystallization temperatures. This is a result of different heterogeneity contents, as this parameter can influence the T_c. On the other hand, T_m is proportional to the lamellar thickness of the crystalline phase (and chemical structure) [29] that is formed, while T_c depends on chemical structure and nucleation density.

Figure 4.1a shows the DSC cooling scans from the melt and Figure 1b the subsequent second heating scans. WAXS experiments for the same samples after cooling from the melt at 20 °C min^{-1} can be observed in Figure 4.2 and will be discussed below. According to Figure 4.2, in the PEO/PHD blends that are rich in PHD, i.e., 20/80 and 40/60, the only component capable of crystallization is the PHD. This is interesting as it demonstrates that when the blends contain a majority of PHD the crystallization of the PEO phase is hindered and this can be interpreted as a sign of blend miscibility. The 20/80 PEO/PHD blend exhibits two crystallization peaks during cooling from the melt that, according to WAXS are both due to PHD crystals. This is an uncommon behaviour as fractionated crystallization is normally associated with the minor component in blends [30]. Therefore, this peculiar behaviour merits future studies that are outside the scope of the present contribution.

The blends with PEO contents of 50 wt% and higher are all double crystalline blends, as demonstrated by WAXS in Figure 4.2. This means that two crystalline phases are formed, and according to Figure 4.2, the crystalline structure does not change with blend composition (there are no changes in the WAXS reflections). This means that once crystallization starts, phase separation is triggered, and within each crystalline phase, the second blend component is completely excluded from the crystals of the component that is crystallizing.

There is a clear nucleating effect of PHD on the PEO phase, as the crystallization peak for PEO shifts to higher temperatures. This nucleation effect is responsible for the overlap of both crystallization peaks for the 50/50 PEO/PHD into a single peak. The melting of this 50/50 blend occurs, displaying a single endothermic peak at temperatures slightly higher than the melting peak of neat PHD, but we know by WAXS (Figure 4.2) that both phases crystallize separately (they do not share the same crystal lattice). Hence, the single melting peak in

Figure 4.1b corresponding to the 50/50 PEO/PHD is due to a coincident melting process of both crystalline phases.

For the 80/20 PEO/PHD blend, the largest crystallization peak in Figure 4.1a (which should correspond to the PEO phase) is clearly shifted towards higher temperatures. This may suggest that the PHD minor phase acts as a nucleating agent for the main phase (PEO). Since heterogeneous nucleation takes place on a solid phase, this could be due to a transfer of impurities (e.g., polymerization catalyst) present in the PHD phase to the PEO phase. This has already been demonstrated for other blends (e. g., iPP/PS blends [31]). Another possibility that explains this behavior is that the amorphous PHD (in the molten state) may be acting as a nucleating agent for the PEO. This phenomenon has already been observed for other systems in which an amorphous polymer acts as a nucleating agent for a semi-crystalline polymer, for example, atactic polystyrene for polypropylene [32], or poly(vinyl butyral) for poly(butylene succinate) [33].

Both PEO rich blends, i.e., 80/20 and 60/40 PEO/PHD, exhibit clear double endothermic peaks in Figure 4.1b corresponding to the melting of the PHD crystalline phase and the PEO crystalline phase. The differences between the theoretical and experimental blends indicate that the blends are at least partially miscible with most probably an asymmetrical phase diagram, whose precise determination is outside the scope of the present work. Clearly, the miscibility is higher for the blends with larger contents of PHD and limited for blends with higher PEO contents.

4.3.2 Wide Angle X-ray Scattering of PEO/PHD blends

The WAXS study was carried out for the blends to determine if there are any changes in the crystal structure of the neat polymers when mixed. In Figure 2, the diffraction patterns of the polymers and blends at 25 °C are presented. The samples were first heated to the melt and then cooled at 20 °C min^{-1} to reproduce similar conditions to the samples in Figure 4.1a.

The reflections of neat PEO are observed at 19.4° and 23.45°, which are assigned to the (120) and (112) planes respectively [34–36], and the reflections

of neat PHD are presented at 19.85° and 24.29°, and are assigned to the (020) and (110) planes respectively [37,38]. The blends 80/20, 60/40, 50/50 PEO/PHD show the peaks of both crystalline structures without any changes in the 2θ angles, which indicates the two phases crystallize separately and without any modification of the crystalline structure of the neat blend components. On the other hand, in the 40/60 and 20/80 PEO/PHD blends, only the characteristic reflections for PHD are presented, which suggests that the presence of PHD prevents the crystallization of PEO in the blends, possibly because the blends exhibit miscibility in the melt state.

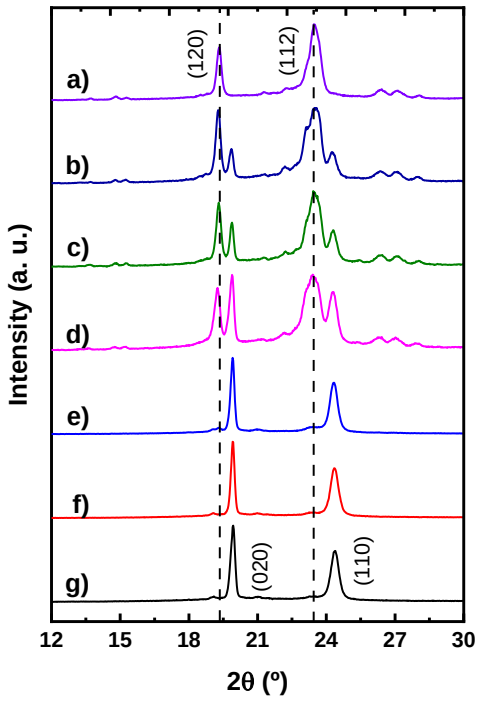

Figure 4.2. WAXS diffractograms of PEO/PHD blends. a) Neat PEO, b) 80/20 PEO/PHD, c) 60/40 PEO/PHD, d) 50/50 PEO/PHD, e) 40/60 PEO/PHD, f) 20/80 PEO/PHD, g) Neat PHD.

4.3.3 Morphology and Crystal growth rate

The morphology and spherulitic growth rate were analyzed by polarized light optical microscopy (PLOM). With this technique, it is possible to measure the isothermal growth of spherulites from the melt in samples that do not have a very large nucleation density. Figure 4.3a and 4.3b show that PEO forms large spherulites, while PHD forms small axialites with high nucleation density. The

superstructures growth rate (e.g., spherulites or axialites) depends on a competition between secondary nucleation and diffusion [39,40].

Figure 4.3 shows the PLOM images for the neat homopolymers and three different compositions, obtained at 40 °C. Neat PEO presents as expected large negative spherulites (Figure 4a), while PHD crystallizes in small axialites (Figure 4.3b). The composition 80/20 PEO/PHD (Figure 4.3c), shows a larger number of the PEO phase spherulites as compared with neat PEO, confirming the nucleation effect of PHD addition reported in Figure 4.1a. The presence of very small PHD phase axialites can also be observed. Figure 4.3d presents the morphology of the 50/50 PEO/PHD blend, where PEO phase larger spherulites can be clearly seen. Some small PHD phase axialites are also observed, indicating that both phases can crystallize. These results for the 80/20 and 50/50 PEO/PHD blends show that both components are able to crystallize under isothermal conditions and are consistent with DSC and WAXS results taken after non-isothermal crystallization.

Finally, for the 20/80 PEO/PHD blend, Figure 4.3e shows that although most of the optical view field is filled with PHD phase axialites, there are some large birefringent structures that are probably constituted by the PEO phase. This is an unexpected observation, as in Figure 4.1 (and Figure 4.2), this sample under non-isothermal conditions has a different behaviour, as only the PHD phase is able to crystallize. Apparently, under isothermal conditions, and given enough time, both phases can eventually crystallize. Nevertheless, as the majority of the sample crystallizes with very small PHD phase axialites, growth rate measurements proved to be impossible.

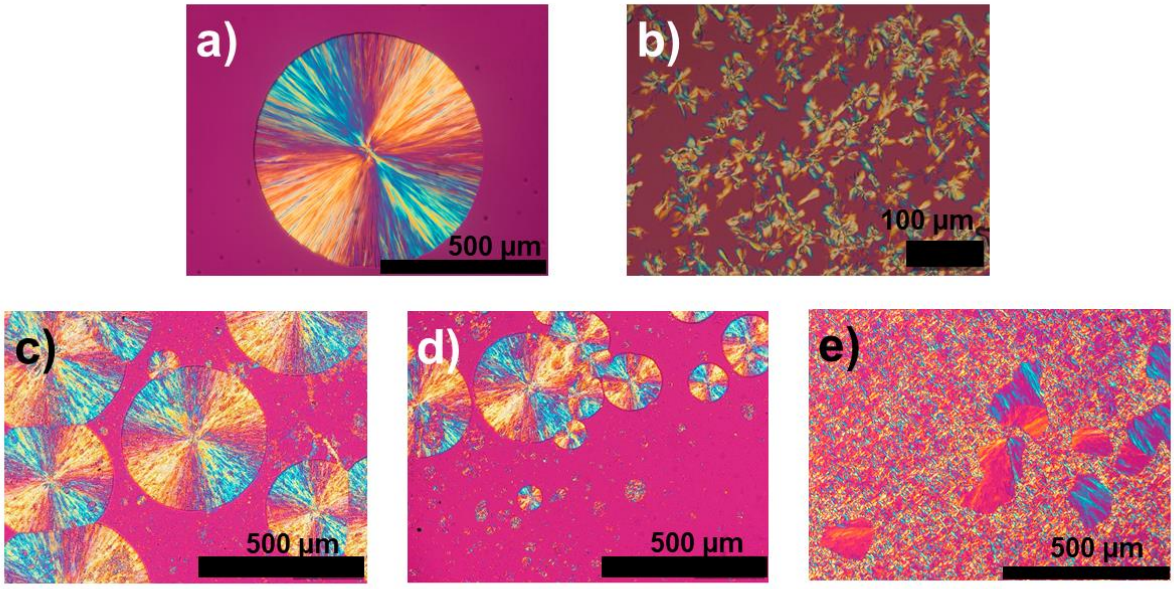

Figure 4.3. PLOM micrographs obtained during isothermal crystallization at 40 °C. a) PEO, b) PHD, c) 80/20 PEO/PHD blend, d) 50/50 PEO/PHD blend, and e) 20/80 PEO/PHD.

The spherulitic growth rate measurements were possible only for neat PEO and the PEO-rich compositions (80/20 and 50/50 PEO/PHD) but not for the rest of the samples, as their nucleation density was too high.

Figure 4.4 shows the spherulitic growth rate as a function of temperature and the solid lines are fits to the Lauritzen and Hoffman theory [41,42], see also the SI. The spherulitic growth rate of the 80/20 PEO/PHD blend matches perfectly with that of neat PEO, a result that indicates immiscibility between the two components for this composition. This result is in line with the DSC melting curves of Figure 1b that show a similar behaviour between the experimental and the theoretical immiscible blend DSC heating scans.

On the other hand, Figure 4.4 also shows the spherulitic growth rate versus temperature for the 50/50 PEO/PHD blend, where a clear decrease in the PEO phase growth rate is observed with respect to neat PEO. This result can be taken as evidence of miscibility between PEO and PHD components, because if they were immiscible, no change in the PEO spherulites growth rate would be expected.

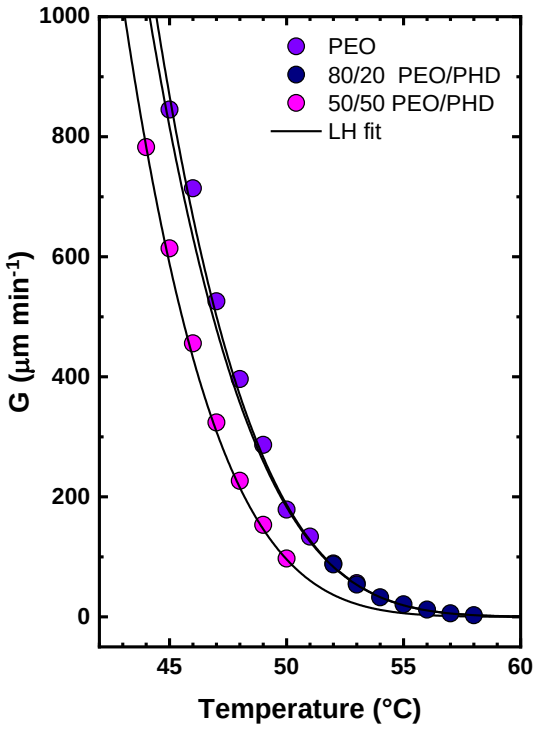

Figure 4.4. Spherulitic growth rate (G) as a function of isothermal crystallization temperature for neat PEO and for the PEO component of the 80/20 and 50/50 PEO/PHD blends.

4.3.4 Non-isothermal DSC of PEO/PHD blends with LiTFSI

LiTFSI salt was added to the 80/20 PEO/PHD blend to evaluate the effect of this salt on the crystallization. In previous work, we demonstrated that LiTFSI acts as a diluent agent that depresses the T_m in these polyethers [27]. Figure 4.5a shows cooling scans from the melt for the 80/20 PEO/PHD blend with different concentrations of LiTFSI (10, 20 and 30 wt% LiTFSI).

In the 80/20 PEO/PHD blend without salt, one main crystallization peak is observed, which results from the crystallization of the PEO phase. It is also possible to observe a low temperature shoulder that corresponds to the crystallization of the PHD phase. Upon salt addition, the T_c of the PEO phase decreases as a function of the LiTFSI concentration (see the arrow that guides the eye in Figure 4.5a), whereas the T_c of the PHD phase remains constant (approx. at 40 °C, see the dashed vertical line in Figure 4.5a). The same effect is observed in the fusion behaviour shown during the second DSC heating scans

(see Figure 4.5b), where the T_m values of the PEO phase decreases (see the arrow that guides the eye in Figure 4.5b) while the T_m value of the PHD phase remains constant at 58 °C (see the vertical dashed line in Figure 4.5b). The above described trends of T_m as a function of salt content can be clearly observed in Figures 4.5c and 4.5d, respectively.

The results shown in Figure 4.5 indicate that the lithium salt prefers to dissolve in the PEO phase rather than in the PHD phase within the 80/20 PEO/PHD blend. This is also corroborated by the decrease in the enthalpies of crystallization and melting of the PEO phase as the salt concentration increases, while those of the PHD phase do not seem to be altered (although the overlapping of signals makes this observation difficult). The behaviour of this blend with lithium salt could be a good solution to the mechanical stability problems that these type of electrolytes present for lithium batteries, as even at high lithium concentrations, the PHD phase remains semi-crystalline, while the PEO/lithium phase becomes fully amorphous at 30% lithium loadings.

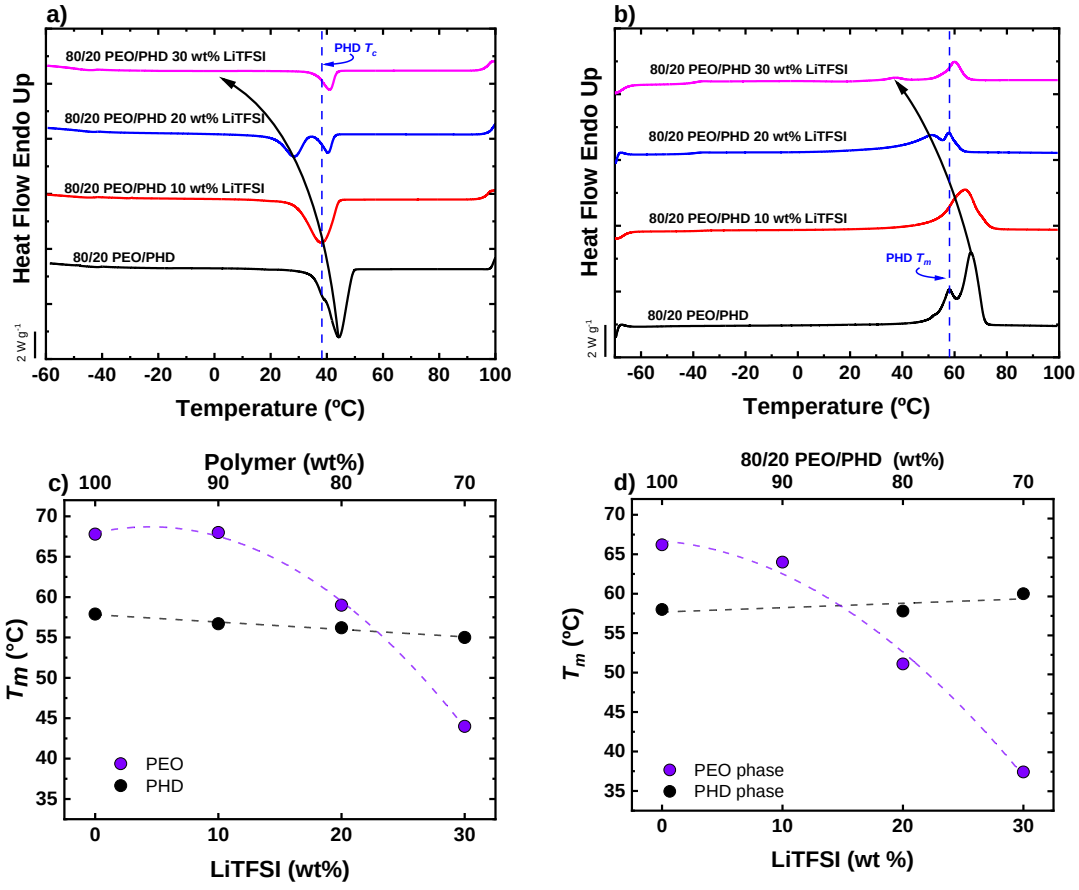

Figure 4.5. DSC for the PEO/PHD blends: a) during cooling from the melt, b) subsequent melting scans, c) change in T_m for the PEO and PHD homopolymers as a function of LiTFSI concentration, d) change in T_m for the PEO and PHD phases within the 80/20 PEO/PHD as a function of LiTFSI concentration.

4.3.5 Isothermal crystallization studies of the PEO/PHD blends with LiTFSI

The spherulitic growth rate was measured for the 80/20 PEO/PHD blend with LiTFSI, but it was only possible to measure the blend with 10 wt% LiTFSI, because there is very high nucleation density with higher amounts of salt and it is not possible to follow the growth of the very small spherulites that quickly impinged on one another. In the SI some PLOM images are shown for PEO and PHD with 20 wt% LiTFSI samples.

Figure 4.6a shows the spherulitic growth rate as a function of crystallization temperature, and the solid lines represent the Lauritzen-Hoffman equation fit. The general trend is that the spherulitic growth rates of neat PEO and the PEO phase within the 80/20 PEO/PHD blend decrease with LiTFSI addition, although the decrease in much higher in the blend. This is because the salt prefers to dissolve in the PEO phase, and, consequently, the LiTFSI concentration in PEO is higher in the blend than in neat PEO.

Isothermal crystallization studies by DSC take into account both nucleation and growth of crystals. Figure 4.6b shows the inverse of the half-crystallization time ($1/\tau_{50\%}$), which represents the overall crystallization rate, as a function of crystallization temperature (T_c), for PEO, PHD, and PEO/PHD blends with 20 wt% LiTFSI. This salt concentration was selected in order to have a clearer comparison of the effect of the salt in the blends.

It is observed that the homopolymers with salt exhibit the lowest values of overall crystallization rates. The blends, however, experience a large increase in overall crystallization as the amount of PEO in the blends increases. As indicated in Figure 6a, the spherulitic growth rate decreases with 10% salt addition. We speculate that this decrease should be equal to or higher with 20% salt addition. Therefore, the synergistic increase in overall crystallization rate shown in Figure 6b when 20% LiTFSI is added to the blends must be due to a very large nucleation effect that offsets the crystal growth rate retardation. The nucleation

effect could be due to the transfer of impurities from the PHD phase to the PEO phase.

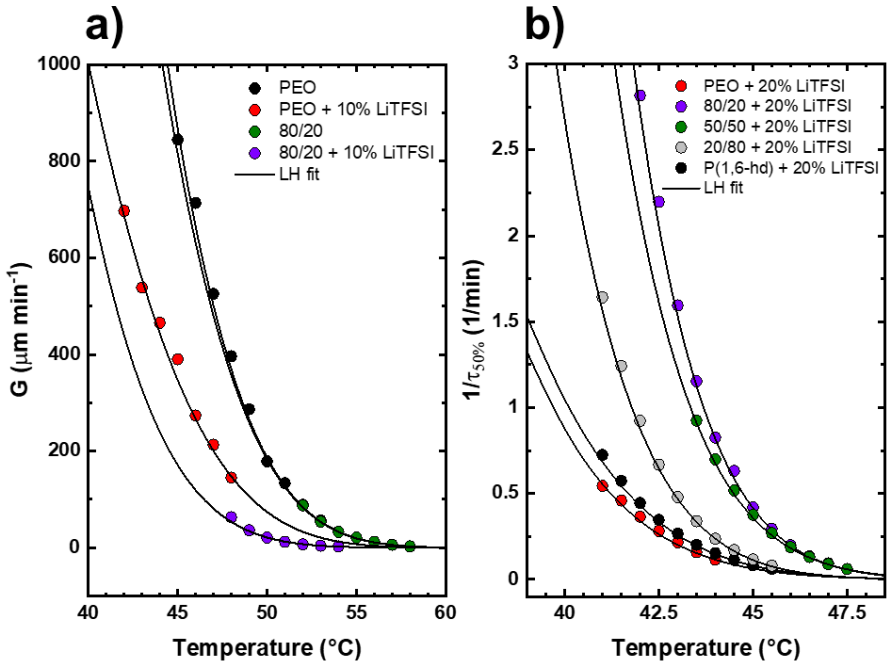

Figure 4.6. a) Spherulitic growth rate of PEO and 80/20 PEO/PHD blends with and without 10% LiTFSI, b) Overall crystallization rate of homopolymers and blends with 20 wt% LiTFSI.

4.3.6 Ionic conductivity

Ionic conductivity is a very important parameter for the use of SPEs, ionic conductivity in polymers takes place in the amorphous phase, and the crystalline phase restricts ionic conductivity [24,43,44]. For this reason, amorphous systems are normally used for this application.

The ionic conductivity was measured by Electrochemical Impdeance Spectroscopy (EIS) for the 80/20 PEO/PHD blends with 20 and 30 wt% LiTFSI, and the values were compared to those obtained with those for neat PEO with salt. Figure 4.7 shows the values of ionic conductivity as a function of temperature for the different blends. PEO presents the highest value of ionic conductivity with 30 wt% LiTFSI, $1.1 \cdot 10^{-3}$ S cm^{-1} at 70 °C. It should be recalled that with such a high salt concentration, PEO does not crystallize and remains amorphous over the entire range of temperatures where the measurements were performed. Furthermore, it is important to note that, with 20 wt% LiTFSI, PEO can crystallize

(although up to a small degree) and therefore presents a small drop in conductivity values in the temperature range where it crystallizes.

In the PEO/PHD blends, there is a drop in the conductivity values at 40 °C (Figure 4.7), which is the temperature at which PHD begins to crystallize. These results are consistent to those obtained by DSC (Figure 4.5). Besides, adding 20 or 30 wt% LiTFSI makes no difference in the ionic conductivity of the polymer blend, perhaps due to a saturation of lithium salt that can be dissolved in the PEO phase [45]. The ionic conductivity values at high temperatures (> 60 °C) for the mixtures are very similar, around ~10^{-3} S cm^{-1}. At lower temperatures, a difference is observed; for example, at 20 ºC the ionic conductivity of the blends PEO/PHD is $9.5 \cdot 10^{-6}$ S cm^{-1}, while the PEO references present a higher ionic conductivity. These results are similar to those presented by Gao, *et al*. [26], wherein a PEO/poly (ether-acetal) blend, the lithium salt prefers to dissolve in PEO, showing conductivities similar to PEO with LiTFSI.

Even though the conductivity values obtained for the 80/20 PEO/PHD blend with 30% LiTFSI are lower than for PEO in the range below 40 °C, we must remember that in the blends, at temperatures below the melting point of PHD, the crystals of PHD will probably reinforce the electrolyte, hence the material will exhibit better mechanical properties.

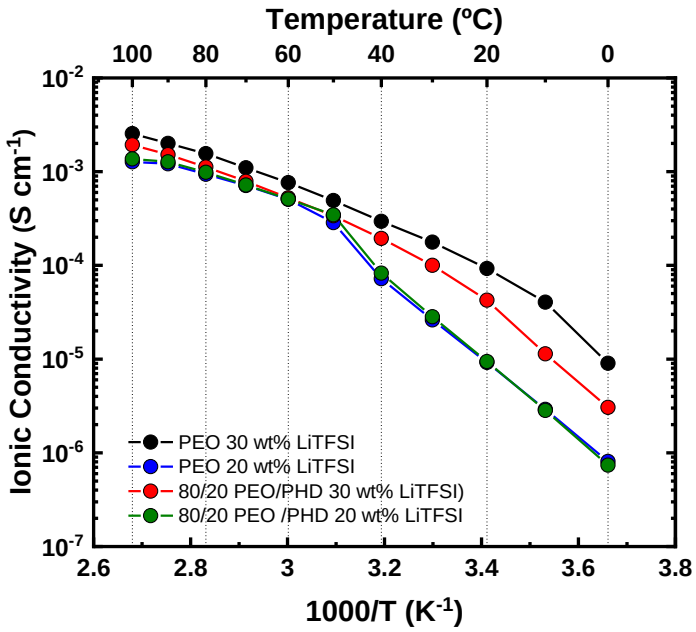

Figure 4.7. Ionic conductivity as a function of temperature for PEO and 80/20 PEO/PHD blends with the either 20 or 30 wt% LiTFSI, as indicated in the inner legend.

4.4 Conclusions

In this chapter, blends of PEO and PHD were prepared by a solvent evaporation method. Taking into account the results obtained by DSC, PLOM and WAXS, it can be concluded that the blends are partially miscible, and the miscibility is a function of blend composition. Blends with higher amounts of PEO have limited miscibility and are double crystalline, while those with higher amounts of PHD exhibit improved miscibility and only the PHD phase can crystallize in them. The PHD phase can nucleate the PEO phase probably by a transference of impurities mechanism.

The addition of a lithium salt (LiTFSI) on the neat polymers and the blends was also studied. The results indicate that the lithium salt preferentially dissolves in the PEO phase and has an insignificant effect on the PHD component, this effect could be one of the keys to improve the mechanical properties of these materials. Even though the salt reduces the spherulite growth rate of the PEO phase within the blends, the overall crystallization rate is enhanced as a result of the strong nucleating effect of the PHD component.

In terms of ionic conductivity, at high temperatures, the conductivity is in the order of ~10^{-3} S cm^{-1}, and as the temperature decreases, the crystallization of PHD is observed.

4.5 References

[1] R. Klein, F.R. Wurm, Aliphatic polyethers: Classical polymers for the 21st century, Macromolecular Rapid Communications. (2015) 1147–1165. https://doi.org/10.1002/marc.201500013.

[2] T.H. Evans, W.L. Hawkins, H. Hibbert, Studies on reactions relating to Carbohydrates and Polysaccharides, Journal of Experimental Medicine. 74 (1941) 511. https://doi.org/10.1084/jem.74.6.511.

[3] E.J. Vandenberg, Organometallic catalysts for polymerizing monosubstituted epoxides, Journal of Polymer Science. 47 (1960) 486–489. https://doi.org/10.1002/pol.1960.1204714947.

[4] M.P. Dreyfuss, P. Dreyfuss, A “living” polymer after cationic initiation, Polymer. 6 (1965) 93–95. https://doi.org/10.1016/0032-3861(65)90018-2.

[5] A. Basterretxea, E. Gabirondo, C. Jehanno, H. Zhu, I. Flores, A.J. Müller, A. Etxeberria, D. Mecerreyes, O. Coulembier, H. Sardon, Polyether Synthesis by Bulk Self-Condensation of Diols Catalyzed by Non-Eutectic Acid-Base Organocatalysts, ACS Sustainable Chemistry and Engineering. 7 (2019) 4103–4111. https://doi.org/10.1021/acssuschemeng.8b05609.

[6] C. Jérôme, P. Lecomte, Recent advances in the synthesis of aliphatic polyesters by ring-opening polymerization, Advanced Drug Delivery Reviews. 60 (2008) 1056–1076.

[7] D.J.A. Cameron, M.P. Shaver, Aliphatic polyester polymer stars: synthesis, properties and applications in biomedicine and nanotechnology, Chemical Society Reviews. 40 (2011) 1761–1776.

[8] M. Lécuyer, M. Deschamps, D. Guyomard, J. Gaubicher, P. Poizot, Electrochemical Assessment of Indigo Carmine Dye in Lithium Metal Polymer Technology, Molecules. 26 (2021) 3079.

[9] Y. Jiang, X. Yan, Z. Ma, P. Mei, W. Xiao, Q. You, Y. Zhang, Development of the PEO based solid polymer electrolytes for all-solid state lithium ion batteries, Polymers. 10 (2018) 1–13. https://doi.org/10.3390/polym10111237.

[10] Z. Xue, D. He, X. Xie, Poly(ethylene oxide)-based electrolytes for lithium-ion batteries, Journal of Materials Chemistry A. 3 (2015) 19218–19253. https://doi.org/10.1039/c5ta03471j.

[11] C. Sun, J. Liu, Y. Gong, D.P. Wilkinson, J. Zhang, Recent advances in all-solid-state rechargeable lithium batteries, Nano Energy. 33 (2017) 363–386. https://doi.org/10.1016/j.nanoen.2017.01.028.

[12] Q. Ma, H. Zhang, C. Zhou, L. Zheng, P. Cheng, J. Nie, W. Feng, Y. Hu, H. Li, X. Huang, L. Chen, M. Armand, Ion Conductors Single Lithium-Ion Conducting Polymer Electrolytes Based on a Super- Delocalized Polyanion Angewandte, (2016) 2521–2525.

https://doi.org/10.1002/anie.201509299.

[13] O.E. Geiculescu, J. Yang, S. Zhou, G. Shafer, Y. Xie, J. Albright, S.E. Creager, W.T. Pennington, D.D. DesMarteau, Solid Polymer Electrolytes from Polyanionic Lithium Salts Based on the LiTFSI Anion Structure, Journal of The Electrochemical Society. 151 (2004) A1363. https://doi.org/10.1149/1.1773581.

[14] C. Tao, M.H. Gao, B.H. Yin, B. Li, Y.P. Huang, G. Xu, J.J. Bao, A promising TPU/PEO blend polymer electrolyte for all-solid-state lithium ion batteries, Electrochimica Acta. 257 (2017) 31–39. https://doi.org/10.1016/j.electacta.2017.10.037.

[15] M. Marzantowicz, J.R. Dygas, F. Krok, A. Łasińska, Z. Florjańczyk, E. Zygadło-Monikowska, A. Affek, Crystallization and melting of PEO:LiTFSI polymer electrolytes investigated simultaneously by impedance spectroscopy and polarizing microscopy, Electrochimica Acta. 50 (2005) 3969–3977. https://doi.org/10.1016/j.electacta.2005.02.053.

[16] K. Vignarooban, B.-E. Mellander, I. Albinson, M. Dissanayake, Effect of Different Types of Ceramic Nano-Fillers on Thermal and Transport Properties of PEO 9 LiTf Solid Polymer Electrolyte, in: Solid State Ionics: Advanced Materials for Emerging Technologies, World Scientific, 2006: pp. 623–630.

[17] M.M. Borgohain, T. Joykumar, S. V. Bhat, Studies on a nanocomposite solid polymer electrolyte with hydrotalcite as a filler, Solid State Ionics. 181 (2010) 964–970. https://doi.org/10.1016/j.ssi.2010.05.040.

[18] T. Niitani, M. Shimada, K. Kawamura, K. Kanamura, Characteristics of new-type solid polymer electrolyte controlling nano-structure, Journal of Power Sources. 146 (2005) 386–390. https://doi.org/10.1016/j.jpowsour.2005.03.102.

[19] Z. Xue, D. He, X. Xie, Poly(ethylene oxide)-based electrolytes for lithium-ion batteries, Journal of Materials Chemistry A. 3 (2015) 19218–19253. https://doi.org/10.1039/c5ta03471j.

[20] J.F. Snyder, R.H. Carter, E.D. Wetzel, Electrochemical and mechanical

behavior in mechanically robust solid polymer electrolytes for use in multifunctional structural batteries, Chemistry of Materials. 19 (2007) 3793–3801. https://doi.org/10.1021/cm070213o.

[21] Solid electrolytes based on poly(ethylene oxide)_poly(4-vinyl phenol-co-2-hydroxyethyl methacrylate) blends and LiClO4 _ Elsevier Enhanced Reader.pdf, (n.d.).

[22] R. Tanaka, M. Sakurai, H. Sekiguchi, H. Mori, T. Murayama, T. Ooyama, Lithium ion conductivity in polyoxyethylene/polyethylenimine blends, Electrochimica Acta. 46 (2001) 1709–1715. https://doi.org/10.1016/S0013-4686(00)00775-1.

[23] L. Meabe, T.V. Huynh, N. Lago, H. Sardon, C. Li, L.A. O'Dell, M. Armand, M. Forsyth, D. Mecerreyes, Poly(ethylene oxide carbonates) solid polymer electrolytes for lithium batteries, Electrochimica Acta. 264 (2018) 367–375. https://doi.org/10.1016/j.electacta.2018.01.101.

[24] J. Mindemark, M.J. Lacey, T. Bowden, D. Brandell, Progress in Polymer Science Beyond PEO — Alternative host materials for Li + -conducting solid polymer electrolytes, Progress in Polymer Science. 81 (2018) 114–143. https://doi.org/10.1016/j.progpolymsci.2017.12.004.

[25] H. Xu, J. Xie, Z. Liu, J. Wang, Y. Deng, Carbonyl-coordinating polymers for high-voltage solid-state lithium batteries: Solid polymer electrolytes, MRS Energy & Sustainability. 6 (2020).

[26] K.W. Gao, W.S. Loo, R.L. Snyder, B.A. Abel, Y. Choo, A. Lee, S.C.M. Teixeira, B.A. Garetz, G.W. Coates, N.P. Balsara, Miscible Polyether/Poly (ether–acetal) Electrolyte Blends, Macromolecules. 53 (2020) 5728–5739.

[27] J.L. Olmedo-Martínez, L. Meabe, A. Basterretxea, D. Mecerreyes, A.J. Müller, Effect of chemical structure and salt concentration on the crystallization and ionic conductivity of aliphatic polyethers, Polymers. 11 (2019) 452. https://doi.org/10.3390/polym11030452.

[28] J.A. Faucher, J. V Koleske, E.R. Santee Jr, J.J. Stratta, C.W. Wilson Iii, Glass transitions of ethylene oxide polymers, Journal of Applied Physics. 37 (1966) 3962–3964.

[29] L. Mandelkern, Crystallization of Polymers, 2nd ed. Vo, Cambridge University Press, Cambridge, United Kingdom, 2002.

[30] L. Sangroniz, B. Wang, Y. Su, G. Liu, D. Cavallo, D. Wang, A.J. Müller, Fractionated crystallization in semicrystalline polymers, Progress in Polymer Science. (2021) 101376.

[31] Z. Bartczak, A. Galeski, N.P. Krasnikova, Primary nucleation and spherulite growth rate in isotactic polypropylene-polystyrene blends, 28 (1987) 1627–1634.

[32] Z. Su, M. Dong, Z. Guo, J. Yu, Study of polystyrene and acrylonitrile− styrene copolymer as special β-nucleating agents to induce the crystallization of isotactic polypropylene, Macromolecules. 40 (2007) 4217–4224.

[33] B. Yang, H. Ni, J. Huang, Y. Luo, Effects of Poly (vinyl butyral) as a Macromolecular Nucleating Agent on the Nonisothermal Crystallization and Mechanical Properties of Biodegradable Poly (butylene succinate), Macromolecules. 47 (2014) 284–296.

[34] A.A. Azli, N.S.A. Manan, M.F.Z. Kadir, Conductivity and Dielectric Studies of Lithium Trifluoromethanesulfonate Doped Polyethylene Oxide-Graphene Oxide Blend Based Electrolytes, Advances in Materials Science and Engineering. 2015 (2015). https://doi.org/10.1155/2015/145735.

[35] N. Reddeppa, T.J.R. Reddy, V.B.S. Achari, V.V.R.N. Rao, A.K. Sharma, Electrical and optical characterization of (PEO+PVAc) polyblend films, Ionics. 15 (2009) 255–259. https://doi.org/10.1007/s11581-008-0269-1.

[36] K.K. Kumar, M. Ravi, Y. Pavani, S. Bhavani, A.K. Sharma, V.V.R.N. Rao, Investigations on PEO/PVP/NaBr complexed polymer blend electrolytes for electrochemical cell applications, Journal of Membrane Science. 454 (2014) 200–211.

[37] A. Basterretxea, E. Gabirondo, I. Flores, A. Etxeberria, A. Gonzalez, A.J. Müller, D. Mecerreyes, O. Coulembier, H. Sardon, Isomorphic Polyoxyalkylene Copolyethers Obtained by Copolymerization of Aliphatic

Diols, Macromolecules. 52 (2019) 3506–3515. https://doi.org/10.1021/acs.macromol.9b00469.

[38] S. Kobayashi, H. Tadokoro, Y. Chatani, Structural studies on polyethers,[-(CH2) m- O-] n. VI. The higher members with m= 6–10, 12, Die Makromolekulare Chemie: Macromolecular Chemistry and Physics. 112 (1968) 225–241.

[39] A.T. Müller, Alejandro J., Michell, R. M., Lorenzo, Isothermal Crystallization Kinetics of Polymers, in: Q. Guo (Ed.), Polymer Morphology: Principles, Characterization, and Processing, John Wiley & Sons, 2016: pp. 181–203. https://doi.org/https://doi.org/10.1002/9781118892756.ch11.

[40] R. Mary, A.J. Müller, Progress in Polymer Science Confined crystallization of polymeric materials, Progress in Polymer Science. 54–55 (2016) 183–213. https://doi.org/10.1016/j.progpolymsci.2015.10.007.

[41] J.D. Hoffman, G.T. Davis, J.I. Lauritzen, The rate of crystallization of linear polymers with chain folding, in: Treatise on Solid State Chemistry, Springer, 1976: pp. 497–614.

[42] M. Safari, A. Mugica, M. Zubitur, A. Martínez de Ilarduya, S. Muñoz-Guerra, A.J. Müller, Controlling the isothermal crystallization of isodimorphic PBS-ran-PCL random copolymers by varying composition and supercooling, Polymers. 12 (2020) 17.

[43] P. Yao, H. Yu, Z. Ding, Y. Liu, J. Lu, M. Lavorgna, J. Wu, X. Liu, Review on Polymer-Based Composite Electrolytes for Lithium Batteries, Frontiers in Chemistry. 7 (2019) 1–17. https://doi.org/10.3389/fchem.2019.00522.

[44] M. Marcinek, J. Syzdek, M. Marczewski, M. Piszcz, L. Niedzicki, M. Kalita, A. Bitner, P. Wieczorek, T. Trzeciak, M. Kasprzyk, P. Łęż, Z. Zukowska, A. Zalewska, W. Wieczorek, Electrolytes for Li-ion transport – Review, 276 (2015) 107–126.

[45] S. Lascaud, M. Perrier, A. Vallee, S. Besner, J. Prud'Homme, M. Armand, Phase diagrams and conductivity behavior of poly (ethylene oxide)-molten salt rubbery electrolytes, Macromolecules. 27 (1994) 7469–7477.

Chapter V

5. High Lithium Conductivity of Miscible PEO/Methacrylic Sulfonamide Anionic Polyelectrolyte Polymer Blends

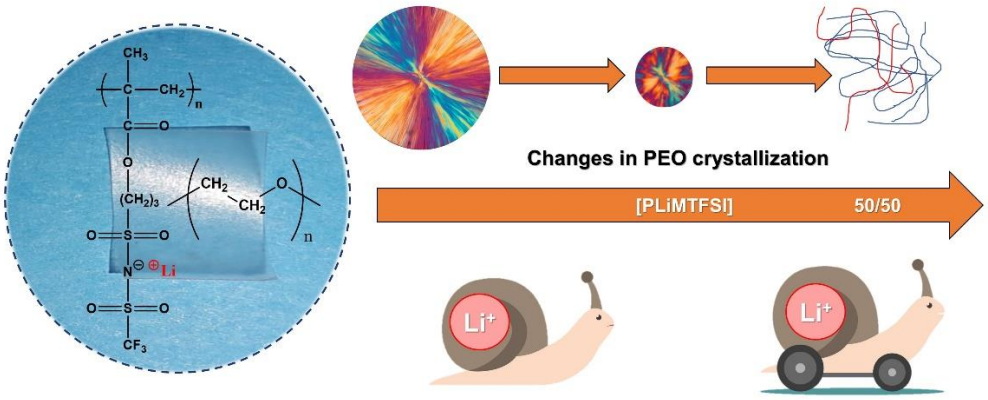

5.1 Abstract

In this chapter, we develop novel single-ion polymer electrolytes (SIPE) by mixing poly(lithium 1-[3-(methacryloyloxy) propylsulfonyl]-1-(trifluoromethanesulfonyl) imide) (PLiMTFSI) and poly(ethylene oxide) (PEO) with different molecular weights. The impact of PLiMTFSI on the crystallization and conductivity of the blends was explored in detail. When PLiMTFSI (an amorphous polymer) is added to PEO, the crystallization ability of PEO decreases. However, blends with high molecular weight PEO (1,000 kg mol^{-1}) experience a lower reduction in crystallinity and melting points. As a result, lower conductivity values were obtained in these blends, which is why most of the study was then focused on blends incorporating a lower molecular weight PEO (100 kg mol^{-1}). We show that the melting point, degree of crystallinity, spherulitic growth, and overall crystallization kinetics decrease with the presence of PLiMTFSI, which are all signs of miscibility. Furthermore, the blends show a single glass transition temperature over the whole composition range. Therefore our results indicate that PEO and PLiMTFSI are miscible, as corroborated by applying the Nishi-Wang equation and obtaining negative χ_{12} values (i.e., the Flory-Huggins interaction parameter) for all blends. Our results show that intermediate molecular weight blends (100 kg mol^{-1} PEO and 50 kg mol^{-1} PLiMTFSI) showed the highest ionic conductivity value. Interestingly, a value of $2.1 \cdot 10^{-4}$ S cm^{-1} was obtained at 70 ºC, which is one of the highest reported so far for a free-standing film of single-ion conducting polymer electrolytes. Finally, employing dielectric spectroscopy, the contribution of ion density and ion mobility on ionic conductivity could be separated. It was found that ion mobility is the parameter that has a greater weight in the conduction process.

J.L. Olmedo-Martínez, L. Porcarelli, Á. Alegría, D. Mecerreyes, A.J. Müller, High Lithium Conductivity of Miscible Poly(ethylene oxide)/Methacrylic Sulfonamide Anionic Polyelectrolyte Polymer Blends, Macromolecules. 53 (2020) 4442–4453. https://doi.org/10.1021/acs.macromol.0c00703.

5.2 Introduction

All-solid batteries including solid polymer electrolytes (SPE), offer advantages for improving the safety of existing lithium batteries [1,2]. Poly(ethylene oxide)s (PEOs) mixed with lithium salts are the most popular solid polymer electrolytes (SPE) for lithium batteries for the past 40 years [3]. However, the ionic conductivity of these PEO/(lithium salt) electrolytes is very low for room temperature use, and the actual lithium-polymer batteries operate at 70 ºC. Many strategies have been studied over the years to improve the ionic conductivity of PEO polymer electrolytes, most of them based on reducing its crystallinity and lowering its glass transition temperature [4–6]. Another drawback of PEO based SPEs is its low lithium transference number or mobility of the lithium ion (t_{Li+} value of approx. 0.2) [7,8].

In the last few years, a series of anionic polyelectrolytes called single-ion polymer electrolytes (SIPEs) has been developed as a new class of solid polymer electrolytes (SPEs). In SIPEs, a highly delocalized anion is attached to the polymeric chain, and the lithium counter-cations possess high mobility. This results in the lithium transference number values being close to unity since lithium ions are fully responsible for the ionic conductivity [9–11]. SIPEs are of particular interest for application in high energy density batteries where the lithium is used as an anode.

The use of single-ion polymer electrolytes in contact with lithium metal anodes limits the formation of lithium concentration gradients in the electrolyte. This holds the promise of avoiding the formation of dendrites, which is the major cause of lithium metal battery failure. Nowadays, the most studied SIPEs are highly delocalized anionic polyelectrolytes, including sulfonamide groups such as lithium poly(lithium 1-[3-(methacryloyloxy) propylsulfonyl]-1-(trifluoromethylsulfonyl) imide) (PLiMFTSI) and its styrenic analog, poly(styrene sulfonyl(trifluoromethylsulfonyl)imide [12]. However, SIPEs homopolymers generally present low ionic conductivity due to the relatively high T_g values of the anionic polyelectrolytes, which limit lithium mobility. These polymers also tend to have poor mechanical properties because of their inherent rigidity, as another consequence of their high T_g values [13,14]. For this reason, anionic polyelectrolytes have been included in a variety of block copolymer formulations

in combination with soft blocks, such as PEO, or hard blocks, like polystyrene, as pioneered by Devaux *et al*.[10]. These SIPE block copolymers typically form microphase separated morphologies where the flexible PEO conducts the lithium cations, while the stiffer polystyrene or similar blocks provide mechanical stability [10,11,15].

Long *et al.* [13], optimized the relationships among chemical composition, morphology, mechanical properties, and ionic conductivity, of the single-ion conducting triblock copolymers. More recently, some of us reported the synthesis of ABA triblock copolymers based on PEO and poly (lithium 1-[3-(methacryloyloxy) propylsulfonyl]-1-(trifluoromethylsulfonyl) imide) (PLiMTFSI). In these triblock copolymers, the mechanical stability was given by the crystallinity of PEO and the block copolymers, which showed a single low T_g (−55 to 7ºC) and a degree of crystallinity which depended on the composition (51 – 0%). As a reference, these triblock copolymers showed the highest ionic conductivity values reported up to now for a SIPE ($\sigma \approx 10^{-4}$ Scm^{-1} at 70°C), and a lithium-ion transference number close to 1 ($t_{Li^+} \approx 0.91$) [11].

It is well known that one of the limitations of block copolymers is that their synthetic methods are complicated and usually costly. Polymer blending is a classic low-cost alternative method for the development of new polymeric materials, which may combine the properties of both individual homopolymers [16]. Blending an amorphous polymer with a semi-crystalline polymer is of significant technological interest for many applications in automotive industry, aerospace or biomedicine. In our particular case, the blending strategy had already been used to develop polymer electrolytes [17–19].

There are several cases in which SPEs have been prepared by mixing polymers and adding some lithium salt. For example, Morris *et al*. [20] prepared polymer mixtures by adding a homopolymer rich in conductive paths (poly(oligo-oxyethylene methacrylate) (POEM)) with lithium salt to a block copolymer (polystyrene-*block*-poly(oligo-oxyethylene methacrylate)), which has a rigid part and a component that helps in the conduction process. By doing this, they found an improvement in the ionic conductivity values. With relation to single-ion polymer electrolytes, Armand *et al*. [12] prepared blends of lithium poly[(4-

styrenesulfonyl) (trifluoromethanesulfonyl imide)] (PLiSTFSI) and PEO, which showed ionic conductivity values of about 10^{-5} S cm^{-1} at 70 °C. Then, they improved the ionic conductivity values by preparing random or block copolymers of PLiSTFSI and ethylene oxide units. In another work, Ma *et al*. [21] reported the synthesis of poly[(4-styrenesulfonyl) (trifluoromethyl (S-trifluoromethylsulfonylimino) sulfonyl) imide) and made blends with high molecular weight PEO. They studied the change in T_g by DSC and also found that the blends showed a high *Li-ion* transference number (t_{Li}^+ = 0.91) and an ionic conductivity of $1.35 \cdot 10^{-4}$ S/cm at 90 ºC.

Interestingly, most of the polymer blends of PEO and anionic polyelectrolytes appeared to be miscible due to the ion-dipole interactions between the free lithium and the attached sulfonamide anion with the ethyleneglycol units. This affected the crystallinity of PEO, however an in-depth study of their miscibility or a quantitative determination of the Flory-Huggins interaction parameters is still lacking [22–24]. In this article, we prepare blends with high lithium conductivity based on poly (ethylene oxide) (PEO) and the methacrylic anionic polyelectrolyte PLiMTFSI for the first time. The effect of the molecular weight of both homopolymers on the ionic conductivity, miscibility and crystallinity of the blends SIPEs was investigated by a variety of techniques and discussed.

5.3 Results

5.3.1 Non-isothermal DSC Results for PEO and PLiMTFSI Blends

The transport of ions in solid polymer electrolytes is regulated by the segmental relaxation of the polymer chains. For this reason, the glass transition temperature (T_g) and the crystallinity degree (X_c) influence the ionic conductivity of the electrolytes [25–28]. In the PEO/PLiMTFSI blends prepared here, the PLiMTFSI component is completely amorphous, while the PEO component can crystallize depending on the composition.

In Figure 5.1, T_m and X_c (degree of crystallinity) values taken from non-isothermal DSC scans are plotted as a function of PLiMTFSI content for the blends. Figure 1a shows the effect of the PEO molecular weight at a fixed

PLiMTFSI molecular weight (5 kg mol^{-1}). In the blends with 100 kg mol^{-1} PEO, the T_m of the PEO component in the blend decreases from 68.7 to 61.8 ºC at 30 wt% PLiMTFSI, while it is completely amorphous at 50 wt%. In the case of 1,000 kg mol^{-1} PEO, the T_m decreases from 70.3 to 58.9 ºC at 50 wt% polyelectrolyte. Additionally, the 50/50 PEO/PLiMTFSI blend has a 21% crystallinity degree, and the 30/70 is amorphous (Figure 5.1c). Hence, the higher the PEO molecular weight, the lower the reduction of crystallinity at constant composition.

The effect of the PLiMTFSI molecular weight is shown in Figures 1b and 1d. At a constant PEO molecular weight (100 kg mol^{-1}), it is observed that the T_m decreases in all cases. With 50 kg mol^{-1} PLiMTFSI, the T_m of the PEO component in the blends decreases from 68.7 to 62.8 ºC at 30 wt% polyelectrolyte. This blend has a crystallinity of 54%, and at 50 wt% it becomes completely amorphous. In the blends with high molecular weight PLiMTFSI, the T_m decreases from 68.7 to 55.2 ºC at 50 wt% PLiMTFSI. It is also necessary to add 70 wt% PLiMTFSI for the electrolyte to be completely amorphous. Based on these results, it is observed that in the 100 kg mol^{-1} PEO and 50 kg mol^{-1} PLiMTFSI blends, there is a larger decrease both in crystallinity and T_m than in the blends with 1,000 kg mol^{-1} PEO.

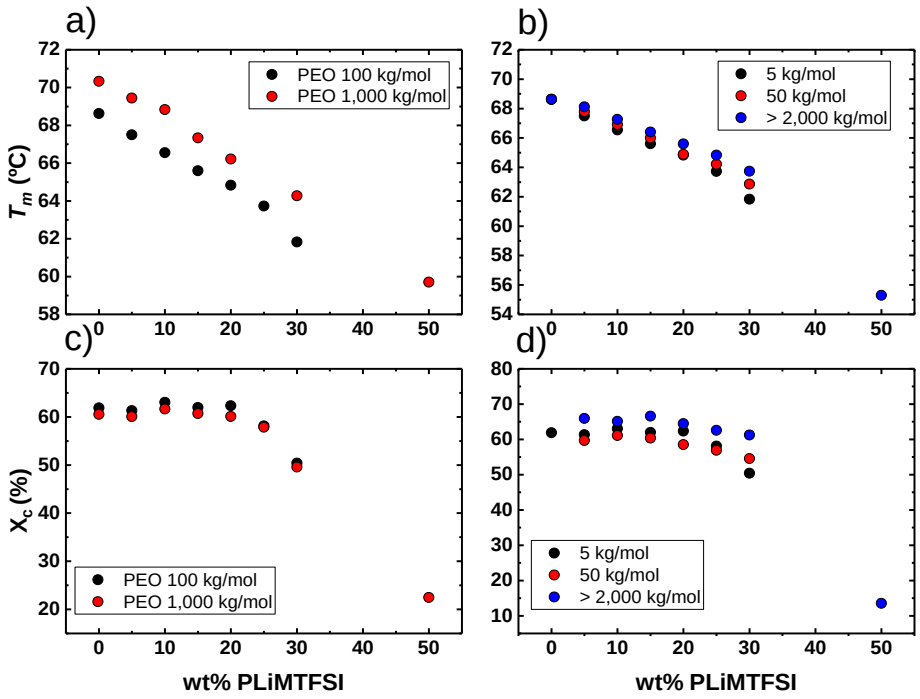

Figure 5.1. Melting points and crystallinity degrees of neat PEO and the PEO component in the blends with different molecular weights. (a) and (c) Blends with 5 kg mol^{-1} PLiMTFSI, the PEO molecular weight values are indicated in the legend. (b) and (d) Blends with 100 kg mol^{-1} PEO, the PLiMTFSI molecular weight values are indicated in the legend.

One of the simplest ways to determine polymer blend miscibility is by examining the glass transition temperature (T_g) [29]. A single T_g generally indicates that the polymers are miscible, whereas in immiscible blends, more than one T_g is observed. Figure 5.2 shows the dependence of the T_g on the composition of the different electrolyte families with 100 kg mol^{-1} PEO. It shows a single T_g in all cases, indicating that PEO and PLiMTFSI are miscible in the amorphous phase for all compositions, and this T_g increases with increasing PLiMTFSI concentration. Porcarelli *et al.* [11] reported SAXS and WAXS measurements for PLiMTFSI-*b*-PEO-*b*-PLiMTFSI triblock copolymers and they also observed a similar behavior, i.e., the materials exhibited a single phase in the melt and in the amorphous state.

The Gordon-Taylor equation was employed to fit the variation of the T_g with respect to the composition:

$$T_{g,blend} = \frac{w_1 T_{g,1} + k w_2 T_{g,2}}{w_1 + k w_2} \quad (5.1)$$

where, w_1 and w_2 are the polymer components weight fractions, $T_{g,1}$ and $T_{g,2}$ are the glass transition temperatures of PEO and PLiMTFSI, respectively, and k is the $\rho_1\Delta\alpha_2/\rho_2\Delta\alpha_1$ ratio. ρ and $\Delta\alpha$ corresponds to the density and the expansion coefficient change at the T_g [30].

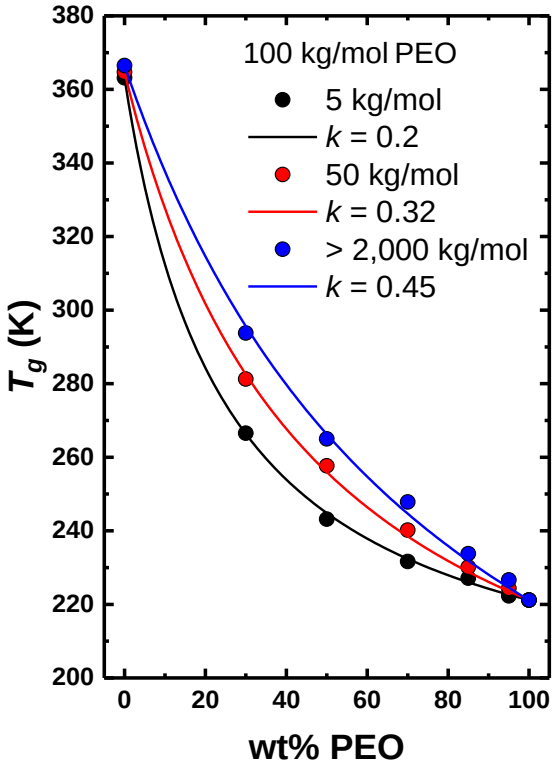

Figure 5.2. Change in T_g for the blends at different PLiMTFSI concentrations and fits to the Gordon-Taylor equation.

Figure 5.2 shows that as expected, the T_g values increase with the molecular weight of the PLiMTFSI. The Gordon-Taylor (G-T) equation is able to fit the experimental data points for the three blend families. The k values obtained from the G-T fits increase with the molecular weight of the polyelectrolyte. This

suggests that minor changes could exist in the density and/or the expansion coefficients of the blend components as the molecular weight of PLiMTFSI increases [30].

The miscibility of a semicrystalline polymer and an amorphous polymer can be evaluated by the depression in melting temperature (T_m), as such change in melting point is associated with the Flory-Huggins polymer-polymer interaction parameter (χ_{12}). The interaction parameter between PEO and PLiMTFSI was calculated using the Nishi-Wang equation, which is based on the Flory-Huggins theory [31,32]. The interaction parameter can be calculated using the following expression:

$$\left(\frac{1}{T_m^0(PEO)} - \frac{1}{T_m^0(blend)}\right) = \left(\frac{RV_2}{V_1 \Delta H_{PEO}^0}\right) \chi_{12} \phi_1^2 \qquad (5.2)$$

where, T_m^0 (blend) and T_m^0 (PEO) are the equilibrium melting temperatures of the blend and the crystallizable polymer (PEO), ΔH^0 is the melting enthalpy of PEO per mol of repeating unit, V is the molar volume of the repeating units of the polymers, and ϕ_1 is the volume fraction of the amorphous polymer in the blend (PLiMTFSI). The subscripts 1 and 2 refer to PLiMTFSI and PEO, respectively, R is the universal gas constant, and χ_{12} is the Flory-Huggins interaction parameter.

The following values were used to calculate χ_{12}: V_1 = 345 cm^3 mol^{-1}, V_2 = 44 cm^3 mol^{-1} and ΔH^0 = 8703 J mol^{-1} [33]. Figure 5.3 shows a plot where the left side of equation 5.2 is represented versus ϕ_1^2. The slope of each line is related to the interaction parameter for each blend family.

The equilibrium melting temperature will be depressed only if χ_{12} is negative. The magnitude of χ_{12}, and the amount of the depression will depend on the strength of the polymer-polymer interactions. χ_{12} decreases as polymer-polymer interactions increase.

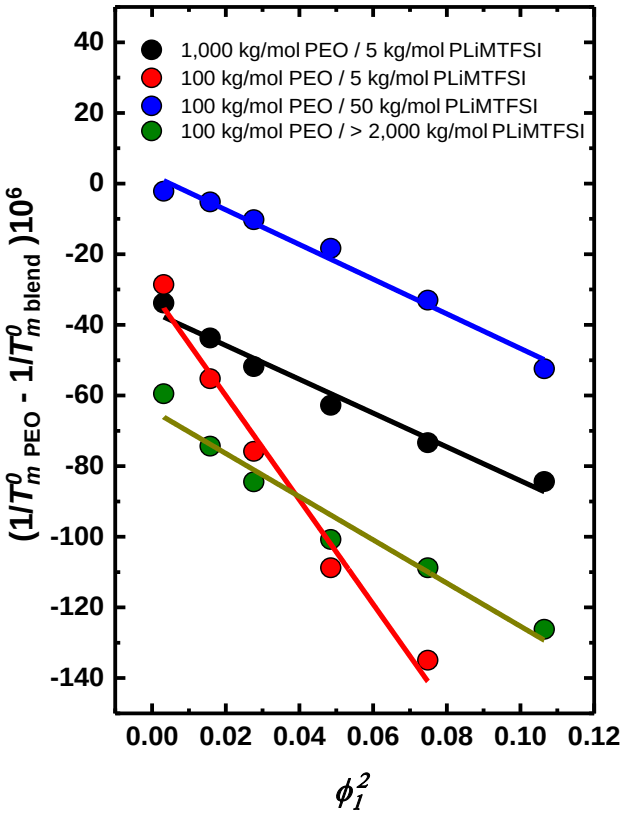

Figure 5.3. Nishi-Wang plot (according to equation 5.2) as a function of blend composition.

None of the lines in Figure 5.3 pass through the origin, as equation 5.2 implies. According to the literature, this could indicate that the interaction parameter (χ_{12}) for these blends may be composition-dependent [31,32], especially for low amounts of PLiMTFSI. However, we have fitted the data to straight lines to be able to calculate approximate interaction parameters according to equation 5.2, that are valid in the composition range explored here.

Table 5.1 lists the χ_{12} values, which are negative for all blends, indicating that PEO and PLiMTFSI are thermodynamically miscible [16,32]. When comparing the effect of the PEO molecular weight, it is observed that the polyelectrolyte is more miscible in the 100 kg mol^{-1} PEO case and, at the same time, miscibility decreases with increasing PLiMTFSI molecular weight. It is well-known that

polymer-polymer miscibility tends to decrease as molecular weight increases, hence the results are consistent with theoretical expectation [34].

Table 5.1. Polymer-Polymer Interaction parameter (χ_{12}) calculated by Nishi-Wang equation.

Blend	χ_{12}
100 kg mol^{-1} PEO / 5 kg mol^{-1} PLiMTFSI	-1.15
1,000 kg mol^{-1} PEO / 5 kg mol^{-1} PLiMTFSI	-0.37
100 kg mol^{-1} PEO / 50 kg mol^{-1} PLiMTFSI	-0.38
100 kg mol^{-1} PEO / > 2,000 kg mol^{-1} PLiMTFSI	-0.47

5.3.2 Spherulitic Morphology and Growth

The morphology and growth rate of spherulites were evaluated with a polarized light optical microscope (PLOM). The images of neat 100 kg mol^{-1} PEO spherulites and PEO/ PLiMTFSI blends obtained at T_c = 50 ºC are shown in Figure 5.4.

Spherulites of neat PEO are larger than those observed when PEO is blended with PLiMTFSI, since the nucleation density of the blends is higher (Figure 5.5). Regular well developed spherulites with Maltese Cross extinction patterns are evident for PEO and PEO blends with low contents of PLiMTFSI. The sign of these spherulites is always negative, as indicated by the extinction colors produced by the introduction of a red tint plate in between the crossed polarizers [35].

When the amount of PLiMTFSI is increased to 30%, the circular shape of the spherulites are distorted and the nuclei density increases even more (Figures 5.4 and 5.5). The change in the nuclei density, as well as the change in morphology, are attributed to the miscibility of the polymers. In the case of the 100 kg mol^{-1} PEO / > 2,000 kg mol^{-1} PLiMTFSI blend, smaller changes are observed in morphology , indicating that this is the least miscible blend from those shown in Figure 5.4.

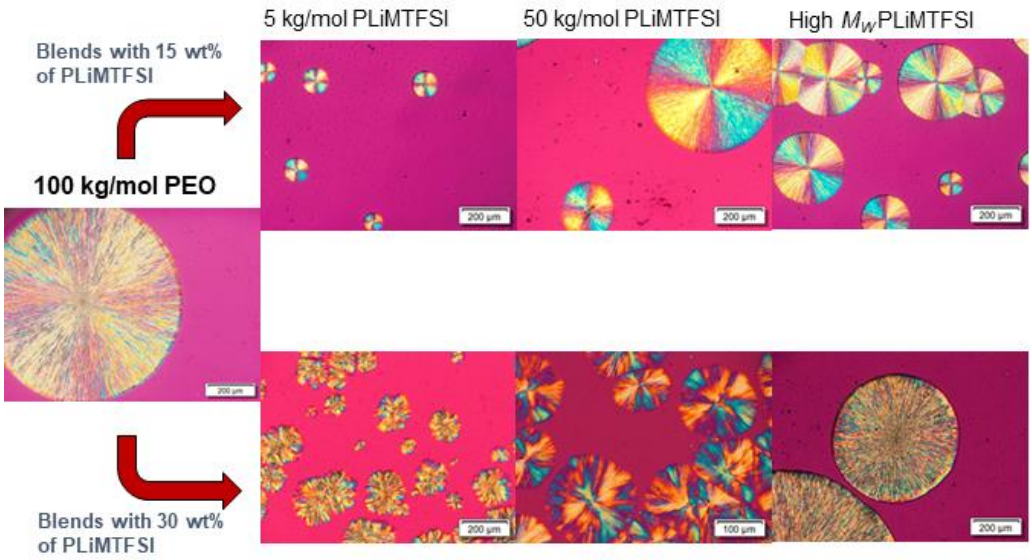

Figure 5.4. Change in the spherulitic morphology of the indicated blends.

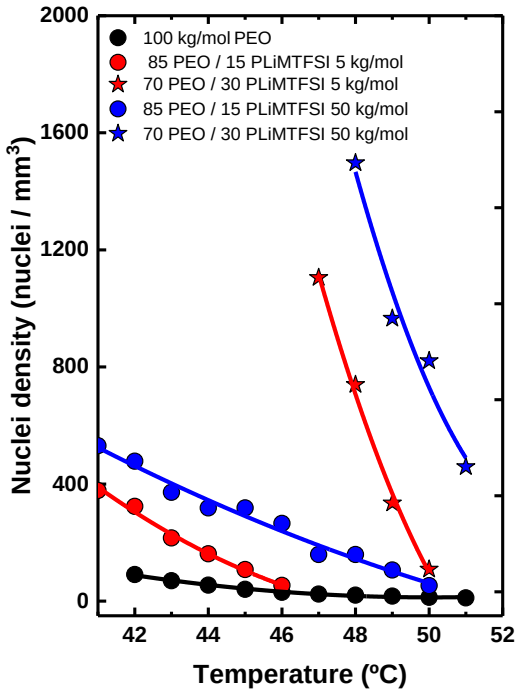

Figure 5.5. Nuclei density of different family blends.

Figure 5.5 shows how the nucleation density measured under isothermal conditions increases with the amount of PLiMTFSI and with its molecular weight. This enhancement of nucleation density can be related to the transfer of impurities from PLiMTFSI to PEO. The increased in nucleation density when the 50 kg mol^{-1} PLiMTFSI is used instead of the lower molecular weight sample (5 kg mol^{-1}) could be related to the changes in miscibility that triggers nucleation in the PEO chains. It should be considered that the phase compositions could change since in general a liquid-liquid phase diagram (which has not been determined in this work) is normally modified by increases in molecular weight.

The crystallization rate is dependent on the energy required to transport the polymer chains to the surface of the growing crystal and also the energy barrier for the creation of secondary nuclei of a critical size [36,37]. These terms depend on the molecular characteristics of each component, such as molecular weight, T_c, T_m and T_g. The addition of a miscible amorphous component causes a dilution effect, resulting in the reduction of the equilibrium melting temperature (T_m^0) [16].

Measurements of spherulitic growth rates were performed by PLOM. The spherulites growth was recorded as a function of time, and then plots of radius versus time were made. The spherulitic growth rate was calculated from the slope of these plots, which were all linear. The results are shown in Figure 5.6. The typical trend of decreasing growth rate with T_c is observed. When polymers crystallize from the melt, the spherulitic growth rate versus T_c curve is a bell shape curve with a maximum at temperatures between T_g and T_m. The left-hand side of the curve is dominated by chain diffusion (data was impossible to obtain in this region, a typical feature of rapidly crystallizing polymers) with a minor contribution from secondary nucleation, while the right-hand side (the zone covered in Figure 5.6) is dominated by secondary nucleation with a minor contribution from diffusion, as polymers at high temperatures have low relative melt viscosities. The probability of forming secondary nuclei decreases as we approach the melting point, and any diffusion contribution also decreases strongly [35].

If the blends were immiscible, no changes in the growth rate of the PEO component would be expected. However, as Figure 5.6 shows for all blends, the growth rate of the PEO component spherulites decreases in comparison to the

corresponding neat PEOs, especially at low crystallization temperatures. This indicates that the more rigid PLiMTFSI chains (that are mixed with PEO chains) are interfering with the secondary nucleation process, slowing it down. This result is the opposite of that observed with primary nucleation, which was enhanced (Figure 5.5) by PLiMTFSI addition. Therefore, the overall isothermal crystallization rate, which can be determined by DSC (see below) and includes both nucleation (i.e., primary nucleation) and growth (i.e., secondary nucleation) should show a competition between these two factors. If the crystallization temperature is too high, the minor contribution of diffusion present in this temperature range (i.e., right-hand side of the bell shape curve) disappears, and the growth rates become very similar or identical at the largest T_c values employed.

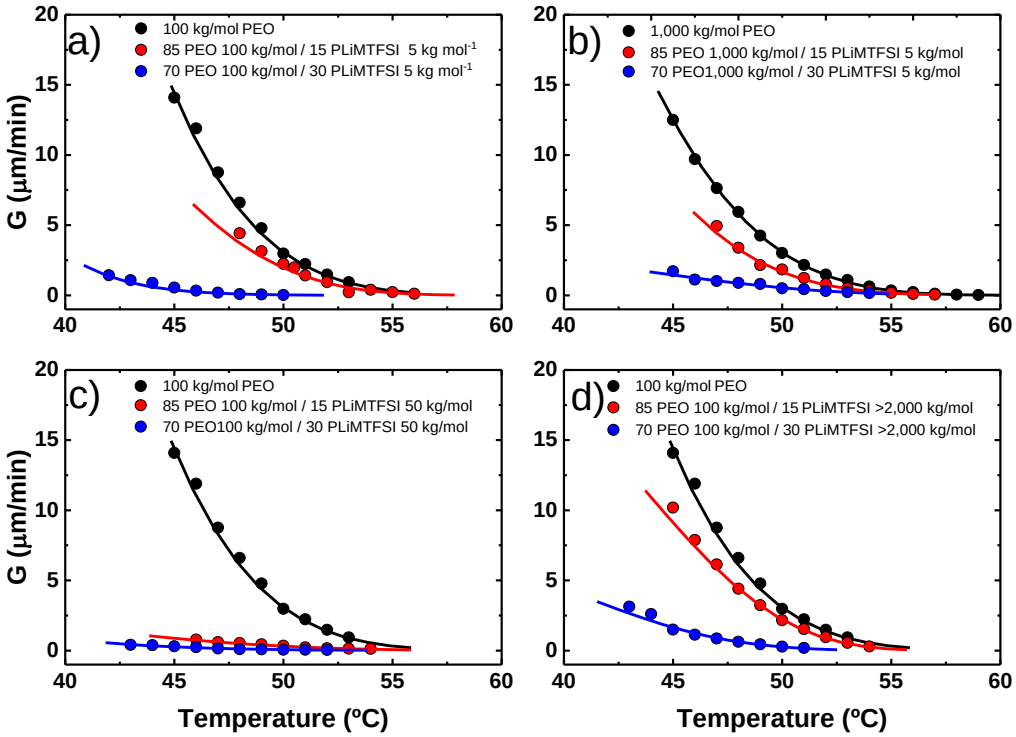

Figure 5.6. Spherulitic growth rate (*G*) as a function of crystallization temperature for: a) 100 kg mol^{-1} PEO / 5 kg/mol PLiMTFSI, b) 1,000 kg mol^{-1} PEO / 5 kg mol^{-1} PLiMTFSI, c) 100 kg mol^{-1} PEO / 50 kg/mol PLiMTFSI, d) 100 kg mol^{-1} PEO / > 2,000 kg mol^{-1} PLiMTFSI. The solid lines are fits to the Lauritzen and Hoffman equation, which are shown to guide the eye.

Figure 5.6 shows very similar decreasing growth rate trends upon PLiMTFSI addition, and in general, the higher the amount of PLiMTFSI, the lower the growth rate. The results are mostly consistent with the values of χ_{12} determined above, as all blends are miscible and hence depress G values, but the specific trends of each blend family do not perfectly coincide with the trends in the interaction parameter. For example, in the particular case of the 100 kg mol^{-1} PEO / 50 kg mol^{-1} PLiMTFSI, both 15 and 30% PLiMTFSI cause the largest reduction in growth rates even though this is not the blend with the lowest PLiMTFSI molecular weight.

5.3.3 Isothermal Crystallization

DSC Isothermal crystallization experiments (which include both primary nucleation and growth) were performed to study how the molecular weight and PLiMTFSI concentration affects the overall crystallization kinetics of PEO. Figure 5.7 shows plots of the inverse of the half-crystallization time ($1/\tau_{50\%}$) as a function of crystallization temperature (T_c) for all blends. The inverse of the half-crystallization time ($1/\tau_{50\%}$) is directly proportional to the overall crystallization rate [33,36]. Unlike spherulite growth, the overall crystallization rate increases at low PLiMTFSI concentrations. At fixed PEO molecular weight, a greater decrease in the crystallization rate is observed for 100 kg mol^{-1} PEO. In both cases, the crystallization rate begins to decrease at 25 wt%. In the case of the 1,000 kg mol^{-1} PEO and 5 kg mol^{-1} PLiMTFSI blend, it is still possible to measure the crystallization rate at 50 wt%, which is consistent with the results of non-isothermal DSC. If we compare the overall crystallization rate for 100 kg mol^{-1} PEO when changing the molecular weight of the PLiMTFSI, it is observed that this rate decreases more with the 50 kg mol^{-1} PLiMTFSI. Furthermore, when using the high molecular weight PLiMTFSI,it was possible to measure the overall crystallization rate up to 50 wt% PLiMTFSI.

The results presented in Figure 5.7 can be rationalized by considering the previously discussed nucleation and spherulitic growth rate results (Figures 5.5 and 5.6). When the amount of added PLiMTFSI is small, the increase in primary nucleation dominates the kinetics, and the overall crystallization rate increases.

However, beyond a specific concentration of PLiMTFSI (typically above 20%), the decrease in growth rate (Figure 5.6) dominates the kinetics and the overall crystallization rate decreases. Hence, the competition between nucleation and growth determines the final overall crystallization kinetics. The specific values of the overall crystallization rate can, therefore, be tailored by changing composition and molecular weight of the blend components.

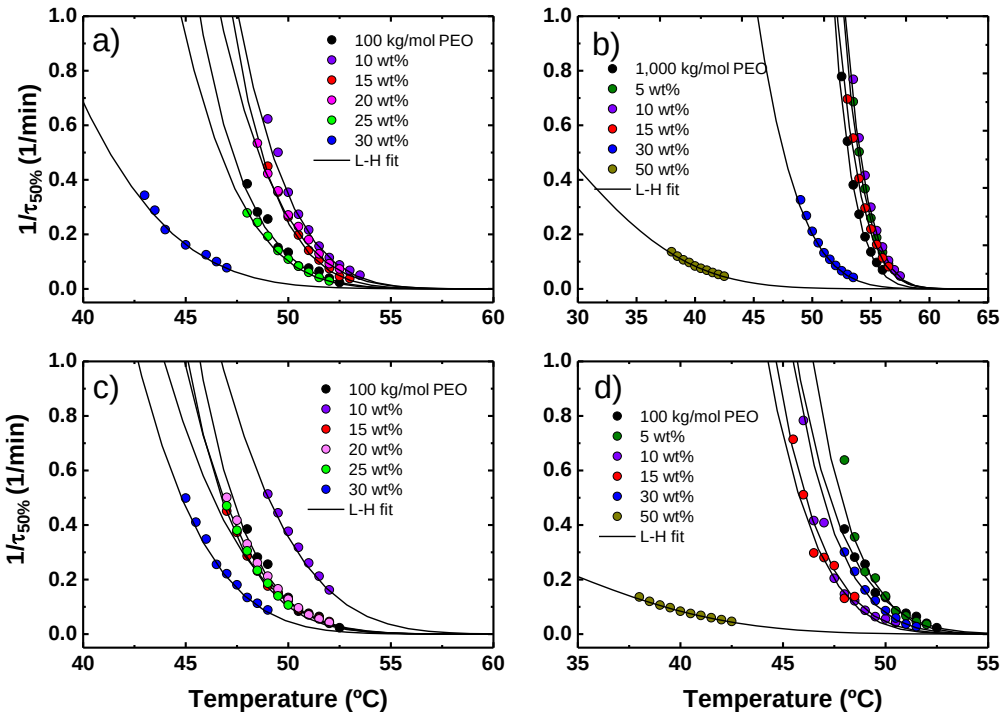

Figure 5.7. Overall isothermal crystallization rates (expressed as the inverse of the half-crystallization time) of the indicated PEO and PEO component in the blend: a) 100 kg mol^{-1} PEO / 5 kg mol^{-1} PLiMTFSI, b) 1,000 kg mol^{-1} PEO / 5 kg mol^{-1} PLiMTFSI, c) 100 kg mol^{-1} PEO / 50 kg mol^{-1} PLiMTFSI, d) 100 kg mol^{-1} PEO / > 2,000 kg mol^{-1} PLiMTFSI. The solid lines are fits to the Lauritzen and Hoffman equation, which are shown to guide the eye.

5.3.4 Ionic conductivity, Li-Ion Density and Li-Mobility

Next, the effect of the PEO molecular weight on the ionic conductivity of the blends was investigated. The temperature dependence of the ionic conductivity for the blends with different molecular weights of PEO and 5 kg mol^{-1} PLiMTFSI is depicted in Figures 5.8a and 5.8b. In the blends with PEO 100 kg

mol^{-1} (Figure 5.8a), the ionic conductivity increases with the amount of polyelectrolyte, and the highest value at room temperature is 2.6·10^{-6} S cm^{-1} at 70 wt% PLiMTFSI. In the case of the blends with 15 and 30 wt%, a decrease in ionic conductivity caused by PEO crystallization is observed from 60 ºC. At 50 and 70 wt% PLiMTFSI, this sudden conductivity drop does not occur because at these PLiMTFSI concentrations the blends are completely amorphous (see Figure 5.1).

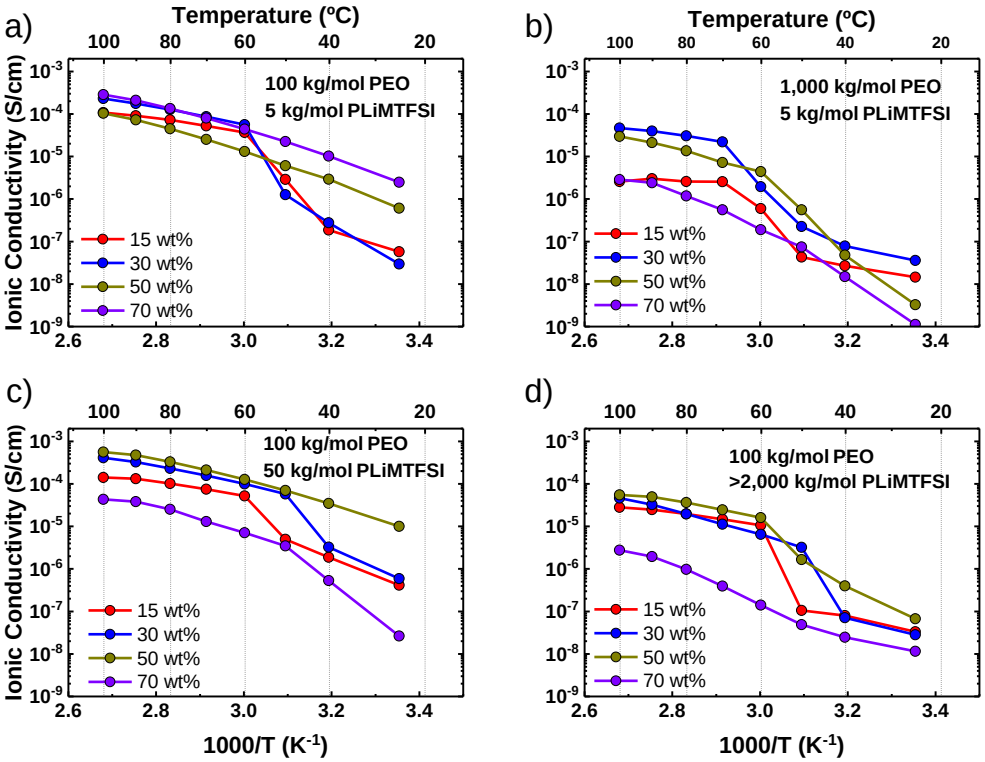

Figure 5.8. Ionic conductivity vs. temperature of different blends.

The ionic conductivity of the blends with 1,000 kg mol^{-1} PEO (Figure 5.8b) is lower than the one of the 100 kg mol^{-1} PEO blends. Besides, it is observed that the blends have higher crystallinity up to 50 wt%, a concentration at which the highest conductivity at room temperature is 3.8·10^{-8} S cm^{-1}. At 70 wt%, the blend is completely amorphous (see Figure 5.1), but the ionic conductivity is the lowest.

The effect of the molecular weight of PLiMTFSI was compared by making blends of 100 kg mol^{-1} PEO and PLiMTFSI at different molecular weights (Figures 5.8a, 5.8c and 5.8d). The general tendency is that increasing the ionic concentration of PLiMTFSI increases the ionic conductivity. The ionic conductivity values are higher with 50 kg mol^{-1} PLiMTFSI, reaching a maximum value at 50 wt% ($2.1 \cdot 10^{-4}$ S cm^{-1}). This conductivity value is greater than the one reported in previous works for single ion conductor electrolytes [2,11,21,38]. This effect is probably due to the high mobility that Li atoms have in these blends, as verified by dielectric spectroscopy. In addition, the blends with > 2,000 kg mol^{-1} PLiMTFSI have lower values of ionic conductivity, perhaps due to the fact that they have a higher T_g than the other blends [39].

To better understand the ionic conductivity process in SIPEs, the ion density (p) and ion mobility (μ) were evaluated by analyzing the electrode polarization (EP) effect [40,41]. For this study, the blends of 100 kg mol^{-1} PEO / > 2,000 kg mol^{-1} PLiMTFSI were selected since in this blend the ionic conductivity is moderate which facilitates the data analysis.

The ionic conductivity (σ), can be expressed as: $\sigma = ep\mu$, where e is the elementary charge. The polarization manifests itself by an increase in the effective capacitance of the cell and an apparent decrease of the real part of the complex conductivity, as the ion accumulation reduces the electric field experienced by the conducting ions. A time scale for conduction can be defined as the time required for the cation motions becoming diffusive, and can be calculated as:

$$\tau_\sigma \equiv \frac{\varepsilon_s \varepsilon_0}{\sigma_{DC}} \qquad (5.3)$$

where, σ_{DC} and ε_s are, respectively, the static conductivity and the statict relative permittivity of the sample (measured when electrode polarization is neglibible), and ε_0 is the permittivity of vacuum ($8.85 \cdot 10^{-12}$ F m^{-1}).The time needed to develop a full electrode polarization can be calculated as:

$$\tau_{EP} \equiv \frac{\varepsilon_{EP}\varepsilon_0}{\sigma_{DC}} \qquad (5.4)$$

where, ε_{EP} is the effective (apparent) permittivity after the electrode polarization is completed.

In the frameworkof the Macdonald and Coelho model [42–44], the electrode polarization is treated as a simple Debye relaxation and the corresponding loss tangent is given as:

$$\tan\delta = \frac{\omega\tau_{EP}}{1 + \omega^2\tau_\sigma\tau_{EP}} \qquad (5.5)$$

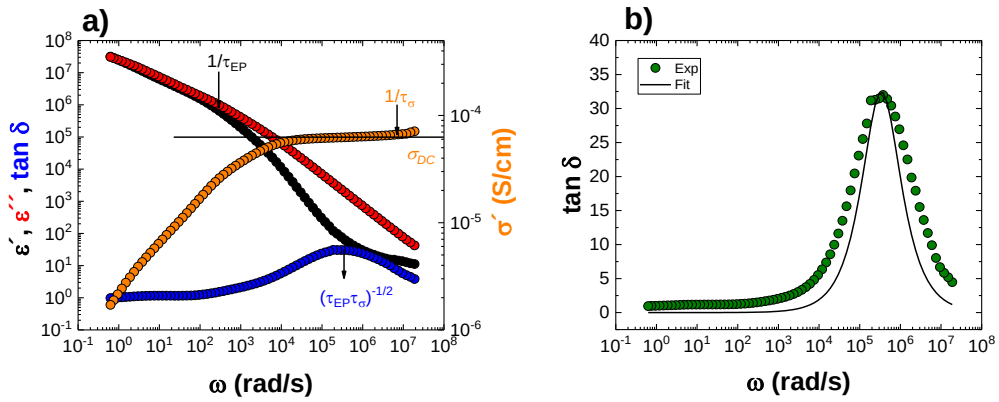

Figure 5.9. a) Dielectric response of 85 PEO 100 kg mol^{-1} / 15 PLiMTFSI >2,000 kg mol^{-1} to an applied AC field at 100 ºC, real part of the dielectric permittivity (ε´), dielectric loss (ε´´), loss tangent (tan δ) and real part of conductivity (σ´). b) Loss tangent (tanδ) as a function of angular frecuency for 85 PEO 100 kg mol^{-1} / 15 PLiMTFSI >2,000 kg mol^{-1} at 100 ºC. Solid curve is a fit of tanδ data to a Debye function (Eq. 5) giving rise to the same peak (frequency and tanδ) values.

Figure 5.9a shows an example of the dielectric response measured at 100 ºC for the 85 PEO 100 kg mol^{-1} / 15 PLiMTFSI >2,000 kg mol^{-1} blend, and it shows where these τ_{EP} and τ_σ values were obtained from. Later, these values were used in equation 5 to fit the tan δ values (Figure 5.9b) in order to verify that the τ_{EP} and

τ_σ values are correct. Figure 5.9b shows the angular frequency dependency. The solid line is the result using equation 5, the criterion used was to obtain the peak at the same frequency as the experimental data and the same value of tan δ at this frequency.

This model allows determining the density of ions that participate in the conduction process and their mobility

$$p = \frac{1}{\pi l_B L^2}\left(\frac{\tau_{EP}}{\tau_\sigma}\right)^2 \tag{5.6}$$

$$\mu = \frac{eL^2\tau_\sigma}{4\tau_{EP}^2 kT} \tag{5.7}$$

where, $l_B \equiv e^2/(4\pi\varepsilon_s\varepsilon_0 kT)$ is the Bjerrum length, L is the thickness of the capacitor, k is the Boltzmann constant, and T is the absolute temperature.

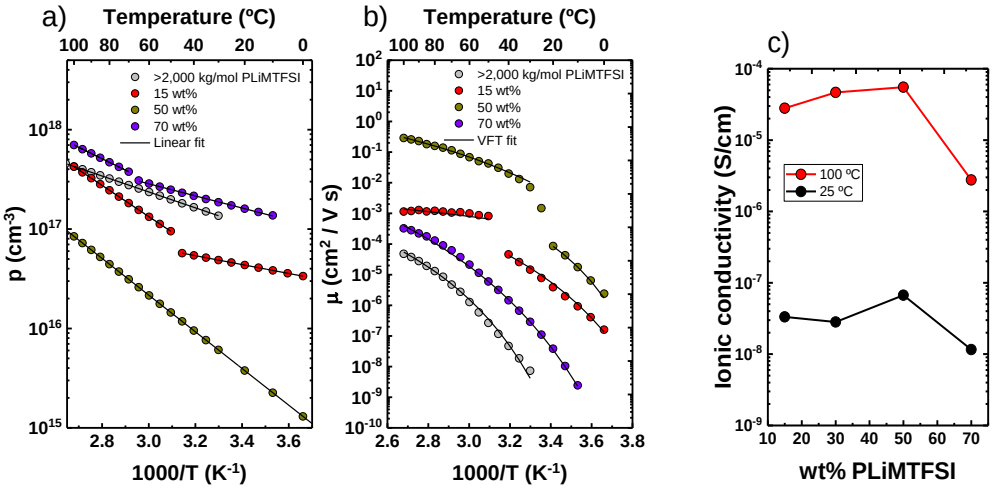

Figure 5.10. a) Free-ion number density, b) mobility of ions for the blends 100 kg mol^{-1} PEO / >2,000 kg mol^{-1} PLiMTFSI, c) ionic conductivity as a function of PLiMTFSI concentration.

Figure 5.10a presents the free-ion number density as a function of 1000/*K* for the blends 100 kg mol^{-1} PEO / >2,000 kg mol^{-1} PLiMTFSI, as well as for neat PLiMTFSI. In all samples, the ion density increases with temperature. The largest number of ions is present in the electrolyte with 70 wt% PLiMTFSI because it is the material with the highest amount of polyelectrolyte and, consequently, there is a greater amount of free lithium ions. In the case of the electrolyte with 15 wt%, a smaller number of free ions is observed. Also, a change in ion density is found near 50 ºC due to PEO crystallization, and the electrolyte with 50 wt% PLiMTFSI has the lowest ion density, maybe due to the fact that per unit of lithium-ion there are fewer places in the PEO to complex the lithium ions compared with the 15 wt% PLiMTFSI blend [45,46]. The temperature dependence of the conducting ion fraction that participates in the conduction process *p(T)* is described by the Arrhenius equation:

$$p(T) = p_{\infty} \exp\left(-\frac{E_a}{RT}\right) \qquad (5.8)$$

where p_{∞} is the conduction ion concentration as $T \rightarrow \infty$, E_a is the activation energy for conducting ions. The parameters obtained by fitting the data obtained above the melting temperature of the PEO are presented in Table 5.2.

Table 5.2. Conducting ion content fitted parameters

Sample	p_{∞} (cm^{-3})	E_a (kJ mol^{-1})
85 PEO / 15 PLiMTFSI	$6.73 \cdot 10^{21}$	30
50 PEO / 50 PLiMTFSI	$7.49 \cdot 10^{21}$	35.35
30 PEO / 70 PLiMTFSI	$8.21 \cdot 10^{20}$	21.93
PLiMTFSI	$5.97 \cdot 10^{19}$	15.33

Figure 5.10b shows the mobility of the ions that participate in the conduction process as determined by EP. Neat PLiMTFSI shows the lowest mobility. For PEO blends, the mobility increases up to a maximum at 50 wt% of both components. An abrupt change in mobility takes place at 15 and 50 wt% of PLiMTFSI when reducing the temperature due to the crystallization of PEO. Low mobility, very similar to that of neat PLiMTFSI, is observed in the case of the blend with 70 wt% of PLiMTFSI. The results of the temperature dependence of the ion mobility were fitted using the Vogel-Fulcher-Tammann (VFT) equation:

$$\mu(T) = \mu_{\infty} \exp\left(-\frac{B}{T - T_0}\right) \tag{5.9}$$

wherein μ_{∞} is the high temperature limit of the mobility, B is an energetic factor and T_0 is the Vogel temperature (at which molecular mobility goes to zero [44,47]).

In this way, we obtained a T_0 value of 245.15 K for neat PLiMTFSI. For the blends, the T_0 values were calculated using the Gordon-Taylor (G-T) equation (Figure 5.11) with k = 0.45, as this was the k value obtained for the fitting of the T_g values. In this calculation, we used a T_0 value of 186 K for neat PEO [48]. The fitting parameters calculated describing the data above the melting temperature of the PEO are presented in Table 5.3.

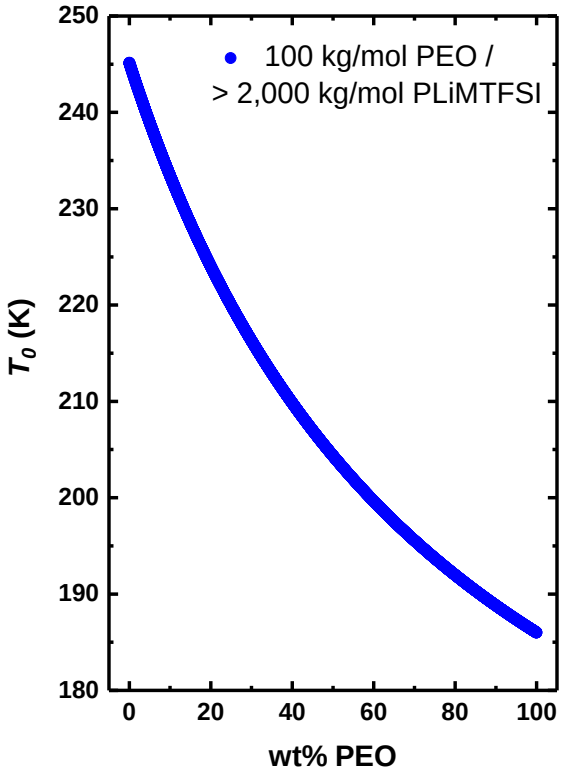

Figure 5.11. Calculation of T_0 values using the Gordon-Taylor equation.

Table 5.3. Ion Mobility fitted parameters

Sample	μ_∞ (cm^2 V^{-1} s^{-1})	B	T_0 (K)
85 PEO / 15 PLiMTFSI	0.01	361.6	190.3
50 PEO / 50 PLiMTFSI	33.5	797	204.4
30 PEO / 70 PLiMTFSI	3.1	1406	216.3
PLiMTFSI	0.14	1005.1	245.15

Figure 5.10c shows the variation of the ionic conductivity of the blends as a function of PLiMTFSI concentration at two constant temperatures (25 and 100 ºC), where it is observed that the highest ionic conductivity in both cases is with 50 wt% PLiMTFSI. Figures 5.10a and 5.10b show that with 50 wt% the ion density

is low, but the mobility of the ions increases more than an order of magnitude as compared to the other compositions. Therefore, we can assume that in this kind of electrolytes, the change of mobility has a stronger effect on the temperature dependence of the ionic conductivity.

5.4 Conclusions

In this chapter, single ion conducting polymer electrolytes blends based on PEO and PLiMTFSI were investigated by changing the molecular weight and the composition of both polymers in the blends from 5 wt% to 70 wt%. The polymer-polymer interaction parameter (χ_{12}) was calculated and found to be negative for all the blends, indicating that the blends are miscible. The isothermal crystallization showed that the crystallization rate and spherulitic growth decreased with the amount of PLiMTFSI. A maximum ionic conductivity value was found in the 50/50 composition blends. Ionic conductivity values were higher when using the 100 kg mol^{-1} PEO and, when comparing the different molecular weights of PLiMTFSI, the best results of ionic conductivity were obtained with the 50 kg mol^{-1} one. The highest conductivity at 70 ºC was $2.1 \cdot 10^{-4}$ S cm^{-1} at 50 wt% 50 kg mol^{-1} PLiMTFSI, probably the best electrolyte to be tested in a battery. The contributions of mobility and the density of ions that participate in the conduction process were separated by employing dielectric spectroscopy, which showed that mobility is the parameter that has a greater effect on ionic conductivity, because it is in the 50/50 composition, which has the highest ionic conductivity, a greater increase in the mobility of lithium ions is observed. Current work in our laboratories involves the use of the high conductivity SIPEs in lithium metal batteries.

5.5 References

[1] J.B. Goodenough, Y. Kim, Challenges for Rechargeable Li Batteries, Chemistry of Materials. 22 (2010) 587–603. https://doi.org/10.1021/cm901452z.

[2] Y. Zhang, A. Lim, W. Cai, R. Rohan, G. Xu, RSC Advances Design and synthesis of a single ion conducting block copolymer electrolyte with multifunctionality for lithium ion batteries †, (2014) 43857–43864. https://doi.org/10.1039/c4ra08709g.

[3] J. Mindemark, M.J. Lacey, T. Bowden, D. Brandell, Progress in Polymer Science Beyond PEO — Alternative host materials for Li + -conducting solid polymer electrolytes, Progress in Polymer Science. 81 (2018) 114–143. https://doi.org/10.1016/j.progpolymsci.2017.12.004.

[4] J.L. Olmedo-Martínez, L. Meabe, A. Basterretxea, D. Mecerreyes, A.J. Müller, Effect of chemical structure and salt concentration on the crystallization and ionic conductivity of aliphatic polyethers, Polymers. 11 (2019) 452. https://doi.org/10.3390/polym11030452.

[5] L.H. Sim, C.H. Chan, N.H.A. Nasir, The effect of molecular mass of PEO and the salt content on its isothermal crystallization behaviour for PEO:LiClO4electrolyte, AIP Conference Proceedings. 1250 (2010) 201–204. https://doi.org/10.1063/1.3469636.

[6] Z. Xue, D. He, X. Xie, Poly(ethylene oxide)-based electrolytes for lithium-ion batteries, Journal of Materials Chemistry A. 3 (2015) 19218–19253. https://doi.org/10.1039/c5ta03471j.

[7] K. Pożyczka, M. Marzantowicz, J.R. Dygas, F. Krok, Ionic Conductivity and Lithium transference number of Poly(ethylene oxide):LiTFSI system, Electrochimica Acta. 227 (2017) 127–135. https://doi.org/https://doi.org/10.1016/j.electacta.2016.12.172.

[8] A.M. Stephan, T.P. Kumar, M.A. Kulandainathan, N.A. Lakshmi, Chitin-Incorporated Poly(ethylene oxide)-Based Nanocomposite Electrolytes for Lithium Batteries, The Journal of Physical Chemistry B. 113 (2009) 1963–1971. https://doi.org/10.1021/jp808640j.

[9] C. Cao, Y. Li, Y. Feng, C. Peng, Z. Li, W. Feng, A solid-state single-ion polymer electrolyte with ultrahigh ionic conductivity for dendrite-free lithium metal batteries, Energy Storage Materials. 19 (2019) 401–407. https://doi.org/10.1016/j.ensm.2019.03.004.

[10] D. Devaux, L. Liénafa, E. Beaudoin, S. Maria, T.N.T. Phan, D. Gigmes, E. Giroud, P. Davidson, R. Bouchet, Comparison of single-ion-conductor block-copolymer electrolytes with Polystyrene-TFSI and Polymethacrylate-TFSI structural blocks, Electrochimica Acta. 269 (2018) 250–261. https://doi.org/10.1016/j.electacta.2018.02.142.

[11] L. Porcarelli, M.A. Aboudzadeh, L. Rubatat, J.R. Nair, A.S. Shaplov, C. Gerbaldi, D. Mecerreyes, Single-ion triblock copolymer electrolytes based on poly(ethylene oxide) and methacrylic sulfonamide blocks for lithium metal batteries, Journal of Power Sources. 364 (2017) 191–199. https://doi.org/10.1016/j.jpowsour.2017.08.023.

[12] R. Meziane, J.P. Bonnet, M. Courty, K. Djellab, M. Armand, Single-ion polymer electrolytes based on a delocalized polyanion for lithium batteries, in: Electrochimica Acta, 2011. https://doi.org/10.1016/j.electacta.2011.03.074.

[13] C. Jangu, A.M. Savage, Z. Zhang, A.R. Schultz, L.A. Madsen, F.L. Beyer, T.E. Long, Sulfonimide-Containing Triblock Copolymers for Improved Conductivity and Mechanical Performance, Macromolecules. (2015). https://doi.org/10.1021/acs.macromol.5b01009.

[14] Y. Long, Lizhen; Wang, Shuanjin; Xiao, Min; Meng, Polymer electrolytes for lithium polymer batteries, Journal of Materials Chemistry A. 4 (2016) 10038–10069. https://doi.org/10.1039/c6ta02621d.

[15] T.A. LaFollette, L.M. Walker, Structural and mechanical hysteresis at the order-order transition of block copolymer micellar crystals, Polymers. 3 (2011) 281–298. https://doi.org/10.3390/polym3010281.

[16] A.G.B. Pereira, R.F. Gouveia, G.M. de Carvalho, A.F. Rubira, E.C. Muniz, Polymer blends based on PEO and starch: Miscibility and spherulite growth rate evaluated through DSC and optical microscopy, Materials Science and Engineering C. (2009). https://doi.org/10.1016/j.msec.2008.09.009.

[17] S. Rajendran, M. Sivakumar, R. Subadevi, M. Nirmala, Characterization of PVA-PVdF based solid polymer blend electrolytes, Physica B:

Condensed Matter. 348 (2004) 73–78. https://doi.org/10.1016/j.physb.2003.11.073.

[18] M.J. Reddy, J.S. Kumar, U. V. Subba Rao, P.P. Chu, Structural and ionic conductivity of PEO blend PEG solid polymer electrolyte, Solid State Ionics. 177 (2006) 253–256. https://doi.org/10.1016/j.ssi.2005.11.014.

[19] S. Rajendran, M. Sivakumar, R. Subadevi, Investigations on the effect of various plasticizers in PVA-PMMA solid polymer blend electrolytes, Materials Letters. 58 (2004) 641–649. https://doi.org/10.1016/S0167-577X(03)00585-8.

[20] M.A. Morris, S.H. Sung, P.M. Ketkar, J.A. Dura, R.C. Nieuwendaal, T.H. Epps, Enhanced Conductivity via Homopolymer-Rich Pathways in Block Polymer-Blended Electrolytes, Macromolecules. 52 (2019) 9682–9692. https://doi.org/10.1021/acs.macromol.9b01879.

[21] Q. Ma, H. Zhang, C. Zhou, L. Zheng, P. Cheng, J. Nie, W. Feng, Y. Hu, H. Li, X. Huang, L. Chen, M. Armand, Ion Conductors Single Lithium-Ion Conducting Polymer Electrolytes Based on a Super- Delocalized Polyanion Angewandte, (2016) 2521–2525. https://doi.org/10.1002/anie.201509299.

[22] Y. Liu, Y. Zhang, M. Pan, X. Liu, C. Li, Y. Sun, D. Zeng, H. Cheng, A mechanically robust porous single ion conducting electrolyte membrane fabricated via self-assembly, Journal of Membrane Science. (2016). https://doi.org/10.1016/j.memsci.2016.02.002.

[23] W.C. Kang, H.G. Park, K.C. Kim, S.W. Ryu, Synthesis and electrochemical properties of lithium methacrylate-based self-doped gel polymer electrolytes, Electrochimica Acta. (2009). https://doi.org/10.1016/j.electacta.2009.03.050.

[24] Y. Chen, H. Ke, D. Zeng, Y. Zhang, Y. Sun, H. Cheng, Superior polymer backbone with poly(arylene ether) over polyamide for single ion conducting polymer electrolytes, Journal of Membrane Science. (2017). https://doi.org/10.1016/j.memsci.2016.12.011.

[25] E.W. Stacy, C.P. Gainaru, M. Gobet, Z. Wojnarowska, V. Bocharova,

S.G. Greenbaum, A.P. Sokolov, Fundamental Limitations of Ionic Conductivity in Polymerized Ionic Liquids, Macromolecules. 51 (2018) 8637–8645. https://doi.org/10.1021/acs.macromol.8b01221.

[26] A. Kisliuk, V. Bocharova, I. Popov, C. Gainaru, A.P. Sokolov, Fundamental parameters governing ion conductivity in polymer electrolytes, Electrochimica Acta. 299 (2019) 191–196. https://doi.org/10.1016/j.electacta.2018.12.143.

[27] V. Bocharova, Z. Wojnarowska, P.F. Cao, Y. Fu, R. Kumar, B. Li, V.N. Novikov, S. Zhao, A. Kisliuk, T. Saito, J.W. Mays, B.G. Sumpter, A.P. Sokolov, Influence of Chain Rigidity and Dielectric Constant on the Glass Transition Temperature in Polymerized Ionic Liquids, Journal of Physical Chemistry B. 121 (2017) 11511–11519. https://doi.org/10.1021/acs.jpcb.7b09423.

[28] F. Fan, Y. Wang, T. Hong, M.F. Heres, T. Saito, A.P. Sokolov, Ion Conduction in Polymerized Ionic Liquids with Different Pendant Groups, Macromolecules. 48 (2015) 4461–4470. https://doi.org/10.1021/acs.macromol.5b00257.

[29] L. Meabe, T.V. Huynh, N. Lago, H. Sardon, C. Li, L.A. O'Dell, M. Armand, M. Forsyth, D. Mecerreyes, Poly(ethylene oxide carbonates) solid polymer electrolytes for lithium batteries, Electrochimica Acta. 264 (2018) 367–375. https://doi.org/10.1016/j.electacta.2018.01.101.

[30] H.A. Schneider, The Gordon-Taylor equation. Additivity and interaction in compatible polymer blends, Die Makromolekulare Chemie. 189 (1988) 1941–1955. https://doi.org/10.1002/macp.1988.021890818.

[31] T. Nishi, T.T. Wang, Melting Point Depression and Kinetic Effects of Cooling on Crystallization in Poly(vinylidene fluoride)-Poly(methyl methacrylate) Mixtures, Macromolecules. (1975). https://doi.org/10.1021/ma60048a040.

[32] Z. Qiu, T. Ikehara, T. Nishi, Miscibility and crystallization in crystalline/crystalline blends of poly(butylene succinate)/poly(ethylene oxide), Polymer. (2003). https://doi.org/10.1016/S0032-3861(03)00149-6.

[33] A.T. Lorenzo, M.L. Arnal, J. Albuerne, A.J. Müller, DSC isothermal polymer crystallization kinetics measurements and the use of the Avrami equation to fit the data: Guidelines to avoid common problems, Polymer Testing. 26 (2007) 222–231. https://doi.org/10.1016/j.polymertesting.2006.10.005.

[34] P.C. Hiemenz, T.P. Lodge, Polymer chemistry, CRC press, 2007.

[35] J.M. Schultz, Polymer crystallization: the development of crystalline order in thermoplastic polymers, Amer Chemical Society, 2001.

[36] A.T. Müller, Alejandro J., Michell, R. M., Lorenzo, Isothermal Crystallization Kinetics of Polymers, in: Q. Guo (Ed.), Polymer Morphology: Principles, Characterization, and Processing, John Wiley & Sons, 2016: pp. 181–203. https://doi.org/https://doi.org/10.1002/9781118892756.ch11.

[37] R. Mary, A.J. Müller, Progress in Polymer Science Confined crystallization of polymeric materials, Progress in Polymer Science. 54–55 (2016) 183–213. https://doi.org/10.1016/j.progpolymsci.2015.10.007.

[38] L. Porcarelli, C. Gerbaldi, F. Bella, J.R. Nair, Super Soft All-Ethylene Oxide Polymer Electrolyte for Safe All-Solid Lithium Batteries, Scientific Reports. 6 (2016) 19892. https://doi.org/10.1038/srep19892.

[39] A. Jourdain, A. Serghei, E. Drockenmuller, U. Lyon, Enhanced Ionic Conductivity of a 1,2,3-Triazolium-Based Poly(siloxane ionic liquid) Homopolymer, (2016) 5–8. https://doi.org/10.1021/acsmacrolett.6b00761.

[40] M. Lee, Y.K. Kwon, J. Kim, U.H. Choi, Effect of Poly(ethylene glycol) Crystallization on Ionic Conduction and Dielectric Response of Imidazolium-Based Copolyester Ionomers, Macromolecules. (2019). https://doi.org/10.1021/acs.macromol.8b02332.

[41] Y. Wang, C.N. Sun, F. Fan, J.R. Sangoro, M.B. Berman, S.G. Greenbaum, T.A. Zawodzinski, A.P. Sokolov, Examination of methods to determine free-ion diffusivity and number density from analysis of electrode polarization, Physical Review E - Statistical, Nonlinear, and Soft Matter Physics. (2013). https://doi.org/10.1103/PhysRevE.87.042308.

[42] J.R. Macdonald, Theory of ac Space-Charge Polarization Effects in Photoconductors, Semiconductors, and Electrolytes, Phys. Rev. 92 (1953) 4–17. https://doi.org/10.1103/PhysRev.92.4.

[43] R. Coelho, R. De Physique, E. Supérieure, Sur la relaxation d ' une charge d ' espace Rui Coelho, 18 (1983) 137–146.

[44] R.J. Klein, S. Zhang, S. Dou, B.H. Jones, R.H. Colby, J. Runt, Modeling electrode polarization in dielectric spectroscopy: Ion mobility and mobile ion concentration of single-ion polymer electrolytes, Journal of Chemical Physics. 124 (2006). https://doi.org/10.1063/1.2186638.

[45] Z. Xue, D. He, X. Xie, Poly(ethylene oxide)-based electrolytes for lithium-ion batteries, Journal of Materials Chemistry A. 3 (2015) 19218–19253. https://doi.org/10.1039/c5ta03471j.

[46] A. Hektor, M.K. Klintenberg, A. Aabloo, J.O. Thomas, Molecular dynamics simulation of the effect of a side chain on the dynamics of the amorphous LiPF6-PEO system, Journal of Materials Chemistry. 13 (2003) 214–218. https://doi.org/10.1039/b206281j.

[47] O. Gedeon, Origin of glass fragility and Vogel temperature emerging from Molecular dynamics simulations, Journal of Non-Crystalline Solids. 498 (2018) 109–117. https://doi.org/10.1016/j.jnoncrysol.2018.06.012.

[48] F. Barroso-Bujans, S. Cerveny, P. Palomino, E. Enciso, S. Rudić, F. Fernandez-Alonso, A. Alegria, J. Colmenero, Dynamics and Structure of Poly(ethylene oxide) Intercalated in the Nanopores of Resorcinol-Formaldehyde Resin Nanoparticles, Macromolecules. 49 (2016) 5704–5713. https://doi.org/10.1021/acs.macromol.6b01285.

Chapter VI

6. Ternary poly(ethylene oxide)/Poly(L,L-lactide) PEO/PLA blends as High-Temperature Solid Polymer Electrolytes for Lithium Batteries

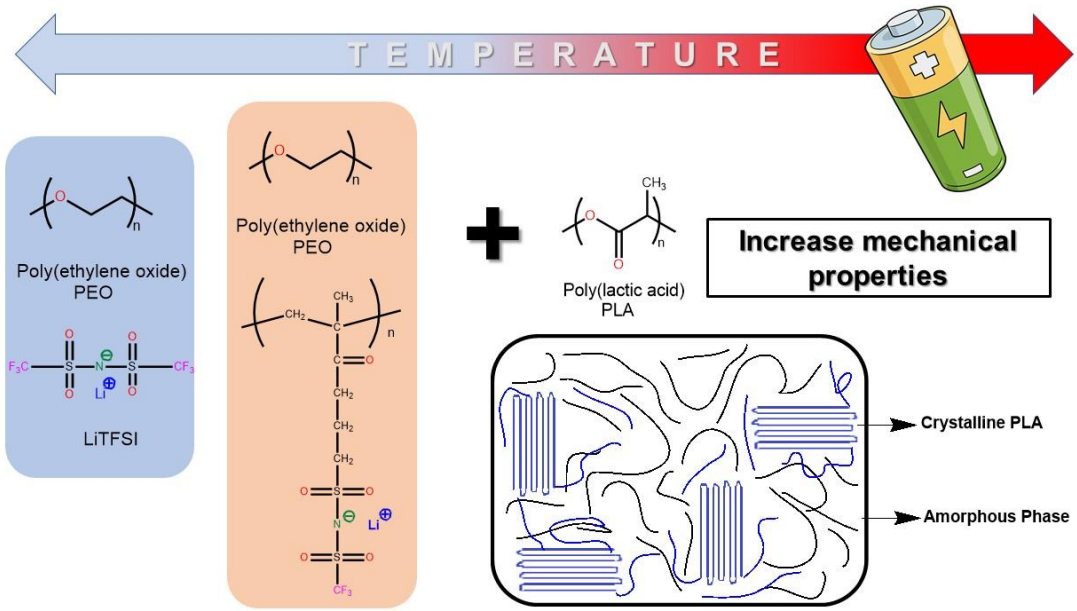

6.1 Abstract

Lithium batteries are rapidly expanding, with demands for high-performance batteries required in many technological fields. However, the restricted temperature operation below 60°C is a problem for a number of applications that require high-energy rechargeable batteries that operate at a high temperature (>100 °C). Poly(ethylene oxide) PEO is the reference solid polymer electrolyte (SPE) actually used in solid-state lithium batteries. However, the application of PEO at higher temperatures is limited due to the loss of mechanical properties. In this article, we show that classical polymer blending strategy of PEO with PLA allows extending its use in batteries at high temperatures (100 ºC). This improvement is due to the mechanical reinforcement of PEO solid electrolytes associated with the presence of PLA crystals. Thus, two solid electrolyte systems based on PEO/PLA blends with either a LiTFSI salt or a lithium single-ion polymer (poly(lithium 1-[3-(methacryloyloxy) propylsulfonyl]-1-(trifluoromethanesulfonyl) imide) (PLiMTFSI)) were investigated and compared. DSC results indicate that regardless of the concentration of LiTFSI or PLiMTFSI in the blend, crystals of PLA are present with melting peaks at 160-170 ºC and the lithium salt distributes preferentially in the PEO rich amorphous phases. The ionic conductivity is negatively affected by the incorporation of PLA in the blends. However, at high temperatures (>70 °C), ionic conductivities in the order of ~10^{-4} S cm^{-1} were obtained for both systems. By DMTA, it was found that the incorporation of PLA increases the mechanical properties of the electrolytes, showing Storage Modulus values of ~10^{6} Pa for the PEO/PLA/LiTFSI system and higher than ~10^{7} Pa for the PEO/PLA/PLiMTFSI system at high temperatures (100 ºC). Finally, both ternary blends were compared in a symmetrical lithium battery at 100 ºC, and the single ion conducting PEO/PLA/PLiMTFSI system presented lower overpotentials, which is reflected in a lower polarization inside the lithium battery. Hence, we demonstrate that the presence of PLA in PEO SPEs increases the possibility of using lithium batteries at higher temperatures.

6.2 Introduction

The development of safe, high-specific-capacity energy storage devices is one of the great challenges of the 21st century. In applications such as portable devices or electric vehicles, lithium-ion batteries currently have no contender in terms of energy density or durability. However, the restricted temperature range of -25 °C to 60 °C is a problem for a number of applications that require high-energy rechargeable batteries that operate at a high temperature (>100 °C) [1]. Lithium metal anodes have a specific capacity of 3860 $mAhg^{-1}$, far superior than graphite anodes used for lithium-ion batteries. However, their use in combination with liquid electrolytes is still limited due to safety concerns, such as leakage, dendrite formation, and thermal stability [2,3]. Solid polymer electrolytes (SPEs) are promising candidate materials to replace organic solvents as electrolytes in lithium batteries and mitigate the safety issues connected to the use of lithium metal electrodes. Poly(ethylene oxide) (PEO) is the most studied host polymer due to its capacity to dissolve lithium salts [4,5]. It is currently used in commercially available solid-state lithium metal batteries for the electric vehicle running at 60 ºC. PEO exhibits high ionic conductivity (~10^{-3} S cm^{-1}) with lithium salts such as lithium bis(trifluoromethanesulfonyl)imide (LiTFSI) at relatively high temperatures (70 ºC) [6,7].

However, PEO has specific problems to be used as a solid electrolyte for batteries, such as the low ionic conductivity at low temperatures, mainly due to the crystallization of the PEO. Several strategies have been developed to solve these problems, such as the synthesis of random [8] or block copolymers [9], as well as crosslinking [10–12], or the incorporation of nanoparticles [13]. In parallel, many researchers are looking for polymer electrolytes with higher ionic conductivity than PEO, which allow battery operation at low or high temperatures. Another additional issue is the poor mechanical properties of the electrolytes as PEO becomes amorphous when lithium salts are added, and the mechanical properties decrease [14], in particular at temperatures over its T_m (>65 ºC).

A common method used in the polymer industry to improve the mechanical properties of polymers is polymer blending. It has advantages over other methods, e.g., it requires less energy and helps obtain materials with the properties of the parent homopolymers involved. For instance, poly(methyl

methacrylate) (PMMA), polystyrene (PS) [15], or poly(lactide) (PLA) [16] have been used as stiffer polymers to maintain the structural integrity of the polymer electrolyte. Of particular interest is the use of PLA (with high L contents) as it is a semi-crystalline polymer and is a widely used bio-based polymer due to its good mechanical properties, biodegradability, and biocompatibility [17]. This makes it a suitable material for applications in different areas such as chemical engineering, medical equipment, electronic devices, and industrial packaging. Recently, Xie *et al.*, found that lithium bis(trifluoromethanesulfonyl)imide (LiTFSI) is thermodynamically miscible with PLA, and a small amount of LiTFSI can accelerate the crystallization of PLA. Also, the anion has a strong interaction with the PLA [18]. In addition, the interaction between the carbonyl group of PLA with Li-ions from LiTFSI has also been reported [19].

Given these special characteristics of PLA, we decided to investigate PEO/PLA blends, as these polymers have partial or total miscibility in their amorphous regions depending on composition and molecular weight of the homopolymers. However, their crystals segregate and do not co-crystallize regardless of the ratio between the polymers [20]. This special feature in this blend is suitable for SPEs, since the presence of PLA crystals can increase the mechanical properties of the solid polymer electrolytes, in particular at temperatures between the T_m of PEO(> 65 ºC) and the T_m of PLA (<150 ºC).

In this chapter, two ternary blends based on PEO and PLA were investigated (Figure 6.1), one with LiTFSI, which presents conductivity due to the movement of the two ions present. In this system, the effect of the concentration of LiTFSI in the crystallization of PEO and PLA was investigated in detail. The second system is a ternary blend in which poly(lithium 1-[3-(methacryloyloxy) propylsulfonyl]-1-(trifluoromethanesulfonyl) imide) (PLiMTFSI) is used as a lithium single-ion conducting polymer. The ionic conductivity and mechanical properties of these ternary blends were then evaluated. Finally, their performance as solid polymer electrolytes in a symmetrical lithium battery at a high temperature was evaluated (i.e., 100 ºC).

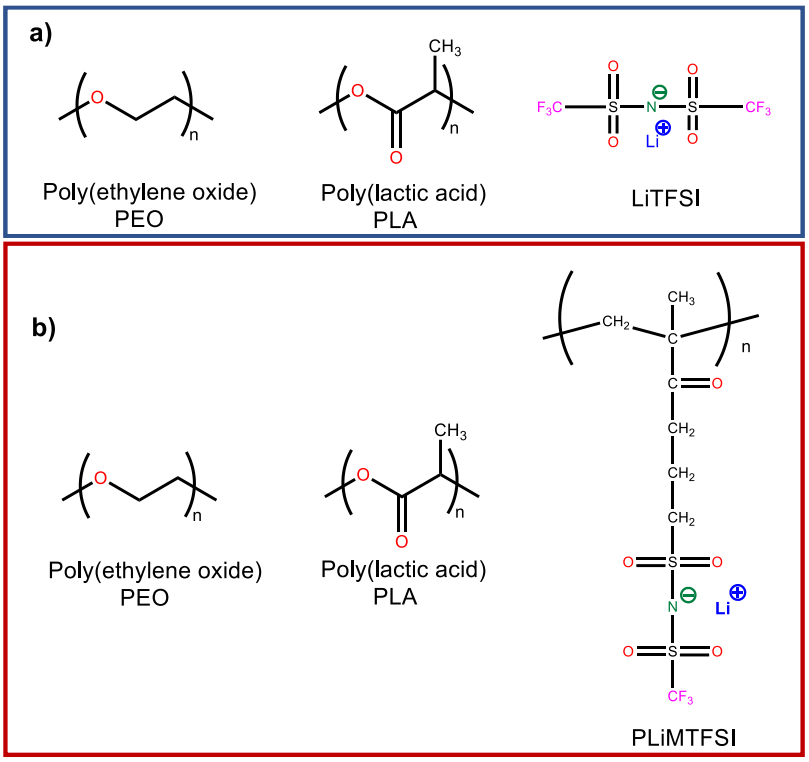

Figure 6.1. Chemical structures of the compounds used in the two electrolyte systems, a) double ion conduction ternary blends, and b) single ion conduction ternary blends.

6.3 Results

6.3.1 Non-isothermal DSC of PEO/PLA/LiTFSI blends

Figure 6.2 shows the non-isothermal DSC results for the PEO/PLA/LiTFSI blends. It must be noted that the first heating scans reflect the thermal history of the blends that were prepared from solution followed by vacuum drying, as specified in the experimental part. For the different blend compositions, PLA crystals are present since during the drying process of the blends the PLA-rich phase was able to crystallize (solvent-induced crystallization). This indicates that in solvent-cast and dried films of the blends, PLA crystals are always present. These PLA crystals will be present during the ionic conductivity measurements (which are performed at temperatures well below the melting point of PLA crystals), and they will provide good mechanical properties to the prepared electrolytes.

During the first heating scan, in the blend without LiTFSI (Figure 6.2a), i.e., the neat PEO/PLA blend, the sequential melting of PEO and PLA is observed.

During cooling (Figure 6.2b), both PEO and PLA phases crystalize in the neat PEO/PLA blend. However, the crystallization exotherm corresponding to the PLA-rich phase is broad and small and cannot be clearly appreciated at the scale shown in Figure 6.2b, but the melting of PLA crystals can be seen in Figure 6.2c (notice the absence of cold crystallization). During the second heating scan of the neat PEO/PLA blend (Figure 6.2c), the T_m of PEO component is observed at 59.6 ºC. This value is nearly 5 degrees lower than that obtained for neat PEO (see Figure 6.2c). This melting point depression of the PEO-rich phase is caused by the PLA presence in the blend. PEO is known to be miscible or partially miscible (depending on its molecular weight) with PLA. In fact, neat PLA cannot crystallize during cooling, as shown in Figure 6.2b, and remains amorphous, as demonstrated by the lack of fusion in Figure 6.2c. However, when it is mixed with PEO, the PLA component in the blend can crystallize during cooling and subsequently melt, as shown in Figures 6.2b and 6.2c [21,22]. This is a result of the miscibility with PEO that acts as a plasticizer for PLA inducing its crystallization.

The results presented in Figure 6.2 indicate that the PEO/PLA/LiTFSI blends are partially miscible with PEO-rich and PLA-rich phases that co-exist and where the Li salt prefers the PEO-rich phase. The existence of two phases has also been demonstrated by DMTA, where two clear T_gs were found located at values in between those of the parent homopolymers (see DMTA section below). In the blends with a lithium salt, the melting temperature and the degree of crystallinity of PEO decrease as a function of LiTFSI concentration until at 30 wt% LiTFSI, the PEO-rich component in the blend becomes completely amorphous. In contrast, the melting temperature of the PLA phase remains constant, indicating that the salt prefers to dissolve in the PEO phase. During cooling (Figure 6.2b), only the crystallization peak of the PEO phase is present, and it decreases with increasing lithium concentration in the blend, the PLA-rich phase does not crystallize during cooling at 20 ºC min^{-1}. During the second DSC heating scans (Figure 6.2c), the PEO phase melts, and its latent heat of fusion decreases as Li salt concentration increases, a consistent result with the crystallization of the PEO-rich phase observed in Figure 6.2b. On the other hand, the PLA-rich phase exhibits cold crystallization during the second DSC heating scan followed

by melting. Since the T_m of PLA does not change with salt concentration, it is concluded that LiTFSI prefers to dissolve in PEO. As the mechanical properties of polymers are directly related to crystallinity degree, the presence of PLA crystals suggests that the mechanical properties of these electrolytes could be enhanced in comparison to PEO/LiTFSi blends.

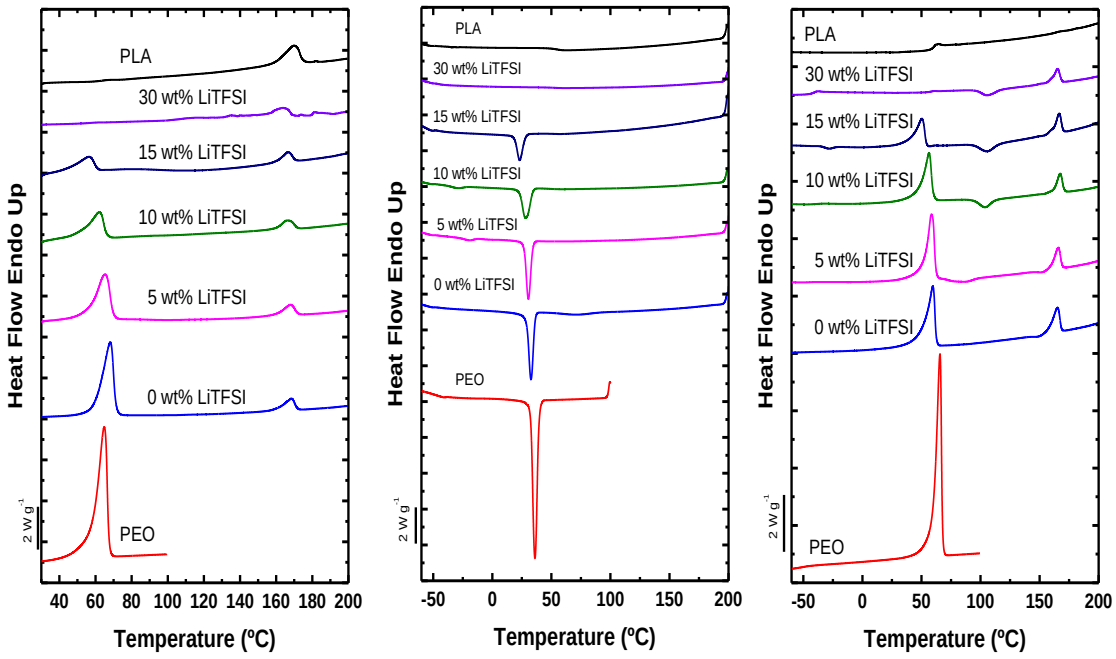

Figure 6.2. Differential scanning calorimetry (DSC) for PEO/PLA/LiTFSI electrolytes, a) first scans at 20 ºC min^{-1}, b) cooling scans at 20 ºC min^{-1}, and c) second heating scans at 20 ºC min^{-1}

6.3.2 Isothermal crystallization of the PEO-rich phase within PEO/PLA/LiTFSI blends

Isothermal crystallization studies were carried out in the DSC for PEO/PLA/LiTFSI blends, to study the effect of LiTFSI on the overall crystallization kinetics of the PEO-rich phase in the presence of PLA-rich phase crystals. A heat treatment was performed to ensure that the PLA-rich phase was crystallized before monitoring the isothermal crystallization of the PEO-rich phase. It is worth mentioning that this study was only performed for the PEO/PLA/LiTFSI blends because in the PEO/PLA/PLiMTFSI blends, the PEO-rich phase is amorphous.

The isothermal crystallization measured by DSC includes both primary nucleation and crystal growth. Figure 6.3a shows the inverse of the half-crystallization time ($1/\tau_{50\%}$) (this value is directly proportional to the overall crystallization rate [23,24]) as a function of the crystallization temperature (T_c) for all blends.

When comparing the crystallization kinetics of neat PEO and the PEO/PLA blend without salt, it is observed that the PEO-rich component in the blend needs a higher supercooling to crystallize. The T_g of PLA is much higher than that of PEO, and since at least part of the PLA is miscible with PEO, the PLA chains within the PEO-rich phase in the blend hinder both secondary nucleation and molecular diffusion, so the overall crystallization rate decreases [25,26].

In the blends with LiTFSI, the overall crystallization rate decreases as the salt concentration increases, a result that is consistent with those found by non-isothermal DSC (Figure 6.2). The supercooling needed for crystallization increases with an increasing salt concentration in the system. Figure 6.4 presents the same study for neat PEO with LiTFSI: a similar behavior is observed, as the overall crystallization rate decreases as a function of salt concentration. However, in the blends that contain PLA, the crystallization rate of the PEO-rich blends is higher in comparison with the overall crystallization rate of neat PEO with Li salt.

Figure 6.3b presents the values of the normalized isothermal crystallization enthalpy (ΔH_c) as a function of T_c for the PEO/PLA/LiTFSI blends. The value of ΔH_c has been normalized by dividing the experimental values by the weight fraction of PEO in the blend. It is directly proportional to the crystallinity of the PEO-rich phase, and it decreases with increasing LiTFSI concentration, as expected for PEO/LiTFSI blends [27,28].

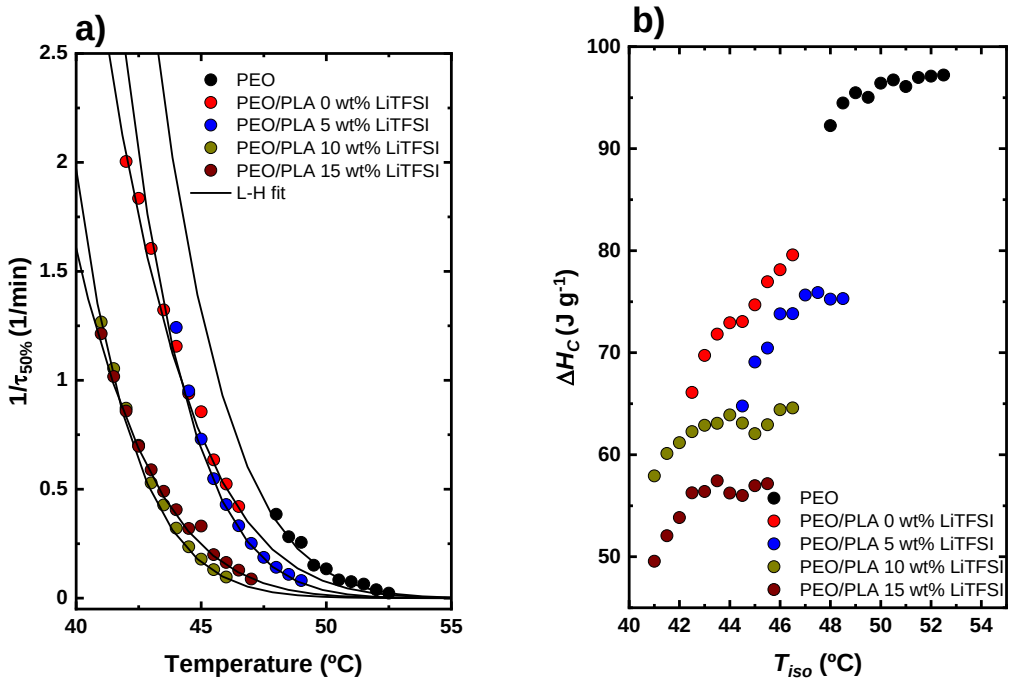

Figure 6.3. a) Overall crystallization rate of PEO in PEO/PLA/LiTFSI electrolytes (expressed as the inverse of the half-crystallization time). The solid lines are fits to the Lauritzen and Hoffman equation, b) Crystallization enthalpy (ΔH_c) of PEO in the different electrolytes as a function of isotherm temperature (T_{iso}).

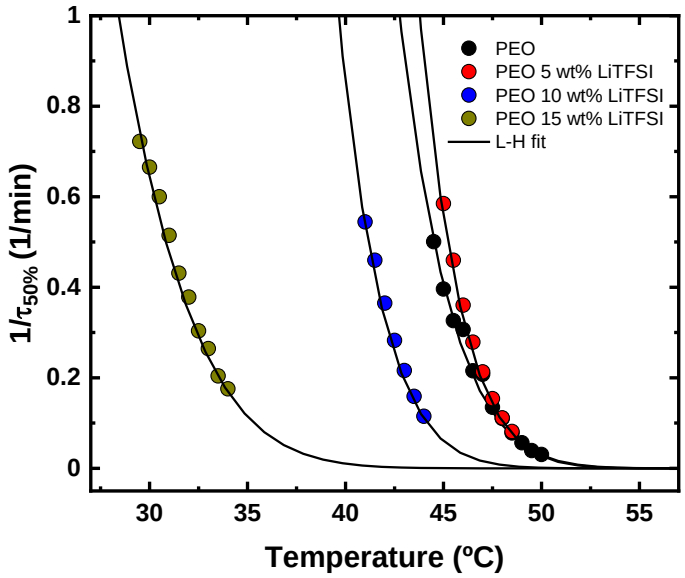

Figure 6.4. Overall crystallization rate of PEO with different LiTFSI concentration (expressed as the inverse of the half-crystallization time). The solid lines are fits to the Lauritzen and Hoffman equation.

6.3.3 Non-isothermal DSC of PEO/PLA/PLiMTFSI ternary blends

In Chapter 5 were prepared binary blends of PEO/PLiMTFSI electrolytes and demonstrated using the Nishi-Wang approach that these two polymers are miscible (negative Flory-Huggins interaction parameter), and we also determined the ratio between them to have the highest ionic conductivity values [29]. Figure 6.5 shows the non-isothermal DSC for the PEO/PLA/PLiMTFSI blends. The first DSC heating scans for the blends (Figure 6.5a) show that the neat 50/50 PEO/PLiMTFSI blend is amorphous, as already reported by us in a previous study [29]. We previously found that PEO and PLiMTFSI blends are miscible, and the degree of interchain interaction is so high that PEO chains cannot crystallize, as they cannot phase segregate during cooling from a mixed melt. [29].

Figure 6.5b also shows that at 20 ºC min^{-1} the neat PLA sample cannot crystallize and therefore exhibits no traces of crystals in Figure 6.5c (i.e., second DSC heating run). PLA has some limited solubility in the PEO/PLiMTFSI; hence, two distinct phases are formed, i.e., a PLA-rich phase and a PEO/PLiMTFSI-rich phase. A clear indication for partial miscibility is provided by the fact that the PLA component in the blend can crystallize during the second heating scan via cold crystallization (Figure 6.5c), something that does not happen in neat PLA.

Figure 6.5a shows the first heating scans of the blends that were prepared from solution followed by vacuum drying, as specified in the experimental part. For the different blend compositions, it is observed that the T_m value of the PLA crystals remains constant, but the intensity of the endothermic melting peak increases with the amount of PLA in the blend, demonstrating that during the drying process of the blends, the PLA-rich phase crystallizes (solvent-induced crystallization). This is an important observation since it indicates that in solvent-cast and dried films of the blends, PLA crystals are always present. These crystals will be left unmolten during ionic conductivity measurements and will provide good mechanical properties to the prepared electrolytes.

Figure 6.5b shows the DSC cooling scans at 20 ºC min^{-1}, the results indicate that none of the samples can crystallize during cooling from the melt [29].

The second DSC heating scans are shown in Figure 6.5c. PLA exhibits an endothermic step at 60 ºC that corresponds to its T_g, and the PEO/PLiMTFSI blends also exhibit a single T_g value at a temperature of -14.5 ºC.

The blends exhibit two T_g values in Figure 6.5c, one located below -10 ºC corresponding to the PEO/PLiMTFSI-rich phase and another one around 55 ºC corresponding to the PLA-rich phase. The two T_g values in the blends are shifted slightly with respect to that of the neat PLA and PEO/PLiMTFSI blend due to the partial miscibility between the components (see Table 6.1). Above the T_g of the PLA-rich phase, all blends exhibit cold crystallization (at around 100 ºC) and finally the melting of the PLA crystals at around 160 ºC.

The behavior is very similar to the PEO/PLA/LiTFSI system, where the PLA crystals remain in the electrolyte at temperatures below 150 ºC. The presence of PLA crystals will reinforce the mechanical properties of the electrolytes.

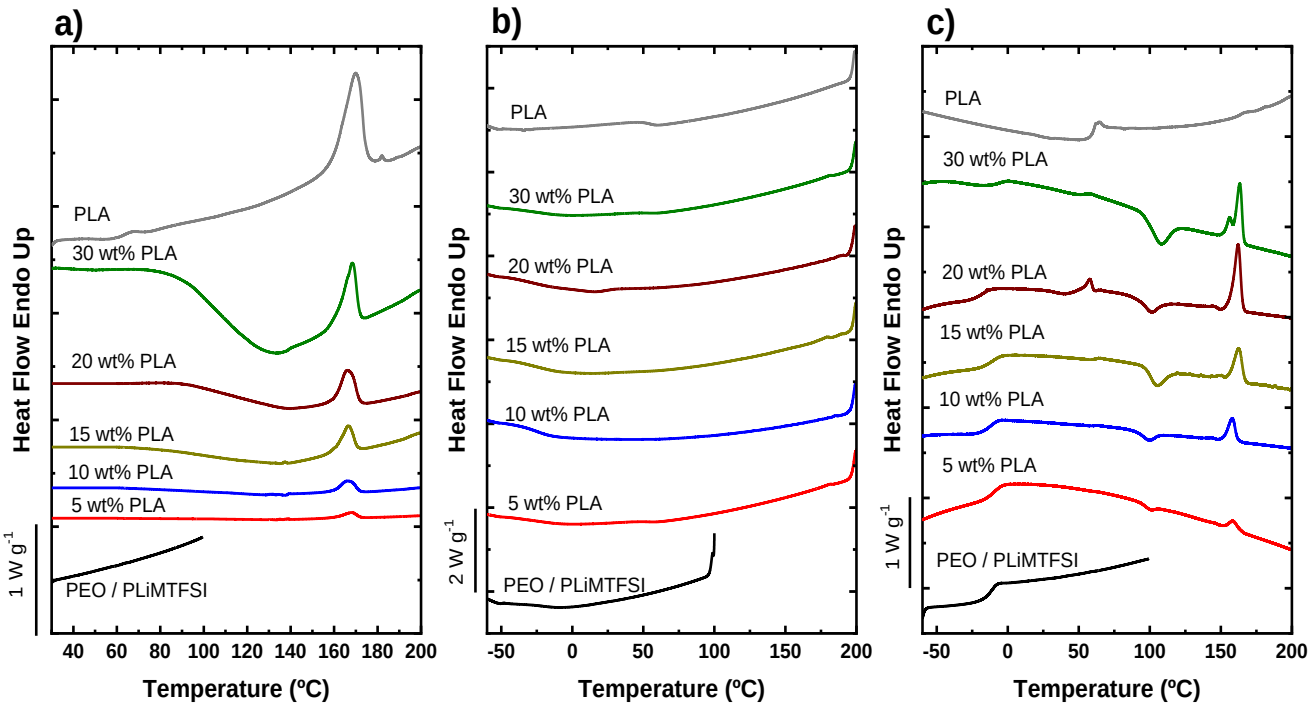

Figure 6.5. DSC scans for PEO/PLA/PLiMTFSI electrolytes, a) first scans at 20 ºC min^{-1}, b) cooling scans at 20 ºC min^{-1}, and c) second heating scans at 20 ºC min^{-1}

Table 6.1. Values of thermal transitions in both electrolyte systems (data taken during the second heating).

Sample	T_m (ºC) **PEO**	ΔH_m (J g^{-1}) **PEO**	T_{cc} (ºC) **PLA**	ΔH_{cc} (J g^{-1}) **PLA**	T_m (ºC) **PLA**	ΔH_m (J g^{-1}) **PLA**	T_g (ºC) **PEO**	T_g (ºC) **PLA**	T_g (ºC) **PEO/PLiMTFSI**
PEO	68.5	132.4	-	-	-	-	-58	-	-
PLA	-	-	-	-	-	-	-	61	-
60 PEO 40 PLA 0 wt% LiTFSI	59.6	111.3	-	-	165.1	51	-48.3	-	-
60 PEO 40 PLA 5 wt% LiTFSI	58.4	106.1	87	16.1	165.8	35.5	-43.9	-	-
60 PEO 40 PLA 10 wt% LiTFSI	56.4	91.1	103.9	30.8	167.4	33.9	-38.8	-	-
60 PEO 40 PLA 15 wt% LiTFSI	50.3	76.7	105.4	35.9	166.6	38.2	-30	-	-
60 PEO 40 PLA 30 wt% LiTFSI	-	-	105.7	30.4	165.2	36.4	-41.7	57.7	-
50 PEO 50 PLiMTFSI 0 wt% PLA	-	-	-	-	-	-	-	-	-18.7
50 PEO 50 PLiMTFSI 5 wt% PLA	-	-	105.1	36	164.8	40	-	54.8	-16.7
50 PEO 50 PLiMTFSI 10 wt% PLA	-	-	105.7	21.5	165.2	28	-	54.2	-14.5
50 PEO 50 PLiMTFSI 15 wt% PLA	-	-	104.7	20	164.2	28.6	-	55.3	-11.2
50 PEO 50 PLiMTFSI 20 wt% PLA	-	-	102.5	21.5	164.2	33	-	55.5	-10.1
50 PEO 50 PLiMTFSI 30 wt% PLA	-	-	105.4	41.8	166.1	48.7	-	53	-5.6

6.3.4 Ionic conductivity

Electrochemical impedance measurements are performed starting from high to low temperatures, in a range from 100 ºC down to room temperature, to measure the ionic conductivity of the polymer electrolytes. As shown above, in the non-isothermal DSC results (Figures 6.2 and 6.5), the prepared electrolytes contain PLA crystals formed during the drying process of the electrolytes. Only the PEO phase will be molten at 100 ºC, as the melting point of PLA is much higher (in the range 160-170 ºC).

Figure 6.6 shows the ionic conductivity values as a function of temperature for the two systems. For the PEO/PLA/LiTFSI system (Figure 6.6a), the ionic conductivity increases as a function of salt concentration, up to a maximum of ~10^{-4} S cm^{-1} at high temperatures. Then, during cooling from 100 ºC down to room temperature, the crystallization process of PEO takes place at around 60 °C, as indicated by a drop in ionic conductivity. The ionic conductivity shows a lower value with increasing salt concentration, because the salt dissolves in the PEO-rich phase. It must be remembered that the crystallinity degree of the PEO–rich phase decreases with the increase in salt concentration until at 30 wt% LiTFSI the PEO-rich phase becomes completely amorphous. Therefore, the electrolyte with the highest ionic conductivity is the PEO/PLA/LiTFSI blend with 30% LiTFSI salt, i.e., it displays a conductivity value of $1.01 \cdot 10^{-5}$ S cm^{-1} at 25 ºC and $1.65 \cdot 10^{-4}$ S cm^{-1} at 100 ºC.

In the PEO/PLA/PLiMTFSI system (Figure 6.6b), the conductivity of the 50 PEO/ 50 PLiMTFSI blend without PLA and that of the blends with different PLiMTFSI concentrations are presented. These electrolytes do not present PEO crystallization processes in the temperature range in which the experiments are performed, so no conductivity drops are observed. The highest conductivity is displayed by the blend without PLA, and when increasing the PLA concentration, the ionic conductivity decreases. The electrolytes with PLA concentrations between 5 and 20 wt% present closer values, but when adding to the blend 30 wt% PLA, the conductivity decreases significantly.

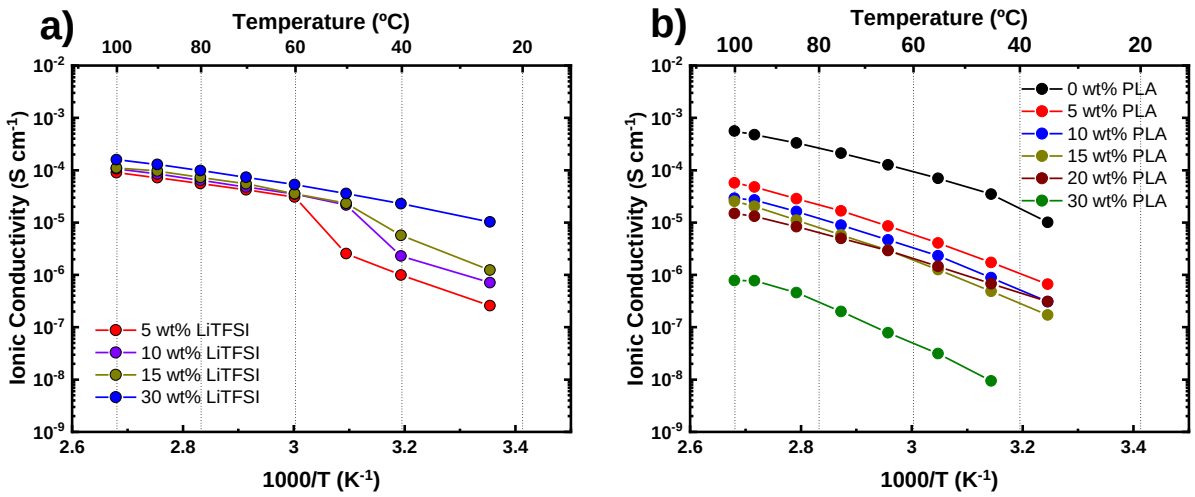

Figure 6.6. Ionic conductivy values of a function of temperature for: a) PEO/PLA/LiTFSI system, and b) PEO/PLA/PLiMTFSI system.

6.3.5 Mechanical Properties: DMTA

It has been reported that dendrite growth can be suppressed if the shear modulus of the electrolyte is larger than 1.8 times that of lithium, i.e., a value close to 6 GPa [30]. But normally, the mechanical properties of electrolytes decrease with the addition of lithium salts, because the salt acts as a diluent for the polymers [28], that is why several strategies have been carried out to increase the mechanical properties of these electrolytes. Another option to suppress dendrite growth is to use single ionic conduction electrolytes, because with these materials, there is no polarization within the cell and no dendritic growth [9,10,31].

Figure 6.8 shows the temperature dependence of the storage modulus *G´* for the two systems. They both show at very low temperatures, in the glassy state, modulus values that are in the order of ~10^9 Pa (for the sample without LiTFSI and in the second system for the two samples analyzed with 15 and 30 wt% PLA). Figure 6.7 show the modulus as a function of temperature for neat PEO and neat PLA. For these polymers, the alpha relaxation process, which is the mechanical manifestation of the glass transition temperature, is observed by DMTA at -51 ºC and 66 ºC for PEO and PLA respectively.

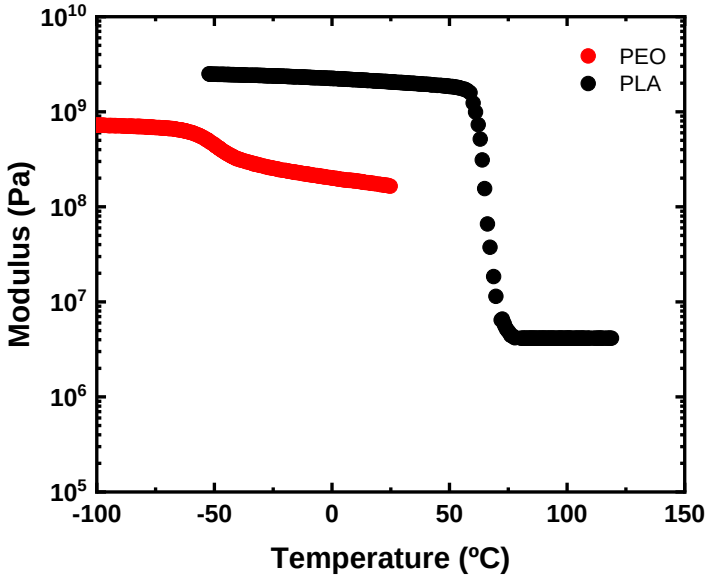

Figure 6.7. DMTA of neat PEO and neat PLA.

In the case of the PEO/PLA blend without salt for the first system (Figure 6.8a), the T_g of the PEO-rich phase and the PLA-rich phase appears at -37 and 50 ºC respectively, these shifts in the T_g values in comparison with those of the neat polymers is a clear indication of partial miscibility. The miscibility between PEO and PLA depends on the molecular weight. Complete miscibility can be achieved if low molecular weights are employed. Still, when high molar masses are involved, as in the present case, only partial miscibility is achieved, leading to the formation of a PEO-rich and a PLA-rich phase [32,33].

Figure 6.8a also shows the plasticizing effect of the Li salt, which causes important reductions in the PEO-rich phase crystallinity. Such decreases in crystallinity cause significant reductions in the storage modulus $G´$, as evidenced by the vertical shift of the modulus versus temperature curves to lower values.

For the PEO/PLA/LiTFSI system (Figure 6.8a), all samples show a drop in moduli at around -50 ºC, i.e., at temperatures close to the T_g of the PEO-rich phase. A more significant modulus drop occurs around 60 ºC, at temperatures close to the melting of the PEO-rich phase crystals and the T_g of the PLA-rich phase. Nevertheless, the modulud values at these high temperatures are higher

when compared to the values found in the literature for the PEO/LiTFSI system [34,35] at 100 ºC (~10^6 Pa with 30 wt% LiTFSI).

For the PEO/PLA/PLiMTFSI system (Figure 6.8b), the modulus at very low temperatures is practically the same for the two samples analyzed. Additionally, the T_g of the PEO/PLiMTFSI blend can be observed by the drop in storage modulus at -20 ºC, which agrees well with the DSC results. The second modulus drop at 60 ºC corresponds to the T_g of PLA-rich phase, since in this system, PLA is partially miscible with the PEO/PLiMTFSI blend and therefore, the T_g value for the PLA-rich phase is approximately 6 degrees lower than that observed for neat PLA by DMTA. As the PLA concentration increases, an increase in the modulus at high temperatures is clearly observed because the sample contains a higher amount of PLA-rich phase crystals. The storage modulus reaches a value of about ~10^7 Pa for the electrolyte with 30 wt% PLA at 100 ºC.

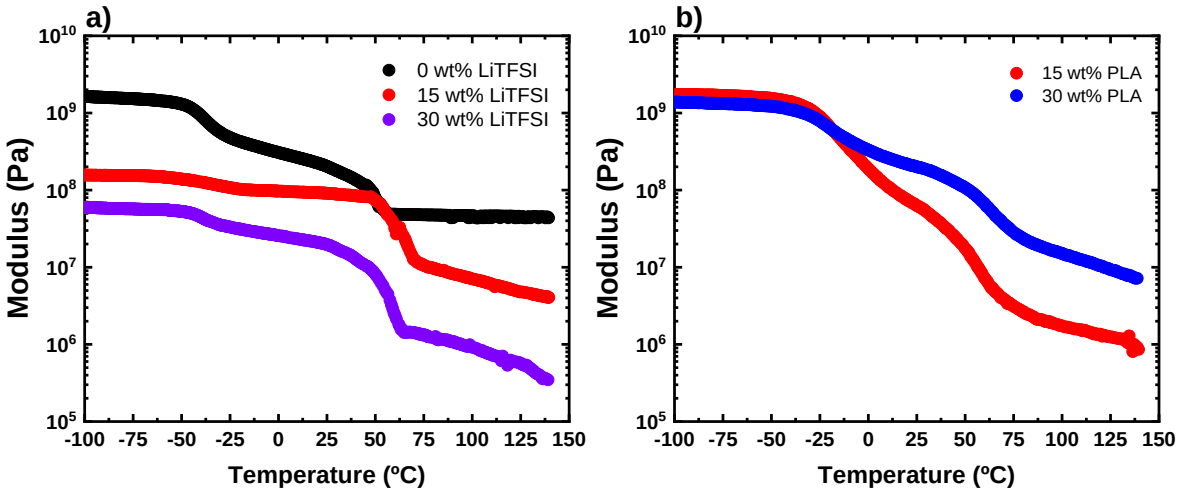

Figure 6.8. DMTA of: a) PEO/PLA/LiTFSI system, and b) PEO/PLA/PLiMTFSI system.

6.3.6 Lithium-ion transference number (tLi+) and linear sweep voltammetry (LSV)

The lithium-ion transference number (t_{Li}^+) is related to the fraction of the total electrical current carried in an electrolyte given by the movement of lithium cations. The transference number is directly related to the mobility of both the anion and the cation, according to the following equation [36]:

$$t_a = 1 - t_{Li^+} = \frac{\mu_a}{\mu_a + \mu_{Li^+}} \quad (6.1)$$

where t_a is the anion transference number, t_{Li^+} is the lithium-ion transference number, μ_a is the anion mobility, and μ_{Li^+} is the lithium-ion mobility.

If the value of the lithium transfer number is 1 (as in the case of single ion polymer electrolytes), then t_a is equal to zero, and according to equation 6.2 of the time for dendrite formation, it becomes infinite, or in the case that the value is not exactly 1, the time becomes very large [36,37].

$$\tau = \pi D \left(\frac{eC_0}{2Jt_a}\right)^2 \quad (6.2)$$

where D is the ambipolar diffusion coefficient, e is the electronic charge, J is the effective electrode current, and C_0 is the initial lithium concentration.

Figure 6.9, 6.10 and Table 6.2 presents the lithium-ion transference number (t_{Li^+}) for blend PEO/PLiMTFSI and two electrolytes of each system with PLA, measured at 70 ºC. For the PEO/PLA/LiTFSI system, the values were calculated for the electrolytes with 15 and 30 wt% LiTFSI, and they are 0.47 and 0.55, respectively. These values are higher compared to that of the PEO/LiTFSI systems, which is around 0.2 [38]. The reason for this difference is related to the complexation of the carbonyl groups of amorphous PLA with the lithium cations, and because the coordination between the carbonyl groups and the lithium cations is weaker. This effect has been reported for other systems, for example, in polycarbonates [39] or polyether/polyester blends [40].

For the PEO/PLA/PLiMTFSI system, t_{Li^+} was obtained for the electrolytes with 5 and 15 wt% PLA. The advantages of using single ion polymer electrolytes are that they avoid the dendrite formation during charge/discharge cycles and that there is no polarization inside the cell. Single ion polymer electrolytes have the anion grafted in the polymer backbone. In the present case, the t_{Li^+} is around 0.8 with 5 wt% PLA and 0.86 with 15 wt% PLA, these values correspond to this type of electrolytes. Moreover, as in the case of the PEO/PLA/LiTFSI system, the transport number increases a little, since the value for the PEO/PLiMTFSI blend

is 0.76 (Figure 6.9), and when adding the PLA, this value increases due to the coordination between the carbonyl groups of PLA and the lithium cations.

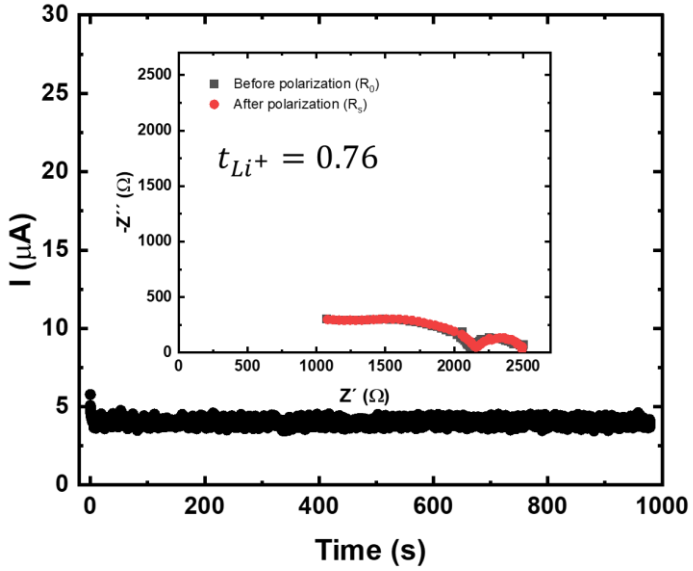

Figure 6.9. ac- and dc-measurements for the lithium ion transference number measurements for 50 PEO/50 PLiMTFSI electrolyte.

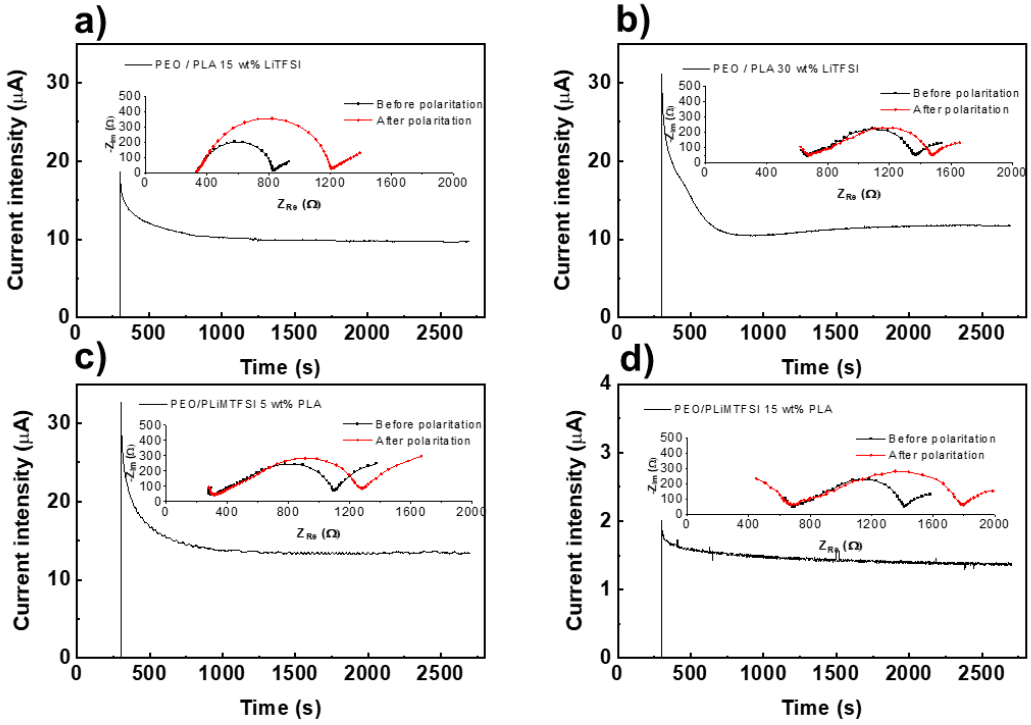

Figure 6.10. ac- and dc-measurements for the lithium ion transference number measurements for: a) PEO/PLA 15 wt% LiTFSI, b) PEO/PLA 30 wt% LiTFSI, c) PEO/PLiMTFSI 5 wt% PLA, and d) PEO/PLiMTFSI 15 wt% PLA electrolytes.

Table 6.2. Lithium-ion transference number for the different electrolytes.

Electrolyte	t_{Li^+}
PEO/PLA 15 wt% LiTFSI	0.47
PEO/PLA 30 wt% LiTFSI	0.55
PEO/PLiMTFSI 5 wt% PLA	0.82
PEO/PLiMTFSI 15 wt% PLA	0.86

The electrochemical stability of SPEs is very important for practical application in energy storage devices [41]. Linear sweep voltammetry experiments for two electrolytes of each system are presented in Figure 6.11. All four electrolytes measured are electrochemically stable above 4 V, which is one of the requirements for the application of these materials [5] and to ensure the safe application of these electrolytes in 4 V lithium secondary batteries. When scanning towards more anodic values, an increase in current is observed, attributed to the electrolyte decomposition at the interface with the electrode. In the case of the PEO/PLA/LiTFSI system, both with 15 and 30 wt%, the electrochemical stability is above 5 V, and in PEO/PLiMTFSI/PLA system with 15 wt% PLA, the value is 4. 4 V. This value is very similar to that reported by Porcarelli *et al.* [9] for PLiMTFSI-PEO-PLiMTFSI copolymers. The difference in the stability values between the systems is due to the fact that the PLiMTFSI starts to degrade at lower potentials, while the LiTFSI is more stable, but both systems have higher stability at 4 V.

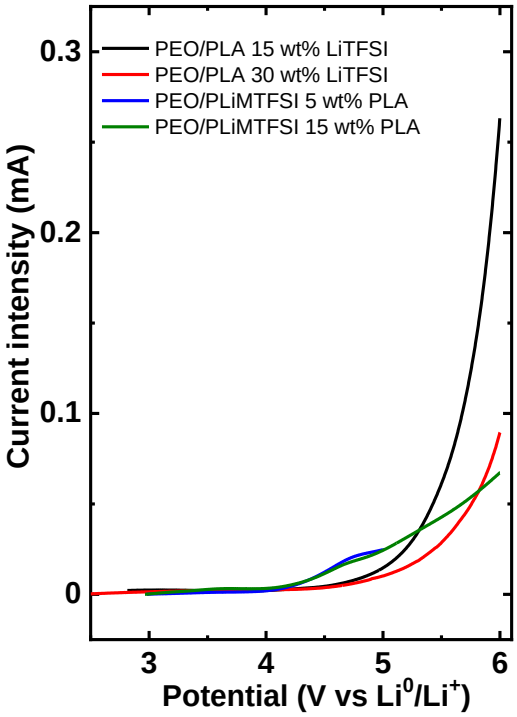

Figure 6.11. Linear sweep voltammograms (v = 10 mV s^{-1}) obtained in the stainless steel/SPE/Li^0 cell at 70 ºC.

6.3.7 Symmetrical cells

A way to evaluate the solid polymer electrolytes against lithium is to perform strip-plate tests of a Li/Li symmetrical cell at different current densities [42]. Figure 6.12 displays the cell polarization as a function of time for PEO/PLA 15 wt% LiTFSI and PEO/PLiMTFSI 15 wt% PLA, at 0.1, 0.2 and 0.5 mA cm^{-2} current densities. These tests were performed at 100 °C, which is a considerably higher temperature test than most reported values for symmetrical lithium cells. For PEO/PLA 15 wt% LiTFSI electrolyte, a stable voltage is observed with the passing of the cycles, with an overpotential of 20, 75, and 130 mV without short circuit. For PEO/PLiMTFSI 15 wt% PLA electrolyte, a stable voltage is observed with the passing of the cycles, with an overpotential of 0.3, 0.6, and 1.5 V. However, signs of short circuits are visible at the higher current density.

When the overpotential increases considerably, a short circuit could occur in the cell. This increase indicates that it has reached a critical value of charge

density, further increasing the charge density, a short circuit occurs within the cell. This is because at a higher current density, the Li^+ ions penetrate into the voids of the solid electrolyte, where a higher reaction kinetics for dendrite growth takes place [11,43].

Lee, *et al*. compared a single-ion and a two-ion electrolyte and concluded that single-ion electrolytes exhibit a higher overpotential, because there is a higher impedance for the single-ion system at higher currents [44]. In general, our results are encouraging and suggest that both families of electrolytes can be used for high-temperature lithium metal cells.

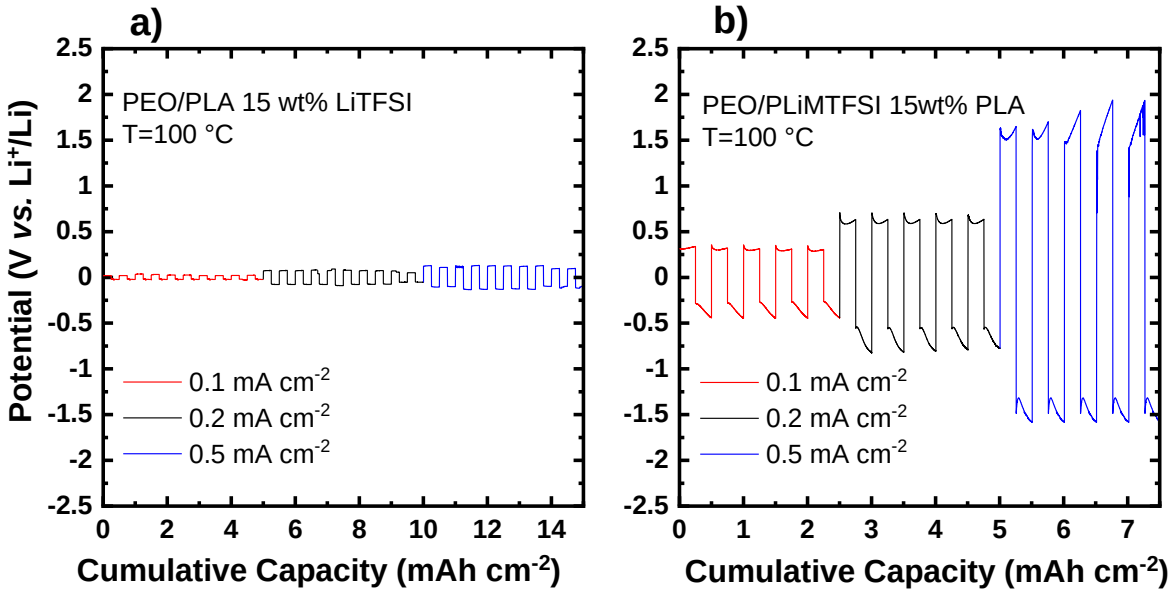

Figure 6.12. Plot of the over potential as a function of time for a symmetrical lithium cell cycled at 0.1, 0.2 and 0.5 mA cm^{-2} at 100 °C with (a) PEO/PLA 15wt% LiMTFSI and (b) PEO/PLiMTFSI 15%wt PLA.

6.4 Conclusions

In this chapter, new solid polymer electrolytes were designed by polymer blending of a high T_m PLA into conducting PEO for high temperature lithium batteries. Thus, two polymer electrolyte PEO/PLA ternary blend systems were prepared, one with dual-ion conduction (i.e., with LiTFSI) and the other with single-ion conduction (with PLiMTFSI). By means of DSC, it was demonstrated that PEO and PLA in the presence of LiTFSI and PLiMTFSI are partially miscible. PLA crystals exist regardless of the concentration of LiTFSI and PLiMTFSI, indicating that both the salt and the single ion polymer prefer to dissolve in PEO.

Moreover, the presence of PLA in both systems increases the mechanical properties of the solid electrolytes. This is an advantage, as these electrolytes could be used at high temperatures (i.e., 100 °C). Ionic conductivities in the order of 10^{-4} S cm^{-1} were obtained in both systems at 100 ºC. The electrolytes were shown to be stable at potentials higher than 4 V. Finally, both ternary blends were compared in a symmetrical lithium battery at 100 ºC. Both solid polymer electrolytes showed promising performance and demonstrated lithium metal plating and striping, while the single ion conducting PEO/PLA/PLiMTFSI system presented lower overpotentials. Hence, we demonstrate that a simple polymer blending strategy and the presence of PLA in PEO SPEs opens the possibility of running lithium metal batteries at high temperatures.

6.5 References

[1] D.R. Wright, N. Garcia-Araez, J.R. Owen, Review on high temperature secondary Li-ion batteries, Energy Procedia. 151 (2018) 174–181.

[2] J.-C. Daigle, A. Vijh, P. Hovington, C. Gagnon, J. Hamel-Pâquet, S. Verreault, N. Turcotte, D. Clément, A. Guerfi, K. Zaghib, Lithium battery with solid polymer electrolyte based on comb-like copolymers, Journal of Power Sources. 279 (2015) 372–383.

[3] Q. Zhang, K. Liu, F. Ding, X. Liu, Recent advances in solid polymer electrolytes for lithium batteries, Nano Research. 10 (2017) 4139–4174.

[4] J. Mindemark, M.J. Lacey, T. Bowden, D. Brandell, Progress in Polymer Science Beyond PEO — Alternative host materials for Li + -conducting solid polymer electrolytes, Progress in Polymer Science. 81 (2018) 114–143. https://doi.org/10.1016/j.progpolymsci.2017.12.004.

[5] S.B. Aziz, T.J. Woo, M.F.Z. Kadir, H.M. Ahmed, A conceptual review on polymer electrolytes and ion transport models, Journal of Science: Advanced Materials and Devices. 3 (2018) 1–17. https://doi.org/10.1016/j.jsamd.2018.01.002.

[6] Blue Solutions, (2021). https://www.blue-solutions.com/en/battery-technology/ (accessed August 10, 2021).

[7] D. Devaux, R. Bouchet, D. Glé, R. Denoyel, Mechanism of ion transport in PEO/LiTFSI complexes: Effect of temperature, molecular weight and end groups, Solid State Ionics. 227 (2012) 119–127. https://doi.org/10.1016/j.ssi.2012.09.020.

[8] T. Morioka, K. Nakano, Y. Tominaga, Ion-Conductive Properties of a Polymer Electrolyte Based on Ethylene Carbonate/Ethylene Oxide

Random Copolymer, Macromolecular Rapid Communications. 38 (2017) 1600652.

[9] L. Porcarelli, M.A. Aboudzadeh, L. Rubatat, J.R. Nair, A.S. Shaplov, C. Gerbaldi, D. Mecerreyes, Single-ion triblock copolymer electrolytes based on poly(ethylene oxide) and methacrylic sulfonamide blocks for lithium metal batteries, Journal of Power Sources. 364 (2017) 191–199. https://doi.org/10.1016/j.jpowsour.2017.08.023.

[10] M. Álvarez Tirado, L. Castro, G. Guzmán-González, L. Porcarelli, D. Mecerreyes, Single-Versus Dual-Ion UV-Cross-Linked Gel Polymer Electrolytes for Li–O2 Batteries, ACS Applied Energy Materials. 4 (2021) 295–302.

[11] L. Meabe, T.V. Huynh, D. Mantione, L. Porcarelli, C. Li, L.A. O'Dell, H. Sardon, M. Armand, M. Forsyth, D. Mecerreyes, UV-cross-linked poly (ethylene oxide carbonate) as free standing solid polymer electrolyte for lithium batteries, Electrochimica Acta. 302 (2019) 414–421.

[12] P. Sutton, M. Airoldi, L. Porcarelli, J.L. Olmedo-Martínez, C. Mugemana, N. Bruns, D. Mecerreyes, U. Steiner, I. Gunkel, Tuning the properties of a UV-polymerized, cross-linked solid polymer electrolyte for lithium batteries, Polymers. 12 (2020). https://doi.org/10.3390/polym12030595.

[13] A.R. Polu, H.-W. Rhee, Effect of TiO2 nanoparticles on structural, thermal, mechanical and ionic conductivity studies of PEO12–LiTDI solid polymer electrolyte, Journal of Industrial and Engineering Chemistry. 37 (2016) 347–353.

[14] S. Klongkan, J. Pumchusak, Effects of nano alumina and plasticizers on morphology, ionic conductivity, thermal and mechanical properties of PEO-LiCF3SO3 solid polymer electrolyte, Electrochimica Acta. 161 (2015) 171–176.

[15] R. Prasanth, V. Aravindan, M. Srinivasan, Novel polymer electrolyte based on cob-web electrospun multi component polymer blend of polyacrylonitrile/poly (methyl methacrylate)/polystyrene for lithium ion batteries—Preparation and electrochemical characterization, Journal of Power Sources. 202 (2012) 299–307.

[16] N. Zhang, A. ling Zhang, Q. fang Liu, M. Zhang, Q. Li, F. fang Li, Effect of liquid crystal ionomer intercalated montmorillonite nanocomposites on PEO/PLA solid polymer electrolytes, Ionics. 24 (2018) 3805–3813. https://doi.org/10.1007/s11581-018-2519-1.

[17] F. Carrasco, P. Pagès, J. Gámez-Pérez, O.O. Santana, M.L. Maspoch, Processing of poly (lactic acid): Characterization of chemical structure, thermal stability and mechanical properties, Polymer Degradation and Stability. 95 (2010) 116–125.

[18] K. Xie, J. Shen, L. Ye, Z. Liu, Y. Li, Increased gt Conformer Contents of PLLA Molecular Chains Induced by Li-TFSI in Melt: Another Route to Promote PLLA Crystallization, Macromolecules. 52 (2019) 7065–7072. https://doi.org/10.1021/acs.macromol.9b01188.

[19] I. Osada, S.M. Hosseini, S. Jeong, S. Passerini, Novel Ternary Polymer Electrolytes Based on Poly(lactic acid) from Sustainable Sources, ChemElectroChem. 4 (2017) 463–467. https://doi.org/10.1002/celc.201600653.

[20] A.J. Nijenhuis, E. Colstee, D.W. Grijpma, A.J. Pennings, High molecular weight poly(L-lactide) and poly(ethylene oxide) blends: Thermal characterization and physical properties, Polymer. 37 (1996) 5849–5857. https://doi.org/10.1016/S0032-3861(96)00455-7.

[21] D. Saha, S.K. Samal, M. Biswal, S. Mohanty, S.K. Nayak, Preparation and characterization of poly (lactic acid)/poly (ethylene oxide) blend film: effects of poly (ethylene oxide) and poly (ethylene glycol) on the properties, Polymer International. 68 (2019) 164–172.

[22] Y. Eom, B. Choi, S. Park, A study on mechanical and thermal properties of PLA/PEO blends, Journal of Polymers and the Environment. 27 (2019) 256–262.

[23] A.T. Lorenzo, M.L. Arnal, J. Albuerne, A.J. Müller, DSC isothermal polymer crystallization kinetics measurements and the use of the Avrami equation to fit the data: Guidelines to avoid common problems, Polymer Testing. 26 (2007) 222–231. https://doi.org/10.1016/j.polymertesting.2006.10.005.

[24] A.T. Müller, Alejandro J., Michell, R. M., Lorenzo, Isothermal Crystallization Kinetics of Polymers, in: Q. Guo (Ed.), Polymer Morphology: Principles, Characterization, and Processing, John Wiley & Sons, 2016: pp. 181–203. https://doi.org/https://doi.org/10.1002/9781118892756.ch11.

[25] Z. Gan, B. Jiang, J. Zhang, Poly (ε-caprolactone)/poly (ethylene oxide) diblock copolymer. I. Isothermal crystallization and melting behavior, Journal of Applied Polymer Science. 59 (1996) 961–967.

[26] J.K. Palacios, J. Zhao, N. Hadjichristidis, A.J. Müller, How the complex interplay between different blocks determines the isothermal crystallization kinetics of triple-crystalline PEO-b-PCL-b-PLLA triblock terpolymers, Macromolecules. 50 (2017) 9683–9695.

[27] B. Kumar, S.J. Rodrigues, S. Koka, The crystalline to amorphous transition in PEO-based composite electrolytes: role of lithium salts, Electrochimica Acta. 47 (2002) 4125–4131.

[28] J.L. Olmedo-Martínez, L. Meabe, A. Basterretxea, D. Mecerreyes, A.J. Müller, Effect of chemical structure and salt concentration on the crystallization and ionic conductivity of aliphatic polyethers, Polymers. 11 (2019) 452. https://doi.org/10.3390/polym11030452.

[29] J.L. Olmedo-Martínez, L. Porcarelli, Á. Alegría, D. Mecerreyes, A.J. Müller, High Lithium Conductivity of Miscible Poly(ethylene oxide)/Methacrylic Sulfonamide Anionic Polyelectrolyte Polymer Blends, Macromolecules. 53 (2020) 4442–4453. https://doi.org/10.1021/acs.macromol.0c00703.

[30] M.D. Tikekar, S. Choudhury, Z. Tu, L.A. Archer, Design principles for electrolytes and interfaces for stable lithium-metal batteries, Nature Energy. 1 (2016) 1–7.

[31] A. Kisliuk, V. Bocharova, I. Popov, C. Gainaru, A.P. Sokolov, Fundamental parameters governing ion conductivity in polymer electrolytes, Electrochimica Acta. 299 (2019) 191–196. https://doi.org/10.1016/j.electacta.2018.12.143.

[32] M. Baiardo, G. Frisoni, M. Scandola, M. Rimelen, D. Lips, K. Ruffieux, E. Wintermantel, Thermal and mechanical properties of plasticized poly (L-lactic acid), Journal of Applied Polymer Science. 90 (2003) 1731–1738.

[33] H. Younes, D. Cohn, Phase separation in poly (ethylene glycol)/poly (lactic acid) blends, European Polymer Journal. 24 (1988) 765–773.

[34] M.A.S.A. Samir, L. Chazeau, F. Alloin, J.-Y. Cavaillé, A. Dufresne, J.-Y. Sanchez, POE-based nanocomposite polymer electrolytes reinforced with cellulose whiskers, Electrochimica Acta. 50 (2005) 3897–3903.

[35] A. Thiam, C. Martinez-Cisneros, Y. Molméret, C. Iojoiu, J.-Y. Sanchez, PEO: An immobile solvent?, Electrochimica Acta. 302 (2019) 338–343.

[36] C. Brissot, M. Rosso, J.N. Chazalviel, S. Lascaud, Dendritic growth mechanisms in lithium/polymer cells, Journal of Power Sources. 81 (1999) 925–929. https://doi.org/10.1016/S0378-7753(98)00242-0.

[37] W. Xu, J. Wang, F. Ding, X. Chen, E. Nasybulin, Y. Zhang, J.G. Zhang, Lithium metal anodes for rechargeable batteries, Energy and Environmental Science. 7 (2014) 513–537. https://doi.org/10.1039/c3ee40795k.

[38] K. Pożyczka, M. Marzantowicz, J.R. Dygas, F. Krok, Ionic Conductivity and Lithium transference number of Poly(ethylene oxide):LiTFSI system, Electrochimica Acta. 227 (2017) 127–135. https://doi.org/https://doi.org/10.1016/j.electacta.2016.12.172.

[39] L. Meabe, T.V. Huynh, N. Lago, H. Sardon, C. Li, L.A. O'Dell, M. Armand, M. Forsyth, D. Mecerreyes, Poly(ethylene oxide carbonates) solid polymer electrolytes for lithium batteries, Electrochimica Acta. 264 (2018) 367–375. https://doi.org/10.1016/j.electacta.2018.01.101.

[40] L. Meabe, S.R. Peña, M. Martinez-Ibañez, Y. Zhang, E. Lobato, H. Manzano, M. Armand, J. Carrasco, H. Zhang, Insight into the ionic transport of solid polymer electrolytes in polyether and polyester blends, Journal of Physical Chemistry C. 124 (2020) 17981–17991. https://doi.org/10.1021/acs.jpcc.0c04987.

[41] N. Vassal, E. Salmon, J.-F. Fauvarque, Electrochemical properties of an alkaline solid polymer electrolyte based on P (ECH-co-EO), Electrochimica Acta. 45 (2000) 1527–1532.

[42] Y. Zhang, W. Lu, L. Cong, J. Liu, L. Sun, A. Mauger, C.M. Julien, H. Xie, J. Liu, Cross-linking network based on Poly (ethylene oxide): Solid polymer electrolyte for room temperature lithium battery, Journal of Power

Sources. 420 (2019) 63–72.

[43] S.-S. Chi, Y. Liu, N. Zhao, X. Guo, C.-W. Nan, L.-Z. Fan, Solid polymer electrolyte soft interface layer with 3D lithium anode for all-solid-state lithium batteries, Energy Storage Materials. 17 (2019) 309–316.

[44] R. Rohan, T.-C. Kuo, M.-W. Chen, J.-T. Lee, Nanofiber single-ion conducting electrolytes: an approach for high-performance lithium batteries at ambient temperature, ChemElectroChem. 4 (2017) 2178–2183.

Chapter VII

7.Flame retardant polyphosphoester copolymers as solid polymer electrolyte for lithium batteries

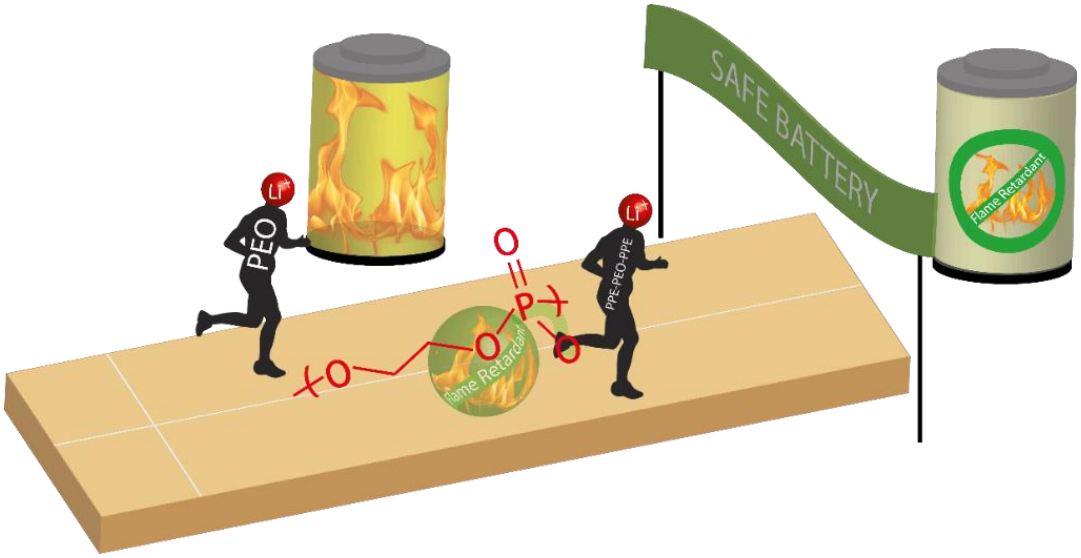

7.1 Abstract

Solid-state lithium batteries are considered one of the most promising battery systems due to their high volumetric energy density and safety. Poly(ethylene oxide) (PEO) is the most commonly used solid polymer electrolyte in solid-state batteries. In this chapter, we introduce new polyphosphoester polymer electrolytes, which show improved flame retardant properties in comparison with PEO. For this purpose, new polyphosphoester copolymers were synthesized, including phosphoester, poly(ethylene glycol) (PEG) and UV cross-linkable vinyl units. Solid polymer electrolyte films based on polyphosphoester copolymers and lithium bis(trifluoromethanesulfonyl)imide (LiTFSI) were prepared by curing under UV-light. The crystallinity present in the copolymers due to the PEG segment decreases with the amount of salt in the electrolyte, as seen by DSC. Solid polymer electrolytes based on polyphosphoester copolymers show ionic conductivity values as high as $2 \cdot 10^{-4}$ S cm^{-1} at 70 °C. FTIR analysis showed that lithium cations complexed with phosphoester groups provoked an increase in the lithium transference number to 0.26 as compared to that of PEO 0.17. Pyrolysis flow combustion calorimetry (PCFC) or micro-calorimetry results demonstrated the improved flame retardancy of the polyphosphoesters in comparison to a reference PEO-based polymer electrolyte. The selected polyphosphoester solid electrolyte was investigated in a solid-state lithium cell Li0/polymer electrolyte/LFP battery showing specific capacity retention close to 80% and coulombic efficiency greater than 98% over 100 cycles at 70 °C.

J.L. Olmedo-Martínez, L. Meabe, R. Riva, G. Guzmán-González, L. Porcarelli, M. Forsyth, A. Mugica, I. Calafel, A.J. Müller, P. Lecomte, Flame retardant polyphosphoester copolymers as solid polymer electrolyte for lithium batteries, Polymer Chemistry. 12 (2021) 3441–3450.

7.2 Introduction

In the XXIst century, a consolidated energy storage system will revolutionize the technology demanded in electric vehicles or in smart grid facilities [1]. Lithium metal batteries with a specific capacity of 3860 mA h g^{-1} could be a competitive candidate to prevail among other battery chemistries. The electrolyte is one of the key components in the performance of the battery. Classic electrolytes are normally based on flammable organic solvents and lithium salts (e.g. 1 M LiPF6-EC/EMC). For this reason, solid-state batteries are seen as the most promisingfuture battery technology in applications where safety is a must, such as in electric vehicles. In this sense, solid polymericelectrolytes (SPEs) composed of a polymer as a host matrix of lithium salt have been presented as a safer option due to their low flammability. The gold standard solid polymer electrolyte for lithium battery applications is poly(ethylene oxide) (PEO), owing to its excellent ability to solvate lithium salts [2,3]. The high ionic conductivity values reached at 70 °C, and good chemical and thermal properties make PEO-based solid-state batteries able to run at temperatures >70 °C. However, PEO still shows limitations for batteries that run at room temperature or make use of new generation high voltage cathodes. For this reason, alternative polymer electrolytes to PEO are actively being searched, which offer advantageous properties such as higher ionic conductivity, electrochemical window, or lithium transference number, which allow improving the performance of Solid-State Batteries. In this respect, little effort has been devoted in designing polymers to improve the flame retardancy of PEO polymer electrolytes.

One of the first options to improve the safety of lithium batteries was to introduce components such as phosphates into the liquid electrolyte [4,5], but increasing the amount of these compounds in the electrolyte decreased battery performance. Another idea studied was the use of $Mg(OH)_2$ as a separator or in polymer electrolytes. In particular, the use of polymer/$Mg(OH)_2$ systems improved the flame resistance by increasing the hydroxide concentration and improved the physical adhesion between the electrode, and the separator [6,7].

It is known that the presence of nitrogen or phosphorus atoms in the structure of additives or polymers promotes the carbonization of the polymer on heating and reduces the amount of volatile combustible products [8]. Within the

study of flame retardants in polymer electrolytes, trimethyl phosphate has been used as a solvent, which helped to decrease the flammability of electrolytes containing ethylene carbonate (EC) and propylene carbonate (PC) [9]. More recently, Xiang, *et al.* [10] proposed the use of 1,3-dioxolane (PDE) polymerized in situ with the addition of tris(pentafluorophenyl)borane (TB) additive, the in situ formation of PDE improved the flame retardant properties and the incorporation of TB contributed to the stabilization of the solid electrolyte interface (SEI). Other examples found in the literature include the use of additives such as pyrrolidinium- and imidazolium-based ionic liquids due to their non flammable/non-volatile property [11–13]. Polyphosphoesters (PPEs), containing phosphoester bonds in the main chain, are biodegradable and biocompatible, and therefore, their principal application is described in biomedicine, mainly known in drug delivery systems [14–16]. Apart from this, PPEs possess excellent thermal stability, fire resistance, and attractive mechanical properties [17]. In fact, organic flame retardants that contain phosphorus groups have attracted much attention in industrial applications [18,19]. As a representative study, Wang et al., reported a polyphosphonate that shows excellent flame retardancy, which was able to prolongate the time to ignition. A meaningful reduction of the peak heat release rate (HRR) by 57% and a decrease of the specific extinction area was reported [20]. However, the use of polyphosphoesters as SPEs in batteries has been poorly explored. Initial works, reported the synthesis and evaluation of different polyphosphoesters as SPEs, show an ionic conductivity values of $\sim 10^{-6}$ S cm^{-1} at 70 °C, which are very low for practical use of these materials in lithium batteries [21]. The use of phosphonate molecules as flame retardant additives in SPEs has also been reported [22].

In this chapter, we synthesized new tailor-made polyphosphoester copolymers and evaluated them as polymer electrolytes for lithium solid state batteries. The new polyphosphoester polymer electrolytes were characterized in terms of thermal and electrochemical properties. Particular attention was paid to investigate the flame retardancy of the polyphosphoester copolymers using pyrolysis flow combustion calorimetry (PCFC) or microcalorimetry. Additionally, the most promising polyphosphoester polymer electrolyte was evaluated in a lithium metal/polyphosphoester/lithium iron phosphate solid state lithium cell

through charge–discharge tests. During the discussion of results, PEO used as a reference for being the reference solid polymer electrolyte in lithium batteries nowadays.

7.3 Results

7.3.1 Solid polymer electrolytes based in polyphosphoester copolymers by UV-curing

In this chapter, three different polyphosphoester copolymers were synthesized according to the procedure described by Vanslambrouck, *et al* [23]. Figure 7.1 shows the chemical structure of the polyphosphoester copolymers, which were designed to include PEG segments, polyphosphester groups and vinyl functional groups. The PEG segments are known to be the best groups for solvating salt in polymer electrolytes. In addition, the phosphoesters functionalities are expected to improve flame retardancy. Since polyphosphoesters are typically low T_g polymers which are viscous liquids at room temperature, we choose to add some vinyl functionalities to be able to crosslink the polyphosphoesters copolymers and thus obtain solid-free standing films. Thus, two triblock copolymers (P1 and P2) with a central block of PEG and two lateral blocks made of hydrophobic polyphosphoesters containing 50 mol% of unsaturated pendant group were synthesized. The difference between P1 and P2 copolymers relies on the number of phosphoester subunits in the lateral blocks. A third copolymer exclusively made of polyphosphoester was also prepared as polymer reference without PEG sequence (P3).

Figure 7.2 shows the typical UV-curing of one polyphosphoester copolymers in the presence of LiTFSI salt and a photoinitiator. As a result of the cross-linking of the initial liquid like low T_g polyphosphoester a free-standing solid polyphosphoester film including LiTFSI was obtained as shown in the picture, Figure 7.2.

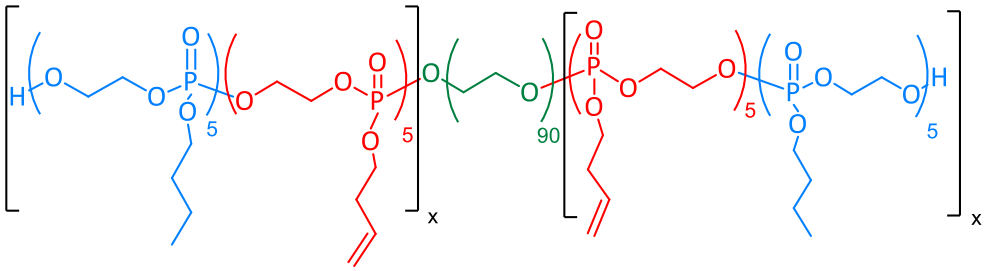

P1 M_n = 7,600 g /mol

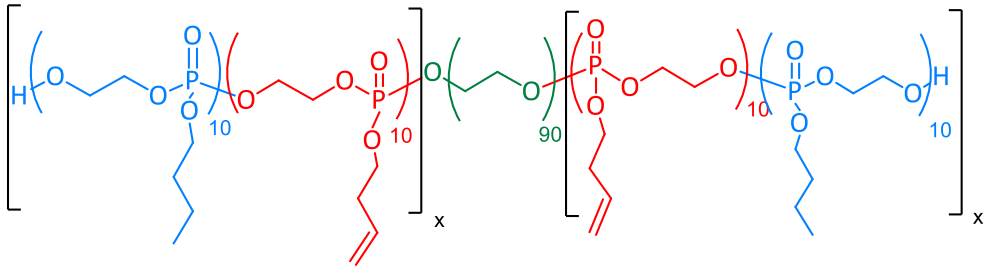

P2 M_n = 11,000 g /mol

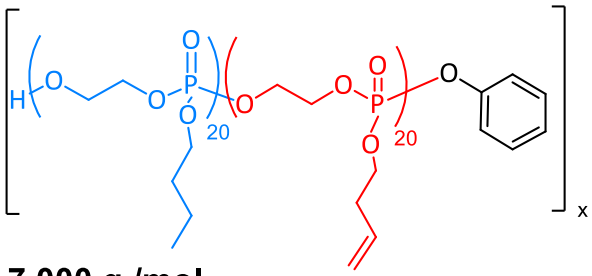

P3 M_n = 7,000 g /mol

Figure 7.1. Chemical structure of the three different polyphosphoester copolymers investigated in this work.

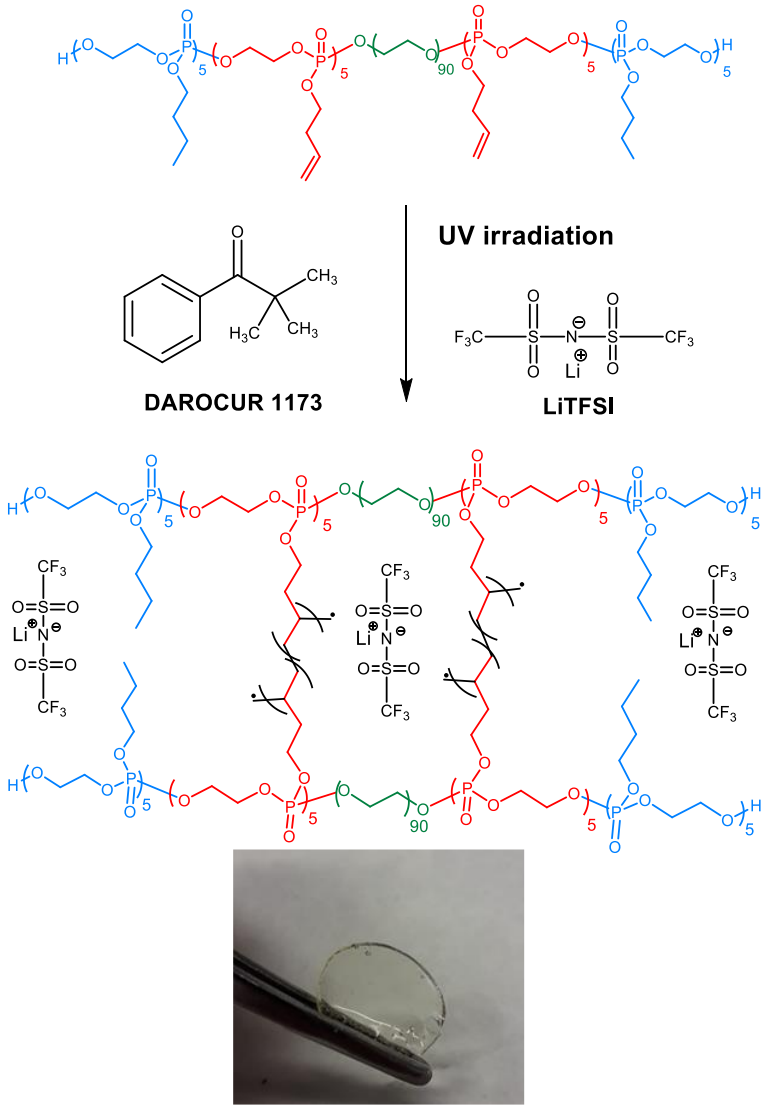

Figure 7.2. Schematic representation of the ultraviolet curing of the polyphosphoester copolymers.

7.3.2 Differential scanning calorimetry (DSC)

It is well known that for the design of new SPEs, amorphous polymers with a low glass transition temperature (T_g) are preferred due to favorable segmental motion for improved ionic conductivity [24] For this reason, the thermal properties of synthesized PPE-SPEs were evaluated by DSC. Figure 7.3 shows the DSC results for the different copolymers and the corresponding blends; non-crosslinked and crosslinked systems with 15 and 30 wt% LiTFSI. In the neat synthesized polymers, two different thermal behavior have been analyzed, P1 and P2 are semicrystalline materials, instead, P3 is an amorphous copolymer. The melting enthalpy (ΔH_m) values for the copolymers P1 and P2 are respectively

72 and 53 J g^{-1}, which represents 34 and 25% crystallinity degree, which decreases further with the addition of Li salt until the material is completely amorphous. The semi-crystallinity of the P1 and P2 is derived from the presence of the polyethylene oxide block, where the analyzed melting temperature (T_m) in both cases is around 40 °C. However, the molecular weight of the PEG block in the copolymers is 4000 g mol^{-1} and the T_m values are lower than those reported for PEG of this molecular weight (~55 °C (ref. [25] and [26])). This lowering of T_m can be associated to the introduction of another block, phosphoester group, where the PEG crystallization is hindered and restricted [27]. Moreover, the addition of LiTFSI to these copolymer matrices, results in a decrease of the T_m, increasing the amorphous phase, Figure 3a and b. As it can be observed in Figure 3a, the T_m in P1 decreases with 15 wt% LiTFSI from 43 °C to 35 °C, and when the electrolyte is crosslinked, following a similar trend, the T_m decreases to 33 °C. Beyond, when 30 wt% LiTFSI is added to the SPEs, P1 and P2 become completely amorphous polymers, with a glass transition temperature (T_g) of −43 and −48 °C, respectively. Figure 7.3c shows the DSC heating scans of P3 copolymer, where it can be corroborated that P3 is completely amorphous owing to the lack of EG units in the polymer. Non-crosslinked and crosslinked electrolytes are completely amorphous and, in all cases, the T_g values are as low as around −45 °C without significant variation.

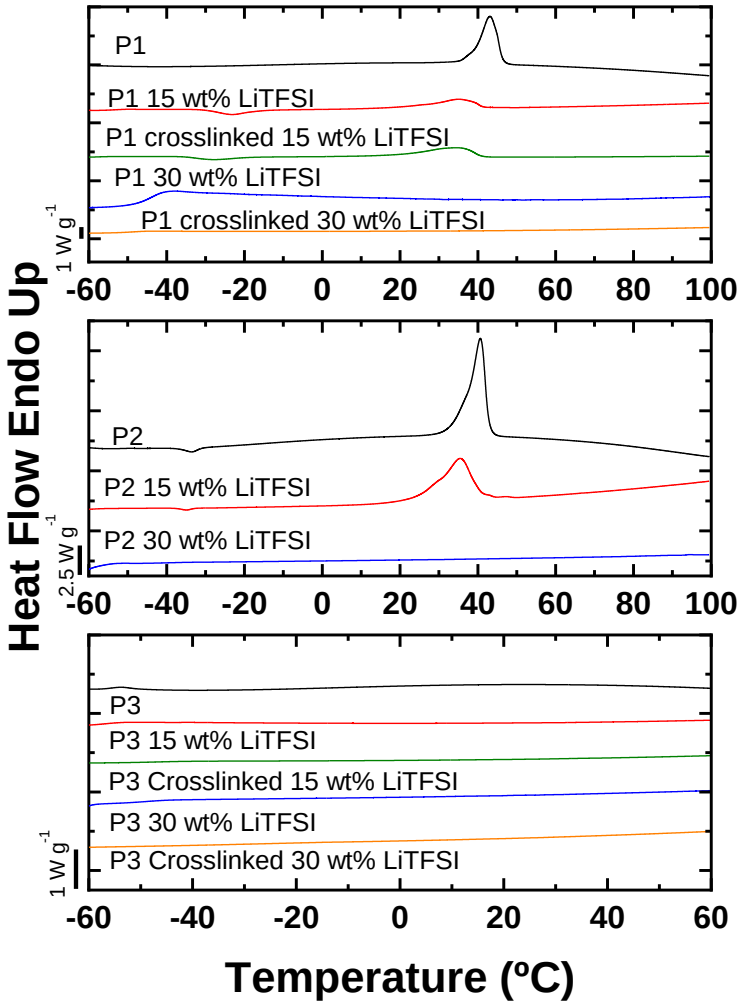

Figure 7.3. DSC heating scans of the different polyphosphoester with LiTFSI.

7.3.3 Dynamic mechanical thermal analysis (DMTA)

Figure 7.4 shows the DMTA results of the P1 copolymer crosslinked and the electrolytes of this copolymer crosslinked with 15 and 30 wt% LiTFSI. DMTA was performed for the crosslinked polymers since the polymers not crosslinked with LiTFSI were viscous liquids, to which this experiment could not be performed. The graph presents the modulus value as a function of temperature, at low temperatures the polymers are in a glassy state [28], and the storage modulus E′, is constant from −100 to −40 °C, where the modulus decreases as the T_g of the polymer passes, these results corroborate those presented by DSC.

In the case of crosslinked P1 without LiTFSI, there is another drop in the modulus, which is attributed to a fusion of the part containing PEG segments, in the case of electrolytes, the T_g at −40 °C is observed and the modulus decreases as a function of the salt concentration in the system, even so, the values of the modulus at 70 °C, $1.56 \cdot 10^6$ Pa with 15 wt% LiTFSI and $6.6 \cdot 10^5$ Pa with 30 wt% LiTFSI, are comparable with other values reported in the literature [29–31].

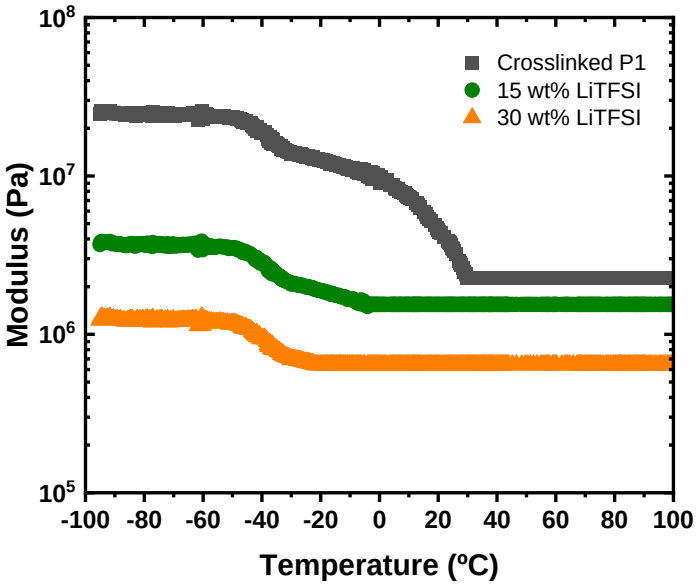

Figure 7.4. DMTA of crosslinked electrolytes.

7.3.4 Microcalorimeter characterization

A microcalorimeter is a bench-scale instrument used to determine the flammability parameters of materials under laboratory conditions. The more important parameters are the heat release rate (HRR) and peak heat release rate (PHRR). Figure 7.6 shows these parameters as a function of time and temperature.

The thermal stability of the polymers was also observed by TGA (Figure 7.5), and it is observed that the decomposition temperature (T_d) of the polymer shows a similar trend compared to PHRR values obtained in the microcalorimeter runs (Table 7.1). Combustibility depends as much on fire conditions as on polymer composition [32], in this case, the PEO was taken as a reference, since the copolymer P1 has a PEG block in its chemical structure. The behavior of the

temperature at peak heat release rate (PHRR) in the graphs (Figure 7.6a) shows that the PEO needs above 400 °C for this material to catch fire, when adding LiTFSI to the PEO this temperature is a bit higher, but they are the ones that need the least time for ignition. In the case of materials with phosphoester groups, the temperature necessary for ignition is 328 °C and decreases when adding lithium salt, but the fire-retardant property is observed in Figure 7.6b, where it is necessary a longer time for ignition. Table 7.1 shows the quantitative results obtained by this technique: it is observed that the following parameters; the heat release capacity (HRC), which is related to the fire hazard of the material and total heat release (THR), which is the amount of heat released throughout the decomposition, decrease when LiTFSI is added, and at the same time these values are lower in the electrolytes based on the copolymers, which proves that flammability of these materials is decreased.

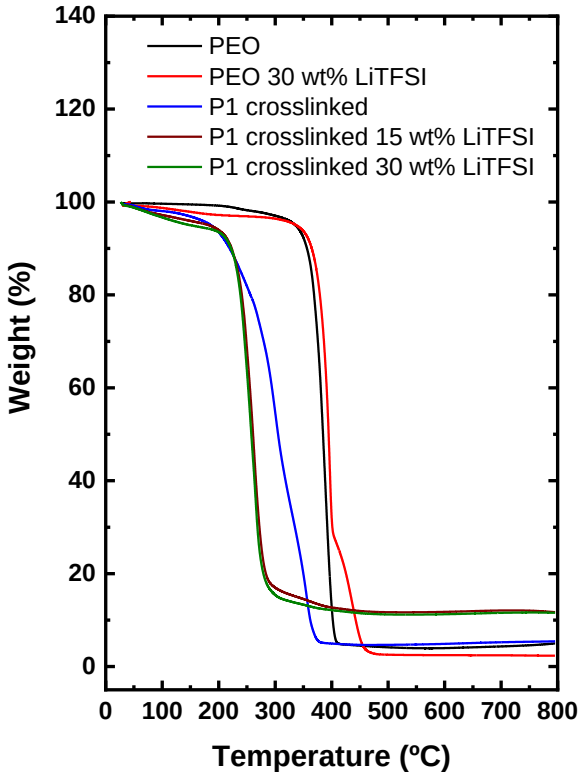

Figure 7.5. TGA of the different polymers.

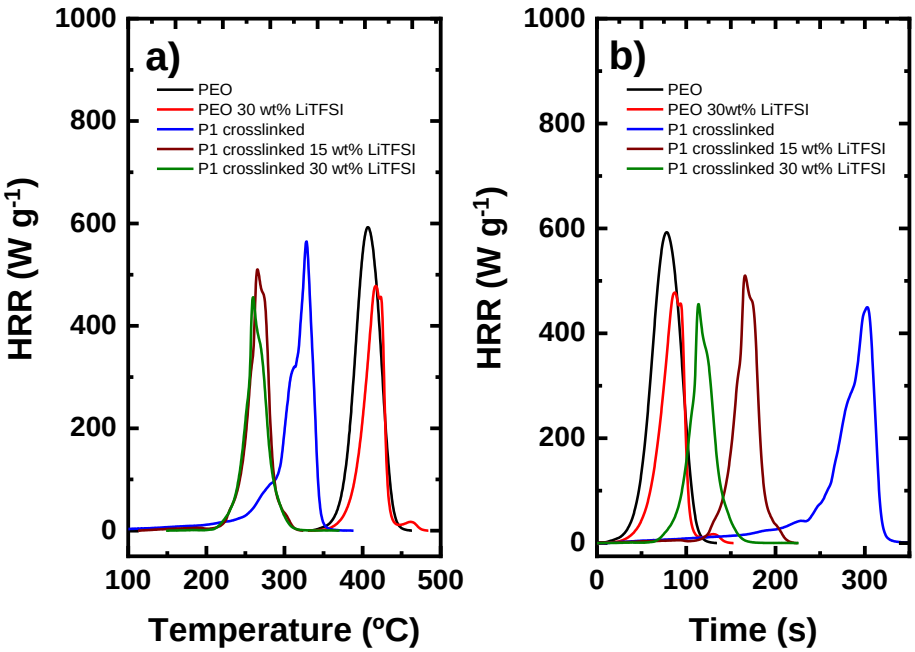

Figure 7.6. Microcalorimeter test as a function of a) Temperature, and b) Time.

Table 7.1. Microcalorimeter data.

Sample	HRC (J $g^{-1}K^{-1}$)	Peak HRR (W g^{-1})	Total HR (KJ g^{-1})	T_p (°C)	T_d (°C)
PEO	600	592.91	23.90	406.74	387
PEO 30 wt% LiTFSI	544.68	545.26	16.07	421.1	416
P1 crosslinked	418.4	420.12	20.57	324.57	298
P1 crosslinked 15 wt% LiTFSI	525.2	525.5	16.32	265.8	265
P1 crosslinked 30 wt% LiTFSI	459.93	449.09	14.44	259.32	259

7.3.5 Ionic conductivity and Li-ion transference number (t_{Li}^+)

Next, the ionic conductivity of the prepared SPEs was evaluated. Figure 7.7 shows the ionic conductivity as a function of temperature for the different non-crosslinked SPEs. In the ionic conductivity experiments, PEO was used as a reference. Figure 7.7a shows the behavior of ionic conductivity of all copolymers and PEO with 15 wt% LiTFSI. The behavior is directly related to the amount of

ethylene oxide units in the polymer structure; the ionic conductivity decreases with the increase in phosphoester concentration in the copolymer (PEO > P1 > P2 > P3). In addition, PEO, P1 and P2 with 15 wt% of salt present some crystallinity, as shown in the DSC results (Figure 7.3), but being such a low crystallinity, the drop in ionic conductivity values is not appreciated. In the case of P3, as it is completely amorphous, no drop is evidenced with the temperature decrease. Figure 7.7b shows the ionic conductivity data corresponding to the SPEs with 30 wt% LiTFSI. All SPEs are amorphous and provide a superior ionic conductivity with respect to that of the 15 wt% LiTFSI-SPEs. The same behavior occurs with SPEs containing 15 wt% LiTFSI, the highest values of ionic conductivity are obtained with PEO, and the newly developed polymers follow the same tendency as in 15 wt% LiTFSI-SPEs, i.e., P1 > P2 > P3. All in all, P1–30 wt% LiTFSI offers the remarkable high ionic conductivity value among the synthesized polymers, $5 \cdot 10^{-4}$ S cm^{-1} at 70 °C and $3 \cdot 10^{-5}$ S cm^{-1} at 25 °C. Among the synthesized copolymers P1 and P3 are selected to improve the mechanical properties in order to further evaluate the effect of phosphoester groups. Figure 7.7c and d represent the ionic conductivity comparison of non-crosslinked and Uvcrosslinked P1 and P3 materials, Figure 7c shows the electrolytes with 15 wt% LiTFSI, whereas Figure 7.7d, the electrolytes with 30 wt% LiTFSI. The ionic conductivity values slightly decrease when the polymer is crosslinked, as the polymer structure becomes more rigid, which is also evidenced in the DSCs, where the T_g of the crosslinked electrolytes is slightly higher, Figure 7.3. Nevertheless, a compromised balance between good mechanical properties and a good ionic conductivity have been succeeded with UV-crosslinked polymer P1 30 wt% LiTFSI: $2 \cdot 10^{-4}$ S cm^{-1} at 70 °C and $1.9 \cdot 10^{-5}$ S cm^{-1} at 25 °C.

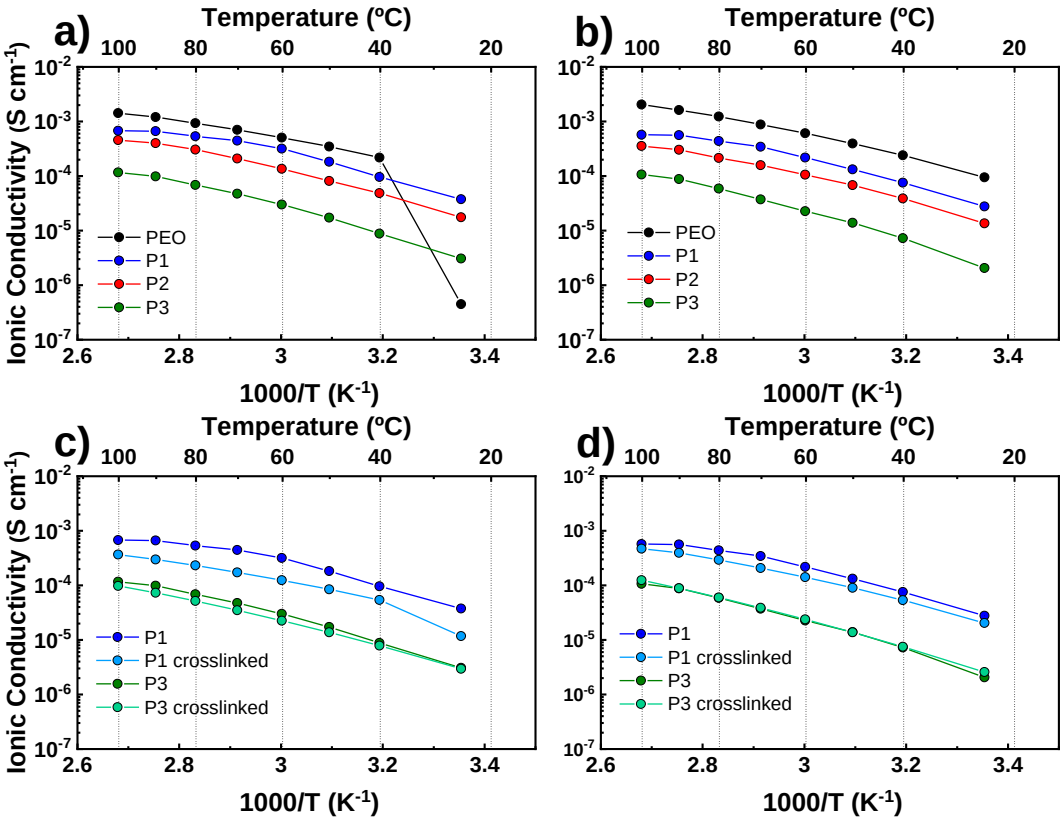

Figure 7.7. Ionic conductivity of PEO and polyphosphoester copolymers, a) with 15 wt% LiTFSI, b) with 30 wt% LiTFSI, c) P1 and P3 crosslinked with 15 wt% LiTFSI and d) P1 and P3 crosslinked with 30 wt% LiTFSI.

The lithium transference number (t_{Li^+}) of the selected crosslinked P1-SPE is calculated using the Bruce and Vincent method [33] (Figure 7.8). The Li-ion transference number at 70 °C for this electrolyte is 0.26. This value is slightly higher compared to PEO-based SPE with 30 wt% LiTFSI, which is close to 0.17 [34]. The increase in the number of lithium transport could be due to the fact that there are new complexing groups in the polymer, such as –P=O groups, as suggested in FTIR analysis, (section 7.3.6). To the same extent that has been studied in other polymer chemistries (e.g., polycarbonates [35,36] or polyesters [37]), the coordination between P=O and lithium cation could be weaker than EG units, and therefore, the lithium mobility is promoted.

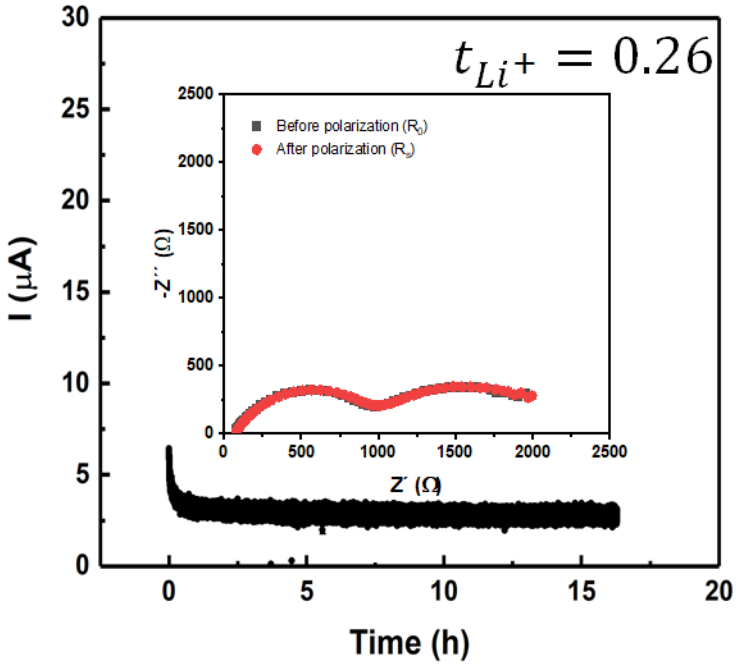

Figure 7.8. ac- and dc-measurements for the lithium ion transference number measurements crosslinked P1 30 wt% LiTFSI electrolyte.

7.3.6 Fourier transform infrared spectrometry (FTIR) analysis

FTIR spectrum of electrolytes provides information on how LiTFSI cations and anions are complexed in the host polymer. Generally, the lithium ions are solvated by EG units in the polymer backbone of PEO-SPEs [38,39]. The study of coordination environments is evaluated for non-crosslinked P1 and P3 copolymers. Even if P1 copolymer provides the most promising ionic conductivity, for an easier evaluation of the role of phosphoester groups in the matrix, P3 copolymer is included in this study, where there is no PEG block in the polymer structure. Figure 9a displays the FTIR spectra for P1 based SPEs (in this case, P1 and P2 have the same discussion since they have the same chemical structure), whereas Figure 7.9c corresponds to P3 based SPEs. In all cases two LiTFSI concentrations are evaluated: 15 and 30 wt% LiTFSI.

The study of FTIR range is focused between 1400–900 cm^{-1}, being the range in which the possible coordination vibration of salt with the phosphoester groups is expected. In P1, the bands that correspond to P–O–C (1060 cm^{-1}) and P=O (1277 cm^{-1}) are slightly shifted to lower wavenumbers, which might be

attributed to the coordination bond formed between oxygen atoms from ether group and phosphate and lithium ion. This indicates the favorable interaction between the lithium ions and the copolymers. The bands that correspond to $TFSI^-$ anion are also represented in the FTIR spectra range. The asymmetric S–N–S stretching mode [40] in non-coordinating environment, appears in 1059 cm^{-1}, whereas when the TFSI anion is presented in ion aggregates, the vibrations is shifted 1140 and 1197 cm^{-1} [41]. The vibration in 1324 and 1345 cm^{-1} correspond to C–SO_2–N bonding mode [42,43], 1197 cm^{-1} is the symmetric stretching mode of CF_3 [44], 1243 cm^{-1} that correspond to asymmetric SO_3 vibrations [44]. Also, the bands 1243, 1324, and 1345 cm^{-1} represent the contact ion pair Li^+TFSI^- [41]. Due to the intensity and the wavenumber of the peaks, it can be said that most of the TFSI anions are in clusters.

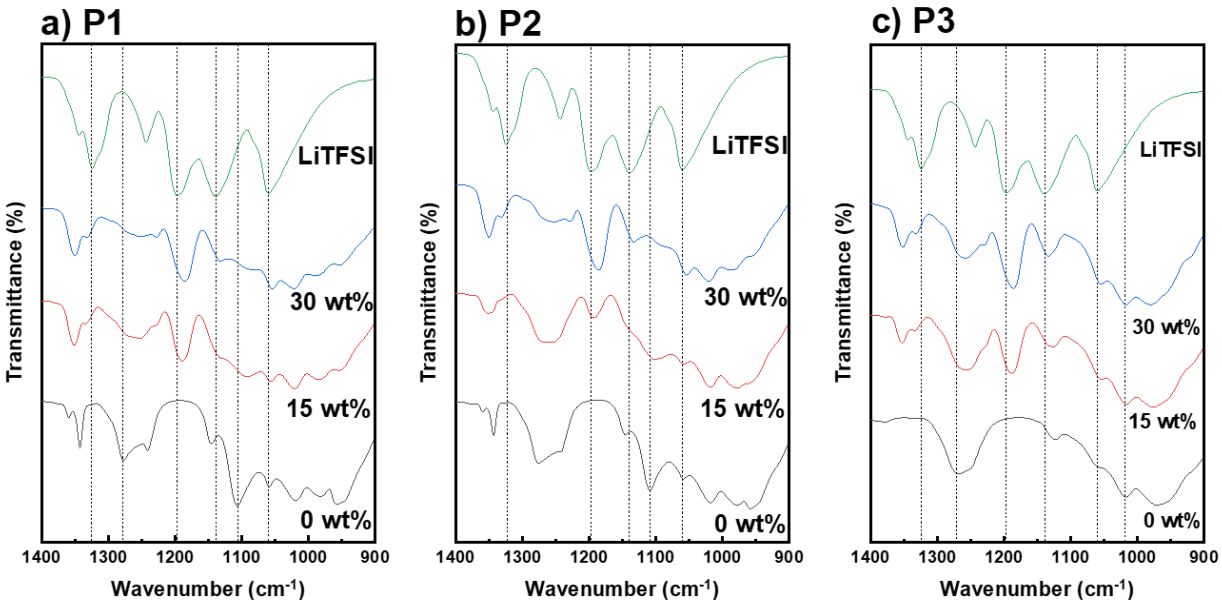

Figure 7.9. FTIR of a) P1 with LiTFSI, b) P2 with LiTFSI, and c) P3 with LiTFSI

7.3.7. Battery test

Owing to the ionic conductivity of UV-crosslinked P1 shown at 70 °C, $2 \cdot 10^{-4}$ S cm^{-1} and its improved flame retardancy this copolymer was chosen to be investigated in solid-state batteries. An important difference between using liquid electrolytes and SPEs is the contact between the electrolyte and the electrode, whereas when using a liquid electrolyte, all the pores of the electrode

are filled with electrolyte facilitating the transport of charge, while in solid state batteries, conduction is more difficult in the cathode. For this reason, P1/LiTFSI was also chosen to use as a binder, to ensure ionic conduction within the porous structure of the cathode and crosslinked P1 30 wt% LiTFSI as a solid polymer electrolyte. The lithium/polyphosphoester/ lithium iron phosphate cell (Figure 7.10) was tested at a C-rate of C/10 between 4 and 2.5 V at 70 °C. The decrease in the first few cycles can be explained by the sequestration of lithium ions, possibly due to the formation of a passivation layer at the electrode/electrolyte interface [45]. Even if a capacity drop can be observed among the cycles, 112 mA h g^{-1} in the 1st cycles, 74 mA h g^{-1} in the 100th cycle (71.8% and 47.5% of the theoretical value with respect to $LiFePO_4$ cathode), good efficiencies (>98%) have been disclosed, that confirms the reversibility of the lithium ion intercalation process as well as the electrochemical stability of the polyphosphoester copolymer electrolyte. Even if cell composition can be optimized for an improved battery performance, these results indicate the good efficiency of the battery using this cathode composition and electrolyte.

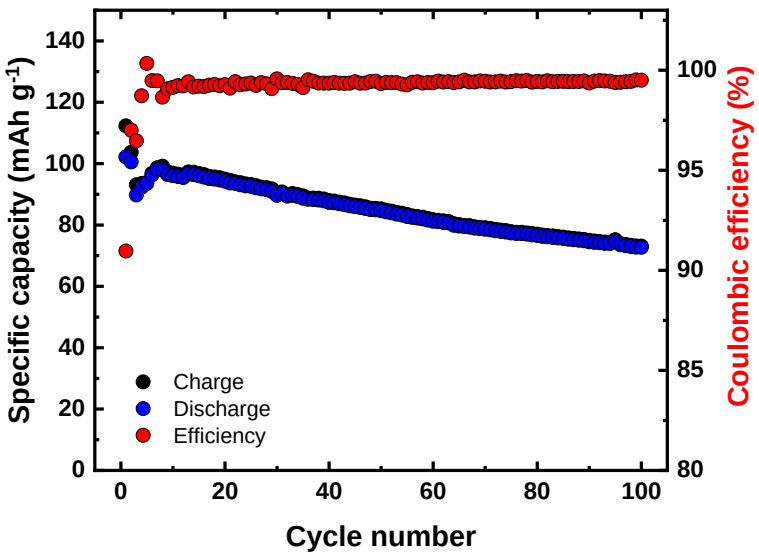

Figure 7.10. Specific capacity versus cycle number profile of the Li/crosslinked P1 30 wt% LiTFSI/$LiFePO_4$ cell at 70 °C.

7.4 Conclusions

Three different polyphosphoester-based copolymers were successfully synthesized, two triblock copolymers with a central PEG segment and one random copolymer only composed of polyphosphoester to be studied as solid polymer electrolytes for lithium batteries. The crystallinity of the copolymers having a PEG central segment decreases with the incorporation of LiTFSI, and the ionic conductivity in these electrolytes is slightly lower than in the PEO reference system. The presence of PEG segments positively affects the ionic conductivity, the conductivity found at 70 °C for the copolymer P1 with 30 wt% LiTFSI was equal to $2 \cdot 10^{-4}$ S cm^{-1}. By FTIR, it was concluded that lithium cations also complexed with phosphoester groups, which caused a slight increase in the number of lithium transfer, obtaining a value of 0.26, which is higher than that of the PEO/LiTFSI system. The lithium/ polyphosphoester/ $LiFePO_4$ cell based on synthesized P1 copolymer with 30 wt% LiTFSI, maintains a coulombic efficiency greater than 98% with specific capacity values that decrease a little with the number of cycles. Interestingly, the fire resistance of these electrolytes was tested, and it was observed that the presence of phosphoester groups acts as flame retardant, which may help for the safety of the batteries devices.

7.5 References

[1] M. Forsyth, L. Porcarelli, X. Wang, N. Goujon, D. Mecerreyes, Innovative Electrolytes Based on Ionic Liquids and Polymers for Next-Generation Solid-State Batteries, Accounts of Chemical Research. 52 (2019) 686–694. https://doi.org/10.1021/acs.accounts.8b00566.

[2] J. Mindemark, M.J. Lacey, T. Bowden, D. Brandell, Progress in Polymer Science Beyond PEO — Alternative host materials for Li + -conducting solid polymer electrolytes, Progress in Polymer Science. 81 (2018) 114–143. https://doi.org/10.1016/j.progpolymsci.2017.12.004.

[3] P. Barai, K. Higa, V. Srinivasan, Lithium dendrite growth mechanisms in polymer electrolytes and prevention strategies, Physical Chemistry Chemical Physics. 19 (2017) 20493–20505.

https://doi.org/10.1039/c7cp03304d.

[4] H.F. Xiang, H.Y. Xu, Z.Z. Wang, C.H. Chen, Dimethyl methylphosphonate (DMMP) as an efficient flame retardant additive for the lithium-ion battery electrolytes, Journal of Power Sources. 173 (2007) 562–564.

[5] Y.E. Hyung, D.R. Vissers, K. Amine, Flame-retardant additives for lithium-ion batteries, Journal of Power Sources. 119 (2003) 383–387.

[6] A.M. Stephan, Review on gel polymer electrolytes for lithium batteries, European Polymer Journal. 42 (2006) 21–42. https://doi.org/10.1016/j.eurpolymj.2005.09.017.

[7] S. Kim, T. Han, J. Jeong, H. Lee, M.-H. Ryou, Y.M. Lee, A flame-retardant composite polymer electrolyte for lithium-ion polymer batteries, Electrochimica Acta. 241 (2017) 553–559.

[8] M. Le Bras, S. Bourbigot, G. Camino, R. Delobel, Fire retardancy of polymers: the use of intumescence, Elsevier, 1998.

[9] X. Wang, E. Yasukawa, S. Kasuya, Nonflammable trimethyl phosphate solvent-containing electrolytes for lithium-ion batteries: I. Fundamental properties, Journal of The Electrochemical Society. 148 (2001) A1058.

[10] J. Xiang, Y. Zhang, B. Zhang, L. Yuan, X. Liu, Z. Cheng, Y. Yang, X. Zhang, Z. Li, Y. Shen, A flame-retardant polymer electrolyte for high performance lithium metal batteries with an expanded operation temperature, Energy & Environmental Science. (2021).

[11] P.-L. Kuo, C.-H. Tsao, C.-H. Hsu, S.-T. Chen, H.-M. Hsu, A new strategy for preparing oligomeric ionic liquid gel polymer electrolytes for high-performance and nonflammable lithium ion batteries, Journal of Membrane Science. 499 (2016) 462–469.

[12] D.R. MacFarlane, N. Tachikawa, M. Forsyth, J.M. Pringle, P.C. Howlett, G.D. Elliott, J.H. Davis, M. Watanabe, P. Simon, C.A. Angell, Energy applications of ionic liquids, Energy & Environmental Science. 7 (2014) 232–250.

[13] S.B. Kale, T.C. Nirmale, N.D. Khupse, B.B. Kale, M. V Kulkarni, S.

Pavitran, S.W. Gosavi, Cellulose-Derived Flame-Retardant Solid Polymer Electrolyte for Lithium-Ion Batteries, ACS Sustainable Chemistry & Engineering. 9 (2021) 1559–1567.

[14] T. Steinbach, F.R. Wurm, Poly (phosphoester) s: A new platform for degradable polymers, Angewandte Chemie International Edition. 54 (2015) 6098–6108.

[15] K.N. Bauer, H.T. Tee, M.M. Velencoso, F.R. Wurm, Main-chain poly(phosphoester)s: History, syntheses, degradation, bio-and flame-retardant applications, Progress in Polymer Science. (2017) 61–122. https://doi.org/10.1016/j.progpolymsci.2017.05.004.

[16] Z.E. Yilmaz, C. Jérôme, Polyphosphoesters: New trends in synthesis and drug delivery applications, Macromolecular Bioscience. 16 (2016) 1745–1761.

[17] K.D. Troev, Polyphosphoesters: Chemistry and Application, 2012.

[18] C. Zhang, T.F. Garrison, S.A. Madbouly, M.R. Kessler, Recent advances in vegetable oil-based polymers and their composites, Progress in Polymer Science. (2017) 91–143. https://doi.org/10.1016/j.progpolymsci.2016.12.009.

[19] A.B. Morgan, J.W. Gilman, An overview of flame retardancy of polymeric materials: Application, technology, and future directions, Fire and Materials. (2013) 259–279. https://doi.org/10.1002/fam.2128.

[20] H.O. Pastore, A. Frache, E. Boccaleri, L. Marchese, G. Camino, Heat induced structure modifications in polymer-layered silicate nanocomposites, Macromolecular Materials and Engineering. 289 (2004) 783–786.

[21] S. Iliescu, N. Plesu, G. Ilia, Synthetic routes to polyphosphoesters as solid polymer electrolytes for lithium ion batteries, in: Pure and Applied Chemistry, 2016: pp. 941–952. https://doi.org/10.1515/pac-2016-0702.

[22] M.F. Rectenwald, J.R. Gaffen, A.L. Rheingold, A.B. Morgan, J.D. Protasiewicz, Phosphoryl-Rich Flame-Retardant Ions (FRIONs): Towards

Safer Lithium-Ion Batteries, Angewandte Chemie. 126 (2014) 4257–4260.

[23] S. Vanslambrouck, B. Clement, R. Riva, L.H. Koole, D.G.M. Molin, G. Broze, P. Lecomte, C. Jérôme, Synthesis and tensioactive properties of PEO-b-polyphosphate copolymers, RSC Advances. 5 (2015) 27330–27337.

[24] D. Devaux, L. Liénafa, E. Beaudoin, S. Maria, T.N.T. Phan, D. Gigmes, E. Giroud, P. Davidson, R. Bouchet, Comparison of single-ion-conductor block-copolymer electrolytes with Polystyrene-TFSI and Polymethacrylate-TFSI structural blocks, Electrochimica Acta. 269 (2018) 250–261. https://doi.org/10.1016/j.electacta.2018.02.142.

[25] D. Fischer, The effect of molecular weight and deposition temperature on the formation of poly (ethylene oxide) films using the femtosecond pulsed laser deposition, Polymer Crystallization. 3 (2020) e10153.

[26] L. Mandelkern, Crystallization of Polymers, 2nd ed. Vo, Cambridge University Press, Cambridge, United Kingdom, 2002.

[27] H. Schmalz, A. Knoll, A.J. Müller, V. Abetz, Synthesis and characterization of ABC triblock copolymers with two different crystalline end blocks: Influence of confinement on crystallization behavior and morphology, Macromolecules. 35 (2002) 10004–10013. https://doi.org/10.1021/ma020983f.

[28] A.S. Shaplov, L. Goujon, F. Vidal, E.I. Lozinskaya, F. Meyer, I.A. Malyshkina, C. Chevrot, D. Teyssié, I.L. Odinets, Y.S. Vygodskii, Ionic IPNs as novel candidates for highly conductive solid polymer electrolytes, Journal of Polymer Science Part A: Polymer Chemistry. 47 (2009) 4245–4266.

[29] M. Álvarez Tirado, L. Castro, G. Guzmán-González, L. Porcarelli, D. Mecerreyes, Single-Versus Dual-Ion UV-Cross-Linked Gel Polymer Electrolytes for Li–O2 Batteries, ACS Applied Energy Materials. 4 (2021) 295–302.

[30] J. Shim, L. Kim, H.J. Kim, D. Jeong, J.H. Lee, J.-C. Lee, All-solid-state lithium metal battery with solid polymer electrolytes based on polysiloxane

crosslinked by modified natural gallic acid, Polymer. 122 (2017) 222–231.

[31] P. Sutton, M. Airoldi, L. Porcarelli, J.L. Olmedo-Martínez, C. Mugemana, N. Bruns, D. Mecerreyes, U. Steiner, I. Gunkel, Tuning the properties of a UV-polymerized, cross-linked solid polymer electrolyte for lithium batteries, Polymers. 12 (2020). https://doi.org/10.3390/polym12030595.

[32] J.C. Markwart, A. Battig, T. Kuckhoff, B. Schartel, F.R. Wurm, First phosphorus AB2 monomer for flame-retardant hyperbranched polyphosphoesters: AB2: Vs. A2 + B3, Polymer Chemistry. 10 (2019) 5920–5930. https://doi.org/10.1039/c9py01156k.

[33] J. Evans, C.A. Vincent, P.G. Bruce, Electrochemical measurement of transference numbers in polymer electrolytes, Polymer. 28 (1987) 2324–2328. https://doi.org/10.1016/0032-3861(87)90394-6.

[34] K. Pożyczka, M. Marzantowicz, J.R. Dygas, F. Krok, Ionic Conductivity and Lithium transference number of Poly(ethylene oxide):LiTFSI system, Electrochimica Acta. 227 (2017) 127–135. https://doi.org/https://doi.org/10.1016/j.electacta.2016.12.172.

[35] B. Sun, J. Mindemark, K. Edström, D. Brandell, Polycarbonate-based solid polymer electrolytes for Li-ion batteries, Solid State Ionics. 262 (2014) 738–742. https://doi.org/10.1016/j.ssi.2013.08.014.

[36] L. Meabe, T.V. Huynh, N. Lago, H. Sardon, C. Li, L.A. O'Dell, M. Armand, M. Forsyth, D. Mecerreyes, Poly(ethylene oxide carbonates) solid polymer electrolytes for lithium batteries, Electrochimica Acta. 264 (2018) 367–375. https://doi.org/10.1016/j.electacta.2018.01.101.

[37] L. Meabe, S.R. Peña, M. Martinez-Ibañez, Y. Zhang, E. Lobato, H. Manzano, M. Armand, J. Carrasco, H. Zhang, Insight into the ionic transport of solid polymer electrolytes in polyether and polyester blends, Journal of Physical Chemistry C. 124 (2020) 17981–17991. https://doi.org/10.1021/acs.jpcc.0c04987.

[38] D. Devaux, R. Bouchet, D. Glé, R. Denoyel, Mechanism of ion transport in PEO/LiTFSI complexes: Effect of temperature, molecular weight and end groups, Solid State Ionics. 227 (2012) 119–127.

https://doi.org/10.1016/j.ssi.2012.09.020.

[39] M. Piszcz, O. Garcia-Calvo, U. Oteo, J.M. Lopez del Amo, C. Li, L.M. Rodriguez-Martinez, H. Ben Youcef, N. Lago, J. Thielen, M. Armand, New Single Ion Conducting Blend Based on PEO and PA-LiTFSI, Electrochimica Acta. 255 (2017) 48–54. https://doi.org/10.1016/j.electacta.2017.09.139.

[40] S. Ahmad, H.B. Bohidar, S. Ahmad, S.A. Agnihotry, Role of fumed silica on ion conduction and rheology in nanocomposite polymeric electrolytes, Polymer. 47 (2006) 3583–3590. https://doi.org/10.1016/j.polymer.2006.03.059.

[41] D. Hambali, Z. Osman, L. Othman, K.B.M. Isa, N. Harudin, Magnesium (II) bis(trifluoromethanesulfonimide) doped PVdC-co-AN gel polymer electrolytes for rechargeable batteries, Journal of Polymer Research. 27 (2020) 1–12. https://doi.org/10.1007/s10965-020-02083-8.

[42] R. Kumar, J.P. Sharma, S.S. Sekhon, FTIR study of ion dissociation in PMMA based gel electrolytes containing ammonium triflate: Role of dielectric constant of solvent, European Polymer Journal. 41 (2005) 2718–2725. https://doi.org/10.1016/j.eurpolymj.2005.05.010.

[43] S. Ramesh, C.W. Liew, Dielectric and FTIR studies on blending of [xPMMA-(1 - X)PVC] with LiTFSI, Measurement: Journal of the International Measurement Confederation. 46 (2013) 1650–1656. https://doi.org/10.1016/j.measurement.2013.01.003.

[44] S. Ramesh, K.H. Leen, K. Kumutha, A.K. Arof, FTIR studies of PVC/PMMA blend based polymer electrolytes, Spectrochimica Acta - Part A: Molecular and Biomolecular Spectroscopy. 66 (2007) 1237–1242. https://doi.org/10.1016/j.saa.2006.06.012.

[45] L. Porcarelli, A.S. Shaplov, M. Salsamendi, J.R. Nair, Y.S. Vygodskii, D. Mecerreyes, C. Gerbaldi, Single-Ion Block Copoly(ionic liquid)s as Electrolytes for All-Solid State Lithium Batteries, ACS Applied Materials and Interfaces. 8 (2016) 10350–10359. https://doi.org/10.1021/acsami.6b01973.

Chapter VIII

8.Conclusions

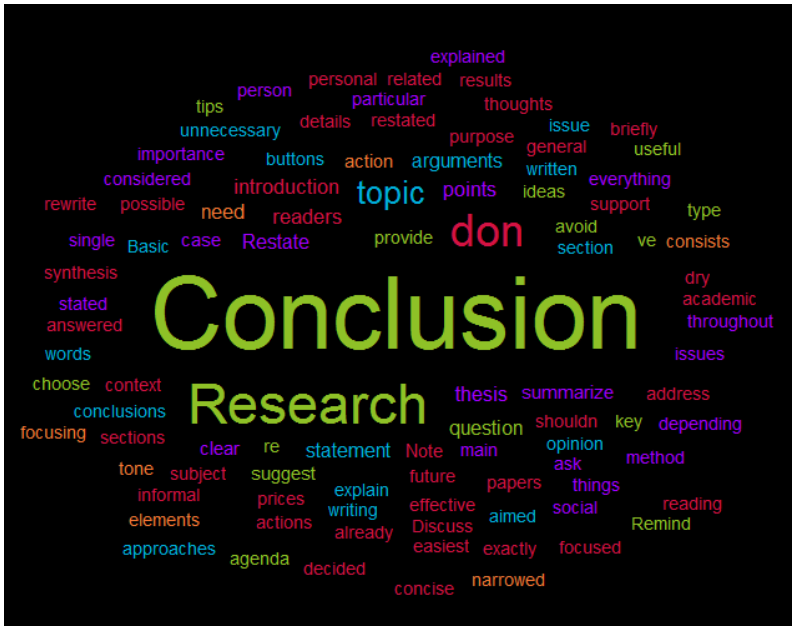

8.1 General Conclusions

The objective of this thesis was to prepare and characterize different polymeric systems, to be used as solid polymer electrolytes for lithium batteries. The main characteristic of this work is that these electrolytes were prepared with the purpose of investigating the relationship between the crystallinity, ionic conductivity, mechanical and thermal properties and its performance as solid electrolytes in lithium batteries. PEO was used in all the systems studied, and the change in the crystallinity of this polymer is studied in detail. New Solid polymer Electrolyte systems were prepared by physical blending of polymers as well as by preparing block copolymers.

Chapter I presents a general introduction to the thesis, the structure of the thesis, as well as the general background knowledge that is necessary for a correct understanding of the content of the thesis. In **Chapter II**, all the experimental techniques used in the development of the thesis are described, as well as the materials, synthesis, and preparation of electrolytes of each chapter.

In **Chapter III**, different aliphatic polyethers were investigated as solid polymer electrolyte matrices with LiTFSI and the effect of the number of methylene units in the repeating unit of the polyethers on the crystallinity and ionic conductivity was compared. It was shown that LiTFSI acts as a diluting agent for aliphatic polyethers, which reduces the crystallization rate and crystallization temperature. It was also found that increasing the number of methylene units in the repeating unit of the polyether decreases the ionic conductivity, with PEO being the polyether with the highest ionic conductivity. Applying the Flory-Huggins theory, we demonstrated that LiTFSI acts as a thermodynamic diluent. Finally, we calculated the equilibrium melting temperature and the equilibrium enthalpy of fusion for poly(oxydecamethylene) for the first time.

Given the results obtained in Chapter III, in **Chapter IV**, blends of PEO and poly(1,6-hexanediol) PHD were prepared, by studying the blending of the polymers without LiTFSI, it was concluded that the blends are partially miscible, and that the miscibility is a function of the blend composition. Adding LiTFSI to the PEO/ poly(1,6-hexanediol) (PHD) blend showed that the lithium salt prefers to dissolve in the PEO and that this effect may be one of the keys to improving the mechanical properties of these electrolytes.

In **Chapter V**, a single-ion polymer electrolyte was prepared by blending of PEO and PLiMTFSI in a wide range of compositions (between 5 and 70 wt%), and the polymer-polymer interaction parameter was calculated (χ_{12}). It was found that in the whole range of compositions the polymers are miscible. In addition, the molecular weight of both polymers was varied, and the ideal ratio between the polymers was found to show the best ionic conductivity values, i.e., 50 PEO/50 PLiMTFSI (PEO of 100,000 g mol^{-1} and PLiMTFSI of 50,000 g mol^{-1}). By means of dielectric spectroscopy, the contribution of mobility and density of ions participating in the ionic conductivity process was obtained, and it was concluded that mobility is the parameter that has a greater weight in the process.

In Chapter V, a single-ion polymer electrolyte was prepared, which theoretically has advantages in terms of safety, since there is no polarization inside the battery, and as a continuation of this chapter and of Chapters III and IV, in **Chapter VI,** ternary electrolytes were developed having as main components PEO and poly(lactic acid) (PLA), this last one with the purpose of increasing the mechanical properties of the system at 100 ºC, in addition, given the high melting temperature of PLA, to be able to use these electrolytes in a at high temperatures. The systems developed were PEO/PLA/LiTFSI and PEO/PLA/PLiMTFSI. By means of DSC, it was demonstrated that PEO and PLA in the presence of LiTFSI and PLiMTFSI are partially miscible. These lithium ion-contributing materials prefer to dissolve in PEO, this was reflected in the mechanical properties of the electrolytes, since the elastic modulus of both systems increased. In addition, the electrolytes were shown to be stable at high potentials (>4 V). When evaluating these systems in symmetric cells at 100 °C, both systems showed good performance, offering the possibility of obtaining safe electrolytes for high temperature batteries.

Chapter VII, presents different polyphosphoester copolymers to be used as SPEs, the great advantage of these materials is that they have flame retardant properties. Therefore, they were studied as electrolytes with LiTFSI, these polymers were crosslinked to increase the mechanical properties of the electrolytes, by FTIR it was concluded that the lithium cations are also complexed by the phosphoester groups, and this causes an increase in the number of lithium transport. The flame retardant properties were evaluated with a microcalorimeter,

showing that this property is not lost upon the addition of the lithium salt. Finally, a lithium/SPE/$LiFePO_4$ battery was assembled, and it was shown that the coulombic efficiency was maintained, remaining higher than 98%.

8.2 List of publications

[1] **J.L. Olmedo-Martínez**, L. Porcarelli, G. Guzmán-González, I. Calafel, M. Forsyth, D. Mecerreyes, A.J. Müller, Ternary poly(ethylene oxide)/Poly(L,L-lactide) PEO/PLA blends as High-Temperature Solid Polymer Electrolytes for Lithium Batteries, ***Submitted.***

[2] **J.L. Olmedo-Martínez**, M. Pastorio, E. Gabirondo, A. Lorenzetti, H. Sardon, D. Mecerreyes, A.J. Müller, Polyether Single and Double Crystalline Blends and the Effect of Lithium Salt on Their Crystallinity and Ionic Conductivity, Polymers. 13 (2021) 2097.

[3] **J.L. Olmedo-Martínez**, L. Meabe, R. Riva, G. Guzmán-González, L. Porcarelli, M. Forsyth, A. Mugica, I. Calafel, A.J. Müller, P. Lecomte, Flame retardant polyphosphoester copolymers as solid polymer electrolyte for lithium batteries, Polymer Chemistry. 12 (2021) 3441–3450.

[4] S. Chen, M.N. Renny, L. C. Tomé, **J.L. Olmedo-Martínez**, E. Udabe, E.P.W. Jenkins, D. Mecerreyes, G.G. Malliaras, R.R. McLeod, C.M. Proctor, Reducing Passive Drug Diffusion from Electrophoretic Drug Delivery Devices through Co-Ion Engineering, Advanced Science. (2021) 2003995.

[5] R.D. Olmo, N. Casado, **J.L. Olmedo-Martínez**, X. Wang, M. Forsyth, Mixed ionic-electronic conductors based on PEDOT:PolyDADMA and organic ionic plastic crystals, Polymers. 12 (2020). https://doi.org/10.3390/polym12091981.

[6] K. Saito, C. Jehanno, L. Meabe, **J.L. Olmedo-Martínez**, D. Mecerreyes, K. Fukushima, H. Sardon, From plastic waste to polymer electrolytes for batteries through chemical upcycling of polycarbonate, Journal of Materials Chemistry A. 8 (2020) 13921–13926. https://doi.org/10.1039/d0ta03374j.

[7] C. Habel, J. Maiz, **J.L. Olmedo-Martínez**, J. V. López, J. Breu, A.J. Müller, Competition between nucleation and confinement in the crystallization of poly(ethylene glycol)/ large aspect ratio hectorite nanocomposites, Polymer. 202 (2020). https://doi.org/10.1016/j.polymer.2020.122734.

[8] **J.L. Olmedo-Martínez**, L. Porcarelli, Á. Alegría, D. Mecerreyes, A.J. Müller, High Lithium Conductivity of Miscible Poly(ethylene oxide)/Methacrylic Sulfonamide Anionic Polyelectrolyte Polymer Blends, Macromolecules. 53 (2020) 4442–4453. https://doi.org/10.1021/acs.macromol.0c00703.

[9] A.P.S. Martins, A.F. De Añastro, **J.L. Olmedo-Martínez**, A.R. Nabais, L.A. Neves, D. Mecerreyes, L.C. Tomé, Influence of anion structure on thermal, mechanical and CO2 solubility properties of uv-cross-linked poly(Ethylene glycol) diacrylate iongels, Membranes. 10 (2020) 1–18. https://doi.org/10.3390/membranes10030046.

[10] P. Sutton, M. Airoldi, L. Porcarelli, **J.L. Olmedo-Martínez**, C. Mugemana, N. Bruns, D. Mecerreyes, U. Steiner, I. Gunkel, Tuning the properties of a UV-polymerized, cross-linked solid polymer electrolyte for lithium batteries, Polymers. 12 (2020). https://doi.org/10.3390/polym12030595.

[11] **J.L. Olmedo-Martínez**, L. Meabe, A. Basterretxea, D. Mecerreyes, A.J. Müller, Effect of chemical structure and salt concentration on the crystallization and ionic conductivity of aliphatic polyethers, Polymers. 11 (2019) 452. https://doi.org/10.3390/polym11030452.

8.3 Conference presentations

1. International discussion meeting on Polymer Crystallization (IDMPC2019), San Sebastián, Spain, 20-23 October, 2019.

Poster: Crystallization and miscibility of solid polymer electrolytes. **Jorge L. Olmedo-Martínez**, David Mecerreyes, Alejandro J. Müller.

2. XXIII International Materials Research Congress (IMRC2019), Cancún, México, 18-23 August, 2019.

Oral presentation: Poly(ethylene oxide)/anionic polyelectrolyte blends for single ion lithium conducting polymer electrolytes. **Jorge L. Olmedo-Martínez**, Luca Porcarelli, Alejandro J. Müller, David Mecerreyes.

3. X Congreso de Jóvenes Investigadores en Polímeros (JIP2019), 2019, Burgos, Spain, 23-23 May.

Oral presentation: Effect of chemical structure and LiTFSI concentration on the crystallization and ionic conductivity of aliphatic polyethers. **Jorge L. Olmedo-Martínez**, Leire Meabe, Andere Basterretxea, David Mecerreyes, Alejandro J. Müller.

4. 6th Young Polímero Scientists Conference & 10th ECNP Short Course, San Sebastian, Spain, October, 2018.

Poster: Effect of chemical structure and salt concentration on the ionic conductivity and crystallization of different polyethers. **Jorge L. Olmedo Martínez**, Andere Basterretxea, Haritz Sardon, Leire Meabe, Alejandro J. Müller, David Mecerreyes.

8.4 Collaborations

This thesis has been carried oun in collaboration with various universities.

Part of the electrochemical characterization of Chapters VI and VII were developed at Deakin University (Melbourne, Australia) during 5 months intership (February 15, 2020 – July 15, 2020) at Institute for Frontier Materials under the supervision of Dr. Luca Porcarelli and Prof. Maria Forsyth.

The copolymers used in Chapter VII were synthesized by Dr. Raphaël Riva and Prof. Philippe Lecomte at the Center for Education and Research on Macromolecules (CERM), CESAM Research Unit, University of Liège (ULiège) in Liège, Belgium.

8.5 Future Work

A PhD thesis has a defined period of time, so that aspects or ideas remain which can serve as a basis for another project:

- Normally, polymeric systems that are used as SPEs have a wide electrochemical characterization for a direct application of the material, but within polymer science, they are very interesting systems to study.
- To study the blends presented in Chapters V and VI, with different cations, e.g., sodium, potassium or magnesium.
- The copolymers studied in Chapter VII are very interesting for the development of safe electrolytes for lithium batteries. The preparation of copolymers of higher molecular weight could be studied, since these were of small molecular weight, and their effect on battery performance could be evaluated.Also, blends could be prepared with the single ion polymer synthesized in Chapter V and blended with these copolymers.

Resumen y Conclusiones

En este trabajo de estudiaron diferentes sistemas de electrolitos poliméricos, con el objetivo de ser utilizados en baterías de litio. Los sistemas poliméricos desarrollados se prepararon con la finalidad de mejorar las prestaciones de los electrolitos sólidos actuales en términos de conductividad iónica, numero de transferencia de litio, propiedades mecánicas a elevada temperatura o resistencia a la llama. El polióxido de etileno (PEO) es el polímero mas utilizado en la actualidad como electrolito de polímero sólido en baterías de litio, ya que presenta los valores mas altos de conductividad iónica, pero tiene algunos parámetros mejorables como su estabilidad térmica, electroquímica y propiedades mecánicas. En esta tesis, se utilizó PEO y se estudió el efecto sobre la cristalinidad del PEO la adición de sal de litio (LiTFSI) y diferentes polímeros. Los sistemas de electrolitos estudiados en esta tesis fueron preparados como mezclas de polímeros y utilizando copolímeros de bloque.

En el **Capitulo I** se presenta una introducción general de la tesis, la estructura de la misma, así como el conocimiento general básico necesario para el correcto entendimiento de la tesis. En el **Capitulo II**, se explican todas las técnicas experimentales utilizadas en el desarrollo de la tesis, además, se presentan los materiales, síntesis y preparación de electrolitos por cada capitulo de resultados.

El **Capitulo III** se estudiaron diferentes poliéteres alifáticos con la incorporación de LiTFSI y se evaluó el efecto del numero de unidades de metileno en la unidad repetitiva del polímero sobre la cristalinidad de los polímeros, así como el efecto de la concentración de LiTFSI en la conductividad iónica. Se encontró que, LiTFSI actúa como un agente diluyente para los poliéteres alifáticos, el cual reduce la velocidad de cristalización y la temperatura de cristalización de estos polímeros. Se observó que, al aumentar el numero de unidades de metileno en la unidad repetitiva la conductividad iónica disminuye, el PEO es el poliéter que presenta los valores de conductividad más áltos. Se aplicó la teoría de Flory-Huggins, para demostrar que el LiTFSI es un diluente termodinámico para estos polímeros, con los resultados obtenidos aplicando

estas ecuaciones se calculo por primera vez la temperatura de fusión en equilibrio termodinámico y el la entalpia de fusión en equilibrio para el poli(oxidecametileno).

Dados los resultados obtenidos en el Capitulo III, en el **Capitulo IV**, se prepararon mezclas de PEO y poli(1,6-hexanodiol) (PHD), lo primero fue estudiar los la mezcla de los polímeros sin LiTFSI, en esta parte, se concluyó que las mezclas son parcialmente miscibles, y que la miscibilidad entre estos polímeros está en función de la composición de la mezcla. Al incorporar LiTFSI en la mezcla 80PEO/20PHD, se demostró que la sal de litio prefiere disolverse en el PEO, y que PHD permanece cristalino, mientras que el PHD permanece cristalino a grandes concentraciones de LiTFSI, la principal conclusión de este Capitulo es que la mezcla de dos polímeros semicristalinos puede ser una de las claves para mejorar las propiedades mecánicas de los electrolitos poliméricos.

El **Capitulo V** presenta un sistema se electrolitos poliméricos de conducción única, esto quiere decir que solo el catión de litio se mueve a través del electrolito, y que el anión permanece inmóvil. Mezclas de PEO y PLiMTFSI se prepararon en un amplio rango de composiciones (entre 5 y 70 wt%). Se calculo el parámetro de interacción polímero-polímero (χ_{12}), y este valor es negativo, indicando que en todo el rango de composiciones los polímeros son miscibles. Además, se estudio el efecto del peso molecular de ambos polímeros, variando estos dos parámetros (composición y peso molecular) se logró encontrar una relación ideal entre los polímeros así como los pesos moleculares con los cuales el electrolito presenta la conductividad mas alta (50 PEO/50 PLiMTFSI con PEO de 100,000 g mol^{-1} y PLiMTFSI de 50,000 g mol^{-1}).

Por medio de espectroscopia dieléctrica, se descompuso la ecuación de conductividad iónica, pudiendo conocer la contribución de la movilidad y la densidad de iones, con este estudio se demostró que el parámetro más importante es la movilidad de los iones.

En el Capitulo V, se preparó un electrolito de conducción única, lo cual en teoría tiene muchas ventajas en términos de seguridad de la batería, dado que no hay polarización dentro de la batería, pero los electrolitos PEO/PLiMTFSI presentaban bajas propiedades mecánicas, por este motivo, y como

continuación de los Capítulos III y IV, en el **Capitulo VI**, se desarrollaron dos sistemas de electrolitos de composición ternaria, teniendo como componentes comunes entre los sistemas PEO y poli(ácido láctico) (PLA). El PLA se añadió con la finalidad de aumentar las propiedades mecánicas de los sistemas, además, el PLA tiene una temperatura de fusión (T_m) alta, alrededor de 160 ºC, lo que permite la utilización de estos electrolitos a altas temperaturas de manera segura. Los sistemas desarrollados fueron PEO/PLA/LiTFSI y PEO/PLA/PLiMTFSI. Por medio de DSC se demostró que el PEO y PLA en presencia de LiTFSI o PLiMTFSI son parcialmente miscibles. Y que los materiales proveedores de cationes de litio prefieren disolverse en el PEO, este efecto se vio reflejado en las propiedades mecánicas, ya que el modulo elástico de ambos sistemas incrementó. Además, los electrolitos mostraron estabilidad a altos potenciales (>4 V), lo cual es un requisito de seguridad de estos materiales. Los mejores electrolitos se evaluaron en celdas simétricas a 100 ºC, ambos sistemas mostraron un buen rendimiento, ofreciendo la posibilidad de obtener electrolitos seguros para baterías de alta temperatura.

En el **Capitulo VII**, se utilizaron distintos copolímeros de tipo polifosfoester para ser evaluados como electrolitos poliméricos, la ventaja que presentan estos copolímeros es la propiedad de resistencia a la llama, la cual es característica de los grupos fosfoesters, estos copolímeros tienen un bloque central de PEO, el cual puede acomplejar sales de litio. Es importante remarcar que estos copolímeros fueron enviados al POLYMAT del instituto CERN, Bélgica. Al añadir LiTFSI, estos copolímeros tenían propiedades mecánicas muy bajas, por lo que aprovechando los dobles enlaces polimerizables en el copolímero, se decidió entrecruzar los polímeros para aumentar las propiedades mecánicas. Por medio de FTIR se concluyo que los cationes de litio son también acomplejados por los grupos fosfoester, y esto causa un aumento en el numero de transporte de litio. Las propiedades como retardante a la llama se evaluaron en un microcalorímetro, mostrando que esta propiedades se mantiene en los electrolitos. Finalmente, el electrolito que presentó la mayor conductividad iónica se evalúo en una celda litio/electrolito/$LiFePO_4$, la cual mostro una eficiencia coulombica >98% después de 100 ciclos.

Finalmente, en el **Capitulo VIII**, se presentan las conclusiones generales de la tesis, así como los artículos científicos publicados durante los 4 años de tesis y la presentación de trabajos en congresos.